Universitetet i Stavanger

DET TEKNISK-NATURVITENSKAPELIGE FAKULTET

MASTEROPPGAVE

Studieprogram/spesialisering: BÆREKRAFT/ENE	Vår.....semesteret, 2014..... Konfidensiell
Forfatter: Per Hassel Sørensen	…… (signatur forfatter)
Fagansvarlig: Veileder(e): Bjørn Hjertager	
Tittel på masteroppgaven: Engelsk tittel: VELOMOBILE: redefined	
Studiepoeng: 30	
Emneord: **Pedelec, series hybrid, electronic transmission, battery management, hydro-pneumatic, active balancing, life-cycle, thermoplastic, self-reinforced composite**	Sidetall: …78 …… + vedlegg/annet: Appendix A,B,C :..50 Appendix D,E,F:...86 Appendix G:……194 Stavanger, 16. juni 2014…….. dato/år

Universitetet
i Stavanger

VELOMOBILE: REDEFINED

Constructing a unique human powered vehicle with electric assist,

to save you & the world

Per Hassel Sørensen

STAVANGER, NORWAY

Abstract

Greenhouse gas emissions from production and use of personal motorized transport must be kept to a minimum to avoid dangerous climate change. More sustainable options must be found.

Bicycles can be used for most local trips within cities and give additional health benefits. Adding electric assist to bicycles improve the range but lack the creature comfort offered by even the least attractive car.

The described electric assisted velomobile construction bridges the gap between cars and electric assisted bicycles while maintaining exercise benefits, reasonable safety, low maintenance, high sustainability and very low cradle-to-grave energy consumption compared to cars.

This documentation describes new solutions for velomobiles and it is the intention of the author to put on the market a vehicle with most if not all of the novel design elements described herewith. The *Veloquad* described has a unique set of qualities making it a truly revolutionary vehicle, not only evolutionary:

- The use of a series hybrid drive with two motors not only benefits a simpler drive train for a four wheeled vehicle. It also enables the use of low cost mass produced motors for pedelecs, a clean and uncluttered platform chassis, and easy adjustment of the pedals position relative to the cyclist. The suggested implementation contains enabling solutions on how to adopt to legislative rules within the European Union on electric assisted cycles (EPAC/PEDELEC).

- The adoption of high tech battery control system with active balancing and wide operating temperature is an enabling technology for the series hybrid electronic transmission.

- The suggested use of PET based self-reinforced thermoplastic composite for aerodynamic vehicle body parts being light, energy absorbing and recyclable is not new, but the use of such materials in velomobiles has not been described in available sources. This also enable shipping of partially assembled vehicles at low cost and with large environmental benefits.

- Nevertheless, the most important contribution is the hydro-pneumatic suspension system. This is in the view of the author the most important enhancement of the velomobile. It enables space efficient parking, low air drag and a smooth and comfortable suspension necessary for 'creature comfort' when riding. It makes the vehicle both practical and hopefully adds 'awesomeness'. If successfully performed, it will transform the *velomobile* from a rare oddity to "*I really want one"* class of vehicle.

Keywords (not included in the title): ***Pedelec, series hybrid, electronic transmission, battery management, hydro-pneumatic, active balancing, life-cycle, thermoplastic, self reinforced composite.***

About the author

Growing up near Scandinavia's largest bicycle factory as neighbour, Per Hassel Sørensen started early to make his own bicycles. Five years ago he built his first velomobile from a Dutch kit. He added an electric assist motor and a homemade battery with surplus li-ion cells from electric scooters. This velomobile is his daily transport. While studying at University of Stavanger for an MSc in sustainable energy, he decided to explore the possibilities of improving the velomobile to make the vehicle more suitable for the masses.

Per has maintained a strong interest in practical application of new technology. His interest for electronics and computer programming dates back to his early teens. At 16 he got his own computer, a KIM-1 with 1 kilobyte RAM opening a new universe of opportunities for this young man. The successive years of self motivated learning and formal education allowed him a career in the computer industry starting while studying and extended more than 20 years. During the latest 15 years Per has shifted from software and programming to full scale product development on instrumentation and process equipment for industrial use. Today, he is a key member of the Zaptec development team creating new power solutions for electric vehicles and spacecrafts.

Author testing his self-constructed prone bike with friends, ca 1981.

Source: P. A. Hassel-Sørensen

Aknowledgements

This master thesis has not been created in solitude. I have had the privilege of both standing on the shoulders of giants and also been supported by everyone around me. I am perpetual grateful to all who in their own capacity has assisted me in so many ways, endured my absence from the daily chores, respond to my queries - large and small and also advised and guided me in what for me is a new territory, but for some is just another thesis. Thank you all for your patience.

I am most obliged to thank Professor Bjørn Hjertager at University of Stavanger for his kind support. He has been both a dedicated and attentive tutor as well as a top-ranking specialist in his field. Prof. Hjertager has been instrumental in addressing the structuring of the thesis and provide open-minded guidance on how to approach the problem in an efficient manner. He also offered guidance to include all critical items at the appropriate place. Also, it is important to point out that learning was very much a part of our discussions. As one gets the hands dirty while digging into a topic for a master thesis, a seasoned tutor can successfully convey a structured way of thinking and learning. Prof. Hjertager has mastered this art fully.

Many thanks also to Mr. Andreas Fuchs, the grand old man of series hybrid bicycle technology. Having worked in the field in excess of 15 years, he is widely recognized for all his contributions to the field. He has with a most kind and inspiring flair responded and elaborated on all my questions and been a great motivator in my work.

My first idea on developing a practical velomobile as the backbone of urban personal transport is most certainly inspired by Mr. Frederik Van De Walle. His thesis from KTH a decade ago is still valid and important.

I would also like to thank the grandfather of human powered vehicles, Professor Emeritus at MIT David Gordon Wilson. He has brought human powered technology from the garden sheds of the enthusiasts and boffins to a recognized scientific level. His contribution as president of the International Human Powered Vehicle Association and editor of its journal is monumental. He has also written Bicycling Science, a major reference for human powered vehicles.

With solid academic background in industrial design and almost 30 years experience from the industry, Njård R. Lone is both knowledgeable and an old friend. He has generously supported this work as a resourceful discussion partner and has been vital resource on design, ergonomics and mass production details. Our encouraging and educational monthly meetings has been a great motivation.

Mr Miles Hellon has been most kind and generous to spend his time to proofread the manuscript. Many thanks for your patience and attention to detail.

Painter Oddny Friestad has been very enthusiastic and has supplied me with her fantastic handmade illustrations of velomobile bodies with eye-opening decorations.

My thanks and gratitude will also go to all the people and companies who has provided advice, parts, materials and guidance. I most sincerely hope to return all your favours by shortly completing a working prototype.

Finally I would like to thank my colleagues, friends and family for their support and patience. Especially my wife and children who has shown so much patience and encouragement during the studies leading up to this. I am profoundly grateful to you all and I hope our efforts will lead to a more sustainable future, for us, our children and future generations.

Table of Contents

"The global effort for sustainability will be won, or lost, in the world's cities, where urban design may influence over 70 percent of people's Ecological Footprint."

Source: (Global footprint network, 2008)

List of Pictures

List of Figures

List of Tables

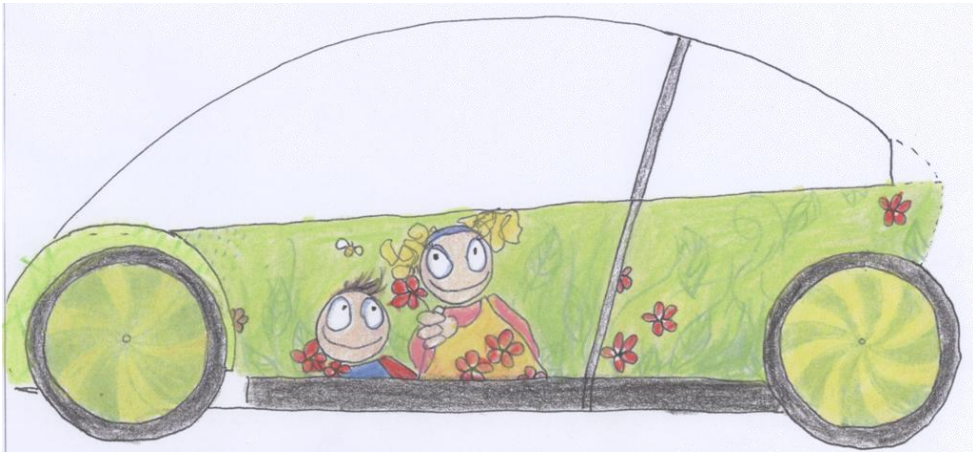

Illustration: Oddny Friestad

Acronyms and symbols

AWD	*All Wheel Drive*	Propulsion on all wheels of vehicle. Favoured on off-road and a must for all-terrain vehicles.
BLDC	*BrushLess DC*	Motor type normally used for motor assisted cycles
BMS	*Battery Management System*	Electronic system being part of a battery used to monitor and/or control the cells in the battery to prevent dangerous situations and damage to the cells.
BMX	*Bicycle Motocross*	Bicycle racing on small tracks, typically mix of dirt and paved surface with undulations, baked curves and jumps. BMX is now a sanctioned racing class within UCI.
C_d	*Coefficient of drag*	The dimensionless fluid drag coefficient for a body.
C_dA	*Drag Area*	Drag coefficient for a given body with a specific size.
CFD	*Computational Fluid Dynamics*	Solving fluid flow problems using numerical methods.
COG	*Centre of Gravity*	Geometric position of the centre of mass.
COTS	*Commercial, Of The Shelf*	Mass produced items readily available at short or zero lead time and at a favourable cost.
C_p	*Coefficient of pressure*	Dimensionless indicator of relative pressure differences.
C_{rr}	*Coefficient of Rolling Resistance*	Rolling resistance coefficient.
DALY	*Disability Adjusted Life Years*	Impact indicator on human health used in life cycle assessment analysis.
DGPS	*Differential GPS*	GPS system with improved accuracy compared to standard GPS.
EEA	*European Economic Area*	A group of countries consisting of Iceland, Liechtenstein and Norway that since 1994 has been allowed to participate in EU's internal market without being EU members.
EPAC	*Electrically Power Assisted Cycles*	European Union classification of cycles with electric motor assist with continuous maximum output power of 250 W and a maximum assisted speed of 25 km/h, and where the motor does not deliver power when the cyclist stop pedalling.
ET	*Electronic Transmission*	A series hybrid drive train for use on cycles.
FEA	*Finite Element Analysis*	A numerical method that can be used to verify mechanical integrity of parts and assemblies by simulating load and stress on computer models.
GHG	*Green House Gases*	Gases that contributes to the greenhouse effect.
GWP	*Global Warming Potential*	The potential greenhouse gas effect of emissions acting on the global climate. Measured in kg CO_2 equivalents
HPV	*Human Powered Vehicle*	Vehicles driven mainly by human power
ICE	*Internal Combustion Engine*	Engine directly driven by gases from combustion of flammable fuels, usually from fossil fuel sources, where the combustion occurs inside the engine.

IP	*Intellectual Property*	Patents, copyrights, trademarks and similar immaterial rights
LCA	*Life-cycle Assessment*	A technique used to assess all the environmental impacts a product or resource has during all the stages from cradle to grave. Also called Life-cycle analysis.
$LiFePO_4$	*Lithium-iron phosphate*	A li-ion cell chemistry class known for being robust, relatively low cost and having good safety. Often used in large battery packs for ships and buses and stationary use. Also used in aviation.
PED	*Pressure Equipment Directive*	EU directive (97/23/EC) specifying safety requirements for pressure equipment within EU/EEA. PED is sometimes used for all pressure safety related directives including S*imple Pressure Vessels [SPVD]* (2009/105/EC), *Transportable Pressure Equipment [TPED]* (99/36/EC), *Gas Appliances Directive [GAD]* (2009/142/EC) and A*erosol Dispensers [ADD]* (75/324/EEC).
PEDELEC	*Pedal-Electric*	A cycle with electric motor assist, see also EPAC.
PET	*Polyethylene terephthalate*	A termoplastic polymer resin in the polyester family, third most used plastic worldwide. Easy and efficient to recycle.
PETG	*PET, glycol-modified*	A PET copolymer made from replacing ethylene glycol with cyclohexane dimethanol (CHDM) making a clear polymer.
SOC	*State of Charge*	How fully charged a battery is in percent of maximum energy storage capacity.
τ	*"tau"*	Shear stress [N/m^2]. Shear stress on walls are usually g τ_w
UCI	*Union Cycliste Internationale*	The international cyclist union founded in Paris in 1900. UCI defines technical requirement for cycles used in cycle sport.
UIS	*University of Stavanger*	University located in Stavanger, Norway.
V2G	*Vehicle to Grid*	Two way communication between vehicle and network.
V2V	*Vehicle to Vehicle*	Communication between vehicles within a certain distance.
y^+	*"y plus"*	Dimensionless wall distance used in fluid models. It is made dimensionless by multiplying physical wall distance with the ratio of friction velocity divided on kinematic viscosity.

Cars cause problems. They cost a fortune to run with their diesel and petrol engines. They produce poisonous emissions and greenhouse gases and consume massive amounts of limited resources. And they make you fat. Compared with cars are bicycles much better, both for you and the environment. Unfortunately, few use them for personal transport. The challenge is how to get more people to use cycles instead of cars. This thesis describes how to construct a human powered vehicle with electric assist that seek to mate comfort and practicality from cars with the low environmental impact and healthy lifestyle from cycling.

1. Introduction

Local combustion of fossil and bio-fuels make emissions that create local air pollution detrimental to humans, animals and plants. In many countries more people die from airborne pollution from cars than from traffic accidents (Caiazzo, Ashok et al. 2013). Combustion of fossil fuels is in addition a huge contributor of greenhouse gases, mainly CO_2, that is very likely to cause worldwide havoc in a not too distant future (IPCC 2014).

Electric cars are better for the environment but still require massive amount of energy for production and use (Simonsen 2010). And even electric cars make you fat.

One of the largest global health issues is the increasing obesity and health problems caused by lack of exercise, partly caused by extensive use of motorized personal transport (WHO 2014). In many nations lack of exercise is the single greatest cause of death. More than 20% of the deaths in the US population is attributed to underutilizing the human body (Booth and Hargreaves 2011). Using pedals both for getting moving and as exercise is a magic bullet, helping both yourselves and the environment.

1.1 Problems to solve

Traditional bicycles have been available for over a hundred years but lack weather protection and high speed capability and offer zero crash protection.

Electric assisted bicycles, or *pedelecs*, remove the burden from pedalling up steep hills or in strong headwind. But they do not remedy the problem of lack of weather protection, nor do they offer any crash protection.

Streamlined *velomobiles*, cycles with a body, are much faster, have at least some weather and crash protection but lack the 'creature comfort' a modern car offers.

The target of thesis is to document how to construct an electric assisted velomobile within a sustainable envelope with the following qualities:

1. **Easy for occupants to enter and leave vehicle**
2. **Having lower air drag than a racing bike**
3. **Excellent ride comfort independent of road conditions**
4. **Complete weather protection including roof and windscreen**
5. **First class cornering stability**
6. **Small parking space**
7. **Room for passenger (child up to 25 kg) within cabin**
8. **Human powered propulsion with motor assist using no derailleur, or gears, nor chains**
9. **Improved safety compared to existing velomobiles**
10. **Easy to mass produce and to ship the 'IKEA' way; with some easy end-user assembly required**

By itself each of these targets are not something special, but balancing the various requirements without compromising each other results in a unprecedented multidisciplinary optimized vehicle. It is simply unique.

1.2 Unsolved problem

An important issue is how to improve the acceptance of velomobiles. This is a very broad problem and involve psychology, infrastructure, economy, sociology, culture, fashion etc. This will not be targeted directly in this thesis. Only where technical issues clearly influence the acceptance of velomobiles will this issue be discussed. For looking further into this problem, *Frederik Van De Walle's* (2004) thesis is a good start.

1.3 Unique solutions

This thesis describes many unique improvements to the velomobile to reduce the gap between cars and human powered vehicles while maintaining sustainability:

- Two hub motors, one in each rear wheel, is the only propulsion - no greasy chains
- An electronic transmission complying to pan-European requirements for electric assisted cycles
- A battery pack specially developed for electronic transmission on cycles in Nordic climate
- Hydro-pneumatic rear suspension with optimum ride comfort
- Rear end including seats can be raised with hydraulics to ease entry and exit
- Protective zones to absorb and distribute impact energy in case of collision
- Body in self-reinforced thermoplastic is strong and light and can be fully recycled
- Vehicle can be stored on its rear end to minimize required parking space

Together with other not so unique, but still important solutions, this thesis describes how to build a series hybrid velomobile targeted as a year-round personal transport for Nordic countries. The focus is on practicality, safety, low maintenance and high sustainability. The motivation is the ongoing and escalating climate change primarily caused by excessive human consumption of fossil fuels - coal, oil and gas. Velomobiles have the potential of reducing the emissions from transport by a factor of ten, compared with electric cars on renewable energy and a factor of at least forty compared with modern cars traditional and hybrid ICE cars. They also make less queue and require less parking space and provide exercise.

1.4 Structure

This document is divided into the following sections:

WHY: Current status and why changes are required

The WHY section contain information about motivation, a short history on cycles and some background on a why changes to the *velomobile*, the vehicle in question, are needed.

WHERE: Areas where new and improved solutions are needed

WHERE goes into details on which weaknesses exists where in the currently available vehicles and describe why current design contains compromised solutions.

HOW: Development of some of the required solutions

In HOW the focus is on the major solutions and how they are developed. Deeper understanding of this process can be found by examining the various appendixes and cited reference material.

WHEN: Discussion, conclusion and further work

The final section WHEN contains a discussion of the construction including a description on why this is a unique vehicle. Exiting thoughts about possibilities for further work can be found here.

The increased car usage is in conflict with necessary reduction of GHG emissions. Cycles could have been much better for personal transport but bicycle racing regulations has severely limited improvements, especially in aerodynamics.

2. WHY: reasons for improving velomobiles

2.1 Motivation

Climate change

Green house gas (GHG) emissions from worldwide burning of fossil fuels have doubled in less than 40 years. CO_2 emissions from fossil fuels caused by human activity are currently interfering with the global climate system. This may cause massive and catastrophic climate changes as documented by thousands of scientists (IPCC 2014).

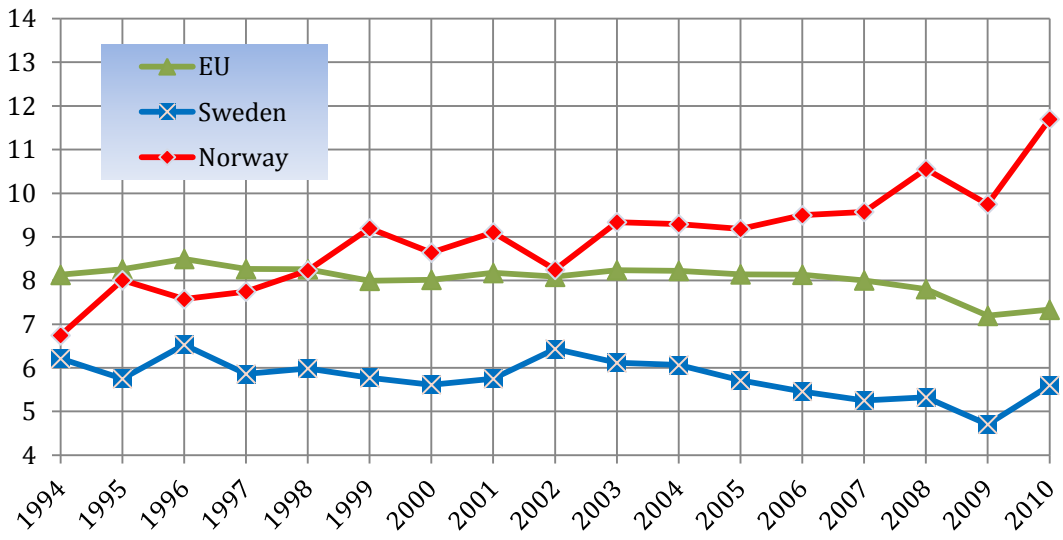

Figure 1 - CO2 emissions per capita 1994-2010

Source: The World Bank, WDI tables

Carbon budget

According to data validated by IPCC (2014) we must limit emissions to around 600 GtC CO_2 to have at least 50% chance of avoiding dangerous climate change. For the last 20 years Norway has increase per capita emissions from 6.7 ton in 1994 to 11.7 ton in 2010. Norway had in 2010 twice the emission of Sweden and is the only Scandinavian Country with rising CO2 emissions, as shown in *Figure 1*. To get to a sustainable level we need to reduce emissions per capita to less than 1 ton CO2 per year, a reduction to 1/10 of current emission level.

Efficiency

A major contribution to CO2 emissions are personal transport by cars. Around 20% of Norwegian emissions comes from the transport sector, where private cars contribute around half, 5.6 Mt for 2012 (SSB 2012) while in Sweden private cars contributed twice as much, 11.1 Mt (NVV 2012). This is around 1.1 t per capita for both countries. In Norway emissions from cars have increased despite official fuel consumption per km have decreased around 25% due to more efficient motors, vehicles and hybrid technologies. This is partly because ac-

cumulated mileage has increased but also because laboratory emission data for new cars has diverged more and more from real life consumption (Mock, German et al. 2013). In addition, increased traffic cause more congestion within cities which lowers average speed and increase fuel consumption on vehicles with an ordinary ICE engine.

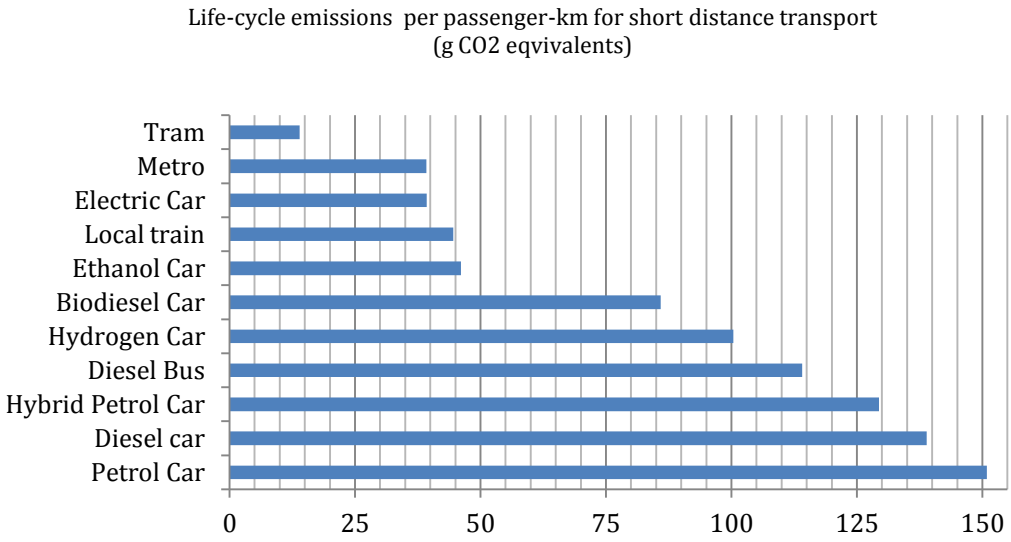

Figure 2 - Total emissions from short distance transport

Source: M. Simonsen, Transport, energi, miljø (TRANSDATA), Vestlandsforskning, 2010

Electric cars using a charged battery as energy source have zero emissions (at the tailpipe), but energy consumption per person per km is still quite high due to the high mass of the vehicle and the vehicle's dependence on electricity and road infrastructure. Even when running electric cars on renewable power sources like wind, hydroelectric or solar, electric cars contributes towards high CO2 emissions per km. Simonsen (2010) used the Norwegian energy mix with high contents of hydroelectric power calculating CO2 equivalents for life cycle emissions of various transport modes. His data shows that electric cars have around 1/3 of the life cycle emissions of a hybrid car and ¼ of a conventional petrol car[1].

From *Figure 2* it is obvious that the use of fossil fuelled cars must be reduced as much as possible. But as the figure shows, electric cars also contribute to emissions. For Norway to stay within the carbon budget we should increase energy efficiency in personal transport by 1000 %. This kind of emission reduction is fully possible by travelling most trips within cities using electrically assisted human powered vehicles (Lemire-Elmore 2004, Walle 2004, Simonsen 2010, Sørensen 2010). To make people select such vehicles instead of cars is the real challenge.

Lack of exercise

Massive documentation exists that lack of exercise is unhealthy (Hwang, Nayak et al. 1998, Walle 2004, Wilson, Papadopoulos et al. 2004, Booth and Hargreaves 2011, WHO 2014), this documentation even go back two millennia. It is major cause of death in many countries but health can easily be improved by light but regular exercise (WHO 2014).

[1] Simonsen use 1.3 passengers including driver per car based on average for short distance commuting, see his discussion on page 38 in his report.

.

.

2.2 Human powered road vehicles

History

The first well known human powered vehicle, or *HPV*, was the *Draisin*, a wooden bicycle made in Germany by *Karl von Drais* in 1816. Later bicycles equipped with chain and pneumatic tires appeared around 1860 and reliable bikes looking like most bikes of today were commercially available in many countries around 1890 as *The Safety Bike* (Wilson, Papadopoulos et al. 2004). These early bikes had a straight posture causing high air resistance at speed. To reduce air resistance a crouched position gave less frontal area resulting in higher speed. Soon special racing handle bars enabling a crouched position became the norm for bikes used in competitons, together with narrow tires and derailleur gears. In the beginning of the 20th century aeroplane development lead to a better knowledge of aerodynamics and attempts were made to decrease the air resistance on cycles. One inventor, *Étienne Bunau-Varilla* and rider *Marcel Berthet* tested in 1913 an aerodynamic shell for a racing bicycle with success, see *Picture 1*. One of his competitiors, *Oscar Egg*, also tried aerodynamic fairings but only partial ones, reducing rear drag (Schmitz 2010). Both Egg and Berthet competed and won the one hour velodrome world speed record several times without fairings from 1907 until 1933 when a recumbent rider smashed the record currently held by Egg by nearly 800 m.

Picture 1 - Marcel Berthet in aerodynamic fairing in 1913

Source: Bibliothèque nationale de France

UCI ban

Recumbent bikes have a lower frontal area compared with racing bikes causing less air drag. This is beneficial at high speed as illustrated in *Picture 2*. From around 1925 until 1934 racers using recumbent bikes were beginning to set records. July 7 1933 *Francis Faure* set a new world record on a recumbent bike riding 45 055 meter in one hour. Shortly after, Berthet in a full faired bicycle, a velomobile, managed almost 50 km. The world records first set with a recumbent unfaired bike and then again using a fully faired velomobile caused disturbance in the cycle world. Were these two innovative bicycles real bikes?

Picture 2 - Recumbent leading the road race Paris-Vichy in 1934

Source: Le Miroir des Sports, No. 769, 19 June 1934

To avoid competitions becoming more dependent on technical innovation and to protect existing bicycle manufacturers, a set of technical requirements forbid fairings and also recumbent bicycles (Walle 2004, Wilson, Papadopoulos et al. 2004, Schmitz 2010). This was decided in 1934 and implemented for all bicycle races arranged by members of UCI, the international cycle union. The new set of rules was very conservative, especially

on frame and wheel design, and is still in place. Any changes causing major improvement to frame, wheel or aerodynamics are not allowed in UCI sanctioned racing. The technical rules are slightly altered now and then but usually to forbid innovative solutions that might give a measurable advantage. Even today the standard UCI 1 hour record is only valid for bicycles technically equal to the bicycle used by *Eddy Merckx* to set the world record in 1972 (Herlihy 2004, Wilson, Papadopoulos et al. 2004, Schmitz 2010).

For organizing racing of non-UCI sanctioned human powered vehicles, *IHPVA-International Human Powered Vehicles Association* was established in 1976. IHPVA in the US and the European organisation WHPVA – *World Human Powered Vehicle Organisation* are currently organizing and maintaining cycle records that fall outside UCI regulations. These international organizations and their national branches are the major development arena for human powered vehicles. (Wilson, Papadopoulos et al. 2004).

Several improvements are needed to make velomobile good enough to be an accepted substitute for a car. Important areas include creature comfort, practicality and safety. Avoiding the need for type approval is also important. The velomobile must legally be an electric assisted cycle for market and cost reasons.

3. WHERE: location of improvement

There are three main problems with current velomobiles from the author's perspective:

1. lack of **creature comfort** - they are primitive compared with even the simplest of cars
2. lack of **practicality** - many velomobiles are not very practical for daily use
3. lack of **acceptance** as an alternative personal transport mode

Improving on **creature comfort** and practicality is the primary target of this thesis. But comfort is intertwined with the **acceptance** factor so there will be some focus on the latter.

3.1 Aerodynamics

To be practical and acceptable, the velomobile must be efficient enough to be propelled by non-athletes. That mean the body must also be aerodynamic. The UCI ban mentioned in the previous chapter prevented further

Machine and rider	Drag coefficient on frontal area, C_D	Frontal area		C_DA	Power to overcome air drag at 10 m/s (22 mile/h)	Power to overcome rolling resistance at 10 m/s for specified total mass (kg) and C_R value		
	C_D	m^2	ft^2	m^2	W	kg	C_R	W
Upright commuting bike	1.15	0.55	5.92	0.632	345	90	0.0060	53
Road bike, touring position	1.0	0.40	4.3	0.40	220	95	0.0045	38
Racing bike, rider crouched, tight clothing	0.88	0.36	3.9	0.32	176	81	0.0030	24
Road bike + Zipper fairing	0.52	0.55	5.92	0.29	157	85	0.0045	38
Road bike + pneumatic Aeroshell + bottom skirt	0.21	0.68	7.32	0.14	78.5	90	0.0045	40
Unfaired long-wheelbase recumbent (Easy Racer)	0.77	0.35	3.8	0.27	148	90	0.0045	40
Faired long-wheelbase recumbent (Avatar Blubell)	0.12	0.48	5.0	0.056	30.8	95	0.0045	42
Vector-faired recumbent tricycle, single	0.11	0.42	4.56	0.047	25.8	105	0.0045	46
Road bike in Kyle fairing	0.10	0.71	7.64	0.071	39.0	90	0.0045	40
M5 faired low racer	0.13	0.35	3.77	0.044	24.2	90	0.003	26
Flux short-wheelbase, rear fairing	0.55	0.35	3.77	0.194	107	90	0.004	35
Moser bicycle	0.51	0.42	4.52	0.214	118	80	0.003	24
Radius Peer Gynt unfaired	0.74	0.56	6.03	0.415	228	90	0.0045	40
Peer Gynt + front fairing	0.75	0.58	6.24	0.436	240	93	0.0045	41
All-terrain (mountain) bike	0.69	0.57	6.14	0.391	215	85	0.0060	50

Table 1 - Drag coefficients of various cycles

Credit: David Gordon Wilson, *Bicycling Science* third edition, and MIT Press

major development on aerodynamic bikes used for competition. The ban targeted only bicycles for sport; a ban for improvement on *transport* did not exist. Unfortunately, the lack of UCI approval prevent many bicycle manufacturers from putting resources into alternative cycle designs. Despite this, some excellent bikes with improved aerodynamic design are now available on the market at reasonable prices. For fully faired cycles, or velomobiles, the offerings are more limited. This is unfortunate since a full fairing can typically increase speed by 50% or more compared to an unfaired bicycle. *Table 1*, reproduced with permission from the book *Bicycling*

Science (Wilson, Papadopoulos et al. 2004), is a list of aerodynamic data for many different bikes. A regular upright bicycle uses 345 W to overcome air drag at 10 m/s. A typical UCI sanctioned race cyclist has a C_dA of around 0.32 m^2, half of the upright bicycle and use 176 W to overcome air drag. C_dA is the drag coefficient C_d multiplied with frontal area A in m^2 and is the most important metric when designing a low drag vehicle and should be as low as possible.

The velomobile Eviestretto used by Russo (2014) has a C_dA around 0.015 m^2, 20 times less. He use only 8.25 W to overcome air drag at 10 m/s. The very low air resistance on *Eviestretto* has been achieved by implementing extreme technologies like riding flat on the back, with head first using a mirror for visual control (Russo 2014).

Picture 3 - VeloX3 at Battle Mountain

Worlds fastest bike has no windows, control by wire using camera and LCD display.

Source: PostNL Press Library

The currently [spring 2014] fastest human powered vehicle, the velomobile *VeloX3* built by the human power team at the University of Delft, set the current world record for the 200 m flying start in September 2013. VeloX3 having a C_dA of 0.02 m^2 was ridden by *Sebastiaan Bowier* at *Battle Mountain*[2] where it achieved a speed of at 133.78 km/h. VeloX3 has an ultra streamlined body which minimize turbulence. There is no windscreen so the rider use a camera and internal LCD screen for visual control (Schuurman 2013). VeloX3 and the specially prepared high altitude test track at *Battle Hill* used for the world record is shown in *Picture 3*.

In section 4.4 some important basics on how to design an aerodynamic body for a velomobile will be described. An iterative development of a functional velomobile body using computational fluid dynamic for drag calculations can be found in appendix C.

[2] The small town of Battle Mountain in Nevada offers both thin air and a very flat and straight section of the nearby Highway 305. The annual IHPVA bike races set often new world records here.

3.2 Functional body

The above-mentioned record velomobiles are pure speed machines and often require a pit crew to start and stop. Most velomobiles have three wheels, and are slower but still fast compared to regular bicycles.

Picture 4 - Three wheeled velomobile

Source: Author

Picture 4 shows a typical design of a three wheeled velomobile. Most velomobiles have sacrificed at least some practicality for higher speed. Most velomobiles are low to reduce frontal and side wind area. The low eye height and long 'bonnet' often makes the road near the vehicle hard to see. They are also narrow to reduce C_dA which diminishes cornering stability. Racing tyres with high pressure reduce rolling resistance, C_{rr} while making the ride uncomfortable and the wheels prone to wear and punctures. For improved body stiffness and low mass the vehicle is often built as a unibody (monocoque) with a stress bearing body without doors and with tall walls, making entry and exit awkward. Also the low seat height makes it cumbersome both to be seated and to exit the vehicle. The thin fairing is light but typically makes a lot of noise when travelling at speed. Fully faired front wheel(s) reduce air resistance but increase turning circle. There are many other similar examples where velomobile designers prioritize speed over practicality (Schmidt 1994, Hwang, Nayak et al. 1998, Sims 1998, Taylor and Blake 1998, Boer 2009). Also, the extended use of thermoset composites made of epoxy, glass and carbon fibre with Kevlar fabric for crash protection is problematic due to the high cost and recycling challenges.

Picture 5 - Velomobiles can be difficult to enter and exit

Source: Author

The cost of a velomobile is often prohibitive, caused partly by expensive materials, but primarily by the limited production volume and a lot of manual labour. In addition shipping costs are quite high due to the large size and fragile materials involved in the constructions (Walle 2004).

An improved velomobile for daily use must target many requirements. For low air resistance and weather protection an aerodynamic velomobile body is a must for an attractive HPV. Preferably it should not be made of thermoset composites as most are difficult to recycle[3]. At the moment scrapped thermoset composites often end up in landfills (La Rosa, Cozzo et al. 2013). Preferred velomobile materials are light and strong and easy to recycle with low conversion losses and which can handle rough handling without becoming scratched, dented or fractured.

A year-round velomobile should have a roof or cover with windows that offers the rider dry transport and good visibility forward and to the sides. A commonly used solution is a clear canopy covering the top of the velomobile, functioning as window and rooftop in a single piece. The drawback of such a solution is the greenhouse effect from the large window area requiring sun shades and good ventilation.

[3] Some glass fibre reinforced plastic, GRP, can be recycled in cement kilns as the mineral composition of glass fibre is similar to raw material mix for certain cement production and the organic part can be used as fuel in the kiln.

Ventilation is very important and must be plentiful, even at winter times. The human engine has a low efficiency, of around 25%. When delivering 100 W mechanical output we produce around 300 W of excess heat that must be removed or else we overheat (Wilson, Papadopoulos et al. 2004). For warm and sunny days it should be possible to ride with 'open windows' or to detach the roof to ride 'topless'.

3.3 Wheels

Wheels are very important for all sorts of cycles. They can cause a lot of trouble. Everyone who has ridden a bike has experienced flat tires. Pneumatic tires were first developed for cycles to improve comfort and reduce rolling friction. Tires and inner tubes has been part of the bicycle wheel for over a century. During WW2, rubber became scarce and some wheels were made using steel springs as replacement as shown in *Picture 6*. This heavy solution did not last past the war.

Picture 6 - Bicycle with springs instead of tyres Right picture shows close-up

Source: Author

Obviously tyre technology is improving but tyres are still a major cause of energy loss when a cycle rolls on the road surface. The rolling resistance when riding at 36 km/h on good non-racing tyres on a typical non-racing bike consume about 40-50 W.

Rolling resistance depends on many parameters, some are rather fixed like tyre size and width, reinforcement material, rubber compound and thread pattern. Others are variable, like temperature, road surface and tyre pressure. Basically, the softer and thinner the tyre is, the easier it rolls. At higher temperature and smother surface, it also rolls better. Tyre pressure is different. There is an optimum air pressure resulting in lowest rolling resistance for each tyre depending on road surface conditions and temperature. Too low pressure results in extensive tyre deformation and internal friction in the tyre. Higher pressure than necessary cause vertical acceleration of vehicle due to imperfect road surface. This vertical acceleration requires energy which would not had been required if the tyre had less pressure and absorbed the imperfection instead. Some recommendations on pressure is usually given by tyre manufacturer but fine tuning must be done on the specific roads experimentally by coasting tests using representative road surface and tyre load (Lafford 2000).

The rolling resistance F_{rr} on level surface can be calculated as:

$$F_{rr} = C_{rr}N$$

where N is the normal force acting perpendicular to direction of rolling, and C_{rr} is the rolling resistance factor. C_{rr} is unique for each tyre at a certain temperature and tyre inflation pressure. C_{rr} primarily reflects the amount of internal friction in the rubber tyre due to flexing under load. The rubber flexes due to load changes during rolling and this flexing converts some mechanical energy to heat and can easily be confirmed by touching car tyres after some driving.

Excluding temperature and road conditions, the easiest way of reducing C_{rr} is by using good tyres with correct tire pressure with regard to laden mass. Using more flexible tyres, typically with thinner cross section and possibly tubeless tyres will also reduce rolling friction, while knobby thread patterns increase C_{rr} (Lafford 2000, Wilson, Papadopoulos et al. 2004)

C_{rr} values for low friction cycle wheels with thread pattern typical for 'city' use when rolling on concrete or smooth asphalt is around 0.004 (Lafford 2000). For a good combination of low rolling resistance and ride comfort, air pressure resulting in 15% 'tyre drop', or reduction of tyre section height, is recommended (Heine 2006). This should be measured with the correct weight per wheel including rider, luggage etc. For a thorough explanation of rolling resistance, chapter 6 in *Bicycling Science* (Wilson, Papadopoulos et al. 2004) is a good start.

Bearing and seal friction

Rolling resistance in the wheel bearings is much less than resistance caused by the tyre and can usually be ignored (Wilson, Papadopoulos et al. 2004). Bearing seals is another matter. Bearing seals have an interface between the two rotating members where there might be friction, depending on the functionality of the seal. This friction is very low for dust proof only seals but quite large for waterproof seals. Bearing suppliers have data on seal and bearing friction.

Wheel size

For saving space, mass and cost, small wheels are better than large wheels. But to reduce rolling resistance larger bicycle wheels are best. In comparative tests large tyres get lower C_{rr} than smaller wheel sizes (Lafford 2000). Unfortunately, using larger than 406 mm front wheels would require a taller body in front and reduce steering wheel angle unless body also was made wider. Most velomobiles have compromised, using medium sized 406 mm wheels, sometimes with a larger rear wheel. Another benefit of reduced diameter is the increased strength for sideways load experienced when cornering at speed assuming same hub and number and strength of spokes. This is due to less spacing on the rim between the spokes, and the increased angle between inner and outer spokes both contribute to lower maximum tension in the spokes.

406 mm is widely used dimension where there is large selection of available tyres. Going below 406 mm the selection of available tyres becomes much smaller. Using the same size for all wheels is preferred. The benefit of

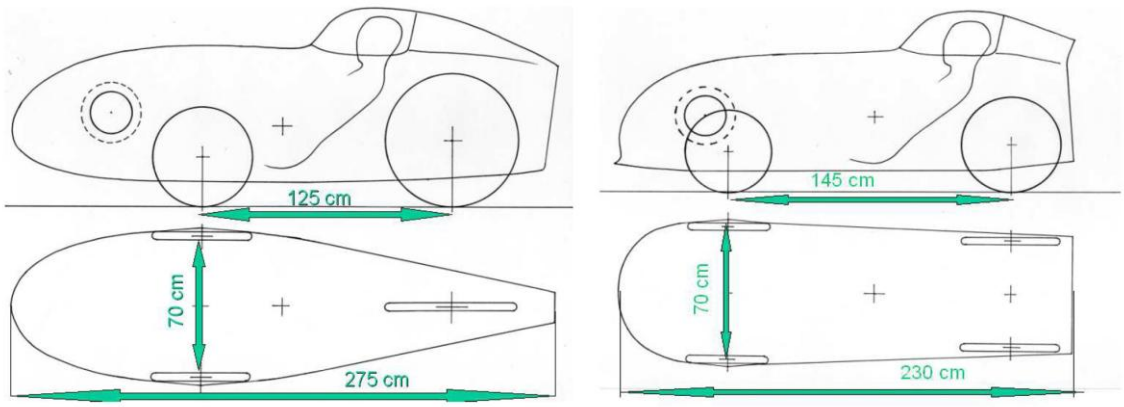

Figure 3 - Typical size of 3 and 4 wheeled velomobiles

Source: Four-wheeled velomobiles. The concept (Kollibay and Neuss 2009)

only needing a single size spare tyre for front and rear make a single tyre size the most sensible solution.

Number of wheels

The number of wheels is important when designing a pedal driven vehicle. The basic rolling resistance formula involves linear relation to the weight on the tyre, so theoretically resistance should be independent of the number of wheels if total mass is held constant. Unfortunately, tests show that more wheels increase rolling resistance and is a typical example of a simple formula being too simple (Wilson, Papadopoulos et al. 2004). A major cause of additional rolling resistance in multitrack vehicles is sideway forces caused by wheels on multitrack vehicles not having perfectly parallel tracks. This causes additional rolling resistance by sideways deformation of the tyres (Zetterström 1998).

Basically, from an efficiency perspective, we want as few wheels as possible. Both one wheeled and two wheeled cycles work, assuming the rider has sufficient training, but single track cycles need continuous movement to maintain balance. One wheeled cycles have the additional challenge of maintaining balance in the direction of travel and are unpractical for most people. Faired vehicles with two wheels can be quite challenging in

windy conditions (Fuchs 1998). There are other practical challenges as well, for example how to keep from falling over when stopping, typically requiring some side support. When focusing on practicality and wanting a vehicle with weather protection, three or four wheels is better.

The author has used a three wheeled velomobile for several years for daily transport, typically travelling 25 km by cycle every day to work and studies, and has overturned three times partly due to the inherent limitations of a three wheel design[4]. There are many compromises in a three wheeled velomobile design which influence safety and practicality (Kollibay and Neuss 2009).

When placing two wheel in front and one in the rear, a so called 'Tadpole' layout, the vehicle must be quite long to accommodate space for the rear wheel as it otherwise interferes with the rider, see *Figure 3*. Also the centre of gravity, *COG*, must be close to front, otherwise the vehicle will easily overturn when cornering. If the *COG* is too close to the front wheels, the rear wheel has a tendency to lift from the ground when braking, causing loss of directional stability.

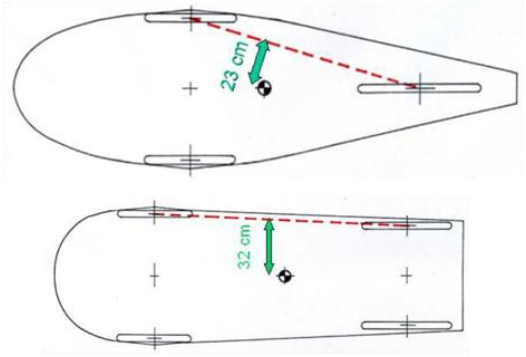

Figure 4 - Distance from COG to tilt line of 3- and 4-wheeled velomobile. The last is more stable

Source: Four-wheeled velomobiles. The concept (Kollibay and Neuss 2009

Having a single wheel in front, a so called 'delta' layout, also has drawbacks. Braking in the corners can lead to the turnover of vehicles as with 'tadpole' designs. Driving two rear wheels becomes complicated, especially with low seating and with rear wheel suspension. Also the vehicle needs to be long or tall in the front, otherwise the steering wheel interferes with the pedals when turning.

Another issue when using three wheelers is the need for three clear tracks for each of the wheels. This can be difficult to manage in off-road conditions or when sharp debris, like glass fragments, lie ahead on the road. Riding in snow and mud also requires more energy when three tracks must be made compared to single or two-track vehicles.

Still, three wheels have several benefits over four wheels, like lower part count and thus less cost plus slightly less rolling and air drag and less mass. But when designing a practical velomobile four wheels is the best compromise when focusing on practicality and safety, as documented by Kollibay and Neuss (2009). One important issue is overall length. Four wheels make the vehicle shorter compared to a 'tadpole' design. Also cornering stability improves by increasing the distance from *COG* to tilt line between the tyres, see *Figure 4*. To distinguish the new *redefined* velomobile design this is given the representative name; *Veloquad*[5].

3.4 Suspension

Exposure to normal vibration levels found on unsuspended cycles is detrimental to creature comfort (Wächter, Zacharias et al. 1998). For low air resistance a heavily reclined seating position is preferred. This requires very good suspension since the recumbent rider cannot suspend herself using the legs and stand on the pedals as on an upright cycle.

Front suspension

A typical front suspension from an velomobile is shown *Figure 5*. It requires cantilever attached wheels where the wheel axle is fixed only on one side. This is a low mass McPherson type construction developed over many years and functions well. As can be seen from the disassembled strut in *Picture 7*, the strut is equipped with two springs. The short red spring is made from a thicker wire tha the long blue spring and acts as the end of stroke damper, preventing bottoming of the suspension. The yellow padding on the centre rod is saturated with a sticky

[4] These overturns did not lead to injuries or stop of journey, only loss of time. But it has always caused damages to vehicle body, once so severe that replacing several body panels was necessary.
[5] A term describing a velomobile with four wheels, coined by *Leo Visscher* of Alligt

lubricant causing high shear stress. When the rod is sliding inside the strut cylinder the padding acts as friction damper.

Figure 5- Front suspension on a 'tadpole' velomobile seen from above

CAD model is based on Alligt Alleweder A4

Source: Author

This front suspension can be supplied with drum brakes or disc brakes. The front wheels have large camber, leaning in on top to maximize traction within a narrow width and also to reduce stress on spokes when cornering fast.

Ride height

For high cornering speeds the centre of gravity need to be as low as possible to reduce the risk of tipping. For a velomobile where the rider is at least half the total mass, that mean the rider(s) needs to be as low as possible in the vehicle. This helps also reducing vehicle height which again decrease frontal area and thus air drag.

Unfortunately, in current velomobiles it is often quite difficult to enter and exit, as can be seen from *Picture 5*. If possible the seat height should be ca 40 cm above ground to ease entry and exit. But for low air resistance and for low *COG* a much lower seat height is required.

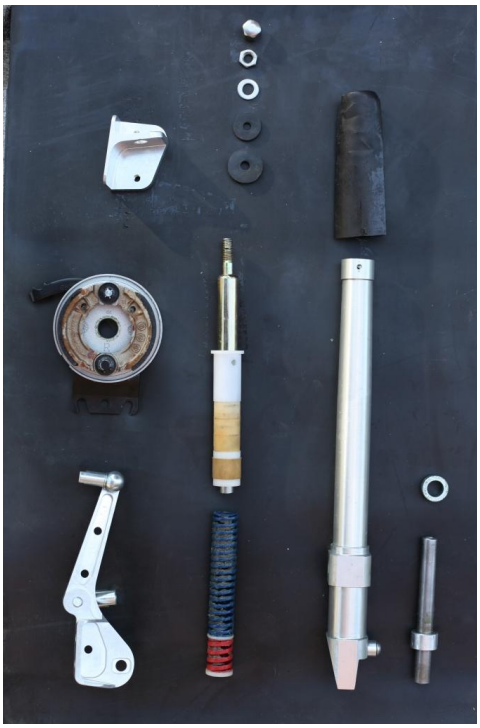

Picture 7 - Front strut parts

Source: Author

Rear suspension

Good suspension is also required on the rear wheels. Probably the springs offering best ride comfort are air springs (Bauer 2011). But air springs need damping as well, usually from a liquid fluid. By combining air spring and hydraulic making a hydro-pneumatic suspension for the rear wheels, raising and lowering the seat becomes possible. Then the dilemma of having normal seat height during entry and exit, while having a low seat for riding can be solved by means of *level adjustable rear suspension*. With sufficiently long stroke will a rear suspension with level adjustment capability offer indirectly seat height control when the rear end of the velomobile is raised at standstill and lowered before moving. This new solution for velomobiles is described further in section 4.9.

Wheelbase
Even when raised it is important to have easy access to the seat, avoiding climbing over a tall sill or sidewall. Distance between seat and front wheels need to avoid lifting feet above front wheels. This require seat to be at a distance from front wheel and the front wheel cover, causing a rather long wheelbase.

A long wheelbase increases the turning circle. So front wheels must be able to do sharp turns to avoid an impractically large turning circle. A long wheelbase also require more ground clearance to pass speed bumps without problems.

3.5 Electric assist

Over the last ten years a new type of cycles has become quite popular for transport use. The electric assisted cycle, or *Pedelec* from Pedal-electric cycle. It has a small electric motor and a battery, to assist the cyclist. This is quite different from a motor-cycle or moped, as a pedelec assist the rider when she/he is pedalling and does not propel the vehicle alone. Sometimes bikes with electric assist are called *e-bike* or *ebike* but then they often have stronger motors than pedelecs and can often travel 30 km/h or faster without pedalling. Ebikes that go faster than 25 km/h on motor are in Norway classified as mopeds which require type approval, helmets, drivers license and insurance and license plates.

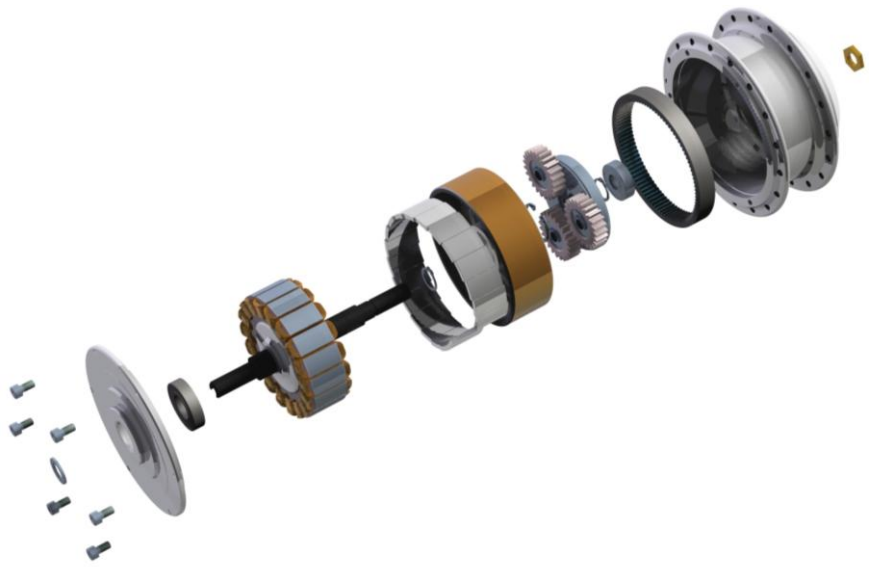

Figure 6 - Exploded view of 3D model of geared hub motor

CAD model is based on front hub motor costing less than USD 100.

Source: Author

Contrary to normal belief, a Pedelec has less energy consumption than a regular bike. Since all the energy for a regular bike comes from food, energy consumption is actually higher due to the low energy efficiency of food production and the low efficiency of human metabolism:

> *"Despite the intuitive sense that electric bikes would require more resources than regular bikes, life-cycle analysis shows that they actually consume 2-4 times less primary energy than human riders eating a conventional diet."* Source: (Lemire-Elmore 2004).

Motors
Pedelec motors are basically of two varieties. Mid motor or hub motor. Some other variants exist, for example those with a separate transmission to driven wheel (Sørensen and Hellon 2009).

Mid motors are located in the bottom bracket and are also called

Picture 8- Geared front motor installed on bicycle

Source: Author

crank drives. They use a chain or belt for transferring energy to the wheel and benefit from any gearing between motor and wheel. They often require special frames and have historically been several times more expensive than hub motors. This might change due to more competition as both *Shimano, Bafang* and *Samsung* have entered the mid motor market which has been dominated by the German company *Bosch* and a few Japanese manufacturers. The current cost of Bafang mid motors bought from China is around USD 350 in single quantities for a bicycle to pedelec conversion kit excluding battery but otherwise complete.

Hub motors have an inverted design where the motor axle is fixed, and the motor housing rotates. This way the motor housing functions as the hub where the wheel spokes are attached. The spoke holes on the flanges of the motor housing can easily be seen in *Figure 6*. Hub motors are manufactured by many different companies, predominantly Chinese. Hub motors often have a high speed low mass motor pulling the hub via an epicyclic gear. A free wheel mechanism prevent drag when not using the motor. Such geared hub motor is shown in the exploded view in *Figure 6* and as installed in *Picture 8*.

Some hub motors use a direct drive construction having a higher mass, higher torque motor with outer rotor. This rotor is also the hub of the bicycle wheel. The author has in the past six years purchased many hub motors from China. Geared hub motors typically cost USD 80 to 90 per unit. Direct drive motors start around USD 100 but usually cost twice as much as a comparable sized (in watt) geared hub motor. Direct drive motors cost more due to more material is needed to achieve sufficient torque at low RPM. Their higher mass makes them not so popular on bicycles, but electric scooters normally use direct drive hub motors because of the robustness of the less complex design. The mentioned prices are for brushless permanent magnet motors with hall sensors needing electronic commutating controller which typically add USD 20 to the cost. Hub motors must be built into a complete wheel with rim and spokes but still cost much less than mid motors.

Battery

A very important part of a Pedelec is the battery. It is usually charged from the mains voltage using a plug-in charger. Some pedelecs can use the motor as a generator to do recuperation or regenerative braking. Then the battery is charged a little every time the electric braking is applied. This is only available on direct drive motors. Geared motors have a built-in free-wheeling mechanism preventing the motor from acting as generator to reduce resistance when not using motor assistance.

Typical energy use is very dependent on speed and terrain. For the hilly terrain typical of Western Norway 10Wh/km is a typical value for unfaired bikes kept near 25 km/h, the official assisted top speed for European Pedelecs. A velomobile pedelec with regeneration typically consume 5 Wh/km at the same speed giving easily twice the battery range compared to the unfaired bike (Sørensen 2010).

Some low cost pedelecs use lead acid cells but these have a low specific energy density and so are rather heavy for use a practical bike. For the last five to ten years li-ion cells with energy densities, lifetime and cost suitable for Pedelec use have become available. Many Pedelec batteries use so-called 18650 cells having a nominal diameter of 18 mm and length of 65 mm. Typical pedelec cells have a specific of energy around 200Wh/kg but this drops typically to half when BMS - *battery management system*, protective housing, sealing to prevent water ingress, internal wiring, temperature sensors, locks, power switches and other necessary parts are added to the battery.

Cell Properties

Li-ion cells are a compromise between many factors; production cost, lifetime, energy density, current capacity, temperature range, charge speed, safety, ease of recycling, IP rights, etc. Li-ion electrochemistry is a moving landscape and the various manufacturers of cells suitable for Pedelec use are continuously improving their products. At a practical level cell performance is arranged by:

1. Specific energy
2. Energy density
3. Specific power
4. Nominal cell voltage
5. Risk classification

Picture 9 - Pedelec battery cells

Source: Author

6. External geometry and size
7. Temperature range for charge and discharge

The first three properties are performance related parameters. *Specific energy* is given in Wh/kg and describes how much electric energy is contained in the cell per mass unit. Battery range is dependent on this property.

Cell	Brand	Mass (g)	Capacity (Wh)	Specific Energy (Wh/kg)	Min.cycles (>80%)	Min charge temp
ICR18650-22P	Samsung	44,5	7,55	169,7	<300	0°C
ICR18650-22	Varta	46	8,14	177	300	0°C
NCR-18650B	Panasonic	47,5	11,54	243	300	0°C
ICR18650H	Molicel	47,5	8,65	182	300	0°C
ANR26650M1B	A123 Systems	76	8,21	108	8000	-30°C

Table 2 - Li-ion cells typical values

Energy density indicate the cell volume needed to contain the energy and is normally given in Wh/l. Specific power shows how fast the cell can be discharged in W/kg and indicates how well the cell handles high loads necessary for hill climbing and fast acceleration.

Nominal cell voltage is directly related to the electrochemistry used in the cell. Having a high cell voltage requires fewer cells in series to achieve the required operational voltage of the battery, reduces the number of interconnections in the battery and reduces the number of voltage stages required on the battery management system. *Picture 9* shows cells from a 48V pedelec battery. It consists of 39 cells connected three in parallel and thirteen in series, or *13S3P*. The white flat cable goes to the battery management circuit board (BMS).

Risk classification is important as cells with a high risk of thermal runaway or other dangerous failure modes will require more support from the infrastructure to achieve an acceptable safety level. *External geometry and size* is to a large degree independent of other properties and is chosen to suit the application's space requirements.

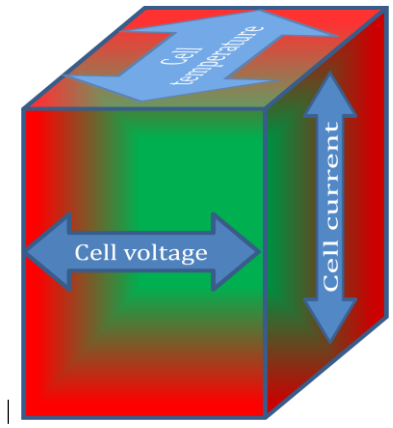

Figure 7 – BMS controlled operative space for a li-ion cell

Source: Author

Temperature

Operating temperature varies between cell types. When designing modern traction batteries for electric cars thermal management is a vital part of the battery system. Pedelec batteries do not use any thermal management other than the written instructions telling the user to take the battery inside for charging and storage in case of cold weather. It is also recommended to not leave it inside a car in warm weather. Longevity of an Li-ion battery pack is highly dependent on cells being kept at optimum temperature during driving or discharge, storage, and charging (Pesaran 2001).

Picture 10 - Pedelec battery label

Source: Author

Charging must normally be performed at a higher minimum temperature compared to storage and discharge. The BMZ pedelec battery pictured can be used down to -17°C but charging must be done between 0°C to 45°C as printed on the label in *Picture 10*. *Table 2* list minimum charge temperature for some cylindrical cells typical for Pedelec use. ANR26650M1B from A123Systems has the lowest energy density but is well suited for winter use in Scandinavia due to it's low minimum charge temperature. Datasheet for this cell can be found in appendix G.

BMS – Battery Management System

To maintain functionality, safety and lifetime of a li-ion battery a battery management system (BMS) is required. The BMS monitors at least *cell voltage*, normally more, operational parameters and control current to/from the cell(s) to keep the voltage, current and temperature within operational space, as illustrated in *Figure 7*. It is important to know that this differs from the real cell's safe operative space which is a much more complex shape as shown in *Figure 8*.

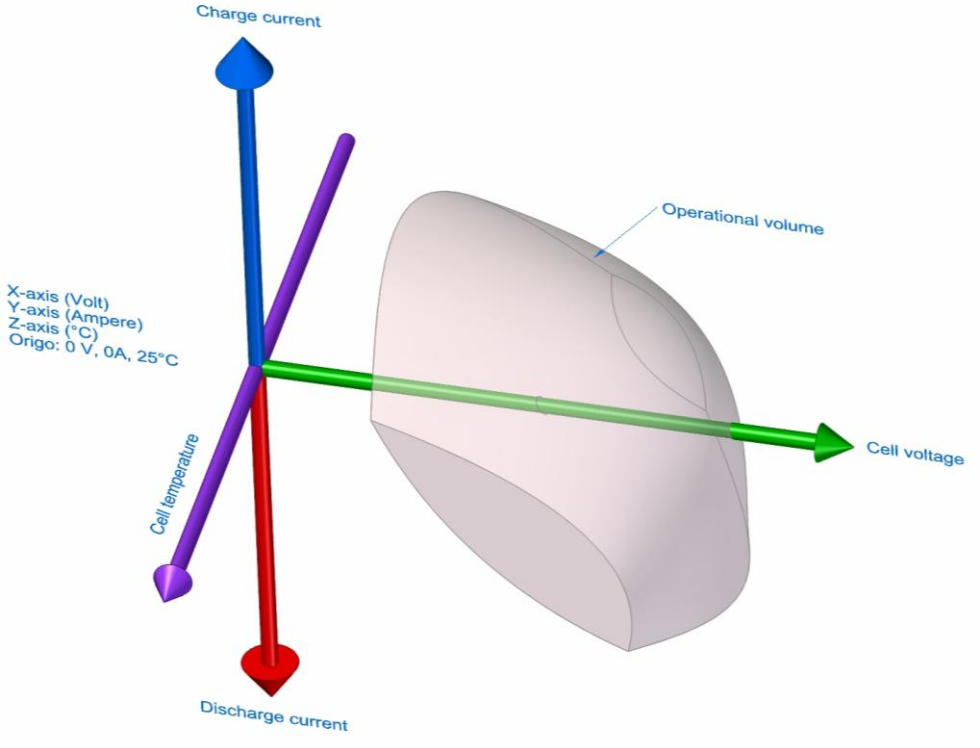

Figure 8 – Safe operative 3D-space of a an imaginary li-ion cell

Source: Author

The three dimensions are; *temperature*, *voltage*, *current.* The shape of the safe space is mainly dependent on cell chemistry but also thermal properties of the cell package. Dimension range of this 3D-space is:

- current, ranging from maximum charge via zero (storage) to maximum discharge,
- voltage, ranging from minimum allowed cell voltage, to maximum charge voltage,
- temperature, ranging from minimum storage temperature to maximum

A fourth dimension, impedance, is also used in some advanced BMS algorithms to compensate for wear ((Andrea 2010). Keeping the operational parameters within the safe space is the responsibility of the BMS. The operational volume of a

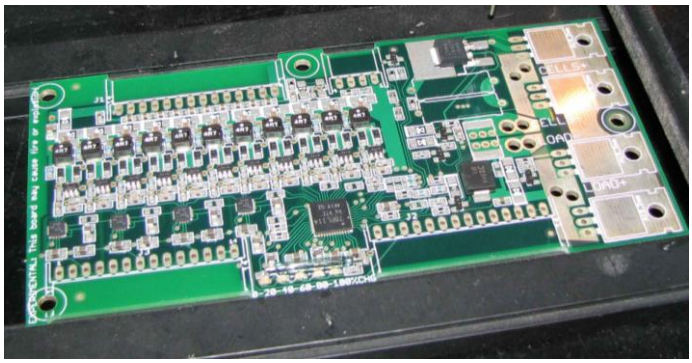

Picture 11 – Assembling a 12 cell (12S) active BMS

Source: Author

real li-ion cell has a complex surface. That requires a *systemic* or inter-dependent BMS algorithm. For example adjusting maximum allowed discharge current to a higher level at medium temperatures when the cell voltage is at a high level. Low cost BMS for Pedelecs normally only limit the operating space within absolute current, voltage and temperature values. Without non-systemic control and with limits set fully within the real operational space, the BMS limits battery performance. If the BMS limits allow some combinations of temperature, current and voltage to extend outside safe space, the cell will end up having reduced capacity or lifetime. A well known example of a BMS not keeping the cells within their safe operational volume is the Think City electric car produced from 1999 to 2003. Due to bankruptcy the BMS algorithm was never fully finished. This BMS lacked the function to reduce the discharge current limit when the cells aged and worn which lead to damaging cell voltage reversal at high discharge currents at *low state of charge - SOC* (Elbilwiki 2014).

For maintaining a long lifetime of the battery, it is also important to monitor the cell temperatures. It is normal to monitor temperature on only one or a couple of the cells to keep cost and complexity low. Normally the temperature difference among the cells in the same battery pack is low so monitoring one cell temperature is often sufficient (Andrea 2010).

Controlling current is relatively easy to perform on batteries during discharge and charging. To control voltage when cells are connected in series is a bit more complicated. Since cells are never completely identical, they will over time diverge in cell voltage. By monitoring the voltage over each series stage and turning on current shunt resistors to "bleed" selected cells during charging, cells can be balanced to the same cell voltage every time the pack is fully charged. Such a balancing system can only be used during charging, otherwise it will reduce the charge of the entire battery.

Active balancing
Some advanced BMSes can also balance the cells during non-charging cycles, transferring energy from the cell(s) with high relative charge to other cell(s) with less charge without using bleeder resistors. BMS that support balancing during usage are especially beneficial for batteries used in electronic transmissions. In this application the battery is continuously charged and discharged during the journey and for regulatory purposes may not be charged via other means, requiring a separate pedelec battery for use only up to the pedelec speed limit. In *Picture 11* the author is building a BMS with active balancing designed for pedelecs.

3.6 Transmission

For transferring the human power to the driven wheel(s) some form of transmission is required to match pedal speed with road speed. For flat roads a fixed gearing works well enough to be acceptable, but in terrain with steeper grades variable gearing is much better. For racing the *derailleur* chain gearing mechanism that was developed during the first half of the 20th century 1900 is the de facto standard due to its low mass and high efficiency. Internal multi-stage gears offer the benefit of less maintenance and tidier look compared with derailleur. The drawback is higher mass and cost and lower efficiency (Wilson, Papadopoulos et al. 2004).

On Pedelecs there is additional complexity caused by the additional electric assist motor. Some motor / transmission combinations simply do not work. For example internal hub gears which change gear by pedalling backwards. They will not work with a mid motor as there is a freewheel in the crank which 'disconnects' the chain when pedalling backwards. This combination would make gearing impossible.

Picture 12 - pendulum pedals

From a Stringbike *recumbent built by Schwinn-Csepel shown at SPEZI2013 in Germersheim, Germany. (Schwinn-Csepel is not connected to bicycle brand Schwinn, part of Dorel Industries.)*

Source: Author

On recumbents with driven wheel(s) in the rear and the pedals in the front the bicycle chain gets quite long. In the *Alleweder* velomobile the chain is over 4 m long, adding considerable mass. Another construction challenge of recumbent cycles is conflicts between the optimal path of the chain and the location of seat, pedals and wheels.

Having more than one driven wheel is another challenge. Without freewheel or differential the connection of the driven wheels by a common shaft cause resistance when turning.

Almost all cycles use pedals attached to rotating crank arms. Alternatives like linear motion pedals, non-circular rotation and pendulum pedals exists but are rarely used. Normally, their benefits seldom outweigh the drawbacks of the added complexity compared to the simplicity of pedaling. However, when altering the basic assumptions for what constitutes a bicycle, innovative solutions must be evaluated. They might be the key to better functional design with less compromise. For example would linear or pendulum pedals reduce the vertical space needed around the pedals compared to a traditional design. This would be very beneficial for a recumbent velomobile. But it would add the complexity of having an oscillating movement propelling the driven wheel(s). A commercial example of pendulum pedals used on a trike is shown in *Picture 12*.

Electronic Transmission
An innovative drive train suitable for cycles is the 'chainless' *electronic transmission, ET,* as advocated by *Andreas Fuchs, Jürg Blatter* and others (Fuchs 1999, Wilson, Papadopoulos et al. 2004). Here the cyclist pedals an electrical generator with electronically controlled resistance and speed. Propulsion is only by electric motor which is fed with power from a generator and from a pedelec battery. In this way no chain or gears are required, except for the fixed gearing to match pedal speed to generator speed, and possibly a fixed gear to match motor with wheel speed. A cycle with ET is a *series hybrid* as understood from the auto industry. Unfortunately,' hybrid' is easily misunderstood in the cycle world. The word 'hybrid' has already been in use for decades to describe a special type of bike being a mix between a practical city bike and a road racing cycle. For this reason Electronic Transmission – *ET* is often used instead. This is the solution selected for the new velomobile construction and will be further explained more in depth later in this paper.

3.7 Regulatory framework

Electrically assisted cycles, or Pedelec's, have some regulatory limitations to make them compatible with existing cycling infrastructure and to keep ebike users in harmony with other cyclists. These regulations have now been harmonized within EU and EEA (EØS) with article 1(h) of *Directive 2002/24/EC* describing type-approval of two and three wheeled motor vehicles. This article states that type approval does not apply to:

"*Cycles with pedal assistance which are equipped with an auxiliary electric motor having a maximum continuous rated power of 0.25 kW, of which the output is progressively reduced and finally cut off as the vehicle reaches a speed of 25 km/h, or sooner, if the cyclist stops pedalling*"

Article 3 of same directive also state that: "*This Directive shall also apply to quadricycles*" so basically that limits a pedelec to:

- Human powered cycles with two to four wheels having pedal assistance
- 250 W continuous maximum mechanical motor assist power measured on the wheel
- 25 km/h top speed with motor assist
- Motor assist only allowed when pedalling[6]

A more thorough definition including test requirements is described in the European product safety standard for pedelecs (EN-15194 2011). Therein is also a reference to the standard used to measure continuous output power (IEC-60034-1 2005).

Control system
For a cycle with electronic transmission – *ET*, there is a risk that the motor power used for transmission is seen as circumventing the motor power limitation as pedelec. This can prevent the velomobile construction from being accepted as a cycle with electric motor assist.

[6]Not included in the directive, but motor assist is allowed up to 6 km/h even when not pedalling. It is a logical consequence of EU/EEA general permission to use motorized vehicles with a max speed of up to 6 km/h on public streets without type approval.

To avoid this from happening, a strict energy and speed control regime must be embedded in the design. One way to achieve this is to use two batteries, one generator battery which is never removed from the vehicle for charging, and a pedelec battery that must be charged from a charger. The generator battery is only charged from the pedal generator.

The pedelec battery can only be used at speeds below 25 km/h while the generator battery is continuously used. If the ET battery gets to a low *state of charge, SOC,* there is not enough energy to maintain current motor speed and the speed is reduced. If the vehicle travels below 25 km/h then energy may come from the assist battery maintaining speed at that level minimum, as long as some pedalling is performed. A suitable control algorithm must facilitate best possible operating conditions for cells, motor and vehicle/cyclist within the legislative framework. Several examples of such algorithms exist in literature and are suitable, at least as good starting point (Fuchs 1999, Embrandiri, Isa et al. 2010, Spagnol, Alli et al. 2012).

3.8 Safety

Improving safety
Cycling safety can be improved by focusing on various areas. Four areas will be addressed here:

- Cars vs cycles
- Impact Energy and Damage
- Visibility
- Stability

Cars vs. Cycles
Every day people on cycles get killed by cars. The high mass and, quite often the high speed of cars involved, makes collisions between car and bicycle very dangerous for the cyclists (Rosen, Stigson et al. 2011). In addition, high speeds increase stopping distance thereby reduces the chance of avoiding potential collisions. Reducing speed of cars would probably be the most efficient way of reducing the number of cyclists killed in traffic (Rosen, Stigson et al. 2011).

Electric cars also kill cyclists. In November 2013, a 40-year old man was hit and killed by a Tesla Model S in Santa Cruz, California while riding a bicycle (Masoner 2013). It is unlikely that Tesla Motors, also located in California, did not know about the fatal accident involving their high profile vehicle. Still, *Elon Musk*, CeO of Tesla Motors, did not count the death of the cyclist when posting in his company's blog five months after the death of the cyclist: "*With a track record of zero deaths or serious, permanent injuries since our vehicles went into production six years ago, there is no safer car on the road than a Tesla."* (Musk 2014).

Figure 9 - Car damages

X-ray show a costly and time consuming repair. to biker's knee and lower leg after low speed collision between cycle and car.

Source: Author

Only considering the occupants in the scope of safety is common in the auto industry. Tesla build cars with exceptional protection for the occupants (NHTSA 2013) but with regard to the previous tragic example even they are still not safe in traffic. In developing technical solutions one must also look on damages and fatalities beyond users/owners. For example a nuclear power plant would not be considered safe even if accidents caused no harm to its own employees, if it damaged its surroundings.

Until a more holistic view on car safety become prevalent or more likely, enforced, cyclists cannot depend on cars for their safety.

Impact Energy and Impact Damage
Being hit by a car travelling even at slow speed is quite damaging if the impact is concentrated on a small area. The author of this paper had a collision with a car while riding a regular bicycle. Even at very low speed the concentrated force resulted in a fractured knee and broken lower leg needing surgery and steel implant, see Fig-

ure 9. A velomobile body is able to absorb, deflect and distribute the collision energy reducing or preventing damage to the occupant(s). This has both been observed by velomobile users (Eastwood 2004, Puchelt 2014) and verified by laboratory testing and simulations (Schmidt 1994, Wilson 1994, Gloger and John 1998). Also the more supine, or recumbent position of the rider in a velomobile, together with lower fall height are likely to reduce the damage an impact will have, especially the risk of head injuries is reduced compared to riding in a regular bicycle where a crash often lead to the cyclist hitting the ground head first.

Plastic composites and fibres has potential to absorb much energy in collisions (Bambach 2013). With sensible compromise between strength and energy absorbing of the external body it is possible to improve on the protection of the velomobile occupants. Today this has little or no focus. There is no traces of extra protection that can be seen on the commercial velomobile body in *Picture 13* which has been cut in half for exhibition purposes. Accepting slightly wider body around the occupant(s) will enable room for crumble zones that can be used to absorb impact energy without gaining extra mass. Such zones also prevent intrusive object from crushing bodies in the cabin. Also deflection and retaining the occupants in their seats help to reduce damages. Gloger and John (1998) set up the following five design guidelines for safer velomobiles:

1. *Velomobiles should have a safety belt system or something with a similar effect*
2. *The structural shape of the vehicle front should be round or elliptical*
3. *Directly around the driver's body there should be a stiff safety panel or an overroll bar*
4. *The velomobile surface should have low friction*
5. *The velomobile front should be deformable, the side panels should be stiff.*

These guidelines are sensible and they are reasonable well documented in their paper. They are, with the possible exception of seat belts, easy to implement. The installation of seat belt for the cyclist could trigger legal implications and should be carefully considered. For the child seat, seat belts are mandatory and accepted.

Visibility

It is obvious that giving cyclists improved visibility would prevent or reduce accidents. Contrasting colours and geometry not easily ignored improve awareness. And the velomobile body is the obvious canvas for eye gripping signage (Boer 2009). By adding unique artistic expression on the velomobile body with the focus on visibility major improvements to safety can be achieved. It is suggested to use unique, single copy decor by professional artists for decorating the outer body so that the vehicle becomes a functional art piece. Thus improving the value of the velomobile and make the cycle unique and personal. Hopefully this will motivate owners to keep the vehicle for a long time extending the lifetime and thereby improve life cycle cost of the velomobile. Unique decor will also deter thefts as a stolen vehicle will be more difficult to sell as it will be instantly recognizable. Artistic examples of such decor are shown in *Figure 10*.

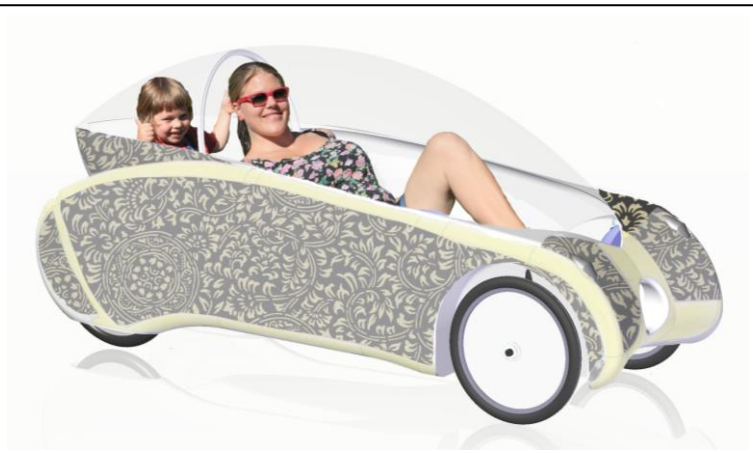

Figure 10 – Artist's illustrations of eye catching velomobile decor for improved visibility

Artist: Oddny Friestad,
Photoshop:Karl P. H. Sørensen

Embedded lights are probably the easiest way of making the vehicle easy to see in the dark. Cyclists are in many countries allowed to use flashing lights. Optimal usage of flashing lights gives high visibility even in daylight conditions. With a translucent body interior lighting can make the velomobile body appear to be glowing in the dark. Also efficient lights for illuminating the road ahead when riding in the dark are needed and can be combined to make an attractive visual impression of the velomobile.

Stability
Stability of the vehicle is paramount for safety. Single track vehicles need to be balanced, relying on predictable friction and zeroing sideway forces. Having three wheels improve stability but four wheels are even more stable at the same width. Riding in slippery conditions like snow and ice or in variable side wind caused by passing cars or gusts also benefits from the extra pair of wheels. A long wheelbase contributes to high speed stability, while a low COG keep cornering speed high and reduce the chance of tipping over.

3.9 Practicality

A major issue is how to get people motivated enough to drop the car and use human powered vehicles instead. Many excuses exists; children to bring, car is needed at work, too long journey, bad weather, they make you look silly etc. To get more people to use velomobiles they must become better for the ones most likely to use them so they need to be targeted at a distinct group of users.

The initial user group has in the design process been young parents as they are most likely to try new solutions, are motivated to reduce emissions, and, with limited resources, they have economic motivation for selecting lower cost solutions. In this context, a velomobile is a smart compromise if daily needs and creature comfort requirements can be met, as shown in *Figure 11*, a velomobile compares favourably with other modes of transport within a city.

Passengers
For this user group there is often a need for bringing children along safely, sometimes more than one. It must be possible to safely bring along a single child up to a certain age. It should also be possible to add a trailer for easy extension of loading capacity so a fixture for a bicycle towing hitch is mandatory.

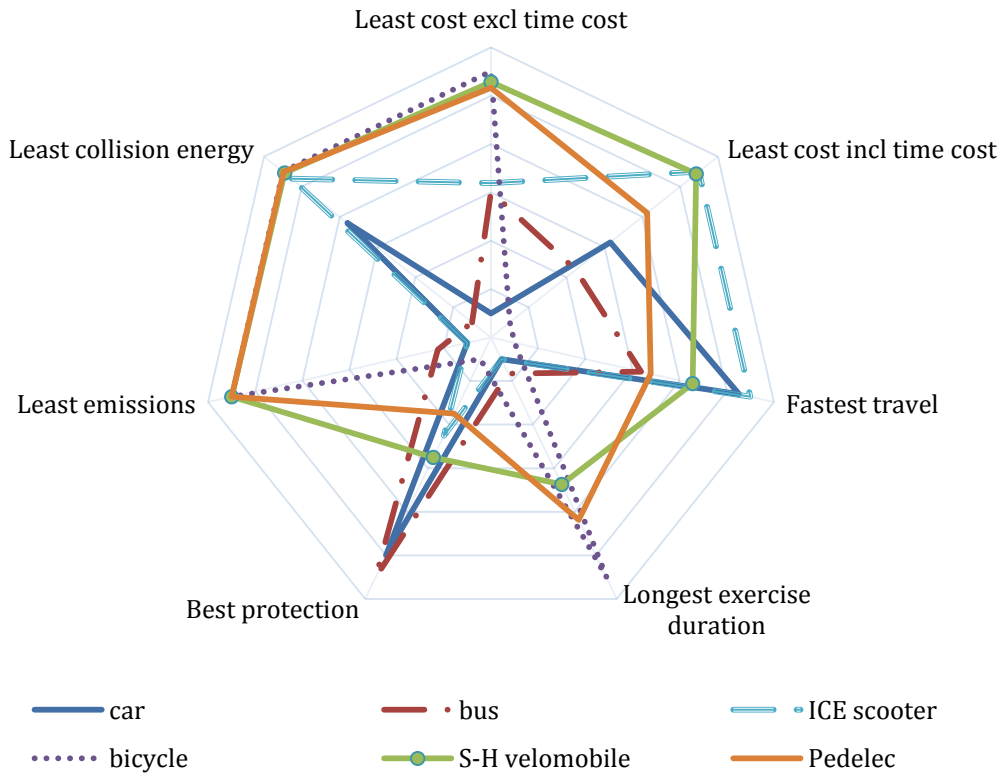

Figure 11 - Comparison of key criteria for various modes of city transport

Source: Author. Key data can be found in Appendix H

Parking and charging
Another issue is parking. To reduce space requirements the velomobile should be able to stand vertically by itself without requiring excessive free height. There must be ways to easily lock the vehicle safely and easy to charge the traction battery either on the vehicle or separately. Especially in cold weather separate charging must be possible. It is few who has access to heated parking area required to maintain sufficient temperature in traction battery within the vehicle.

3.10 Life cycle design requirement

An important requirement for this velomobile design is low environmental impact. Materials chosen should be easy to recycle and have a low environmental impact. That makes usage of thermoset composites problematic as they are difficult to recycle. Another problem is that a cost efficient thermoset composite velomobile should be a unibody design avoiding the extra vehicle mass, cost and complexity of an additional structural frame. This contradicts another requirement, namely easy shipping. This new four-wheeled velomobile, *veloquad*, will likely be sold via mail order. That means shipping must be fairly easy and inexpensive.

With that in mind, and knowing that shipping complete velomobiles is expensive, a platform frame design with a non-structural upper body is preferable. That makes it easy to ship the velomobile partly assembled to reduce shipping volume and to save assembly cost. It also makes it possible to use a compliant body material that does not break or scratch easily. That reduces the risk of body parts arriving damaged or becoming damaged during final assembly by the purchaser.

Final assembly after shipping should require only regular hand tools. Where suitable, the parts used are regular bicycle parts for low cost and ease of repair and replacement. All parts specially made for the vehicle should be easy to recycle.

Life cycle assessment
For a new velomobile design to have a purpose, it must be sustainable. Materials, production methods and transportation must all have a low eco impact in sum. That means not only low energy consumption in the use phase, but also when building and recycling the vehicle. In addition, the practical lifetime must be long, preferably much longer than for a standard bicycle or pedelec. To do a life-cycle assessment, LCA, is a good way to document sustainability.

Substantial information on how to make the new velomobile, including detailed specifications, functionality level and performance. Details of chassis-layout, aerodynamic body, drive train, suspension, steering, brakes, ventilation and life cycle analysis.

4. HOW: Implementing improvements

4.1 Primary design specification

Based on discussions from previous chapters the design has many requirements. Following is a list of specific design requirements:

Primary Layout specification - wheels, dimensions and mass

1. Four wheels - most stable for a narrow vehicle
2. 406 mm ISO bicycle rim diameter - standard on most velomobile front wheels for compact size and low rolling resistance
3. All wheels same size and width - identical wheels are most practical requiring least spare tyres and tubes
4. Width max 800 mm excluding mirrors and extending parts on wheels - wider makes it harder to use it on bicycle paths, just less than 800 mm will let it pass narrow doorways while having space for a crush zone on the sides of the cyclist
5. Height 1100 mm when riding - somewhat arbitrary but lower could be claustrophobic and higher cause more air drag
6. Eye height 750- 800 mm - a bit low but necessary to get low COG
7. Able to store vertical under roof with height 2400 mm - standard ceiling height in Norway
8. Ground clearance at nominal mass should be at least 100 mm - 100 mm is largest allowed speed bumps in Norway
9. Turn radius reasonably small - should be able to U-turn within a normal road width
10. Centre of gravity as low as possible - this reduces the risk of falling over and increase cornering speed, reducing the need for braking, thus saving energy
11. Unladen mass max 50 kg including batteries
12. Max 15 kg when empty on front wheels - For storing vertically, vehicle must be easy to lift in front
13. Nominal mass 120 kg - 70 kg cyclist, same as standard mass for car drivers in Norwegian legislation
14. Laden mass max 200 kg - 100 kg cyclist, 25 kg child, 25 kg luggage
15. Seat one adult with height 140-200 cm - should fit more than the average rider
16. Seat one infant, max 25 kg/7 year - cramped space for larger children

Primary drive train specification - motor, power, battery

17. 100W mechanical power from hub motor(s) should sustain a speed of 30 km/h or more - that should be sufficient for 50W rolling resistance loss and 50W air drag loss
18. Compliant to Pedelec requirements, i.e. shall be a pedal cycle, not a motorcycle - absolutely necessary to allow usage in bicycle paths and on public roads. If classified as a motorcycle/moped it would be much more costly and much more unpractical.
19. Electronic Transmission (series hybrid drive) to avoid need for differential, chains, gears, shifters, and drive shafts - zero maintenance drive train
20. Two (rear) hub motors having a starting torque of 40 Nm and continuous torque of 20 Nm
21. Shall work, albeit require more pedalling, without traction battery, i.e. without electric assist. To be classified as a cycle, it must work as a cycle

22. Battery for electric transmission must work (charge and discharge) down to -30°C - this battery is integral part of electronic transmission and must always work. Low night temperatures in the winter should not prevent vehicle from functioning
23. Large traction battery must work (discharge) down to -10°C - this will give the traction battery suitable temperature range even if being parked outside in the winter for some hours
24. Large traction battery must be easy to remove for charging and storing indoors - most high energy density Li-ion cells require temperatures above 0°C when charging
25. Large traction battery must be possible to lock to vehicle - battery is costly, theft must be prevented

Primary functional Specifications - Safety, chassis, body

26. Passive protection as good as possible without incurring much extra mass - being safe is important, but also feeling safe
27. Aerodynamic non-structural body with low C_dA, preferably less than 0.15 m^2- result is needed to achieve at least 30 km/h with 100 W mechanical input
28. Luggage space minimum 150 litre (with child seat removed)
29. Prepared to attach a towing hitch - A bicycle trailer is sometimes necessary
30. Rear end having hydraulic lifting means to raise rear end to bring seat height to 400 mm minimum - important for vertical storage, large load capacity and vertical storage
31. Full weather protection by canopy - to be an alternative to pedelec, this is required
32. Excellent ventilation to prevent condensation on windows and overheating - 100 W mechanical output from cyclist results in 300 W excess het from same, this must be vented away from body
33. Attractive design using trick of the (automobile) trade as colours, lights, shape, sound, and more - can always be improved upon
34. It must be easy to lock vehicle to stationary item for theft prevention - vehicle is costly, theft must be prevented
35. Aluminium chassis mainly made of sheet metal with blind nit joints, no welding - welding requires careful optimizing to prevent fatigue and corrosion issues
36. Design life time 25 years / 250 000 km - difficult to achieve but is reasonable
37. All made parts shall be easily recyclable - presumed preference for early adopters, possibly a future requirement for all vehicles

4.2 Secondary specifications (guidelines)

When developing the vehicle additional information not easily described in the above mentioned primary specifications are necessary to guide the constructor.

Part selection

Most parts should be mass produced and easily available parts, so-called *COTS, commercial of the shelf*. Preferably bike *COTS* parts for easy procurement of parts when vehicle need service. Long service time is more important than lowest cost. Parts that can be efficiently recycled should be preferred.

Part design

Parts that must be tailor made for this vehicle should be made using production methods resulting in low LCA cost. Production methods should be suitable for production worldwide. No welding or soldering unless absolutely necessary.

Corrosion protection and life time

Parts should have sufficient corrosion protection and life time for lasting 25 years of normal use exposed to the local climate. Parts having insufficient corrosion protection or lifetime is acceptable if this is the least LCA cost alternative.

Seating

To achieve low air resistance seating side by side is discarded. It will also make vehicle wider than design spec.
For safety reasons, seats must be located within a roll cage to protect the occupants. Due to limited space for adjustable seat position it is fixed lengthwise. To adjust for different body length both pedals and steering need to be adjustable. To ease entry and exit from the main seat, it must be possible to move the legs sideways from ground to pedals while sitting in the seat. That means there need to be a distance of approx. 700-800 mm between front wheel housing and the lowermost part of the seat to easily move legs past the wheel housing.

Main seat is a special recumbent seat as supplied by *Alligt Liegfietsen*[7] made of PA6/GF30 (nylon with 30% glass fibre). It is hinged at lower front to allow access to area behind the seat. The upper part is locked in correct seating position and fixed to roll cage when doors are closed to prevent seat from tilting forward during travel. Inclination should be adjustable so that persons with different body length can achieve necessary eye height

Child seat is a modified child bicycle seat with leg fairings cut off to fit inside vehicle. It is attached to a special bracket enabling easy fixing and removal of child seat to floor behind main seat

Steering

Steering is by two sticks on each side of main seat. To prevent conflict during entry and exit they can be folded down. Linkage runs in the centre and is attached to central steering pivot arm below the pedals. The rest is standard front suspension parts as used on Alligt Alleweder A4 and similar velomobiles.

Picture 13 - A fast tadpole velomobile cut in half. Adjusting seat, steering and pedals takes a long time

Source: Author

Pedal generator

The pedal generator made from a crank pedelec motor fits between the front wheels on a bracket which is an integral part of the floor. The position must be easily adjustable to fit riders of different length. Most velomobiles has opening underneath the pedals. This opening has many functions; It is the *Flintstone* type reverse gear[8], it makes it possible to have pedals lower and thus reducing bonnet height, it is a telltale when seen from distance that the vehicle is in fact a cycle as the pedalling feet is visible from underneath, and it is a large ventilation inlet.

In the veloquad there are no openings in the bottom for the feet. The electric motors offers the reverse when needed, the crank arms are short to accommodate a low bonnet, and the pedalling feet are visible thru the canopy. This gives two important benefits; less drag and, most important, the drizzle reaching your feet from the front wheels when cycling in wet conditions is avoided. This drizzle would have been a big problem since the pedals are besides the front wheels, not in front of the wheels as on tadpole velomobiles.

[7] www.alligt.nl

[8] In Flintstones they actually use it also for forward gear, not only reverse.

The need to adjust position of the pedal generator to accommodate a large range of people of different sizes becomes easier when there is no need to make holes for pedals and feet. Also the steering design becomes easier.

Brakes
For front brakes hydraulic disc brakes for tricycles are used as they are self balancing. 180 or 203 mm brake discs improve braking capacity. Hand brake handle is located on right stick. In case of brake failure on front brakes, the left stick also has a hand brake handle operating two mechanical disc brakes, one on each rear wheel. The rear brakes double as a parking brake by applying a clamp on the brake handle when energized. Rear disc callipers are *minimoto* parts made for mini motorcycles and are supplied in symmetric pairs at low cost.

Wheels
For lowest LCA cost use of stainless steel spokes is best and can be easily repaired. Alternative wheel designs are discussed in section 5.3.

Other
Examine drawings in Appendix A for further details on the mechanical design.

4.3 CAD model

The velomobile has a set of requirements making its design challenging. Initially, models of main sub assemblies/components was acquired if available at reasonable cost, or modelled by author from real parts or drawings. The main subassemblies and their sources is listed in *Table 3*.

Part	Source	Comments	Link for download
Front suspension	Author	Modelled from Alligt Alleweder A4 parts and published on Grabcad by Author.	https://grabcad.com/library/allweder_kv4_internals (accessed 2014.05.27, require free registration for download)
Rear suspension	Author	All parts constructed by author.	Not released
Pedal - generator	Grabcad/ Author	Sunstar S03 mid motor made for pedelec	www.grabcad.com/library/pedelec-crank-mid-motor-based-on-sunstar-s03-1
Rider	unknown	95 percentile male	Possible sources: http://mreed.umtri.umich.edu/mreed http://www.3dhumanmodel.com/
Passenger	University of Delft	KIMA 5-6 year old, purchased model.	http://www.3dhumanmodel.com/ Datasheet in Appendix G
Hub motor	Author	Modelled from front hub motor purchased from www.goldenmotor.com. Published on Grabcad by author.	https://grabcad.com/library/golden-motor-250w-geared-hub-motor-for-front-bicyclewheel-minimotor (accessed 2014.05.27, require free registration for download). Drawing of motor geometry for wheel building in appendix A
Electronic Transmission battery	Author	Cells modelled from datasheet on A123 Systems AMR23650B1 $LiFePO_4$ Li-ion cell. BMS modelled from BMS bought from www.EM3ev.com in China	Datasheet for battery cell in appendix G
Main seat	Alligt	Alligt has published CAD models of this seat in different 3D formats	www.alligt.nl/downloads/Aliigt_zitje.zip (accessed 2014.05.26)
Front dual LED lights	Author	Two 3W LED on each side. One wide angle that flash in daylight. one narrow for distance. Designed from scratch and published on Grabcad by author.	https://grabcad.com/library/velo-mirrorlight-1 (accessed 2014.05.27, require free registration for download)

Table 3 - 3D subassemblies and their sources

CAD system used was Solid Edge from Siemens which is very well suited to machine design. It has a good sheet metal functions and has extensive free surface modelling necessary for optimal design of aerodynamic body.

For finding an optimal layout of the various parts a base assembly containing all the main subassemblies was made and various parts relocated until a suitable layout complying with all requirements was found. The base layout is shown in *Figure 12* seen from the side, and in *Figure 13* seen from the top.

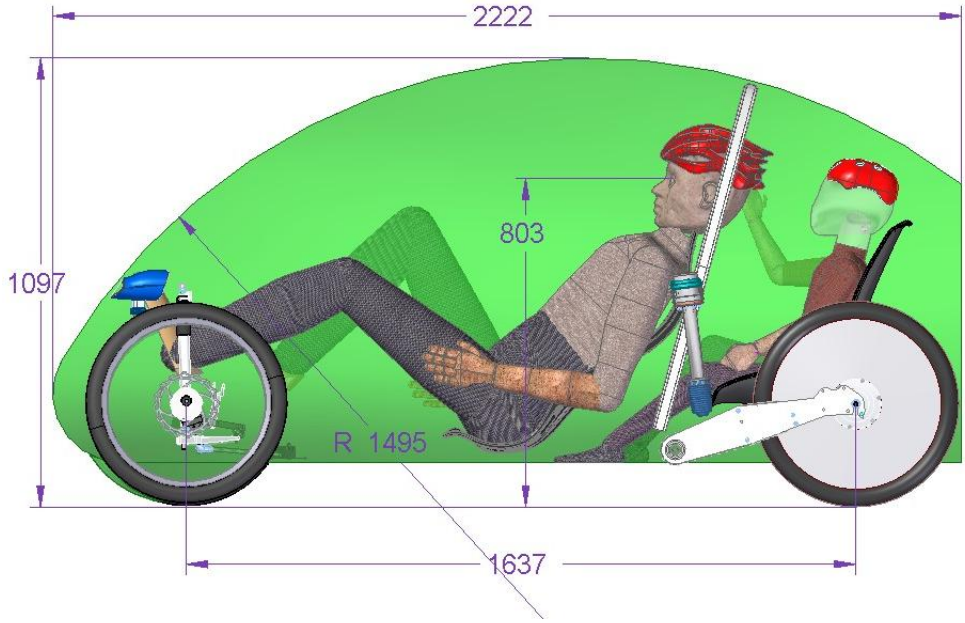

Figure 12 - Basic layout - side view

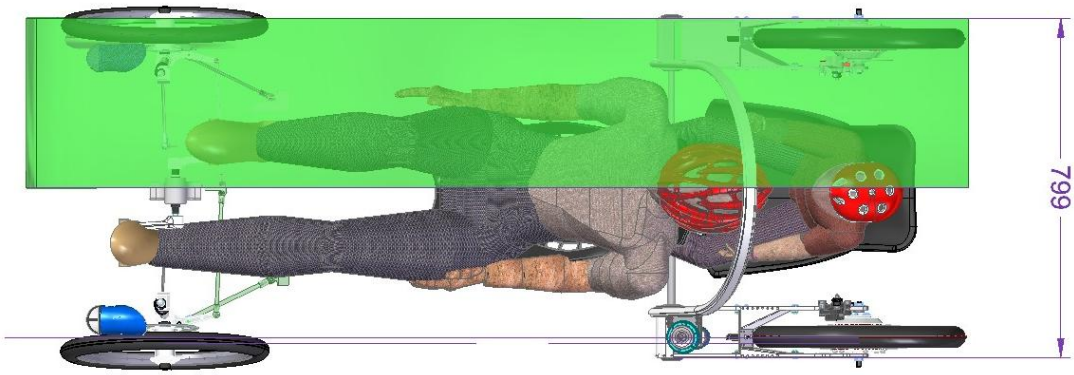

Figure 13 - basic layout - top view

Based on dimensional specifications from section 4.1, a simple body shape, VELO14, large enough to fit all base assembly parts plus occupants of representative size was modelled. Its geometry with dimensions is also shown in *Figure 12* and *Figure 13*. This was the initial starting point of the body geometry. During development several improvements were made and for each major iteration the revised body was named sequentially, i.e. VELO15, VELO16, etc.

Iterations were guided by these three requirements

- Following low drag design principles from the book *The Leading Edge* by Goro Tamai (1999)

- Drag verified by computational fluid dynamic simulation at fixed velocity, 10 m/s (36 km/h)
- Functional body shape that can be easily manufactured at reasonable cost and low mass

The Leading Edge

Goro Tamai's book *The Leading Edge* is a "*how-to manual"* for *"aerodynamic design on ultra-streamlined land vehicles"* (Tamai 1999) contains many well documented examples on how to design ultra-light vehicles for minimum air drag. Important design principles to achieve low drag extracted from this book is, in prioritized order:

1. Frontal area should be as small as possible
2. Lift causes drag and should be minimized
3. Low drag requires little or no flow separation and vortex shedding (induced drag)
4. Maintain laminar flow for as long as possible
5. Body surface should have as few and as small as possible gaps and appendages
6. Necessary body openings for ventilation, wheels, lights etc. should be as small as possible
7. External, i.e. exposed or 'wetted' area on body cause frictional drag and should be minimized
8. Some bodies have a pronounced drag minimum at a certain ground clearance

Following these design principles is easier said than done. Especially when a practical body that can be made at reasonable cost an low mass is sought.

4.4 Air drag

To reduce drag as much as practically possible, the body geometry has been refined over many iterations while making sure that other vital parts functions well. Items like windscreen, ventilation ports, wheels and suspension require specific positions and a streamlined body is of no use if it cannot function on the vehicle.

. The ultimate target was to get CdA down to 0.15 m^2. This is quite difficult when considering the requirement for four wheels and elevation system and avoiding a cramped and claustrophobic cabin.

The initial frontal area for VELO14 is 0.3992 m^2 for the half body, while the final VELO23 body has a frontal area of 0.3283 m^2. To make simulation time acceptable, CFD models contained no details for doors, lights, fasteners etc. Only the basic shape has been simulated, with the exception of wheels and on a couple of simulations; ventilation ports.

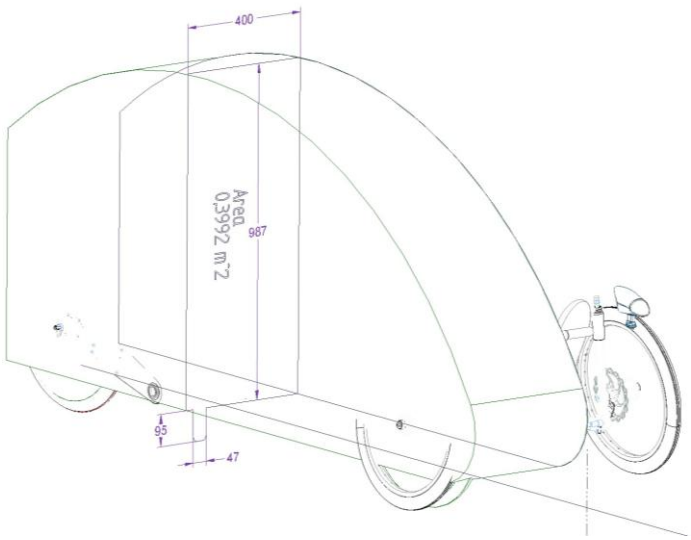

Figure 14 - Frontal area of VELO14

As the body is axis symmetric, only half body was used to reduce simulation time.

Turbulence model

When examining drag at low velocities and with streamlined bodies, CFD turbulence model used in these simulations is important. The *k-ω SST* model (Menter 1993) is a two equation eddy-viscosity model with a shear stress transport [SST] part. That help to handle flow with low Reynold number [R_e] without needing to resolve the boundary layer requiring a very fine mesh (Versteeg and Malalasekera 2007, CFD-Wiki).

However, *k-ω SST* is not optimized for flows containing transitional flow, i.e. laminar flow only partially turning into turbulent flow. The relatively low vehicle speed of the veloquad results in at least some transitional boundary flow. Simulating the body drag using a turbulence model capable of handling transitional flow with accuracy should give a more realistic result, and was suggested by two different CFD specialists with deep knowledege of respectively *Fluent* and *Caedium* CFD software (Smith 2013, Kjeldsen 2014).

Walters and Cokljat (2008) have published a three-equation RANS model for transitional flow. Their model have been implemented in the well known CFD program *Fluent*. This model is also included in *OpenFOAM/Caedium*. The major drawback of this model is the requirement of having y+ of 1 in the cells nearest the walls. y^+ is dimensionless wall height comes from '*law of the wall*', first described by one of the giants in fluid dynamics, *Theodore von Kármán* (1930). From the 'law of the wall' is y^+ defined as:

$$y^+ \equiv \frac{u_* y}{\nu}$$

Where $u_*$is the friction velocity or the velocity nearest the wall, y is the distance to nearest wall and ν is the kinematic viscosity of the fluid. To find the necessary wall distance which is the CFD cell height for the cells touching the surface, given y^+ =1:

$$y = \frac{y^+ \mu}{\rho u_*}$$

Where ρ is fluid density and μ is the dynamic viscosity of the fluid. $u_*$is:

$$u_* = \sqrt{\frac{\tau_w}{\rho}}$$

The wall shear stress, τ_w, can be found using the skin friction C_f with the formula:

$$\tau_w = C_f \frac{1}{2} \rho {U_{freestream}}^2$$

The skin friction can be estimated using Schlichting skin-friction correlation based on local Reynolds number at given position, Re_x , when $Re_x < 10^9$:

$$C_f = [2 \log_{10} Re_x - 0.65]^{-2.3}$$

So the ubiquitous Reynolds number must first be found. The Reynold number at a given point, Re_x, is based on boundary layer length:

$$R_e = \frac{\rho \, U_{freestream} \, L_{boundary\ layer}}{\mu}$$

So, based on estimated length of the boundary layer a wall distance, here the maximum cell height *y*, can be found. For a *freestream* velocity of 10 m/s and a boundary layer length of 1 m the estimated wall distance is 3.4×10^{-5} m, or 0.034 mm. A boundary layer length of 1 cm results in an estimated 0.02 mm wall distance, not much reduction of y even with 1/100 layer length, due to the log function in the formula for the wall shear stress.

Some preliminary CFD runs were performed using k_t-k_l-ω *Low* R_e, the OpenFOAM implementation of (Walters and Cokljat 2008). Unable to make a good enough mesh resulting in suitable y+ values it was not considered worthwhile to use this more accurate but much more resource demanding transitional model. So all iterative simulations has been with the *k-ω SST* likely resulting in somewhat conservative, or high, drag and lift forces.

Verification of simulation

For the CFD simulations the VELO14 body is the inital design of the basic body shape as illustrated in *Figure 12* and *Figure 13*. This initial model was simulated in two different programs, in Caedium by the author and in Fluent by a professional CFD expert (Kjeldsen 2014). When comparing the simulation results from *Caedium* and *Fluent* it became obvious that the Caedium mesh resolution was too low. By repeating the simulation in Caedium with higher resolution good correlation on drag was found, 13.2 N in Fluent and 13.3 N in Caedium. Lift values were more diverse but lift forces require much longer time to converge, as can be seen from the flow simulation report in appendix C.

Body iterations

The second body iteration, VELO15, got more accurate wheel geometry and simulations were performed both with and without rotating wheels. The additional effort defining rotational axes and angular velocity on wheel surfaces required to simulate the rotating surfaces was high. According to Tamai (1999) air drag reduction caused by rotating wheels is compensated by air pumping of the same wheel rotation. This pumping effect cause an angular drag on the wheels leading to higher rolling resistance. This rolling resistance is not calculated, resulting in too optimistic total drag. Consequently, in the consecutive simulations wheel surfaces are not rotating, causing slightly higher air drag results, but closer to real values.

Further iterations progressed towards a final shape that were producible, functional, aerodynamic, and at the same time safe and aesthetic.

Drag of wheels and wheel cutouts

Disc covered wheels have less air drag than wheels with exposed spokes but can make the vehicle more sensitive, possibly even dangerous, at strong side winds. Careful design of steering geometry and vehicle aerodynamics is need to minimize this negative impact (Fuchs 1998, Sims 1998). Covered wheels also reduce cooling of the heat producing components in the hub. Typical example of such hub mounted components is gears, brakes, motors and bicycle light dynamos.

CFD summary

Each CFD simulation iteration had to be fine-tuned to get results that were consistent and stable. The most challenging were the meshing of the surface grid due to the different ways CAD and CFD handles 3D surfaces. In the CAD program solids are created based on a 'history tree' of basic geometry and modifications where each action creates or deletes surfaces. A part of such a 'history tree' from the VELO20 body is shown in *Figure 15*. In CFD, the surfaces should be divided based on their function and the need of local resolution within the fluid model surface mesh. This lead to very time consuming work for each iteration to manually merge surfaces in the CFD environment, and manually split certain surfaces in the CAD program. This was required to get 3D models with optimum surface boundaries leading to good surface and volume meshes.

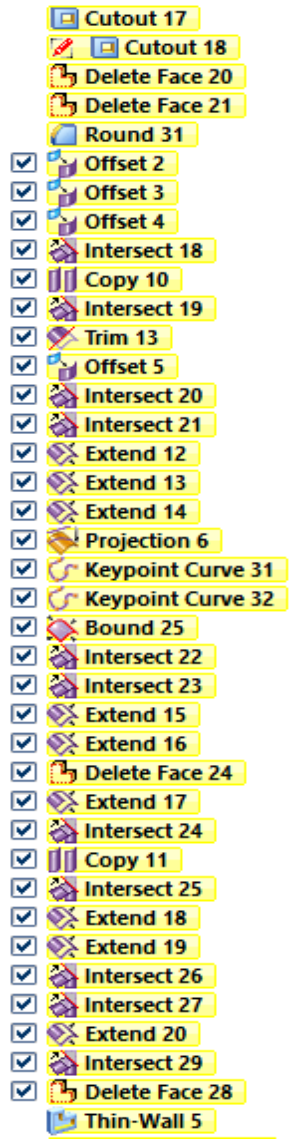

Figure 15 - CAD model history tree

Source: Author

It is interesting to see how much air drag we get at 25 km/h, the maximum pedelec speed, and the speed where the cyclist must propel the vehicle unassisted. We know the force at 10 m/s, 36 km/h is 12 N requiring 120 W. For 25 km/h, 6.9444 m/s, rounded to 6.95 m/s the power required for a body with C_dA of 0.20 m^2 is:

$$P = C_d A \frac{1}{2} \rho V^3 = 0.2 \frac{1}{2}\ 1.205\ \times\ 6.95^3 = 40.5\ [W]$$

This is quite favourable compared to almost all other cycles in *Table 1 - Drag coefficients of various cycles*.

An extract of the CFD results is listed in *Table 4*. VELO23 simulation plots are shown in *Figure 16*, *Figure 17*, *Figure 18* and *Figure 19*. For a complete overview of the CFD simulations, including the data and discussion of the various results, please examine appendix C.

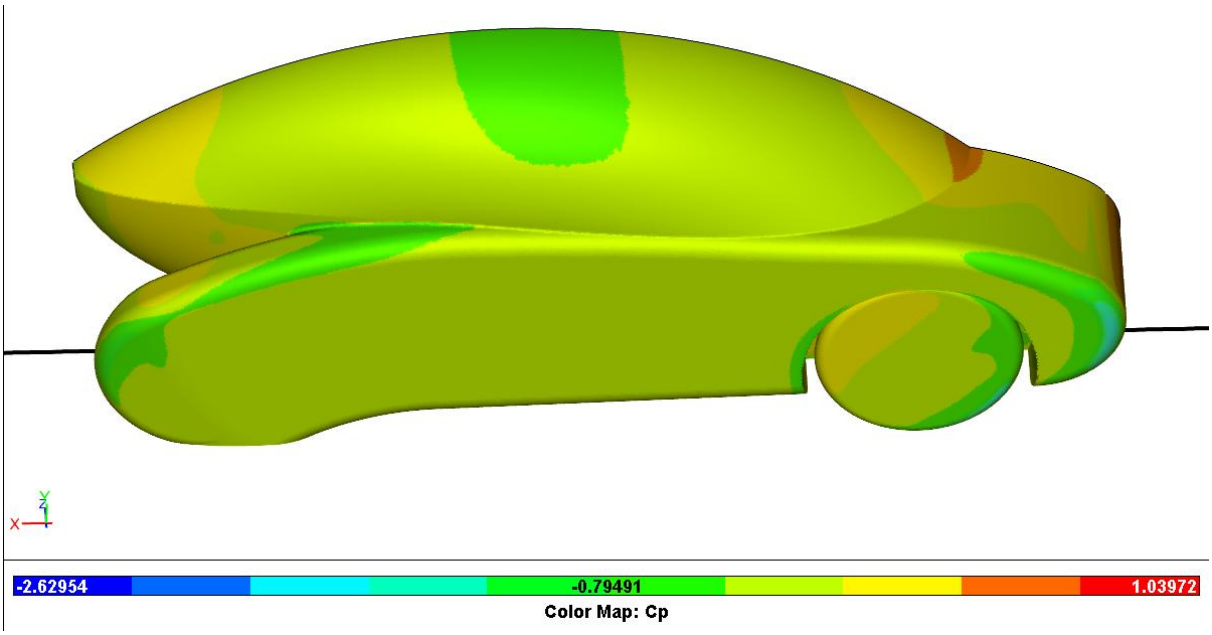

Figure 16 - Plot of Cp, coeffcient of pressure on VELO23

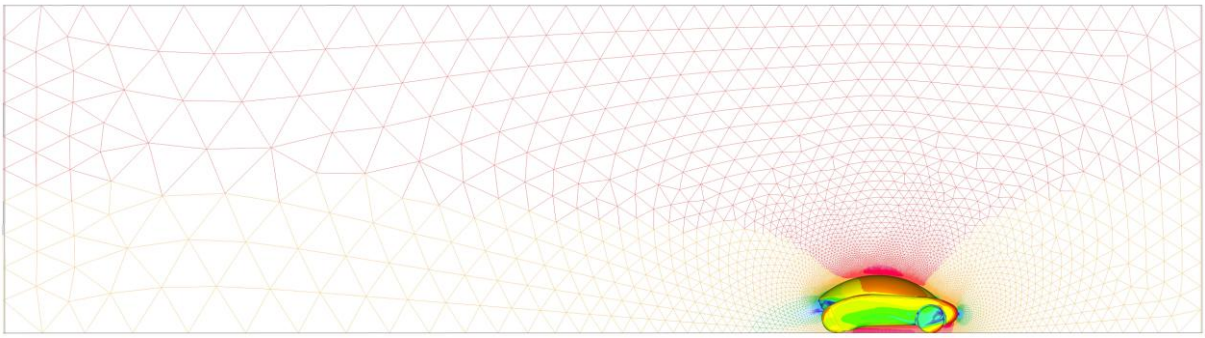

Figure 17 - Velocity plot of VELO23 with surface mesh on the symmetry plane.

This figure illustrates well that the rather large wind tunnel, 6 m upstream and 16 m downstream of the vehicle, is required. The depth is 3 m, simulating only the half wind tunnel due to the symmetric body. There are a total of 8 363 506 elements in this volume mesh, the most detailed that were used in these CFD iterations of VELO bodies.

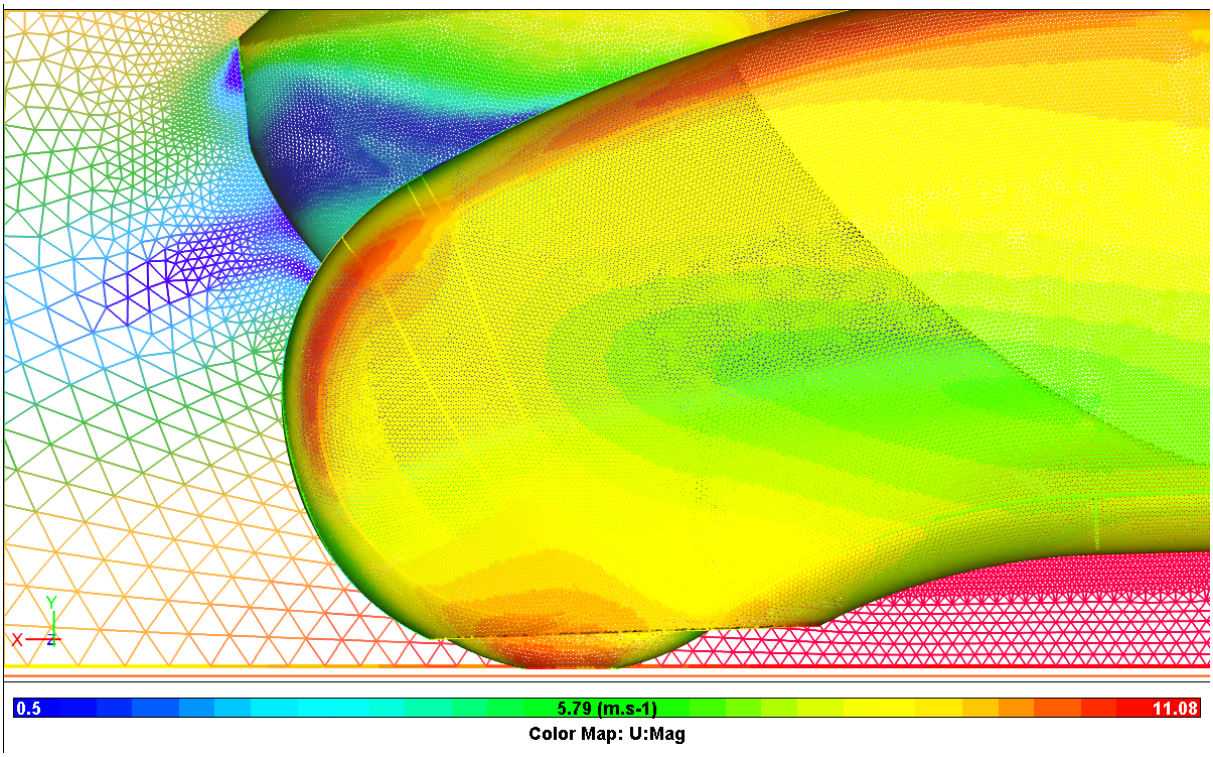

Figure 18 - Details from velocity plot with surface mesh from VELO23

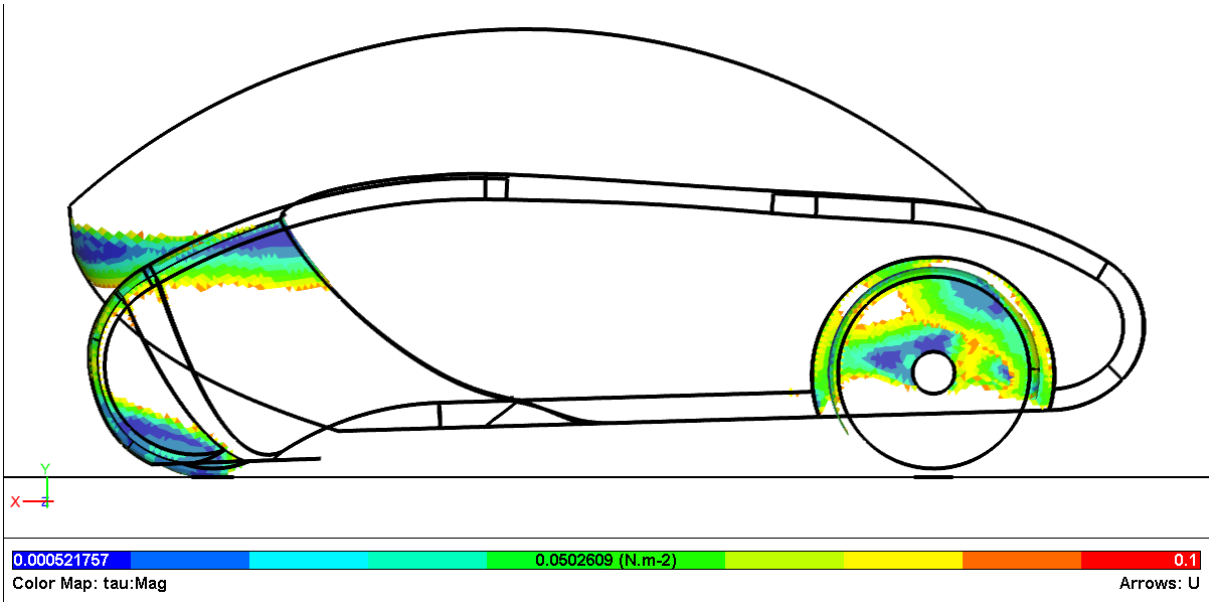

Figure 19 - Plot of τ_w, wall shear stress with values less than 0.08 N/m^2 on VELO23

Geometry	A [m^2]	Changed from previous simulation	Drag [N]	Lift [N]	CdA [m^2]	Comments
VELO14	0.3992	Base model	14.5	5.7	0.48	Simplest geometry that fit
VELO14	0.3992	finer mesh	13.3	5.5	0.44	For verification
VELO14	0.3992	finer mesh	13.5	5.3	0.45	For verification
VELO14	0.3992	fluent verification	13.2	8.5	0.44	Base case
VELO15	0.3788	aerodynamic improve-ment, angular velocity on wheel surfaces	10	-2.2	0.33	Compensated by air pumping
VELO15	0.3788	no angular velocity	12	-1.8	0.40	
VELO16	0.3261	Added wheel carrier rear	9.7	0.2	0.32	
VELO16	0.3261	Refined geometry	9.2	-1.25	0.31	
VELO16	0.3261	Refined geometry	8.8	-1.1	0.29	
VELO17	0.3264	With ventilation			NA	Did not finish
VELO17	0.3264	Refined mesh			NA	Did not finish
VELO17	0.3264	Refined mesh			NA	Did not finish
VELO17	0.3264	Refined geometry			NA	Did not finish
VELO17	0.3264	Refined mesh			NA	Did not finish
VELO17	0.3264	Refined geometry, mesh	9.8	0.2	0.33	
VELO18	0.3268	Streamlined, no vent.			NA	Did not finish
VELO18	0.3268	Refined mesh			NA	Did not finish
VELO18	0.3268	Refined geometry			NA	Did not finish
VELO18	0.3268	Refined geometry, mesh	8.5	-0.8	0.28	Strange oscillation in residuals
VELO18	0.3268	Refined mesh	7.3	0.2	0.24	did not help on residuals
VELO 19	0.3289	Added ventilation ports			NA	Did not finish
VELO 19	0.3289	Merged surfaces	9.25	-2.2	0.31	
VELO 19	0.3289	Refined mesh	8.25	-0.5	0.27	
VELO20	0.3289	Added person in cabin			NA	Meshing failed due to complex 3D
VELO21	0.3254	Streamlined underside, plugged vent			NA	Too high y+ (limit 300)
VELO21	0.3254	refined mesh	8.5	8.75	0.28	
VELO21	0.3254	refined mesh	8.2	-9.2	0.27	
VELO22	0.3232	Flat underside			NA	Did not finish
VELO22	0.3232	Rounded canopy edge R=7mm	9	-9	0.30	Much too high y+
VELO22	0.3232	Rounded canopy edge R=7mm	8	-6	0.27	
VELO23	0.3283	3% camber (front raised 50 mm)	8.25	-8	0.27	Too high y+ (limit 300)
VELO23	0.3283	refined mesh	8	-8	0.27	
VELO23	0.3283	refined mesh	7.2	-7.5	0.24	
VELO23	0.3283	refined mesh, adj. relax f.	6.5	-5	0.22	Changed to lesser relaxation factors
VELO23	0.3283	refined mesh, adj. relax f.	6	0	0.20	Tuned relaxation, many iterations

Table 4 - Summary of CFD results

4.5 Ventilation

To achieve acceptable internal temperatures and demist of windows good ventilation is required.

Heat sources inside the velomobile:

- Cyclist
- Passenger
- Solar radiation
- Drive train parts internal to the velomobile (pedal generator, power electronics, batteries)

Other sources like light, mobile phones and other possible heat sources are small and have been ignored.

Heat from cyclist

Most heat comes from the rider. Plotted in *Figure 20* is the accumulated cooling rate for humans at various wind speed. There are also some lines showing the cooling rate of comparable geometric objects.

Located inside the canopy, the rider is not automatically cooled by moving air as on a regular bicycle. To cool the velomobile rider efficiently, ventilation must provide sufficient air velocity surrounding the rider. The rider mechanical output of 100 W on average creates 300 W of heat given an efficiency of 25% (Walle 2004). From (Wilson, Papadopoulos et al. 2004) we have human body area given as 1,8 m^2 which require cooling at 167 W/m^2. A small person with an estimated body area of 1,5 m^2 maintaining the same power output would require 200 W/m^2. Selecting *Reclining human* , the posture for our velomobile cyclist, from the chart above, an airspeed over the body of 1 m/s removes around 200 W/m^2 of heat. If the ventilation system can achieve an air speed of 1 m/s over the cyclist's body the velomobile offers sufficient cooling for continuous use. If not, the cyclist would heat up more and more and would need to sweat or reduce power to prevent overheating.

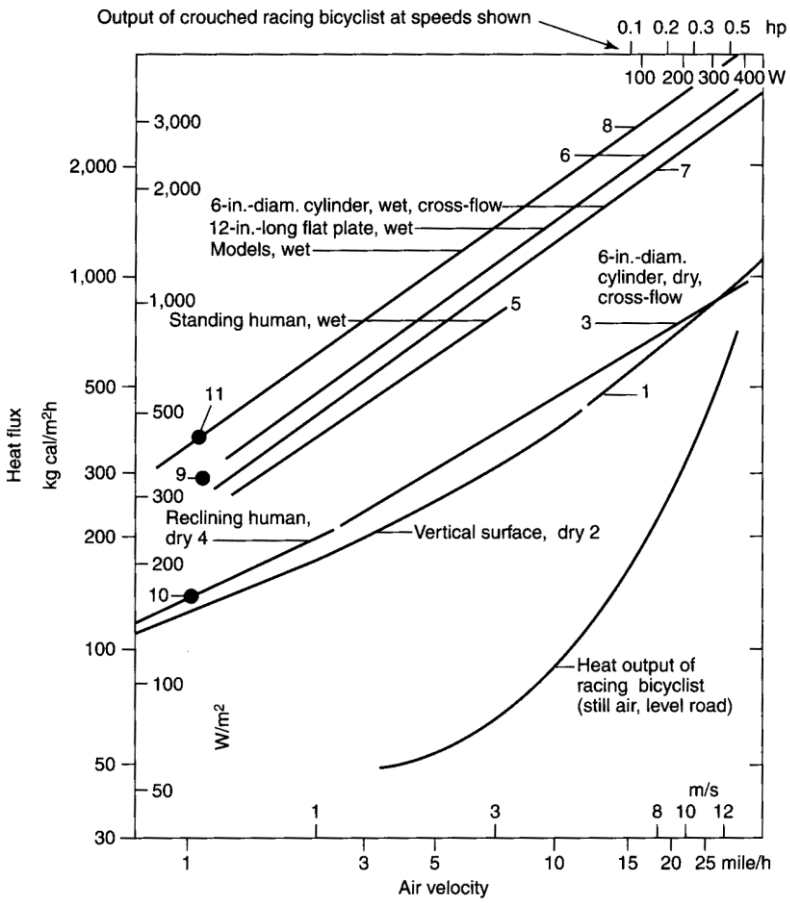

Convective and evaporative heat flows.

Figure 20 - Cooling of humans

Credit: David Gordon Wilson, *Bicycling Science* third edition, and MIT Press

Heat from passenger

The child passenger is preferably sitting still - another good reason why child seats comes with safety belts! Heat from a 6 year old child sitting with moderate activity will vary between 50 to 120 W depending on age, sex and clothing (Parsons 2002).
For sizing the ventilation system 90 W in passenger heat is considered as a sensible estimate.

Heat from solar radiation

Heat from the sun goes directly into the cabin via the canopy. To prevent extreme greenhouse effects, the top of canopy has a reflective film blocking most heat and light[9] having a typical $\eta = 15\%$. Rear sides are covered with a tinted film assuming $\eta = 40\%$ transmission ratio. Canopy material is PETG with UV enhancement having a typical $\eta = 86\%$. A verification of the heat load from the sun is still necessary.

The maximum solar power reaching the earth is 1366 W/m^2 minus the loss of energy from the sun reflected off the earth's atmosphere (Holter, Ingebretsen et al. 2010). This result in $\dot{q} \approx 1000$ W/m^2 at a surface on the ground normal to the sun.

The position of the sun relative to earth is dependent on the geographical latitude, date and time . The *declination*, height, Ψ, of the sun is given by the inclination of earth's axis, α, the geographical latitude φ, and the azimuth of the sun τ. Formulas for calculating the sun's position can be found in (Holter, Ingebretsen et al. 2010):

$$\Psi = \alpha - (90° - \varphi)\cos\tau$$

Azimuth of the sun, $\tau = 0°$ at midnight, with sun in the north, and $\tau = 180°$ at noon, with sun in the south. At summer solstice inclination $\alpha = 23.44°$, but on other days the sun's inclination is given by:

$$\alpha = 23.44° \sin\frac{360°(z + 284)}{365}$$

where *z* is the number of the day in the year, starting with *z*=1 for January 1st. This design is aimed at Nordic countries where the latitude φ is 55°N or higher. Assuming worst case scenario for ventilation , i.e. midday summer solstice far south in Denmark, the declination of the sun is:

$$\Psi = 23.44° - (90° - 55°)\cos 180° = 23.44° + 35° = 58.44°$$

The solar radiation entering through the canopy can then be calculated:

$$\dot{Q} = \dot{q}\eta A$$

where $\dot{q}$ is the sun radiation level in W/m^2, η is the energy transmission ratio of the window glass, and *A* is the projected window area normal to the sun in m^2. On VELO17 the projected window area depends on orientation of the vehicle towards the sun, and Ψ, height of the sun on the horizon.

Since the velomobile use a complex shaped canopy having three different coatings, areas facing the sun were extracted from the CAD model. Two orientations of the vehicle, front and side towards sun were used. In addition to the worst case scenario of high sun, also a low sun of 30° was used to extract area data from CAD model. Each section's area and total ηA for both directions and both heights of the sun is listed in *Table 5*.

		Front 30°		Front 58,44°		Side 30°		Side 58,44°	
	H	*A [m²]*	*ηA [m²]*	*A [m²]*	*ηA [m²]*	*A [m²]*	*ηA [m²]*	*A [m²]*	*ηA [m²]*
Window	86 %	0,519	0,447	0,659	0,567	0,554	0,477	0,574	0,494
Roof	15 %	0,145	0,022	0,244	0,037	0,133	0,020	0,242	0,036
Rear	40 %	0,031	0,013	0,202	0,081	0,281	0,112	0,318	0,127
sum			**0,481**		**0,684**		**0,609**		**0,657**

Table 5 - Values for exposed area of VELO17 canopy at various sun angles

Selecting worst case from *Table 5*, heading a sun high in the sky give a solar radiation heat load via canopy of:

$$\dot{Q} = 1000\ W\ 0.684\ m^2 = 684\ W$$

This is worst case, sun will seldom be this strong. Also some heat will be radiated out, but then, also some heat will come from the body exposed to a strong sun. Due to the large curved canopy, a lot of heat energy caused by solar radiation will enter the interior. Even low sun at the front results theoretically in 481 W of heat.

[9] For example Solar Steel 20 from Hanita Coatings, see appendix G.

On cloudy days the amount of radiation from the sun goes down to 5-10 times less than the maximum calculated values, or 68 to 137 W (Holter, Ingebretsen et al. 2010). Using the largest value for dimensioning the canopy ventilation, it must be possible to ride the vehicle with a fully closed canopy in cloudy weather with estimated 137 W of heat from solar radiation and achieve sufficient ventilation.

In a bright sunny day with solar radiation up to five times as strong it is acceptable to ride the velomobile with the canopy at least partly open to achieve sufficient ventilation. This is an important requirement for the canopy design. This additional ventilation must be verified with CFD to confirm sufficient ventilation and minimize the additional drag cause by the extra opening(s).

Additional functions to help preventing the overheating of the cabin due to too much solar radiation would be beneficial and should be considered. Possible improvements to the current design are discussed in chapter 5.3.

Drive train parts
The drive train has some losses. Based on 100 W mechanical input and 250 W electrical motor power output the heat contributing parts inside the cabin and their estimated losses are:

- Pedal generator 20 W (est. 80% efficiency)
- Rectifiers 8.2 W (est 3 * 0,7 V voltage loss * 4 A)
- Maximum power tracker 10 W (estimated)
- Transmission battery w/BMS 0.4 W (est 100 mΩ resistance sum in all power transistors and 2 A)
- Traction battery w/BMS 1.25 W (est 50 mΩ resistance and 5 A)
- Motor controller 12.5 W (est 95% efficiency on two controllers 50 V and 2.5 A)

Total power loss in drive train inside cabin based on above estimate: 53 W

Total heat load on ventilation
There are a few other heat sources that should be accounted for in this calculation:

- Head lights and LED regulators 10 W
- Fans (probably used when maximum ventilation is needed) 2 x 6W
- Various other consumers like USB charger, control panel and powered speakers 10 W

Based on the data above the total heat needed to be removed is:

- Cyclist: 300 W
- Solar radiation: 137 W
- Passenger: 90 W
- Drive train: 53 W
- Other: 32 W
- **Sum heat loads: 612 W**

Required mass transport
To find out if we have enough air to remove 612 W of heat depends on the air heat capacity. It varies a bit due to humidity, ambient temperature and air pressure but not much so we assume of k_a = 1000 $\frac{J}{K\,kg}$ in these hand calculations. From the simulations in appendix C we have a ventilation flow rate of 0.177 m^3 per second, see the *Ventilation ports* section below. With a density ρ = 1.205 kg/m^3 as used in the simulations, resulting mass flow $\dot{m}$ = 0.21 kg/s. Assuming ambient, or more exactly, inlet air temperature of 15°C, adding 612 W gives a resulting temperature of:

$$T = T_{ambient} + \frac{P_{heat}}{k_a\,\dot{m}} = 15°C + \frac{612\ W}{1000\frac{J}{c°\,kg}\,0.21\frac{kg}{s}} = 17.9\ °C$$

3°C is quite a lot of warming but 612 W is a lot of heat, probably much more heat than for most days. This should work. When and if ventilation is insufficient, primarily caused by sunny weather, the option of opening the canopy is available.

It is also possible to improve ventilation by increasing the ventilation port area in exchange for slightly more air drag. This is what is normal in velomobiles having an opening for the feet underneath the pedals.

Ventilation ports

According to (Tamai 1999), for the ventilation ports and ventilation air flow to cause least damage to body air drag, the:

- intake should be at stagnation point, or area with highest pressure coefficient, *Cp*
- outlet should be parallel to surface air flow in area with low Cp

Cp is the dimensionless *pressure coefficient*, defined as:

$$C_p = \frac{p_{loc} - p_\infty}{\frac{1}{2}\rho {v_\infty}^2}$$

where p_{loc} is the local pressure and p_∞ is the free stream pressure.

From the Cp plots in appendix C the obvious intake location is at the centre front of the vehicle. The outlet location is less obvious. Several low Cp areas can be found on the vehicle but on the rear end, along the rear upper edge of the canopy there is an area with low *Cp* that is preferred. It is easy to reach to adjust opening size using tape or shutters. It also helps to keep airflow along the inside of the canopy to avoid mist. Also to expel warm air an outlet high in the vehicle is preferable.

A model (VELO17) with a tube having an inner diameter of 150 mm with rounded inlet in front centre, and an invert U shaped outlet along canopy rear edge was added to VELO16, see *Figure 21*. At 10 m/s vehicle speed the ventilation tube velocity was 3.4 m/s resulting in air volume rate of 0.177 m^3/s .

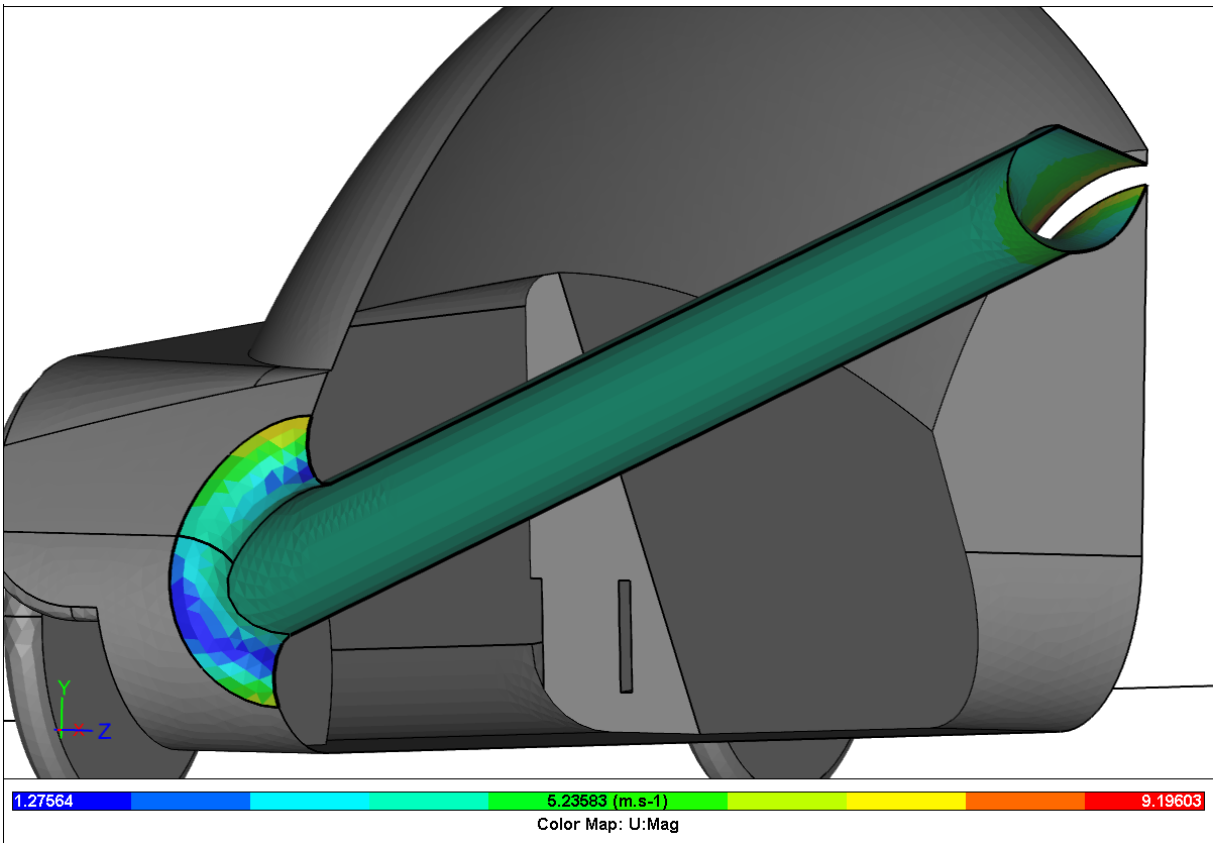

Figure 21 - air velocity from passive ventilation at 10 m/s vehicle speed

The final vehicle will have a much larger cross section, using the inside of the body as the tube. But having the occupants as flow restrictors, and guiding most of the air flow directly on the pedal zone should result in sufficient air flow along the cyclist's body.

Demist
A demist function is needed when stopping in cold air. The cyclist's moist breath will reach the cold window and form mist unless some form of preventive action is taken. Several solutions to reduce this problem have been implemented:

- Small PC fans maintain a flow of air from the outside over the front inside of the canopy
- Inside surface of window is treated with a antifogging coating
- Large distance between front window and cyclist

4.6 Material for aerodynamic body

For the upper body, a material was sought that is:

- Light
- Strong
- Outdoor resistant
- Easy to use
- Low environmental impact
- Easy to recycle
- Reasonable to purchase
- Can be painted/coloured

When turning the body from CFD simulations into the real thing, the materials chosen must be easy to shape according to the CAD model. Due to the double curvatures and the smooth surface requirements casting using an external surface mould is usually required. Most velomobiles tend to be made of thermoset plastic composites. A cast body in GRP or similar materials makes a light and stiff body and the mould(s) does not need to handle high temperatures. But several drawbacks exists, among them are a fragile body, difficult recycling and expensive transport of finished bodies and velomobiles. Fortunately, when using a non stressed body design the choice of using more sustainable body materials are much easier. Due to a metal chassis, there is much less need for stiffness in the body.

Self reinforced polymer
A self reinforced thermoplastic composite made from PET, srPET, is a suitable choice. PET allows canopy and body to use the same plastic material. In addition, self reinforced PET fabric has a very high strength to mass ratio and is commercially available (ApS). srPET from the Danish company Comfil ApS seems to be a good candidate for the body material having been used in building the structural parts of the *Plastiki* 60-foot catamaran that crossed the pacific in 2010 (ApS , Rotschild 2011).

When constructing parts for later recycling it is important to follow recommendations from the recycling industry (RECOUP 2013). When selecting adhesives, paint, films and coatings that attach to the plastic it is important that these materials are compatible with efficient recycling processes or at least do not cause problems when recycling adjacent materials.

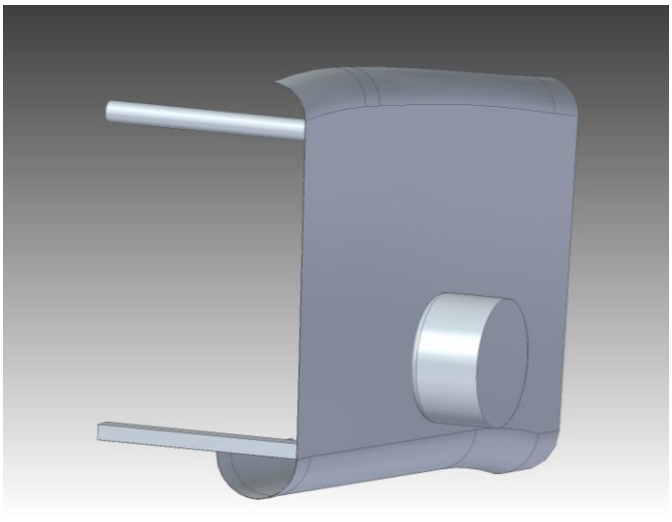

Figure 22 - Door panel for FEM simulation of collision force

srPET strength
srPET is a commingled fabric woven of fibres of both high tenacity PET (HPET) and fibres made of PET with a low melting temperature (LPET). Several compositions and weaves with different properties are commercially available. For highest strength to mass ratio a lay-up consisting of fabric must be designed based on expected load values and major load direc-

tions. As with other composites, available strength primarily depends on fibre direction, lay-up and craftsmanship. The last is important to avoid delaminating layers and loss of shear strength. This usually means that samples must continuously be made from the production batches and tested to verify sufficient quality and strength. With an automatic production process less variations should occur.

srPEt is unfortunately not without its problems. It is complex and time consuming to process, requiring pretty advanced equipment to make strong, light body panels. Heating the parts to high temperatures in a short time is especially demanding. The process window require at least 180°C, preferably 200-220°C for reduced holding time and higher strength, see the process window chart in *Figure 23*.

When the fabric has been put in the mould it is compacted during heating by vacuum. A vacuum bagging sheet typically made from heat resistant silicon rubber is put on top of the fabric and air is evacuated using vacuum pump(s). The vacuum requires good sealing between mould and bagging sheet. Heat must be applied long enough to get good bonding but not longer as extended heating reduces strength of the composite.

Processed sheets of srPET composites are commercially available[10] (ApS). A sheet with 50% HPET + 50% LPET in a 2/2 twill fabric has a yield of 192 MPa, 24.5% elongation before break and a tensile modulus of 5.4 GP when tested with 50% of reinforcement fibres in warp direction. A slightly different lay-up with 80% of reinforcement in warp direction has 256 MPa in yield and 7.4 GPa in modulus which is very impressive. This is approximately the same yield strength as aluminium but at half the density and much lower material cost.

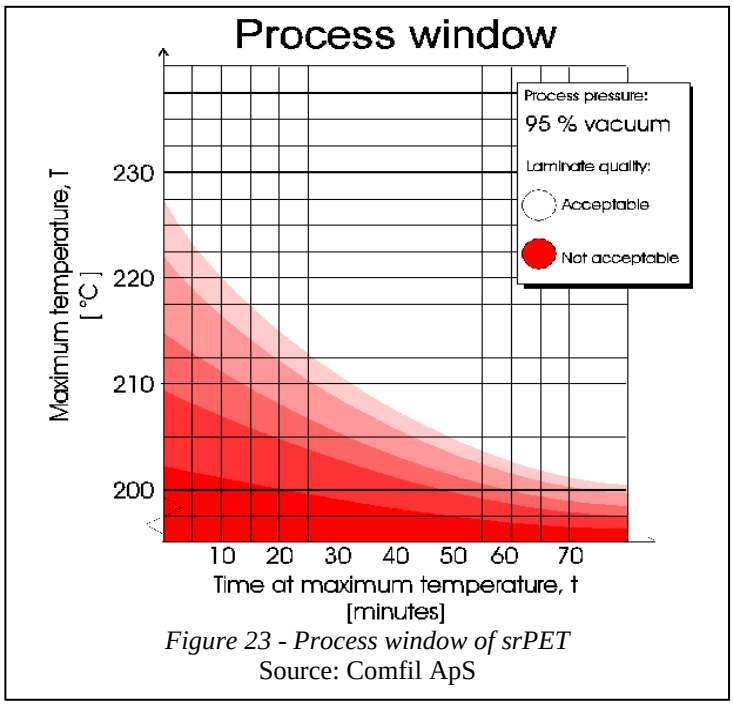

Figure 23 - Process window of srPET
Source: Comfil ApS

Body strength

The body need to be sufficiently strong to cope with normal handling, its own mass plus appendages and additional load from wind and speed. But during transport, storage and, in worst case, collisions, the material will be exposed to much higher stresses. Especially when, acting as a protective cocoon in the case of collision, the velomobile body must be as strong as possible given the limited mass. Various collisions between velomobile and car have been simulated and tested in scale by Stefan Gloger and Harald John (Gloger and John 1998). They recommend a stiff side on the velomobile to prevent intrusion and diverge forces in case of collision. In their tests of a veloquad the occupants experienced collision impacts of 4g. It would have been interesting to do a full transient analysis of an impact that simulate a true collision. Unfortunately, that requires more resources than are available. Instead a much less accurate method, but still indicative of the required qualities, was chosen.

To compare body materials for a velomobile door with crash protecting capabilites, a simple model has been defined consisting of a section from the side of the velomobile body. This section has a 90 degree angled plate where the edge is fully supported. At the other end there are two 300 mm long steel tubes bonded to the panel with the other end of the tubes fully supported. This panel was exposed to a force caused by impact with a Ø180 mm metal cylinder with r=10mm rounded edge, being pushed 50 mm into the plate, see *Figure 22*. This geometry was simulated using a static FEM model using tensile modulus only with the following door panel materials (with mass):

- 0.8 mm sheet metal steel (4.15 kg)
- 2 mm aluminium alloy (3.64 kg)
- 4 mm srPET (3.62 kg)

[10] Thermoformable sheet type 50204 and 50203 from Comfil made of srPET

Steel required a maximum of 7751 N before the sheet buckled in a bit and force fell to 7348 N at 50 mm displacement.
Aluminium required 13290 N, with no buckling phenomena.
4mm srPET required only 3327.5 N and gave little protection, despite being 4 mm thick.
These simulations used a linear material model and are not realistic. Documentation on these simplified simulations can be found in Appendix D.

PET sandwich
If instead of using a single 4 mm thick sheet we made a sandwich construction, putting a lightweight core between two thin sheets of high strength srPET, the panel becomes much stronger without additional mass. Sandwich construction is often used in various structures that need to be light and stiff. To keep the body construction easily recyclable the core should also be made of PET. Fortunately, lightweight foam cores for making sandwich constructions are commercially available in both virgin and recycled PET with various densities and strengths. Datasheet for *Armaform* and *Divinycell* PET cores can be found in Appendix G. When making a geometric model of the same door panel made of two layers of 1 mm srPET with 20 mm Divinycell P100 PET foam in the middle, the mass becomes only 3.03 kg. From a very simplified FEM simulation of a sandwich door panel an impressive force of 9685 N was needed to penetrate 50 mm into the velomobile. That would exceed 4g, even for a fully loaded vehicle.

For realistic simulation elastic-plastic material models using data from material testing is needed to verify real values for impact strength. This would also require a representative CAD model of the vehicle support structure. The body parts should be modelled for production tolerances resulting in conservative panel strength from the simulations. However, that requires expensive resources and takes a lot of time. Unless quantified strength is absolutely necessary, a quicker way to get results is to try to shorten the development cycle by using simpler what-if simulations and comparing outcome of alternative designs. Then use those results to optimize the design to make best possible use of the limited mass budget in a human powered vehicle. It is important to use the available mass budget where the construction benefits most.

If using PET sandwich, long lasting bonds between the different layers are crucial. But inter-layer bond is also vital for pure srPET layers. Shear forces between the layers from an impact could break the bonding which would cause severe loss of strength. It is very important to verify longevity of panels made of PET by accelerated tests involving systemic cycling of temperature and loads. Also other loads due to humidity, ozone, sun, bacteria and fungus should be considered.

Canopy
The canopy should preferably be made of PETG for ease of recycling, safety and cost. Using the same class of polymer as the body also simplifies recycling and waste management in production, reducing cost. Polycarbonate (PC) with the trade name *Lexan*, is even stronger but recycling is not easily available for PC. Acrylic is also an alternative, being more scratch resistant than PETG. Unfortunately, it cracks more easily and would require a thicker and heavier canopy. It is also more expensive.

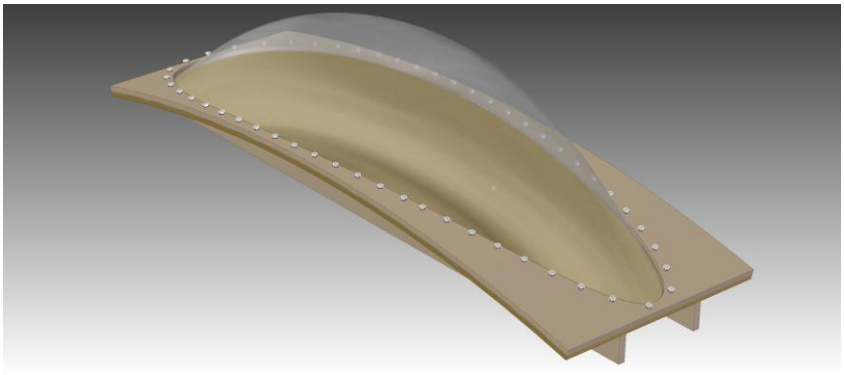

Figure 24 - Thermoforming the canopy

The canopy is made by thermoforming, heating the sheet and then forming the plastic by using air pressure in a thermoforming setup as illustrated in *Figure 24*. The base plate is curved for several reasons; improved look, to increase canopy edge stiffness, to get a more stable mould, possibly increasing view angle thru window for better optics, and last but not least - to fit in the oven.
After blowing the sheet to the required height, see drawing in appendix A, the bubble must be allowed to cool while actively maintaining the air pressure. If the air supply is just cut off, the air inside the bubble will shrink and reduce the pressure when cooling, possibly deforming the canopy.

After removing the canopy from the blow mould and verifying it has the correct shape, it must be stabilized by additional heat curing. Material suppliers have often given advice on this. Another good reference is an Autospeed article (Edgar 2009). This article goes into at least some details on how to blow form canopies.

After the canopy has been shaped and polished it must be accurately cut to fit the rollover protection and the rest of the body. Nice edges are important so cutting should be done according to the instructions from the material supplier. When cutting plastic it is easy to cause local heat stressing of the material. This can cause micro cracks that sooner or later become macro cracks. To avoid this it is normal to do a new heat curing after final cutting and drilling if possible.

Canopy coatings and films
Special material grades for prolonged exposure to UV light from the sun are necessary to avoid the need to replac the canopy prematurely. Also sheets with scratch resistant coatings may be used if they handle the blow forming. On the inside an anti-mist coating would be beneficial. Such special coatings are often applied after forming to prevent damage to the coating during manufacture. Special water repellent coatings on the surface could help the visibility in rainy conditions.

For reducing radiated heat from the sun it would be beneficial to use plastic sheet of a quality that limit heat energy from entering the canopy. Such heat filtering should not reduce visible light by more than 25%, as required for safety glass in car windshields. There must also be reflective films on top and rear as discussed in section 4.5, otherwise solar heat would overwhelm the ventilation capabilities of the vehicle.

For the unlikely event that the canopy fractures, the inside of the canopy can be equipped with a safety film preventing sharp pieces from harming the occupants. Such film is used inside laminated glass and is made of polymers with high tensile strength and good optical properties. Safety films with integral sun filters are available, see appendix G for datasheets on canopy films.

Edge protection
PETG is quite strong and does not fracture easily but in cold weather this might happen. The canopy is less likely to fracture if the edge is equipped with a suitable protection made from a thin aluminium profile or similar. It should not be glued or fixed with screws or nits. Due to different thermal expansion coefficient and shrinkage of the canopy after blow forming this will cause extra stress. Fixing can for example be by a thin elastomer sheet maintaining compression set between edge and profile.

Picture 14 - Typical blind nits assembly technique using clecos, vices

Source: Author

4.7 Chassis

To make a low cost velomobile with a small environmental footprint it is important to use efficient production methods. One of the most efficient production methods available for low volume production is CNC thin sheet metal fabrication. Using highly automated machinery the cost of manufacturing is almost independent on wages, making production possible everywhere.
By using sheet metal construction methods as used on light but highly stressed structures like airplanes, a stiff and light platform frame can be made out of aluminium using CNC tooling at reasonable cost. Aluminium production requires a lot of electric energy. Fortunately, more and more electric energy comes from renewable sources. Aluminium is also very well suited to recycling resulting in a low environmental impact during its life cycle.

Assembly and corrosion
Assembly need to be according to best practice, removing burr from drilled holes and using correct size, length and material of nits and bolts, nuts and washers. Also good tools, especially for pulling blind nits is important, while keeping parts tightly assembled using clecos or similar, see *Picture 14*. Severe corrosion will decimate the

strength. Selection of corrosion compatible materials are necessary, i.e. aluminium sheets and stainless steel fasteners together with corrosion protective coating. Some corrosion are inevitable over time due to road salt and together with suitable drainage and prevention of debris accumulating inside the wheel carriers.

Since the final chassis and body is not finished, drawings or calculations of the chassis is limited to the rear suspension and hydropneumatic suspension. Stress calculations has been done in ANSYS Workbench to verify stiffness and strength. Please see appendix D for documentation.

Some calculations on the rear wheel carriers have been done regarding fatigue. As most stressed parts are made of aluminium these parts must be designed to last longer than the lifetime of the component (25 yrs/250 000 km). Alternatively, if this is difficult to achieve (or document) they must fail safe. Please see appendix D for further documentation on fatigue calculations.

Figure 25 - Elevated entry and exit

Source: Author

4.8 Front suspension and steering

As much as possible of the front suspension is taken from Alligt A4 velomobile kit. An identical vehicle was built by the author in the spring 2010. The parts are readily available for purchase and the author made a CAD model of the suspension parts when he built his own velomobile, see *Figure 5*. The Alligt A4 kit was also used by UIS students Bjørkli and Gjerldstveit (2013) for a bachelor assignment where the students motorised the front wheels. By using this front suspension it is possible to reuse their solution for motorizing the front wheels, if more motor power is required.
Some changes must be done to the central part of the steering linkage. There is less free space between the wheels in the new veloquad due to the relocation of the pedals to this area. In addition, the veloquad uses stick steering as the traditional handle bar comes in conflict with the position of the pedal generator. Otherwise the steering geometry is kept as is.

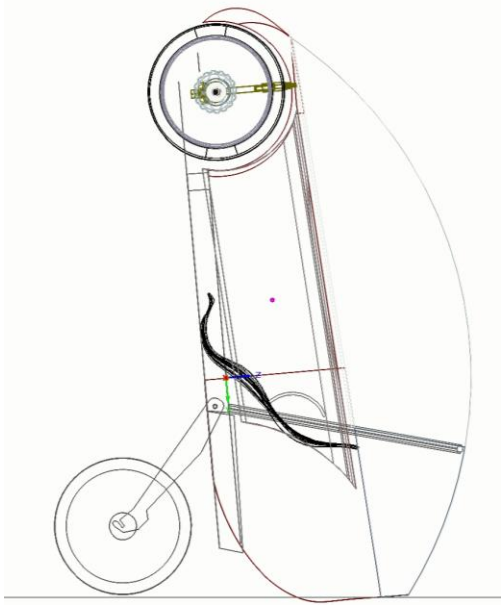

Figure 26 - Vertical parking

Source: Author

4.9 Rear Suspension and elevation system

The rear suspension has two other functions in addition to being the vehicle's suspension system for the rear wheels. It functions as an actuator by lifting the rear chassis including the seat from riding height to a more suitable height for entry and exit, as illustrated in *Figure 25*. The rear suspension is also used as support for vertical parking and storage with the wheel carriers fully extended as shown in *Figure 26*.

Sway bar

The two rear wheel carriers is hinged on a hollow shaft that extends outside of the chassis on each side with the free section extending backwards, see *Figure 27*. Each of the two rear wheel carriers is equipped with a dual ball bearing from a standard bicycle head set used in the front fork steering. A sway bar, or anti roll bar going thru the hollow shaft connects the two wheel carriers. The rear sway bar has several important tasks:

1. **Reducing body roll for improved safety**
   When cornering the sway bar has an important safety function. It will reduce the height of the COG by leveraging some of the weight load from the outer wheel to the inner wheel when cornering. Without the sway bar the vehicle would lean and raise the inside much more, possibly raising COG.

2. **Actuator for sensor used to detect rear wheel height**
   Travelling must be prevented when the vehicle is raised due to the much higher COG of the vehicle. A single sensor or switch triggered by the angular position of the centre area of the sway bar can be used for this sensing task.

3. **Aligning wheel height when raising and lowering the wheels**
   To keep the hydropneumatic light, reliable and reasonably priced, the system should be as simple as possible. Having a sway bar that mechanically links the two rear wheel carriers enables use of a single control valve for lowering and rising the vehicle.

4. **Extra fail safe mechanism preventing wheel carriers from falling off the vehicle in case of failures**
   The rear wheel carriers are quite exposed to wear and damages. Especially the hinge bearing and axle. For a vehicle designed to last for 25 years it is expensive to use materials and hardware in such an exposed position that will last the lifetime of the vehicle. To keep cost low, the vehicle should have wheel carriers that can tolerate a hinge bearing or hinge shaft breakdown without causing danger. A failsafe solution that use the sway bar is logical. It is easy to make the bar capable of acting as hinge and retaining the rear wheel carriers in case of failure. This will allow use of lower cost and lighter parts without sacrificing safety.

To save mass, a large diameter tube would be better than a rod. Material should have low density and suitable torsion stiffness and fatigue properties to outlast the design lifetime of the vehicle.

Rear wheel carrier

The hub motor wheel shaft is fixed to both sides of the wheel carrier, a trailing arm suspension, see *Figure 27*. This allows the use of standard hub motors which require support on both sides. Cantilever hub motors are much more expensive and are currently also much less available than regular e-bike hub motors.

Figure 27 - Wheel layout

Source: Author

The need of attaching the hub motor on both sides requires a wide wheel carrier. It was also important to put the wheels as far apart as possible for optimum stability, given the narrow vehicle width of 800 mm. The wheels also needed to be as far back as possible for ease of entry and to keep the vehicle capable of be stored vertically with a maximum height of 2400 mm.

To achieve low air drag, it is paramount to have a slim, tapered rear end. So by moving the wheel carriers outside the cabin it became possible to taper of the vehicle in three sections, one for the main body and two for the external wheel carriers. This is not aerodynamic perfect and will cause slightly more air drag than a single section, but the CFD analysis shows that it is possible to reach acceptable drag levels, see 4.4.

There are several other reasons for bringing the wheel carriers outside the main cabin body:

- Reducing the width of the platform chassis. Since the chassis is likely to be shipped preassembled, size should be limited as it influence cost of freight.
- When the front part of the canopy is fully opened, it tilts backwards. To prevent strong winds from tipping the vehicle, the edges of the moving canopy go between the fixed canopy section and the rear wheels to keep a low profile and thus less wind exposure.
- Another reason is having the rear suspension outside the cabin prevents passenger (child) from hurting themselves on moving suspension parts without requiring extra covers.
- Noise from the motors and rear wheels are more dampened when they are located away from cabin.

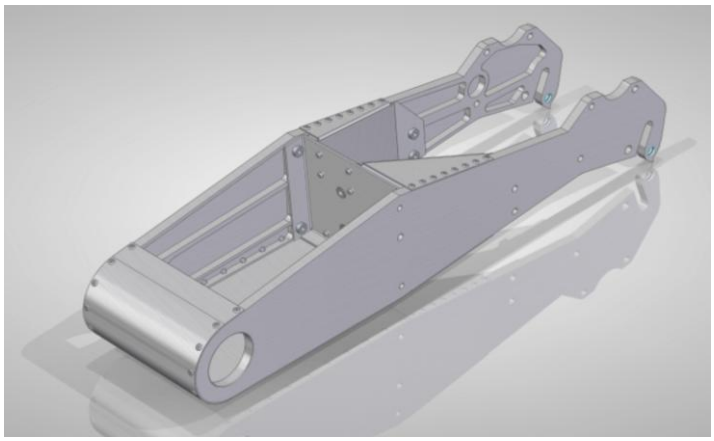

Figure 28 - Rear wheel carrier structural design

Source: Author

Rear wheel carrier construction

The wheel carrier is a box section made from several aluminium sheet metal and two 8 mm plates, see *Figure 28*. This is designed to take advantage of single-sided milling using 2.5D machining and using only an 8 mm end mill cutter for optimum economic production. At higher production volumes the wheel carrier should be redesigned to take advantage of economies of scale. It is also important to do load measurements on the structural parts when in use to see if the load picture is very different from the one envisioned.

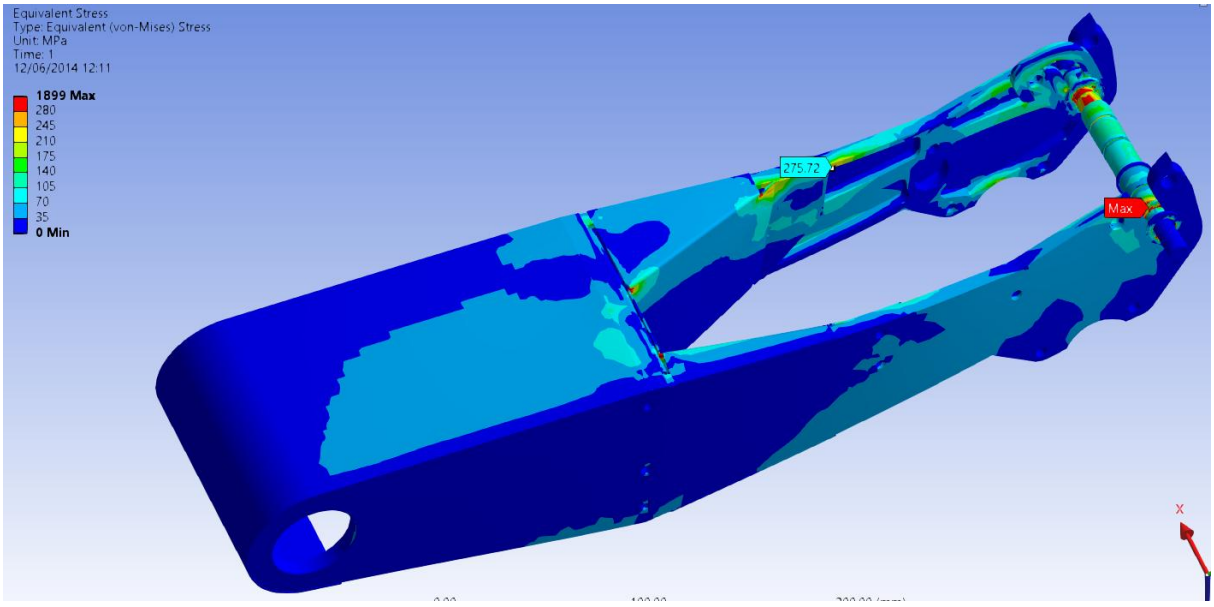

Figure 29 - 800 N vertical and 800 N horizontal as remote load 250 mm from wheel axle

FEM simulations has been done on a simplified model of this structure. The simulated structure was without blind nits, blind nit holes or structural bolts, having been replaced with full bonding between parts to be able to simulate with available software and hardware. This removes stress concentrators likely to initiate cracks from the simulation. To remedy this, areas having large stresses where there are joints should be simulated with the level of details necessary to verify strength of construction as built.

Boundary conditions for stress simulations were based on the following:

- Max allowed vehicle mass 200 kg from specification, see 4.1
- Weigth [N] = 9.81 * Mass [kg]
- Weight distribution left/right 50/50 due to symmetric design
- Weight distribution Front/rear 40/60 estimated based on CAD model
- 35% extra load to try to compensate for the simulated assembly being bonded instead of nitted and bolted assembly

This resulted in a weight load of 800 N. The assembly showed sufficient strength based on von Mises plot to handle a static systemic vertical load of 800 N and a load of 800 N horizontal, comparable to 1 g, as remote load matching the diameter of a 406 mm wheel. Some plastic deformation will happen but the structure is redistribute loads after initial minute plastic deformation so it is unlikely it will progress to failure, see *Figure 29* and *Figure 30*. For further details of the structural simulation of the wheel carrier see appendix D.

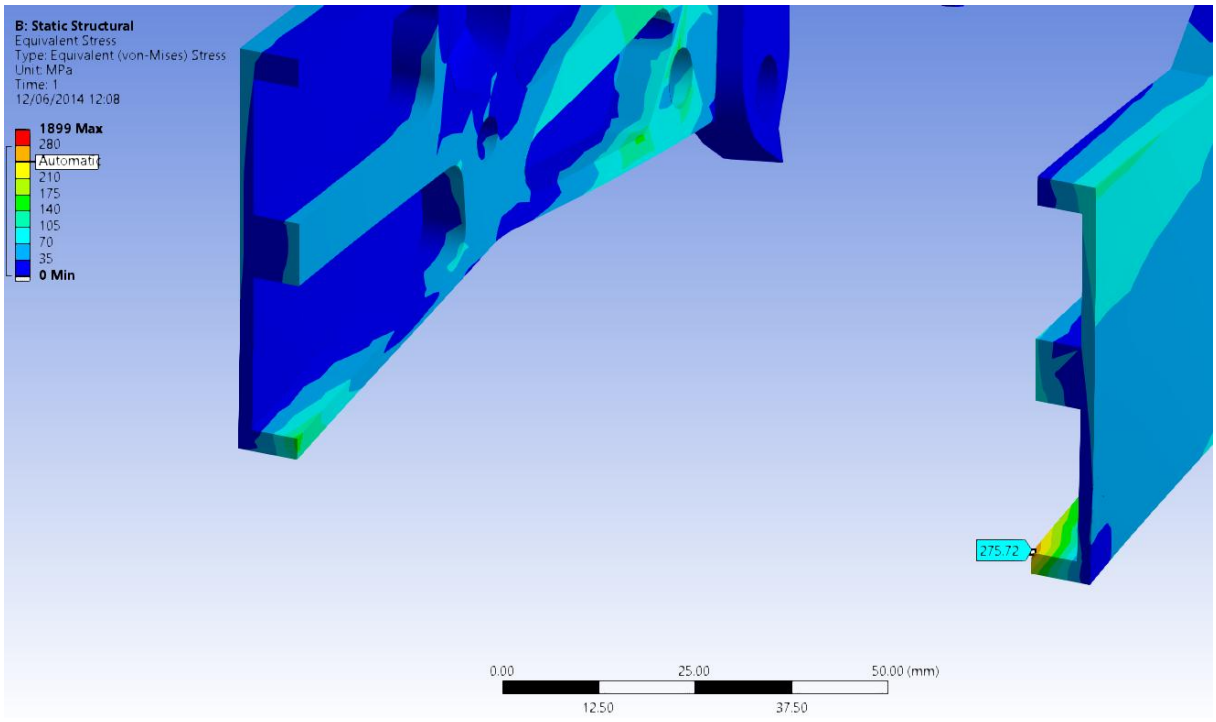

Figure 30 - Close up of cross section showing that max load in wheel carrier is only local

Fatigue

Materials exposed to cyclic stresses have a limited lifetime before fractures occur. For low loads this lifetime is practically unlimited, but for very light and highly stressed structures a used in velomobiles, fatigue is an important design criteria. For city and trekking bicycles the safety standard (EN-14764 2006) describes several fatigue tests. One test described in section D is specifically made for fatigue testing of wheel and tyre assembly:

The tyre shall have a pressure equal to 80% of the maximum tyre pressure as stated on the tyre wall and the wheel assembly shall be put on top of a rotating drum. The wheel axle is loaded to cause a force of 640 N onto the drum which is having a diameter between 500 to 1000 mm, see *Figure 31* and *Figure 32*. The surface of the drum is equipped with 10 mm thick and 50 mm wide chamfered slats with a circumferential distance of at least 400 mm between the slats on the drum. The drum is equipped with a motor that maintains a drum circumferential speed of 25 km/h +/- 10%. The drum propels the wheel for a period of 750 000 impacts from the slats onto the tyre/wheel assembly.

Another test in same standard specifies 450 N full load reversal, i.e. -100% to +100% load in the fatigue test for front forks, for 10^5 cycles.

As it is difficult to extract useful test criteria from these tests to match the wheel carrier design, a simulation of a fatigue test was done based on the same data as for the static load, with the exception that the sideways load was removed

The vertical load of 800 N was applied for a fatigue simulation with 0-100% load cycling, i.e. no load reversals, which showed a lifetime of 10^8 cycles. For the 25 year with 10 000 km per year that represents a full load cycle every 2.5 metre, slightly less than the distance covered by two turns of the wheel. A simulation report can be found in appendix D.

It is suggested that a fatigue test is done in the laboratory using real parts when they are available and that they are tested suitable standards. If no such standards can be found, a possible setup could be two times the perpendicular weight as measured on the wheel with nominal vehicle mass of 120 kg and 0-100% load cycling. A five days continuous test at 25 Hz, the specified max frequency for fork fatigue test in (EN-14764 2006), would return 10^7 cycles.

Another

Torque arm

To prevent the hub motor from unscrewing itself from the wheel carrier or overloading the wheel carrier attachment point for the motor axle, a torque arm on one or both sides of the motor is needed. An example of an existing torque arm made by author from surplus parts can be seen in *Figure 33*.

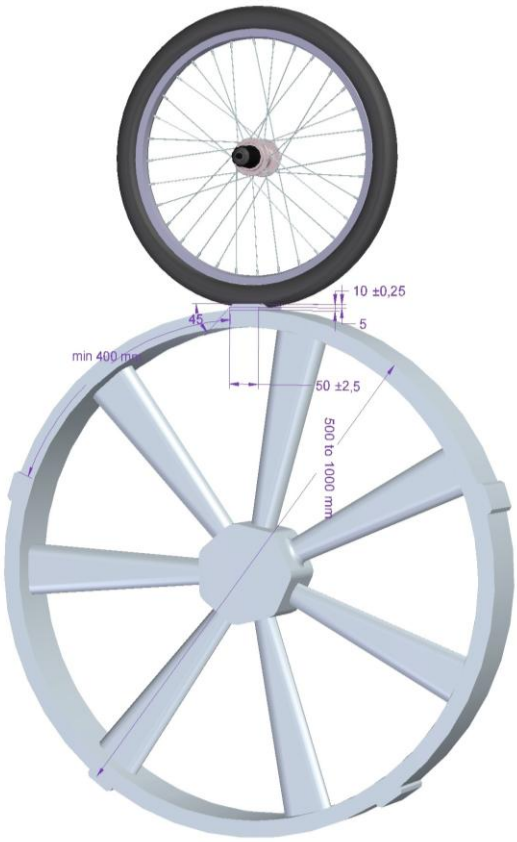

Figure 31 - EN 14764 Fatigue test jig

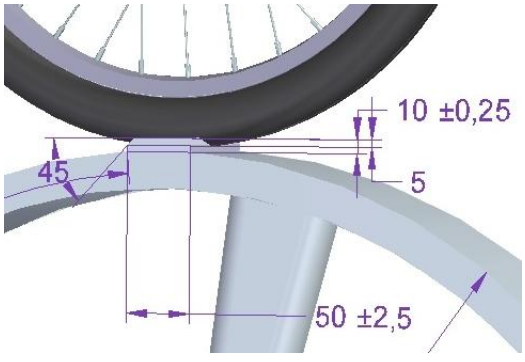

Figure 32 - Test jig details

Source: Model by author based on dimensions from EN 14764:2006 section D.1

Figure 33 - Hub motor torque arm

Source: Author

A torque arm with the added function of pretension has been specifically developed for the motor installation on this velomobile. It consists of a 1/4" thick (6.35 mm) 'G' shaped water/lasercut stainless steel plate. It has been designed to function even with large tolerances for low production cost. Pretension is by a use of a square nut with slanted sides. When this nut is forced into position, the torque arm will clamp the flats on the sides of the motor shaft, see *Figure 34*. With this pretension design there is no backlash when the motors changes torque direction. Without the clamping the repeatedly alternating between accelerating and braking will undo axle nuts over time.

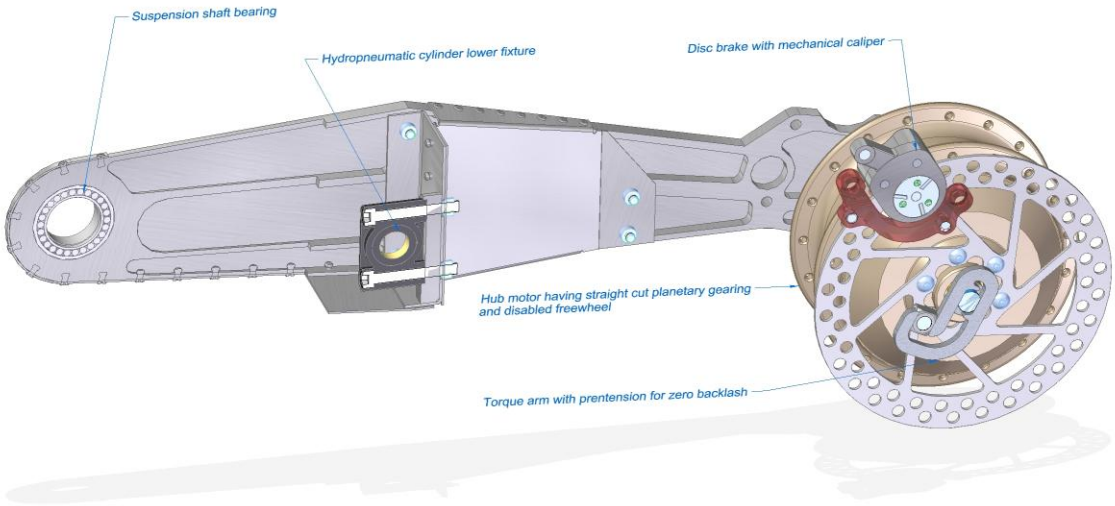

Figure 34 - Illustrative section of rear wheel carrier

Von Mises stress plot and total deflection of the torque arm due to pretension only is shown in *Figure 35*. Similar plots of the torque arm with 25 Nm axle torque is shown in *Figure 38*. As can be seen from these plots, showing stresses larger than 500 MPa in red, the part is highly stressed. This is on purpose to avoid precision machining and instead *bend* the part around the shaft. It might need to be slightly stronger, but there are several variables here that may reduce the stress; axle thickness, some torque taken by friction and wheel carrier slots, variable size of wedge nut, influence from HAZ - heat affected zone, material for the arm etc. The tiny edges on the part are for positioning the arm in correct place while allowing the motor cable to be thread in between.

There are torque arms on both sides of each motor. To make it fit in a narrow space, the torque arm is located on inside of wheel carrier on the brake side, while on the outside on the opposite side of the motor.

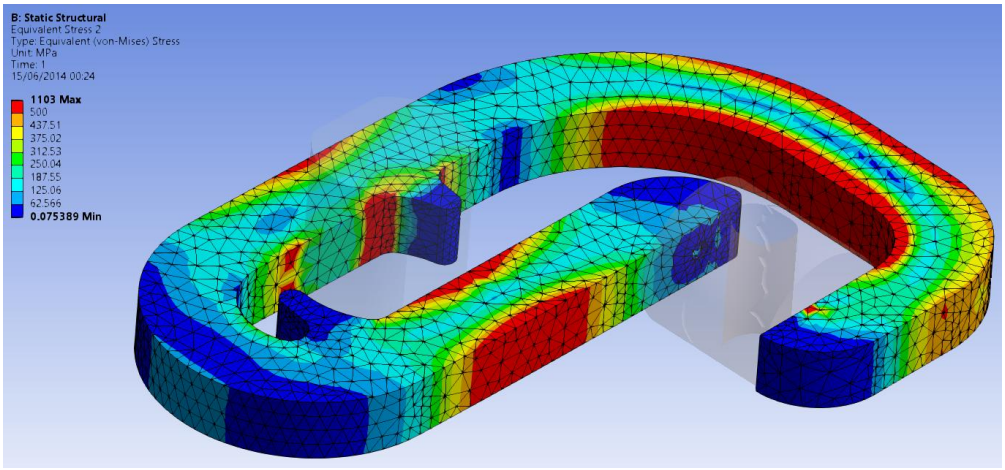

Figure 35 – Torque arm stress from pretension only

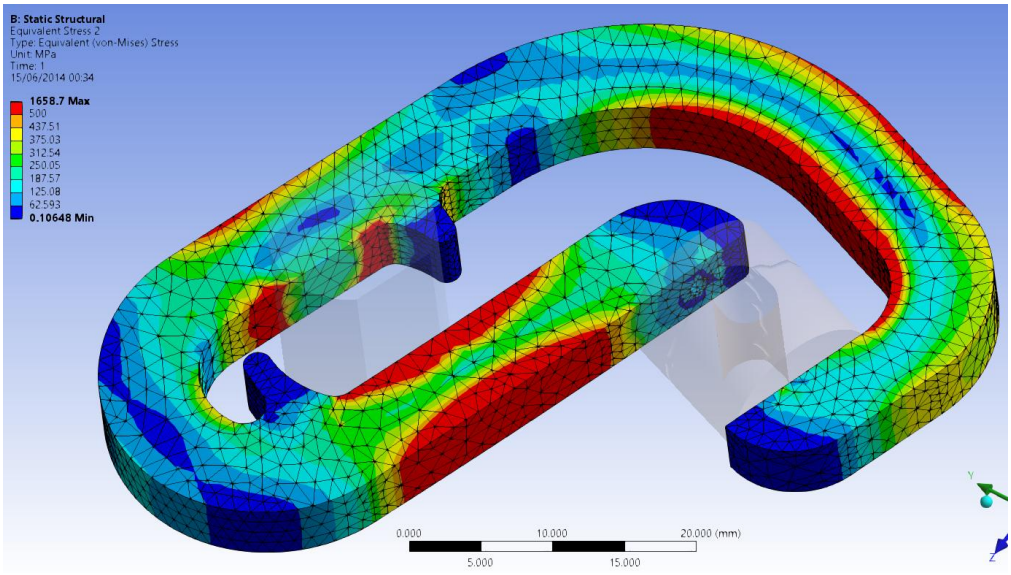

Figure 38 – Torque arm stress for pretension and 25 Nm torque

The attachment for the hydro-pneumatic lower fixture is a spherical shaft bearing made of polymer from *Igus Gmbh*. It is very light, still handles 3350 N for long periods and twice that for short durations. It also absorbs some vibration. The use of polymer ball joints has also been considered for the front suspension, but fail safe solutions has not been found. For the rear wheel carrier this problem is handled by securing with a strong plastic strip going thru the suspension attachment and the wheel carrier keeping them at least partly together in case of fault.

Detailed assembly drawing for the rear wheel carrier with parts including their mass can be found in appendix A.

Rear damper/spring unit suspension

A mechanism to achieve both a comfortable ride and ease of access has been developed by means of a hydro-pneumatic rear suspension. An extra long hydraulic piston and cylinder were required to achieve sufficient height adjustment, as shown in *Figure 36* and *Figure 37*.

This suspension unit use a rolling diaphragm between fluid and gas (air) to achieve a soft ride while having a progressive stronger suspension, common for hydro-pneumatic suspension systems {Bauer, 2011 #2} A cross section drawing can be seen in *Figure 39*. On top is a Schrader valve for air pressure control, while the fluid is filled via inlet underneath the diaphragm guide piston. A detailed assembly drawing of the velomobile hydro-pneumatic rear suspension can be found in Appendix A.

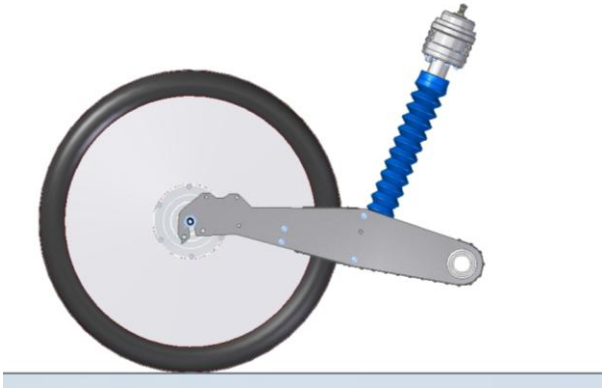

Figure 36 - Normal position

Figure 37 - Raised position

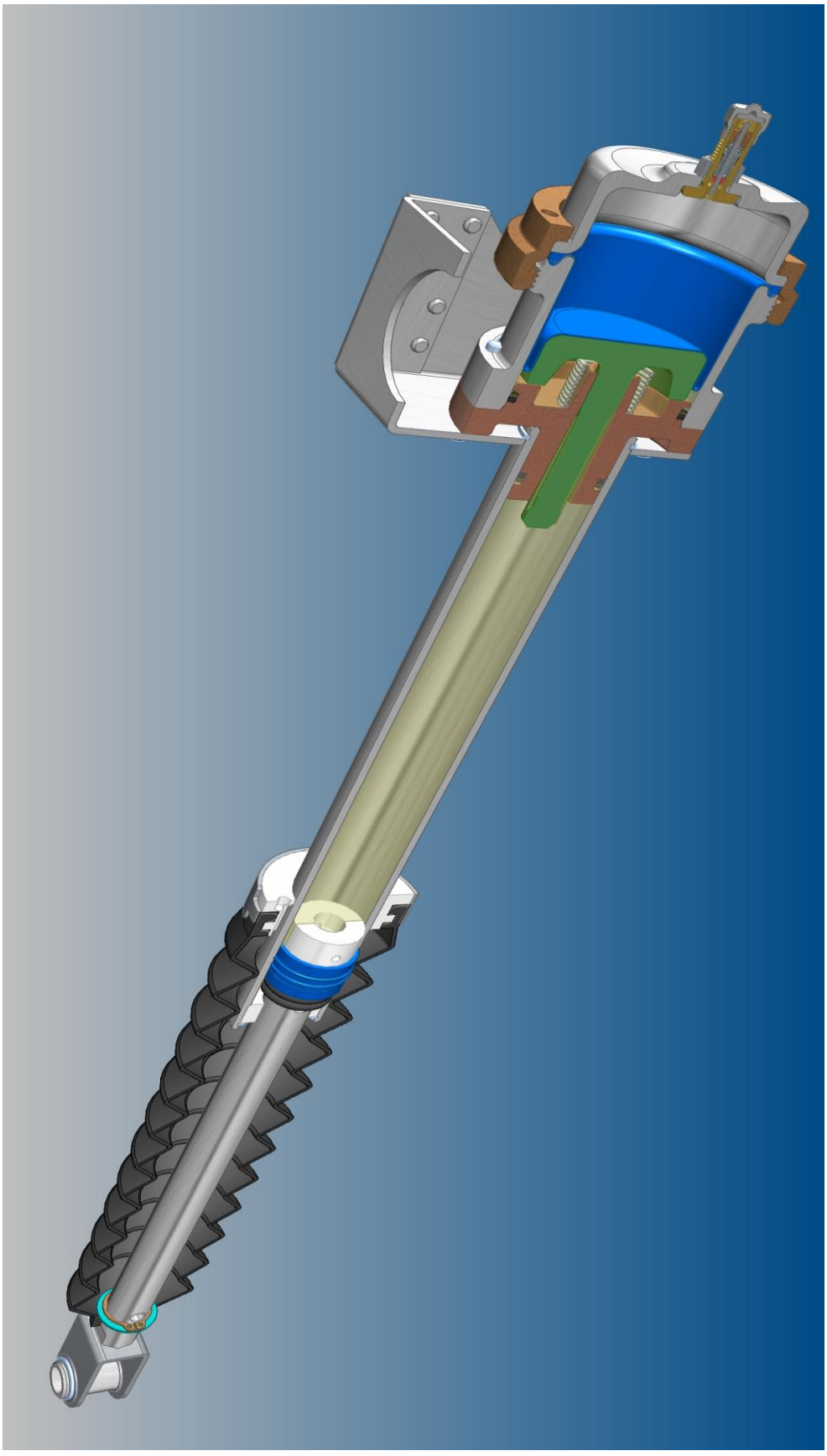

Figure 39 – Hydro-pneumatic suspension for velomobile

4.10 Electronic Transmission

The electronic transmission is a very important part of the veloquad construction. It removes the chain and the gearing, two of the most service intensive parts on a velomobile, and often the dirtiest as well. In addition, it simplifies the complexity of powering more than a single wheel on a velomobile. Having two motors adds little complexity in an electronic solution, and the added redundancy results in a more fault tolerant propulsion system.

Propulsion system overview
The schematic overview in *Figure 40* show the main modules of the propulsion system. The system functions as follows:

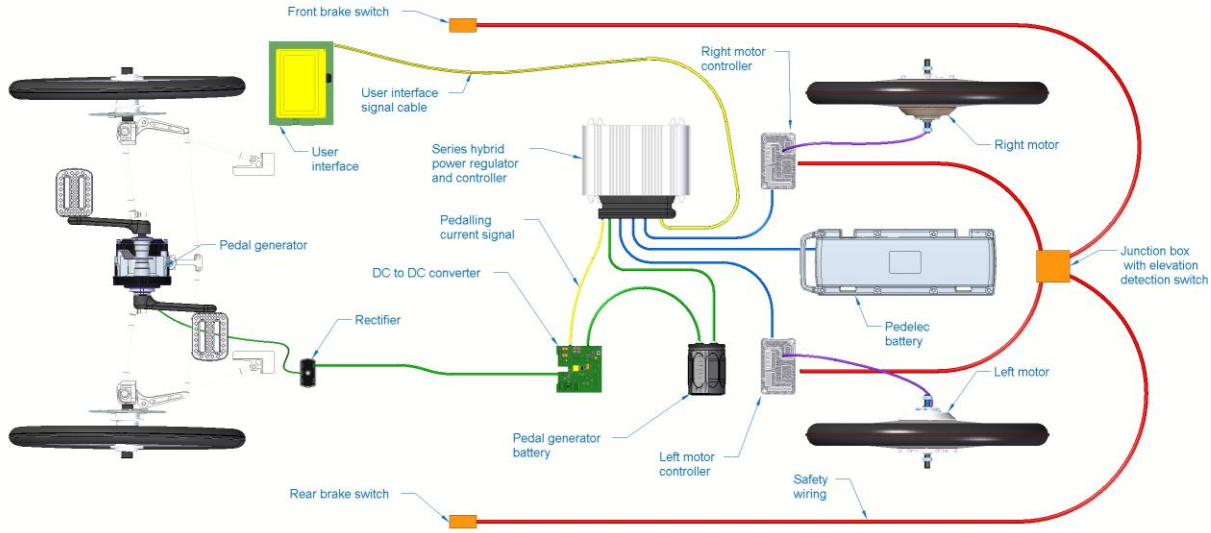

Figure 40 - Schematic overview of the propulsion system modules.

Green wires are energy supplied by the cyclist via the pedal generator. Blue is bidirectional power plus control signals. Violet is motor wiring. Red is safety override wiring which is normally closed. It is directly connected to the motor controllers and will disable the motor power if activated by one of the three override switches. Yellow wires are low power control signals.

1. When the cyclist spin the *Pedal generator* it generates three-phase alternating current, AC, to the *Rectifier*. The rectifier converts the voltage to direct current, DC, but with a variable voltage depending on the speed of the generator.
2. This variable voltage enters the *DC to DC converter* that is used to regulate the generator according to the cyclist preferences on speed and load, plus some feedback from the road [heavier uphill, lighter downhill, etc.]. The *DC to DC converter* is managed by the microcontroller inside the *Series hybrid power regulator and converter - SHPRC.* The *SHPRC* is configured via its *User* interface, a small display alternatively a smart phone or similar.
3. Power from the *DC to DC converter* goes to the *Pedal generator battery*. This battery supplies power to the motors via the *SHPRC* which makes sure that there is always some energy left in the *Pedal generator battery* by reducing speed, if the state of charge, SOC, goes under a certain threshold.
4. Each motor has its own *motor controller* that commutates the stator field of the connected brushless permanent magnet motor. The *motor controllers* are four-quadrant controllers able to both brake and accelerate in both directions of rotation, depending on input signals from the *SHPRC.*
5. Motors are driven by power from the *pedal generator battery* as long as this battery's SOC is within minimum level allowed by the *SHPRC.*
6. The *pedelec battery* supplies a variable amount of <u>additional</u> energy depending on user settings as long as all the following conditions are met:
   - speed is less than 25 km/h
   - there is less than 100% SOC in the Pedal generator battery
   - the cyclist pedals
7. If speed is less than 6 km/h, the vehicle can be propelled from the pedelec battery only, without pedalling, but only when the cyclist operates a manually activated control, selecting forward or reverse motion.

8. If any of the brake switches are operated at speed, positive motor torque is cut, and brake torque is applied by retarding the motors. Braking is preferably by proportional control from brake handle(s). Regenerative power shall only be used to charge the pedelec battery.

Pedal generator

This design implements a Japanese *Sunstar S03* crank motor modified to act as a pedal generator. The pedals powered by the cyclist turn the generator rotor via a fixed gear box that convert the pedal cadence of 60-100 RPM to a much higher speed. Generators with a reasonable low cost and mass, able to handle the required power typically need 1000 to 3000 RPM for highest efficiency.

The Sunstar motor has an intermediate axle with a freewheel so it use a two stage gearing, as illustrated in *Figure 41*. The gear from crankshaft to intermediate is straight cut with 70 teeth driving intermediate shaft with 10 teeth increasing pedal speed 7 times. The output from the intermediate shaft is a helical cut gear with 52 teeth driving the motor shaft with 10 teeth increasing the pedal speed 5.2 times more, resulting in a total gear ratio of 1:36.4. That gives the motor a speed of 3276 RPM when pedalling with a normal cadence of 90.

Since this was originally a crank motor it had to be modified at three points:

1. First the the motor freewheel was reversed by removing and reinstalling the gear marked with 52 [teeth] upside down, reversing the one way clutch located inside the gear.
2. Then the motor controller was replaced with a three phase rectifier
3. The pedal arms had to be swapped from left to right since the direction of rotation for the motor/generator now had changed. Pedals have different threads left and right to prevent them from unscrewing during usage

A step-up converter with fixed voltage output had also to be added to get 48V required for the battery independent on the cyclist pedalling speed.

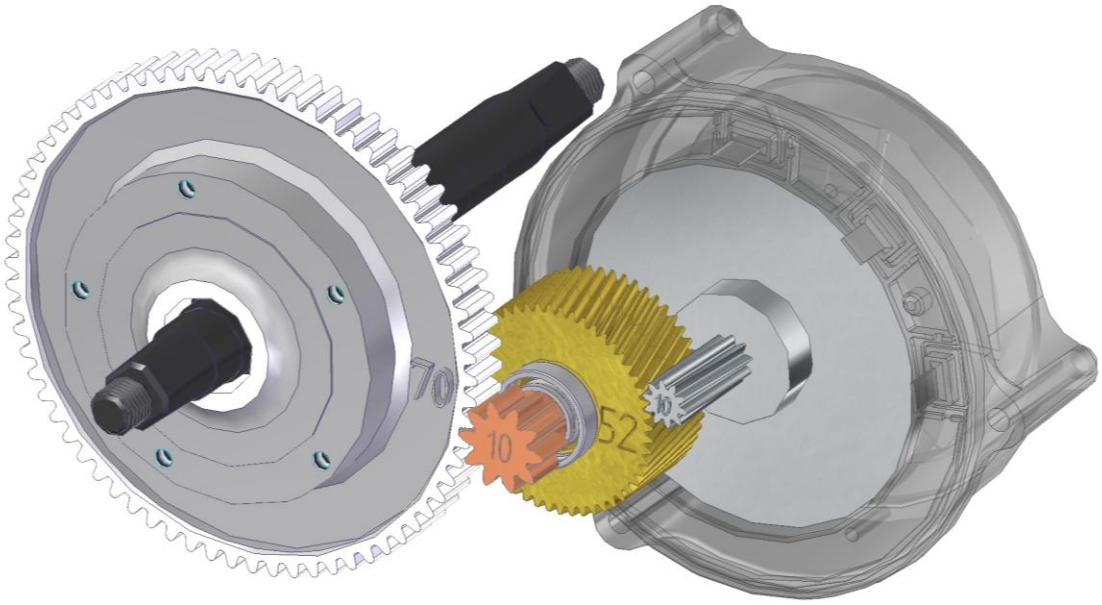

Figure 41 - gearing in pedal generator

Source: Grabcad with additional modelling by author

Generator battery

The pedal power is the only source of energy delivered to the generator battery. The generator battery is necessary for the electronic transmission to work, and it must do so independently of ambient temperature.

AMR23650B1 cells from *A123 Systems* LiFePO4 cells were chosen due to the wide temperature range supported for both charge and discharge cycles. In addition to this, these cells have a long lifetime and high current rating. The datasheet on these cells can be found in appendix G. Building this battery with 16 cells in series and two cells in parallel gives a battery that has ample energy for supplying high current for starting torque. The cells handle pair has a nominal operational voltage of 45V but goes up to 48V when fully charged and down to 42V when fully discharged.

Generator battery BMS

This battery need a BMS that has active balancing as discussed in section 3.5. This is vital since the battery is never connected to a charger which is required for regular pedelec BMS designs to do cell balancing. A 16S. or 16 cells in series, active balancing BMS developed by the author is described in appendix B. This BMS was especially designed for use with electronic transmission and has several levels of protection against damage to the cells.

Pedelec battery

The pedelec battery has a fully charged voltage of 56V but goes down to 42V when fully discharged. The energy consumption of the vehicle is low, around 5 Wh/km at max pedelec speed, so 0.5 kWh capacity should be enough for a 100 km effective range in the summer. However energy consumption goes up and available battery capacity goes down when temperatures are low so 0.8 to 1 kWh of nominal capacity is reasonable for a round-year vehicle. If the cyclist accepts more pedalling, a lighter pedelec battery with less capacity would be sufficient.

Most pedelec BMS lack the ability to turn off charge current via motor controller power connection to save cost. It is important for safety that the BMS used in the pedelec battery has the possibility to fully disconnect energy flow, otherwise the battery may be over charged when going downhill, which can destroy the battery, and can result in exothermal reaction leading to fire. The BMS design shown in appendix B avoid this having a fully bidirectional electronic switch.

Motor and motor-controller

The two motors are brushless DC motors requiring external commutation using three phase stator windings.
For optimum functionality in this application the motors must have their free-wheels disabled to be able to:

1. Do regenerative braking
2. Reverse the vehicle
3. Use the same motor construction on both sides of the vehicle while keeping a symmetric design (brake disc on inside etc.)

The selected motors are originally made as pedelec hub motors for front wheels with disc brake support. They are light, low cost, and fit in a space 100 mm wide. Rear motors are usually heavier and made to fit 135 mm wide space.

When you lock the freewheel on hub motors they are forced to handle bidirectional loads. Some motors use helical gears which runs more silent. Unfortunately, regular hub motors with helical gears have thrust bearings supporting motor loads in one direction only, see *Figure 42*. Current velo-

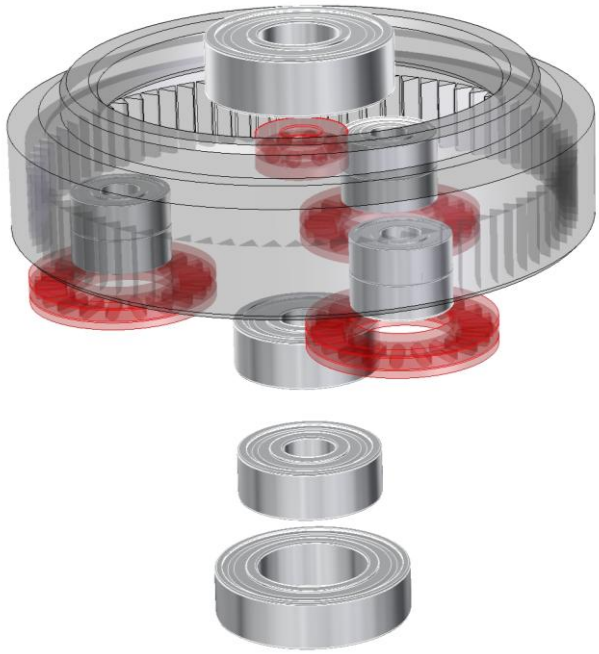

Figure 42 - Helical gears require extra thrust bearings (red)

The figure shows all the bearings in a CAD model of a hub motor with helical gears. All other parts except ring gear is hidden. To use this motor with bidirectional forces an extra set of thrust bearings must be added to the motor construction.

Source: Author

quad design uses hub motors with straight cut gears at the expense of slightly more noise. That is another reason why motors are located outside of the main body.

Commutation can be so-called *sensorless;* vector field based calculated in real time from continuous current and phase measurements from the three phases. Or *sensored;* a much less computing intensive algorithm using *hall sensors* inside the motor to detect exact position of the permanent magnet rotor where phases must be switched. Both work but the best is to use motor controllers supporting both. Sensorless gives least noise and best motor efficiency but needs a certain minimum speed to function. Up to that minimum speed it's nice to have hall sensors. Supporting both also gives the motor controller some fault tolerance. If sensors or the connection to them fails, the motor controller is still able to work, albeit with a simple open loop start-up control at low speed.

At high speed, for instance going down a steep hill, the induced voltage may exceed battery voltage and start to charge connected batteries via the motor controller transistors built-in body diodes. This means that the BMS must be able to disconnect motor current going in reverse[11]. It also means that the motor controller must be able to handle as high a motor voltage as can be generated from back EMF during downhill coasting. This voltage may easily exceed the maximum system voltage.

System controller and user interface

For the *hybrid power regulator and converter - SHPRC,* the electronic transmission controller, three rules are important. Here they are in prioritized order (for the Sci-fi addict, these rules will probably seem familiar[12]):

1. The electronic transmission must not cause any danger
2. Motor and generator must work seamlessly and under control of the cyclist
3. The controller must protect the electronic transmission parts from being destroyed

For safety systems; hardware beats software, especially when documentation for fail safe behaviour is required. For enhanced safety reliable micro-switches with suitable protection against ingress of dust and water are used.

It has been a tradition in pedelecs to have an electric switch built into the brake levers that cut motor power when activated. Normally this switch disables motor power directly by turning off the gate drivers for the power transistors. So it happens immediately and most pedelec motor controllers have this input. A requirement for such a switch does not exist but if there is one its function is formalized in (EN-15194 2011). The benefit for safety is obvious and is a reasonable requirement on the veloquad for both brake levers. In addition, there must be a similar switch for disabling motors when the hydraulic suspension is in raised position. Also a third override switch that is activated when the pedal generator has not been in use for a while is simple to implement in hardware.

These are safety systems that act independently of the software. In addition, a limp home mode should be available that takes electric power from the pedal generator and use it to diretly propel the motor in case of system controller malfunction.

For best possible riding experience the cyclist will require good feedback from the electronic transmission. Likewise, some data from the cyclist, like cadence, pedal torque, body temperature and heart rate would be helpful for the SHPRC to monitor. Not all, but maybe some, would enjoy a bidirectional interface between cyclist and vehicle. Electronic gearing, heart and cadence monitors and rear wheels with integrated torque and power recorders[13] are already in widespread use in bicycle racing.

For integrating the generator and motors with the cyclist there exist several patents and publications (Fuchs 1999, Spagnol, Alli et al. 2012). It is advisable to check out any possible patent infringements before making controller software. Verifying *freedom to operate* is vital in commercial exploitation of new technology. It is also important to check out how current electronic transmission implementations works. The *Mando Footloose* is a pedelec with electronic transmission. Although pricey at almost €4000 it is currently being sold in Asia, Europe, and North America. Nevertheless, testing this bike and possible others with similar propulsion systems will give valuable information on how control algorithms for a good electronic transmission should function.

[11] Most pedelec battery BMSes are made for non-regenerative use where this is not a problem. However, the BMS described in appendix B is designed to handle this well and can disconnect back EMF up to twice the nominal battery voltage.

[12] The famous science fiction author Isaac Asimov defined the vaguely identical *Three laws of Robotics in 1942*

[13] PowerTap has been available for more than

4.11 Parking

Vertical storage
A velomobile requires more space to park than bicycles. To remedy this potential drawback, the veloquad design allows storing the vehicle vertically, as shown in *Figure 26*. The velomobile is then using the same or less floor area than a bicycle. To make it easier to lift the velomobile to upright position, there is a handle underneath the ventilation inlet in front, and another handle on the underside. Motors and batteries are located far back to make it easier to raise the front and to help stabilize the velomobile when raised.

When raised vertically, the veloquad model stands on its rear wheel fenders and the center tail section. It could be beneficial to make cutout for the rear wheels so that it stands on the rear wheels instead of the fenders, increasing friction. The drawback is the increased risk of falling over with insufficiently inflated or flat rear tyres.

When storing several veloquads, for example for rental, it is suggested to store the velomobiles vertically in a storage carousel. With suitable design such a carousel could supply both storage and locking in a confined space, and be completely user operated for reduced operating cost. At outdoor locations the storage carousel could be equipped with solar panels supplying some or all of the electicity for charging the velomobiles. Such a carousel could also use motors on the velomobiles to power the carousel, for loading and unloading vehicles.

Locking
The vehicle has communication means that enables the electric transmission. Without the 'dongle', or 'key fob' or a standard smart phone, it is simply not possible to pedal or use the electric assist. In addition, the motor controllers short the motor phase wires. This brakes the motors very efficiently, preventing theft by someone trying to simply push the vehicle. It is a relatively light vehicle and can literally be carried away. To prevent this it must be secured to a fixed object with a padlock or similar. Three different locking positions are designated for this use. The handle in front for not so secure locking, a handle underneath is somewhat more secure but usually only available when stored vertically, and a strong spring-loaded wire in the rear end that retracts into the vehicle when not in use.
With suitable electronics, any tampering with the vehicle may send off a silent alarm via GPRS or similar wireless communication. In addition to a not so silent alarm locally, if necessary.
The pedelec battery is inside a lockable compartment underneath the child seat, preventing theft primarily by being difficult to locate, and requiring brute force to access. In addition, the battery need a charger, so it has not much value on its own.

Charging
Only the pedelec battery needs charging. This can be done in the vehicle using an external charge socket. For charging the temperature must be within the range required for the cell chemistry. That mean bringing the battery inside a heated building when the ambient temperature is too low.

As both a charging connector and specification for future functions it is suggested to support *EnergyBus*[14], a suggested light vehicle battery and charging standard for pedelecs and other small vehicles. Such a standard could improve accessibility for opportunistic charging without bringing your own charger, and hopefully define geometry for pedelec batteries and thereby enable a large market with batteries at a reasonable cost.

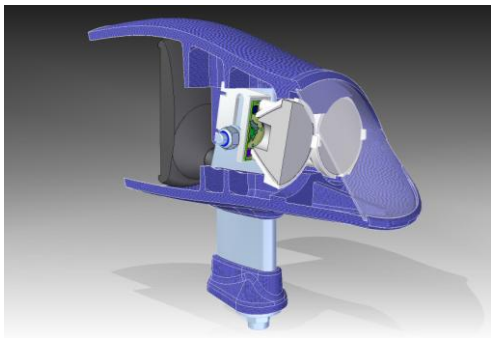

Picture 15 - Velo Mirrorlight has two 3W LED

Source: Author

4.12 Lights and other equipment

Running lights
The veloquad use four 3W LED in front, two on each side. They are located inside a housing originally designed for also containing a velomobile mirror from *B&M*. A cross section of one of the *Velo Mirrorlights* can be seen in *Picture 15*. A 3D model with necessary files for printing the three plastic parts can be found on the repository

[14] EnergyBus is possibly becoming an ISO standard, *ISO 61851-3-1, see www.energybus.org*

listed in section 4.3. Schematic and layout of LED current regulator capable of delivering constant current of 350 or 700 mA, depending on components chosen can be found in appendix B.

Rear lights

The plan is to use the translucent properties of the velomobile body to hide rear lights inside/behind the body for 'coolness' and lower drag. Alternatively, normal rear lights for ebikes with extended voltage range can be readily purchased [15]. A red rear reflex must be externally mounted as required by national cycle regulations.

4.13 Life Cycle Assessment

Producing, using, and finally, scrapping the velomobile makes an environmental impact. To evaluate this impact and to compare it with other means of transportation several methods exists. Such methods are called *life cycle assessments*. To help manage the necessary data for such evaluations, *Ecodesigner*, a report generator for Solid Edge from TRAYAK[16] has been used.

Assessment Method	Analysis Results Option	Default Indicators Shown (units)	Alternative indicators available for configuration
Eco-indicator 99	Damage Assessment	Human Health (DALY)	
		Ecosystem Quality (PDF)	
		Resources (MJ surplus)	
	Single Score	Single Score	
ReCipe	Damage Assessment	Human Health (DALY)	
		Ecosystem Quality (PDF)	
		Resources (MJ Surplus)	
	Single Score	Single Score	
TRACI 2	Selected Impact	Acidification (H+ moles eq)	Carcinogenics (kg benzene eq)
		Eutrophication (kg N eq)	Non Carcinogenics (kg toluene eq)
		Global Warming (kg CO2 eq)	Respiratory effects (kg PM2.5 eq
			Ozone Depletion (kg CFC-11 eq)
			Ecotoxicity (kg 2,4-D eq)
			Smog (kg NOX eq)
IPCC GWP 100a	Selected Impact	IPCC GWP 100a (kg CO2 eq)	
CML 2 Baseline 2000	Selected Impact	Acidification (kg SO2 eq)	Abiotic depletion (kg SB eq)
		Eutrophication (kg PO4 eq)	Ozone Layer depletion (kg CFC-11 eq)
		Global Warming (kg CO2 eq)	Human Toxicity (kg 1,4-DB eq)
			Fresh water aquatic ecotoxicity (kg 1,4-DB eq)
			Marine water aquatic ecotoxicity (kg 1,4-DB eq)
			Terrestrial ecotoxicity (kg 1,4-DB eq)
			Photochemical oxidation (kg C2H4)

Table 6 - Available methods and indicators in Ecodesigner

Source: *Ecodesigner* help screen, Trayak LLC

Ecodesigner

Ecodesigner can generate lifecycle impact reports based on five different impact assessment methods, as shown in *Table 6*. Which methods to chose depends both on the end use of the report and what exists of available data needed to make the assessment. The five available assessment methods supported by Ecodesigner are:

- Eco-indicator 99 (Goedkoop and Spriensma 2001)
- ReCipe Endpoint(Goedkoop, Heijungs et al. 2009)
- TRACI 2 (Bare 2002)
- IPCC 2007 GWP 100a (IPCC 2007)
- CML 2 Baseline 2000[17]

Each method offers damage values for example indicating:

- *Human health*
- *Ecosystem Quality*
- *Resources*
- *Acidification*
- *Global Warming*
- *Ozone Depletion*

[15] Grin Technologies supplies water proof (potted) rear and front LED lights handling wide operating voltages specially made for electric assisted cycles: www.ebikes.ca

[16] http://ecodesigner.trayak.com

[17] Based on various work at the *Institute of Environmental Sciences* (CML) at the *University of Leiden.*

Units most often used are:

DALY	*Disability adjusted life years where different disability causes by diseases are weighted*
PDF·m²·yr	*Potentially Disappeared Fraction from one m^2 area during one year*
MJ surplus energy	*Additional MJ energy required to compensate for lower future ore grade*
GWP	*Global Warming Potential in kg CO_2 equivalents*

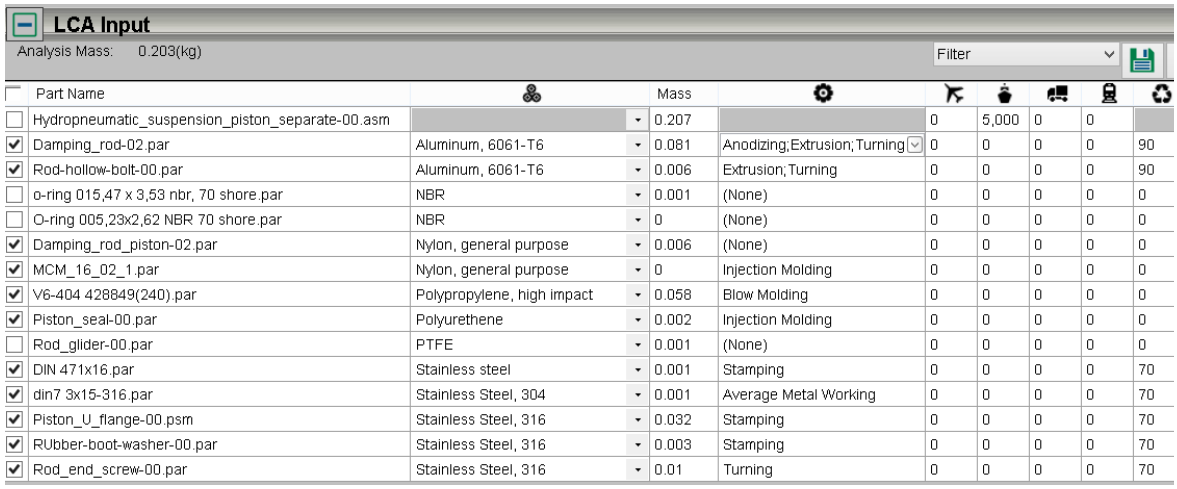

LCA Input

Analysis Mass: 0.203(kg) Filter

Part Name		Mass						
Hydropneumatic_suspension_piston_separate-00.asm		0.207		0	5,000	0	0	
Damping_rod-02.par	Aluminum, 6061-T6	0.081	Anodizing;Extrusion;Turning	0	0	0	0	90
Rod-hollow-bolt-00.par	Aluminum, 6061-T6	0.006	Extrusion;Turning	0	0	0	0	90
o-ring 015,47 x 3,53 nbr, 70 shore.par	NBR	0.001	(None)	0	0	0	0	0
O-ring 005,23x2,62 NBR 70 shore.par	NBR	0	(None)	0	0	0	0	0
Damping_rod_piston-02.par	Nylon, general purpose	0.006	(None)	0	0	0	0	0
MCM_16_02_1.par	Nylon, general purpose	0	Injection Molding	0	0	0	0	0
V6-404 428849(240).par	Polypropylene, high impact	0.058	Blow Molding	0	0	0	0	0
Piston_seal-00.par	Polyurethene	0.002	Injection Molding	0	0	0	0	0
Rod_glider-00.par	PTFE	0.001	(None)	0	0	0	0	0
DIN 471x16.par	Stainless steel	0.001	Stamping	0	0	0	0	70
din7 3x15-316.par	Stainless Steel, 304	0.001	Average Metal Working	0	0	0	0	70
Piston_U_flange-00.psm	Stainless Steel, 316	0.032	Stamping	0	0	0	0	70
RUbber-boot-washer-00.par	Stainless Steel, 316	0.003	Stamping	0	0	0	0	70
Rod_end_screw-00.par	Stainless Steel, 316	0.01	Turning	0	0	0	0	70

Figure 43 - Entering LCA data for CAD assembly
Source: *Ecodesigner* screen copy, Trayak LLC

Using Ecodesigner

When starting EcoDesigner, each part will automatically inherit LCA data based on the part material as defined in the CAD system. The user can then override the inherited LCA data if needed. There are several columns of data for each part, see *Figure 43*. The material, the production methods and the recycling columns are only available for parts, while the remaining columns also include assemblies. Transport distance have four columns, one for each mode of transport; air, sea, road or railway. This allows a mixed mode of transport for each item.

Recycling

Default value for recycling is 0[%]. Everything is then calculated as municipal waste and the impact is defined by the typical impact of the typical incineration and landfill split in the underlying database which is adapted to the selected region.

By changing the recycling value for a part, it will indicate the percentage of the part that is recycled back to base material, thereby reducing need for raw materials. In the suspension piston assembly listed in *Figure 43*, 90% of the aluminium is estimated to be recycled, while the stainless steel parts have only 70% of their material recycled.

Cost

Ecodesigner also includes a cost analysis function where the cost of each part can be calculated based on entered LCA data. That way the various options that influences the life cycle can also be compared on a cost basis. This function requires configuring the cost of the various production means and how they relate to the part's volume, surface or other parameter.

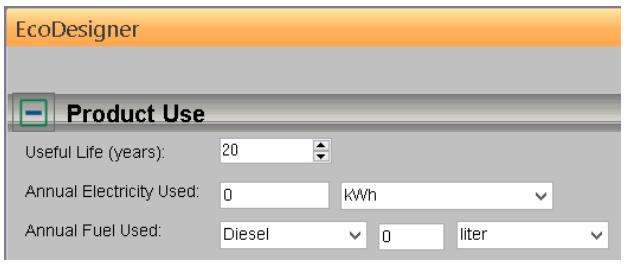

Figure 44 - Entering usage data
Source: *Ecodesigner* screen copy, Trayak LLC

Energy consumption in use phase

Ecodesigner can also be used to calculate the use phase impact based on the energy sources. Then the required amount of fuel and/or electricity is entered under the product use tab, see *Figure 44*. This is useful for many products. For vehicles with additional life cycle costs like maintenance, repair and spare parts, this added complexity is not possible to enter in the Product use tab in EcoDesigner. That is part of the reason why EcoDesigner cannot be used for LCA for the complete vehicle, only for the production phase.

Complex assemblies

For assemblies that does not exist in the CAD system as discrete parts, only as subassemblies, the LCA data must be entered into the database for each assembly. This made it difficult to do assessment on the complex assemblies. For assemblies that use defined materials, EcoDesigner is a very nice tool and give immediate results, see

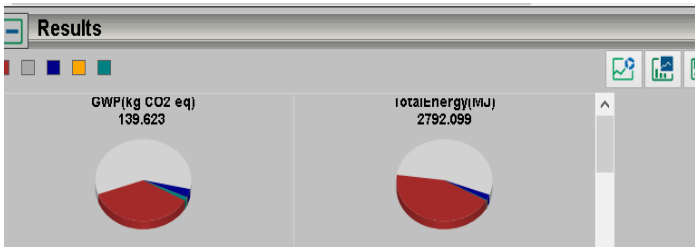

Figure 45 - Pie charts from EcoDesigner

Source: Ecodesigner screen copy, Trayak LLC

Comparing velomobile and car in the production phase

LCA values were extracted for the velomobile and can be found in appendix E. Due to the lacking material data for some parts, the extracted data are incomplete and invalid for a comparison. Assuming equal impact per mass unit for an 1500 kg electric car and the 50 kg velomobile, the electric car use 30 times more material. Based on this comparison, building and recycling a velomobile has only around 3% of the environmental impact compared to building and recycling a car.

Comparing velomobile and car in the use phase

For the use phase a simple calculation can easily be done:

- The design target of the vehicle is 25 years and 250 000 km. Estimating average lifetime of 20 year and 10 000 km / year seem fair enough.
- For the velomobile the estimated electric energy consumption is 10 Wh/km including 50% loss. This loss includes charger, BMS, ventilation, light, USB chargers etc., plus some loss in battery during storage. So the propulsion system ends up with 5Wh/km after losses. That matches available data for electric assisted velomobile (Sørensen 2010). These calculations also disregard any extra food, if required by the cyclist, due to pedalling.
- 10 Wh/km for 10 000 km per year is 100 kWh/year, 2000 kWh in total

An electric car consumes typically 200 Wh per km[18]. If assuming only one third of the losses compared to the velomobile, or 16.67% of the grid power received, each km require 0.24 kWh, or roughly 25 times as much electric energy. ICE cars are not directly comparable as they do not use electric energy, but in Norway, they typically use four times the energy per km compared to electric cars (Simonsen 2010). So it is not wrong to say that the velomobile is 25 to 100 times more energy efficient on transporting 1 adult and a child than a car.

That mean all electric energy necessary for travelling with this velomobile can be produced from a single low-cost solar panel[19]. With two pedelec batteries, the one not in use can be charged during the day.

[18] Consumption varies depending on car, usage, temperature road and weather.
[19] A low cost 160x90 cm solar panel can supply more than 110 kWh/yr with less than 10% conversion loss.

A unique high efficiency solution for personal transport within cities has been presented including technical details and reference materials. Several details can be further refined, including aerodynamics. The best is yet to come, building the real thing. Future possibilities are many including off-road capabilities, flood proofing and autonomity.

5. WHEN: Conclusions, lessons learned and further work

5.1 Conclusions

A repository of documentation on how to build an enhanced velomobile with high efficiency, low energy consumption and low lifecycle cost has been made. This documentation describes new solutions for velomobiles and it is the intention of the author to put on the market a vehicle with most if not all of the novel design elements described herewith. The *Veloquad* described has a unique set of qualities making it a truly revolutionary vehicle, not only evolutionary.

- The use of a series hybrid drive with two motors not only benefits a simpler drive train for a four wheeled vehicle. It also enables the use of low cost mass produced motors for pedelecs, a clean and uncluttered platform chassis, and easy adjustment of the pedals position relative to the cyclist. The suggested implementation enables the adoption to legislative rules within the European Union on electric assisted cycles.

- The adoption of high tech battery control system with active balancing and wide operating temperature is an enabling technology for the series hybrid electronic transmission.

- The suggested use of a thermoplastic self-reinforced composite for vehicle body parts is not new, but the use of such materials in velomobiles has not been described in available sources. This would also be a new solution, with large environmental benefits.

Nevertheless, the most important contribution is the hydro-pneumatic suspension system. This is the most important enhancement of the velomobile. It enables space efficient parking, low air drag and a smooth and comfortable suspension necessary for 'creature comfort' when riding. It makes the vehicle both practical and hopefully adds 'awesomeness'. If successfully performed, it will transform the *velomobile* from a rare oddity to "*I really want one"* class of vehicle. When that happens then this thesis has really been worthwhile.

This is a multi disciplinary engineering documentation bordering into science and research. It has been hard to target the information on a level suitable for the non-specialist. Some of the documentation requires deeper background in the various engineering fields. This has been put into the appendixes and only the conclusions and possible some informative illustrations have been kept in the main text. But the appendixes are not only meant for those who is skilled in the art. The appendixes also contains important and valuable information. It has simply been put there when the amount or depth of information made it unsuitable in the main text.

5.2 Lessons learned

A prototype is important and should have been made. But since this document is a master thesis having definite deadlines the prototype had to be postponed. Only some subassemblies and parts like pedal generator, front suspension, seats and batteries were ready.

It was the plan to first construct a prototype chassis that should be tested on a rolling road. Then a fitting body would have been first constructed in 3D, then be optimized for low air drag using CFD simulations and low mass

using FEA simulations. Transitional air flow is currently very resource consuming to simulate accurately. Improved turbulence models for CFD are still being developed. There is currently no magic CFD bullet that solves your problem. Real engineering problems need adaption of geometry and usually some tweaking of the flow models, requiring good knowledge of the relevant fluid problems and the implemented numerical solution's shortcomings for CFD to be useful.

Another important lesson is that people work for money. When calling or mailing companies for information as a student, it was often with negative result. This was very different from the author's experience with information gathering when working in the oil & gas industry. *'Money talks!'*

5.3 Further work

Much of the construction work has been done, but there is still much to do before all production documentation is ready. All production drawings and files must be finished and the total assembly must be completed in CAD and verified for fit, form & function before making the first vehicles.

An important issue that must be assessed is the production cost. Even though not quantified, cost has been in focus during design and construction. A low production cost is vital to broad success of the velomobile construction. How much it will cost is highly dependent on volume and how 'flat packed' the final product becomes. The two extreme options are a kit of unfinished parts or a complete vehicle. The current idea is a slightly disassembled for easier transport but otherwise ready for use. The level of complexity to be offered to end user need to be decided.

The current design is also not static. It can and must be further improved to achieve the necessary refinement. It is imperative for the vehicle to be tested by different persons in different environments and situations over time to verify durability and functionality. Experience from this test phase must then be used to implement improvements to the design, and retest before starting to mass produce the vehicle.

Improving CFD accuracy
CFD simulations that have been performed contain no details for doors, lights, fasteners etc. Only the basic shape has been simulated. A more detailed 3D model should be simulated to get an understanding of how these details influence drag, and, if possible, reduce the drag caused by such details by relocation or redesign.

CFD turbulence model used, k-ω-SST, uses a boundary layer function that is not optimized for flows containing large areas with transitional flow, i.e. laminar flow partially turning into turbulent flow. The relatively low vehicle speed of the veloquad results in transitional boundary flow. Simulating the body drag using a turbulence model capable of handling transitional flow with accuracy and should give a more realistic result.

Improving ventilation and reducing solar radiation
In direct sun heat load can overwhelm the ventilation capacity. To reduce amount of radiated heat the addition of retractable reflective shades inside the doors could be considered. Also a movable overhead shade, perhaps fabric thread on two thin wires attached to the inside of the canopy, over the cyclist's head should be considered.

Improving wheels
The current wheels take time to repair in cases of flats or broken spokes. *Flevobikes* makes a composite GRP 406 mm wheel with a bolt on flange, as shown in *Picture 16*. Using such wheels instead of

Picture 16 - Composite 406 mm wheel for velomobiles

Source: Author

spoked wheels will make it easy to repair flats if a complete spare wheel was brought along, as used in cars.

Fine tuning the current design

- Series hybrid generator can adjust torque (load) dependent on the pedal angle of rotation. This can be used to compensate for the natural torque ripple caused by humans' legs performing circular pedalling, thereby increasing human efficiency and stamina.
- Direction of pedalling could easily be reversed as tests have shown that this increase pedalling efficiency (Wilson, Papadopoulos et al. 2004)
- Pendulum, or string pedals could reduce the space needed for pedals, improve forward view and increase compatibility with different shoes.
- Windscreen wiper, manually operated to save mass and to avoid excessive wear on windscreen.
- Using plastic for the windshields makes use of windshield wipers problematic as they causes wear on the plastic surface. Adding a wear resistant coating or replaceable film on the windshield area being wiped could be a viable solution.
- Optimizing mechanical design for lower cost production
- Evaluating other self reinforced polymers than srPET
- ABS on rear wheels when doing regenerative braking could eliminate need for manual proportional control of electric braking
- The use of polymer ball joints for the front suspension will potentially save weight, cost and maintenance but need a solution to be fail safe.

Prototype
It is important to make a prototype as soon as possible as the project has now come up to a certain speed, and most of the expensive parts are in place.

Test equipment
It is important to test the electronic transmission including both hardware and software in a controlled environment. A rolling road is a valuable tool when testing control algorithms for the electronic transmission.
The best test environment would be a rolling road on a belt in a wind tunnel. University of Stavanger has been offered surplus ventilation fans from subsea tunnels by the local road traffic authorities. Several of these fans in parallel would likely be needed to make a suitable wind tunnel. Such a wind tunnel could be used for velomobile design but also for scale tests of wind turbines and other uses as well.

5.4 Future versions

Extending the market of the velomobile construction is possible by offering additional functionality.

Tilting velomobile
For higher cornering speed and improved road grip, the hydro-pneumatic suspension can be used to actively lean inwards in corners by transferring hydraulic fluid from inside to outside suspension cylinder. This would require adding hydro-pneumatic suspension also to front wheels and would increase complexity and cost of the vehicle. A well performing implementation of such a modification would likely be well received in the high end market and could demand a major price premium.

Flood proof transport
If motors, batteries and electronics were water resistant enough to be submerged without damage, the vehicle would be able to survive flooding. Flooding is likely to occur much more often in many areas due to climate change (IPCC 2014), so flood proofing is an attractive feature many places. Water proofing hub motors is relatively simple:

- Replace standard ball bearings with bearings equipped with waterproof seals as normally used on farming equipment.
- Make room for and install o-ring seals between housing and lid on motor
- Seal motor cable entry

- Install a semi-permeable breather valve on motor casing to pressure equalise inside of motor without letting water enter[20]

Water proofing electronics typically involve encapsulating the circuit boards within their casing using polymer compounds. Such compounds are typically two-component silicones or polyurethanes with mineral fillers to reduce cost and increase thermal conductivity. Encapsulation depends on heat removal needs. It can be either a thin layer of conformal coating typically used on control electronics or a complete potting often used in power electronics. Mixing is preferably done in special metering and mixing equipment to avoid air entrapment for optimum heat conductivity. Filling the casings is often done in a vacuum chamber where parts have been allowed to dry out for some time before potting. When applying ambient pressure after filling casing with compound in vacuum, the compound will enter even small cavities and bonds well to the electronic parts. For certain a compound like silicone priming is often required as well to achieve a good bonding. Without good bond between compound and parts water may leak into the seam, or joint. For further information on water proofing and encapsulation, *Edward R. Salomon's* book (1986) is a good reference.

Flood proofing batteries require that the batteries are inside a water tight compartment equipped with water tight cables with water proof connectors for power and signal. Connector for charging must be electrically disconnected otherwise galvanic corrosion will occur.

Off-road capability

With the following few changes the vehicle could easily go off-road:

- Increased ground clearance
- Wide BMX tyres
- Extra motors in front wheel hubs for AWD
- Bring COG to centre of vehicle by relocating batteries
- Remove or weaken anti-roll bars, if used

Wider tyres will increase energy consumption of the wheels caused by higher rolling resistance and more air drag. Water proof motors would need water proof bearing seals having higher friction than less capable seals used as standard on bike bearings.
Practicality will be reduced by making the front end heavier to lift. The higher COG due to increased ground clearance and weakened or removed anti-roll will increase risk of tipping when cornering.

Picture 17 - 559 mm fat bike tyre

Source: Author

For extreme all-terrain capabilities additional changes would most likely involve modification of chassis and the body. Large modifications would be necessary to traversing snow, marshes and smaller rivers:

- Shorter wheel base
- Water proofed motors
- Large 'fat bike' wheels as shown *Picture 17*
- Chassis and body water sealed up to a maximum water line

All-terrain capabilities are probably best to implement on a vehicle designed from scratch for proper optimization but the possibility exists to make a truly efficient all-terrain vehicle for civil and military use. Bicycle technology certainly has potential in extreme terrain. A 'tadpole' trike with 559 mm fat bike tyres was used by *Maria Leijerstam* on her the journey to the South pole in 2013 (BBC 2013). She travelled 800 km in 10 days and became the first person to ride a bike to the South pole.

Goods and ambulance transport

Strengthening and extending the chassis rearward from the rollover protection and replacing the rear body with a suitable platform increases transport capacity. If mentioned off-road capabilities has already been implemented,

[20] Example of suitable breather valve can be found in appendix G

the vehicle may be used off-road for transport of light goods, animals or as ambulance for an incapacitated person. This would require moving COG as far forward as possible by relocating the batteries, to avoid risk of tipping backwards. Also relocating the rear wheels farther to each side would improve stability and increase speed.

Autonomity

Many stakeholders are putting a lot of effort into making self-driving cars. Universities, defence agencies, and commercial companies like Nissan, Volvo, General Motors, Volkswagen and others use large resources on developing systems and algorithms capable of driving a car autonomously on public roads. Also Google has used massive resources on developing autonomous cars (Google).

However, the huge impact energy of a heavy vehicle travelling at speed requires very good collision avoidance systems. In traffic, an environment consisting of moving objects with often unpredictable trajectories, it is very resource intensive to travel at high speed. The cost of even very small errors when testing the autonomous systems in traffic can be prohibitive and prevent necessary testing in stochastic environments on public roads.

Google lack the car-centric motivation of other companies working on driverless cars. In May 2014 they published video and pictures showing their own prototype vehicles without steering wheels, brake and accelerator pedals as "they were not needed" (Markoff 2014), see also *Picture 18*. But, Google's new vehicle has a major drawback. It needs faultless autonomity to work. Putting on steering wheel and brake pedals for fault tolerance would then require the driver to have a driver's license.

It is much easier to implement and test autonomity on velomobile pedelecs. These very light human powered vehicles have a minimum of collision energy due to their very low mass, and moderate speed. So the legislative issues are much more forgiving as they are much less likely to cause severe accidents, see *Figure 46*

Also, the much lower average speed of the vehicle make it much easier to process positional and sensory data within the required timeframe, without impairing performance compared to self driven mode. This reduces the cost of the sensors and the control system.

To use a pedelec velomobile as a self driving vehicle, the rider must pedal to legally keep moving, having a built-in 'dead man's switch'. This offers the rider exercise according to individual needs and liking. The vehicle could follow a predetermined route programmed on a map or trained from via points from a previous trip using GPS, DGPS or similar navigational system. Or the vehicle could just follow the road as an auto pilot. Vehicle would need to automatically reduce speed or stop in case of obstacles, or if the rider stops to pedal.

With *vehicle to vehicle*, *V2V*, or *vehicle to grid*, *V2G*, communication, the vehicle could be part of a fleet, travelling together under guidance from a master vehicle or control system. This could enable persons with limited cognitive abilities to travel on tour by themselves or in a group. When not pedalling, or alternatively, hand-cranking the generator, the vehicle could still legally travel at speed up to 6 km/h if the rider get too tired. The vehicle could eventually be fully remote controlled which could be beneficial for riders with severe disabilities. Implementing this possibility would certainly raise some legal issues.

Picture 18 – Google self-driving vehicle prototype with no steering wheel or pedals

Source: Google

Figure 46 – Cuter than Google?

6. Bibliography

Andrea, D. (2010). Battery Management Systems for Large Lithium Ion Battery Packs, Artech House.

ApS, C. "Facts about PET." Retrieved 2014.05.09, 2014, from http://www.comfil.biz/products/new-products/self-reinforced-plastics/srpet.php.

Bambach, M. R. (2013). "Fibre composite strengthening of thin-walled steel vehicle crush tubes for frontal collision energy absorption." Thin-Walled Structures **66**: 15-22.

Bare, J. C. (2002). Developing a Consistent Decision-Making Framework by Using the U.S. EPA's TRACI, EPA.

Bauer, W. D. (2011). Hydropneumatic suspension systems. Berlin ; London, Springer.

BBC (2013). "Maria Leijerstam is first person to cycle to South Pole." Retrieved 2014-06-03, 2014, from www.bbc.com/news/uk-wales-25526541.

Bjørkli, A. and I. L. Gjeraldstveit (2013). Bachelor assignment: Modification of velomobile. Stavanger, Norway, University of Stavanger**:** 105.

Boer, P. d. (2009). Velomobiles in traffic. 6th European Seminar on Velomobile Design. Copenhagen, Denmark.

Booth, F. W. and M. Hargreaves (2011). "Understanding multi-organ pathology from insufficient exercise." Journal of Applied Physiology **111**(October): 2.

Caiazzo, F., et al. (2013). "Air pollution and early deaths in the United States. Part I: Quantifying the impact of major sectors in 2005." Atmospheric Environment **79**: 11.

CFD-Wiki (2014). "SST k-omega model." 2014, from http://www.cfd-online.com/Wiki/SST_k-omega_model.

Eastwood, T. (2004, 2008.11.28). "1.62 Miles - A short ride on a velocycle." 2008.11.28. Retrieved 2014.04.24, 2014, from 2008.11.28.

Edgar, J. (2009). Custom Bubble Canopies. Autospeed. Croydon North Vic 3136, Australia, Web Publications Pty Limited (ABN 38 084 463 507).

Elbilwiki (2014). "Electric car wiki (Norwegian) - Elbilwiki." Retrieved 2014.05.08, 2015, from http://www.elbil.no/wiki/Think:Batteripakke.

Embrandiri, M., et al. (2010). "Supercapacitor/Battery hybrid Powered Electric Bicycle via a Smart Boost Converter " World Electric Vehicle Journal **4**: 280-286.

EN-14764, C.-E. C. F. S. (2006). "City and trekking bicycles - Safety methods and test methods." 88.

EN-15194, C.-E. C. F. S. (2011). Cycles - Electrically power assisted cycles - EPAC Bicycles.

Fuchs, A. (1998). Trim of aerodynamically faired single-track vehicles in crosswinds. Third European seminar on Velomobile Design, Roskilde, Denmark.

Fuchs, A. (1999). Chainless Electrical Human-Power Transmissions and their likely Applications. 4th Velomobile seminar, Interlaken, Switzerland, Future Bike Switzerland.

Gloger, S. and H. John (1998). Investigation of the Passive Safety of Ultra Light Vehicles. Third European seminar on Velomobile Design, Roskilde Technical School, Denmark, Velomobile Forum.

Goedkoop, M., et al. (2009). ReCiPe 2008 A life cycle impact assessment method which comprises harmonised category indicators at the midpoint and endpoint level.

Goedkoop, M. and R. Spriensma (2001). The Eco-indicator 99 A damage oriented method for Life Cycle Impact Assessment Methodolgy Report. Amersfoort, The Netherlands, PRé Consultants b. v. **:** 132.

Google Self-Driving Car Test: Steve Mahan.

Heine, J. (2006). Bicycle Quarterly **5**(4): 1.

Herlihy, D. V. (2004). Bicycle: The History, Yale University Press.

Holter, Ø., et al. (2010). Fysikk og energiressurser (Physics and energy resources). Oslo, By the Authors.

Hwang, P., et al. (1998). Human-Powered Vehicles for Third-Agers as a Mode of Local Transport. Third European seminar on Velomobile Design, Roskilde Technical School, Denmark, Velomobile Forum.

IEC-60034-1 (2005). Rotating electrical machines Part 1: Rating and performance.

IPCC, I. p. o. c. c.-. (2014). Mitigation of Climate change (WGIII) - Summary for Policymakers Fifth Assessment Report (AR5).

IPCC, I. p. o. c. c. (2007). WGI: The Physical Science Basis - Direct Global Warming Potentials**:** Section 2.10.12.

Kármán, T. v. (1930). "Mechanische Ähnlichkeit und Turbulenz." Nachrichten von der Gesellschaft der Wissenschafen zu Göttingen **Fachgruppe 1 (Matematik)**(5): 58-76.

Kjeldsen, M. (2014). Low Re simulation (oral discussions).

Kjeldsen, M. (2014). Verification run of VELO14 in FLuent using k-omega SST. P. H. Sørensen.

Kollibay, I. and J. Neuss (2009). Four-Wheeled Velomobiles. The concept. 6th European Seminar on Velomobile Design. Copenhagen, Denmark**:** 30.

La Rosa, A. D., et al. (2013). "A Comparative Life Cycle Assessment of a Composite Component for Automotive " CHEMICAL ENGINEERING TRANSACTIONS **32**(2013): 6.

Lafford, J. (2000). "Rolling resistance of bicycle tyres." Human Power - technical journal of the IHPVA **50**(1): 5.

Lemire-Elmore, J. (2004). The Energy Cost of Electric and Human-Powered Bicycles**:** 10.

Markoff, J. (2014). Google's Next Phase in Driverless Cars: No Steering Wheel or Brake Pedals. The New York Times. California.

Masoner, R. (2013). "Cyclist killed by Tesla in Santa Cruz County." Retrieved 2014.04.24, 2014, from http://www.cyclelicio.us/2013/cyclist-killed-by-tesla-in-santa-cruz-county/.

Menter, F. R. (1993). "Zonal Two Equation k-ω Turbulence Models for Aerodynamic Flows." AIAA(93).

Mock, P., et al. (2013). From laboratory to road - A comparison of official and 'real-world' fuel consumption and co2 values for cars in Europe and the United States. Washington DC, USA, International council on clean transportation.

Musk, E. (2014). Tesla Adds Titanium Underbody Shield and Aluminum Deflector Plates to Model S. T. Motors. USA. **2014**.

NHTSA (2013). "National Highway Traffic Safety Administration crash test report." from http://www.safercar.gov/Vehicle+Shoppers/5-Star+Safety+Ratings/2011-Newer+Vehicles/Vehicle-Detail?vehicleId=7769.

NVV, N.-. (2012). Utsläpp av växthusgaser från inrikes transporter - Emission of GHG from domestic transport. Retrieved 2014.04.29, 2014, from http://www.naturvardsverket.se/Sa-mar-miljon/Statistik-A-O/Vaxthusgaser-utslapp-fran-inrikes-transporter/#.

Parsons, K. (2002). Human Thermal Environments: The effect of hot, moderate, and cold environments on human health, comfort and performance

Pesaran, A. A. (2001). Battery Thermal Management in EVs and HEVs: Issues and Solutions Advanced Automotive Battery Conference Las Vegas, USA**:** 10.

Puchelt, J. P. (2014). "J.P.'s Alleweder site." Retrieved 2014.04.24, 2014, from http://alleweder.jp-web.de/index.php?page=safety&lang=en.

RECOUP (2013). Recyclability by design. RECOUP. UNited Kingdom.

Rosen, E., et al. (2011). "Literature review of pedestrian fatality risk as a function of car impact speed." Accident Analysis and Prevention. **43**(1): 25-33.

Rotschild, D. d. (2011). Plastiki. New York, USA, Melcher Media.

Russo, F. (2014). "Eiviestretto - The World-Record-Speedbike." Retrieved 2014.05.01, 2014, from http://www.russo-speedbike.com/eiviestretto.html.

Salmon, E. R. (1986). Encapsulation of Electronic Devices and Components, CRC press.

Schmidt, T. (1994). What is HPV safety? Second European seminar on velomobiles/HPV, Laupen Castle, Switzerland, Future Bike Switzerland.

Schmitz, A. (2010). Cyclists Cycling Cycles & Cycle Parts.

Schuurman, M. (2013, 2013.08.22). "Latest work on VeloX3 (Dutch) - Laatste werkzaamheden aan de VeloX3." The Human Power Team Delft & Amsterdam. Retrieved 2014.05.01, 2014, from http://www.hptdelft.nl/nl/index.php?option=com_content&view=category&id=15&layout=blog&Itemid=58&limitstart=40.

Simonsen, M. (2010). Transport, energy and environment. - Final report *Norwegian* (Transport, energi og miljø. -Sluttrapport), Western Norway Research Institute (Vestlandsforskning)**:** 67.

Sims, I. (1998). Stability of Faired Recumpent Tricycles in Cross Wind. Third European seminar on Velomobile Design, Roskilde Technical School, Denmark, Velomobile Forum.

Smith, R. (2013). emails regarding low re and kt-kl-omega in Caedium

Sørensen, P. H. (2010). "What about an electric pedal car? (Norwegian) *Hva med en elektrisk trøbil?* ." Electric bikes and motorcycles. Retrieved 2014.05.05, 2014, from http://elbilforum.no/forum/index.php/topic,2707.0.html.

Sørensen, P. H. and M. Hellon (2009). High efficiency bicycle propulsion system using two motors and epicyclic gearing. Electric Vehicle Symposium - EVS24, Stavanger.

Spagnol, P., et al. (2012). A full hybrid electric bike: How to increase human efficiency. American Control Conference (ACC). Montreal**:** 2761 - 2766.

SSB, S. S.-. (2012, 2014.04.29). "Emissions of greenhouse gases, 1990-2012, final figures." 2014.01.30. from http://ssb.no/natur-og-miljo/statistikker/klimagassn/aar-endelige/2014-01-30?fane=tabell&sort=nummer&tabell=160420.

Tamai, G. (1999). The Leading Edge - Aerodynamic Design of Ultra-streamlined Land Vehicles. Cambridge, MA, USA, Bentley Publishers.

Taylor, T. A. and K. Blake (1998). Designing a practical Velomobile for the Next Century. Third European seminar on Velomobile Design, Roskilde Technical School, Denmark, Velomobile Forum.

Versteeg, H. and W. Malalasekera (2007). An Introduction to Computational Fluid Dynamics:The Finite Volume Method, Prentice Hall.

Wächter, M., et al. (1998). Measurement and Simulation of the Vibrational Stress on Cyclists. Third European seminar on Velomobile Design, Roskilde Technical School, Denmark, Velomobile Forum.

Walle, F. V. D. (2004). The Velomobile as a Vehicle for more Sustainable Transportation. Department for infrastructure. Stockholm, Sweden, Royal Institute of Technology. **Master of Science:** 104.

Walters, K. and D. Cokljat (2008). "A Three-Equation Eddy-Viscosity MOdel for Reynolds-Averaged Navier-Stokes Simulations of Transitional Flow." Journal of Fluids Engineering **130**: 14.

WHO (2014). Obesity and overweight - fact sheet 311.

Wilson, D. G. (1994). What safety measures are needed for HPVs? Second European seminar on velomobiles/HPV, Laupen Castle, Switzerland, Future Bike Switzerland.

Wilson, D. G., et al. (2004). Bicycling science. Cambridge, Mass., MIT Press.

Zetterström, S. (1998). Wheel suspension arrangement in a vehicle. PCT.

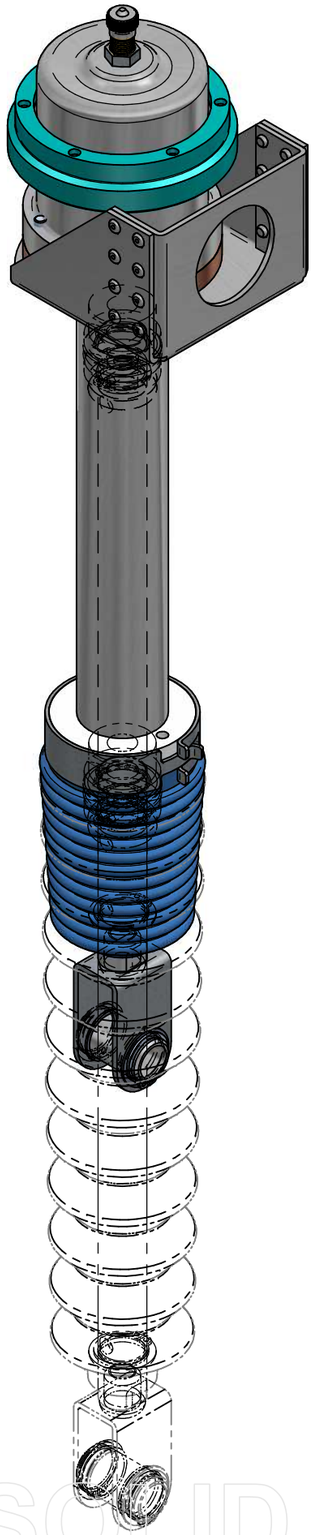

12

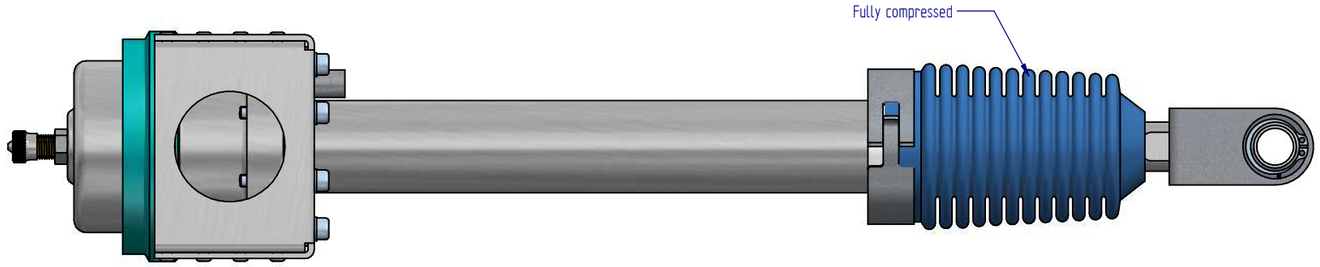

12

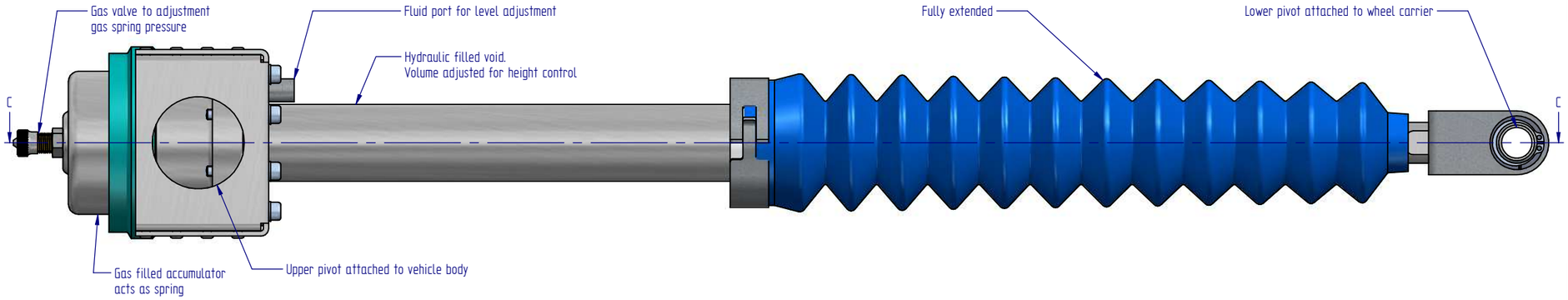

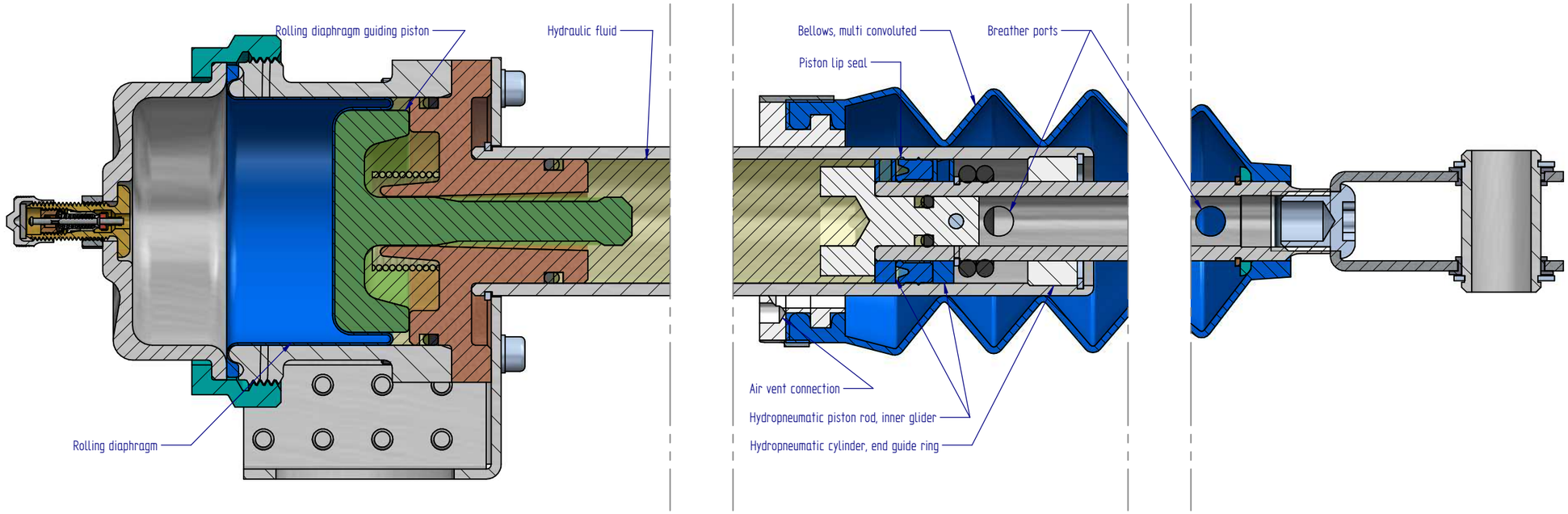

SECTION C-C
1:1

Weight	Volume
986,0 g	462,0 cm^3
Material specification	

Hydropneumatic spring & damper assy

Unless otherwise noted:

All edges to be deburred
All dimensions in mm
Surface roughness, Ra in um:
Dimension tolerances according to ISO 2768-1 class:

Sheet size	Projection	Scale
A3		1:1 unless noted

UIS_MTVR-ASM003-02-B

Sheet: 1 of 2

Velomobile:Redefined
Per H. Sørensen
University of Stavanger

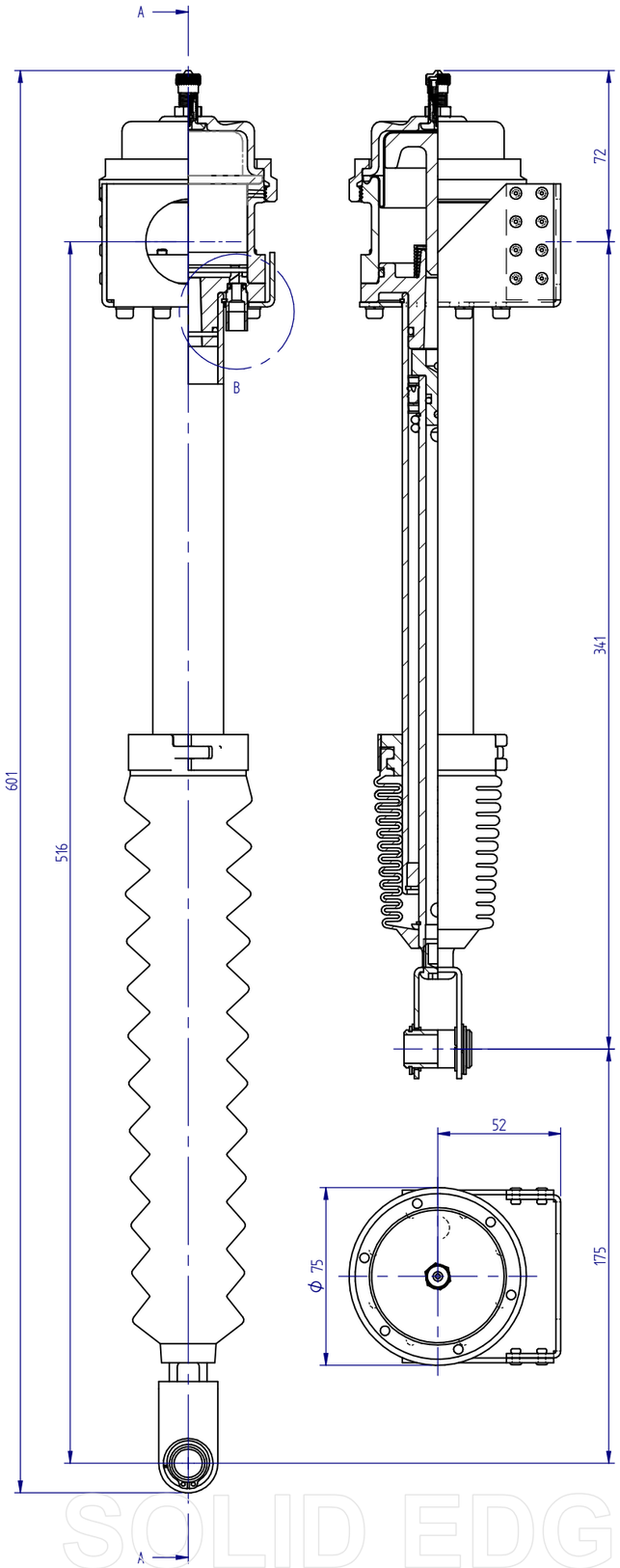

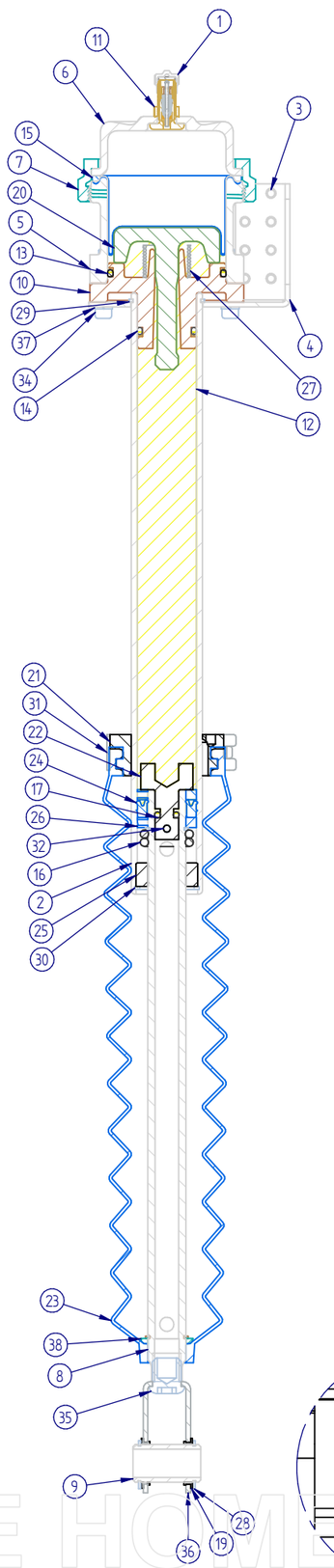

SECTION A-A

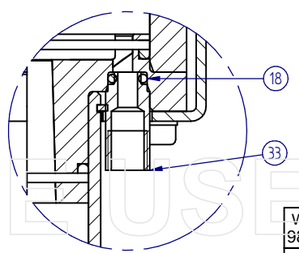

DETAIL B

Item	Title	Document Number	Qty	Material	Material grade	Mass (Item)	Mass (Qty)
1	Schrader 50bar valve assy	Schrader OEM	1			9,2 g	9,2 g
2	Hydropneumatic cylinder, ID25	UIS_MTVR-PAR104	1	Aluminum, 5050		145,1 g	145,1 g
3	Blind rivet	Popnail Ø3.2 L6	16	Aluminum, 5050		0,3 g	4,8 g
4	Hydropneumatic spring & damper, top bracket	UIS_MTVR-PSM101	1	Aluminum, 5050		70,5 g	70,5 g
5	Hydropneumatic accumulator, center	UIS_MTVR-PAR101	1	Aluminum, 6061-T6		107,4 g	107,4 g
6	Hydropneumatic accumulator, top	UIS_MTVR-PAR102	1	Aluminum, 6061-T6		54,0 g	54,0 g
7	Hydropneumatic accumulator, screw ring	UIS_MTVR-PAR103	1	Aluminum, 6061-T6		46,7 g	46,7 g
8	Hydropneumatic piston rod	UIS_MTVR-PAR109	1	Aluminum, 6061-T6		81,1 g	81,1 g
9	Hydropneumatic piston rod, end bracket bolt	UIS_MTVR-PAR112	1	Aluminum, 6061-T6		6,5 g	6,5 g
10	Hydropneumatic accumulator, base	UIS_MTVR-PAR114	1	Aluminum, 6061-T6		97,5 g	97,5 g
11	Scharder valve, external nut	NA	1	Brass, yellow brass		1,5 g	1,5 g
12	Hydraulic fluid	TBD	1	Hydraulic fluid		102,7 g	102,7 g
13	seal	o-ring	1	NBR		1,1 g	1,1 g
14	seal	o-ring 20x2.6	1	NBR		0,5 g	0,5 g
15	Rolling diaphragm	Simrit BFA 50 45 40 2365	1	NBR	50 NBR 253	6,4 g	6,4 g
16	o-ring	o-ring 15.47 x 3.53	2	NBR	N674-70	0,7 g	1,4 g
17	o-ring	O-ring 5,23x2,62	1	NBR	N747-75	0,2 g	0,2 g
18	o-ring, Parker 2-008, 4,47x1,78	Parker # 2-008	1	NBR, 70 sh	N674-70	0,1 g	0,1 g
19	Polymer slide bearing, Ø17, for sheet T=2	IGUS MCM 16-02	2	Nylon, general purpose		0,3 g	0,6 g
20	Guide piston for diaphragm	UIS_MTVR-PAR107	1	Nylon, general purpose		24,1 g	24,1 g
21	Bellows holder, with vent port	UIS_MTVR-PAR108	1	Nylon, general purpose		15,1 g	15,1 g
22	Hydropneumatic piston, end plug	UIS_MTVR-PAR110	1	Nylon, general purpose		5,9 g	5,9 g
23	Bellows, multi convoluted	Simrit V6-404 428849	1	Polychloroprene		77,7 g	77,7 g
24	Piston lip seal	OD 30	1	Polyurethene		1,8 g	1,8 g
25	Hydropneumatic cylinder, end guide ring	UIS_MTVR-PAR106	1	PTFE	Unfilled	4,0 g	4,0 g
26	Hydropneumatic piston rod, inner glider	UIS_MTVR-PAR111	2	PTFE	Unfilled	1,2 g	2,4 g
27	Guide piston spring	UIS_MTVR-PAR115	1	Stainless steel	Spring temper	5,3 g	5,3 g
28	lock ring, external	DIN 471 Ø16	4	Stainless steel	Spring temper	0,7 g	2,9 g
29	Lock ring, external, Ø30	DIN 471 Ø30	1	Stainless steel	Spring temper	1,5 g	1,5 g
30	Seeger ring, for bore, 19mm	DIN 472 19mm	1	Stainless steel	Spring temper	1,6 g	1,6 g
31	Hose clamp, self energized, Ø48		1	Stainless Steel, 304		23,7 g	23,7 g
32	Parallel Pin	DIN 7, OD5 L15	1	Stainless Steel, 304		0,8 g	0,8 g
33	Fluid port hose connection	UIS_MTVR-PAR105	1	Stainless Steel, 304		7,2 g	7,2 g
34	bolt	DIN 912 M4x25	8	Stainless Steel, 316		3,5 g	28,2 g
35	Bolt, M12x1.5 L12, for rod end	UIS_MTVR-PAR113	1	Stainless Steel, 316		9,7 g	9,7 g
36	Hydropneumatic piston rod, end bracket	UIS_MTVR-PSM102	1	Stainless Steel, 316		31,9 g	31,9 g
37	Spring Washer	DIN 127 M4	8	Stainless Steel, 316	A4	0,2 g	1,8 g
38	Washer with rounded outer edge	Washer ID16 OD20	1	Stainless Steel, 316	A4-80	2,5 g	2,5 g

Weight	Volume
986,0 g	462,0 cm^3
Material specification	

Hydropneumatic spring & damper assy

Unless otherwise noted:

All edges to be deburred
All dimensions in mm
Surface roughness, Ra in um:
Dimension tolerances according to ISO 2768-1 class:

Sheet size	Projection	Scale
A3		1:1 unless noted

UIS_MTVR-ASM003-02-B

Sheet: 2 of 2

Velomobile:Redefined
Per H. Sørensen
University of Stavanger

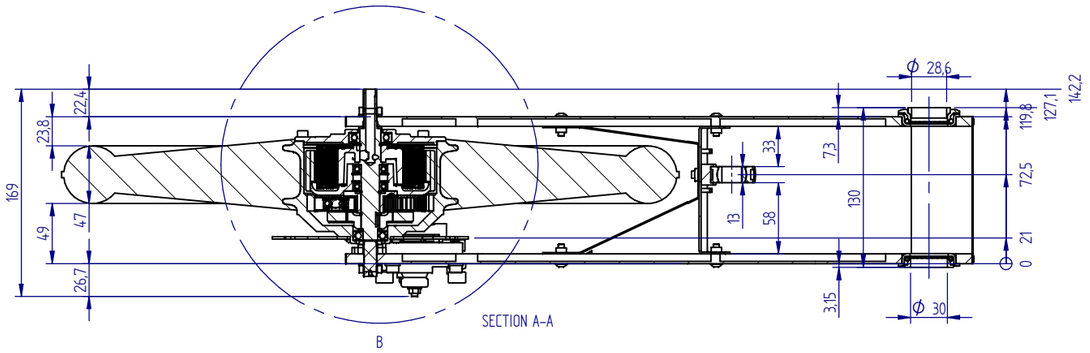

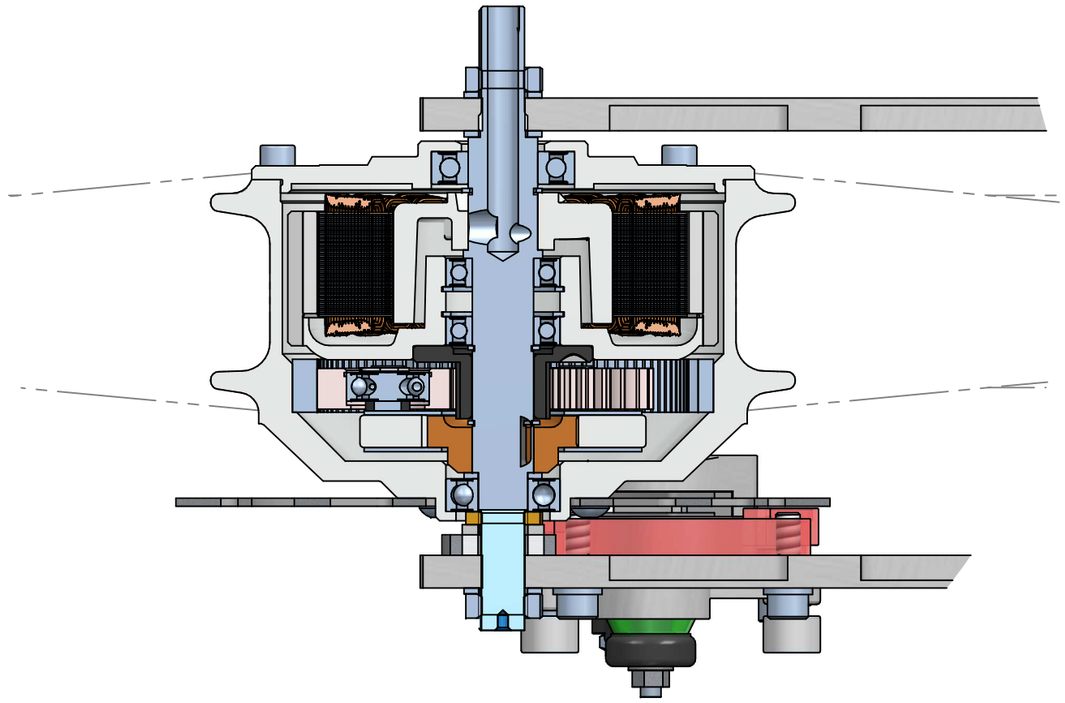
DETAIL B

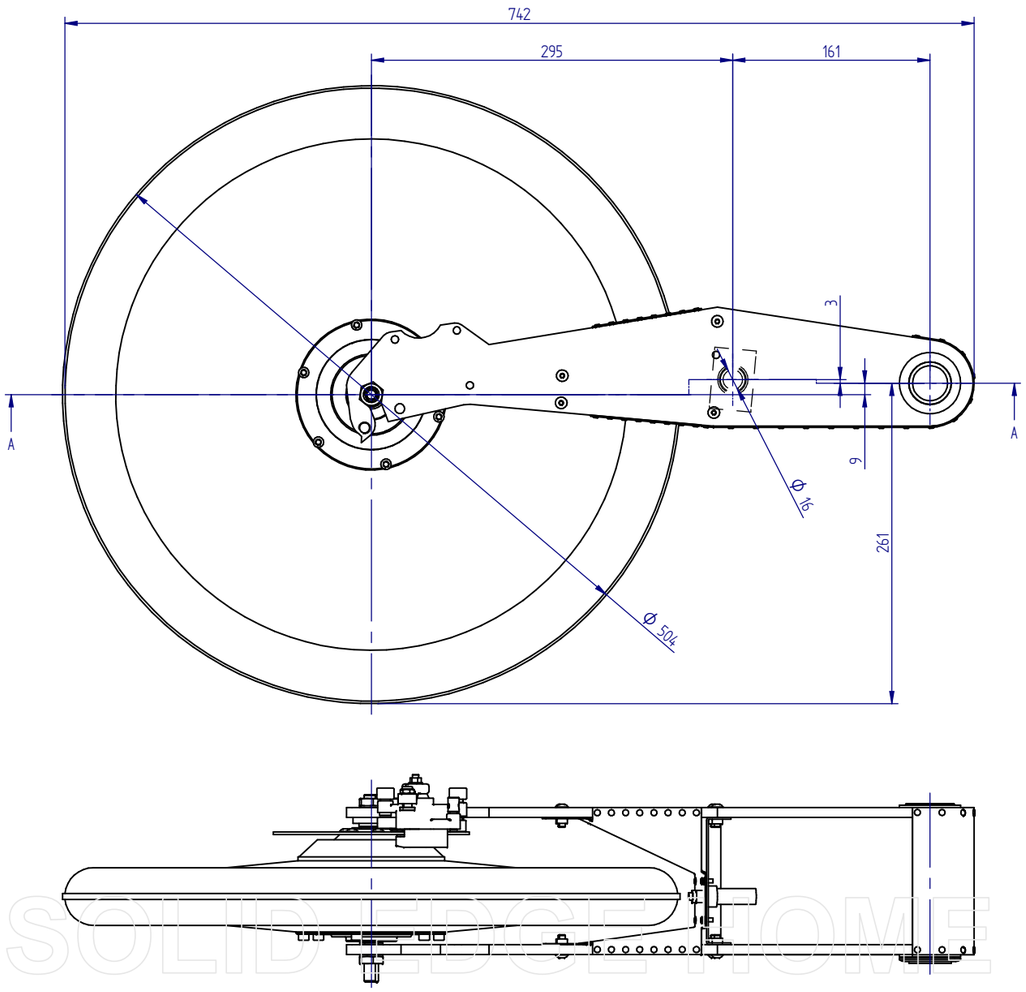

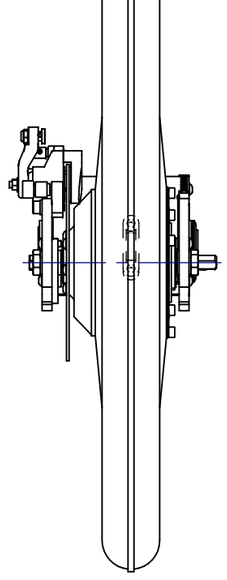

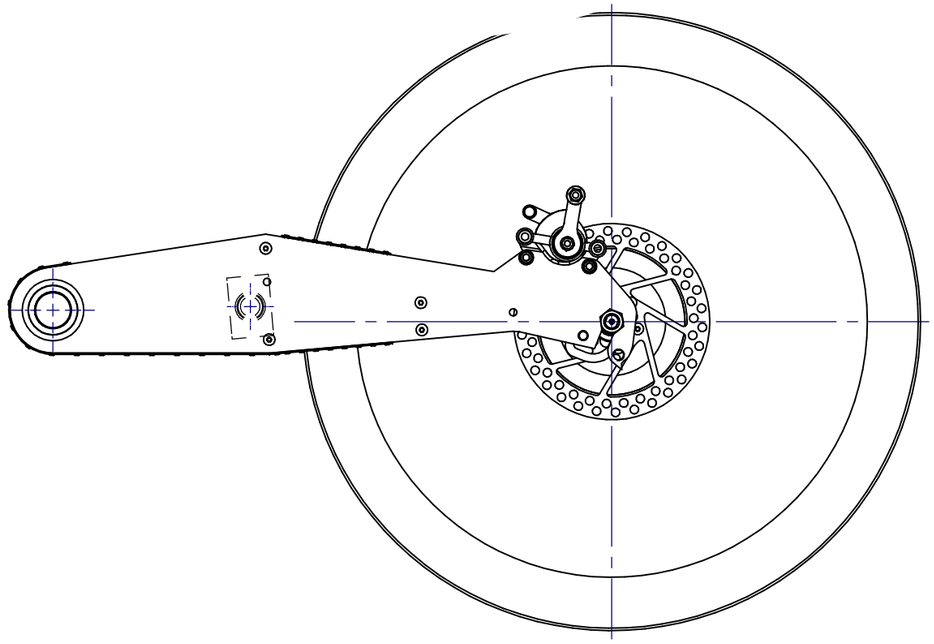

Weight	Volume
5831.3 g	8671.4 cm^3

Material specification

Rear Suspension assembly, right

Sheet size	Projection	Scale
A3		1:1 unless noted

UIS_MTVR-ASM001-11-B

Sheet: 1 of 2

Unless otherwise noted:

All edges to be deburred
All dimensions in mm
Surface roughness, Ra in um:
Dimension tolerances according to ISO 2768-1 class:

Velomobile:Redefined
Per H. Sørensen
University of Stavanger

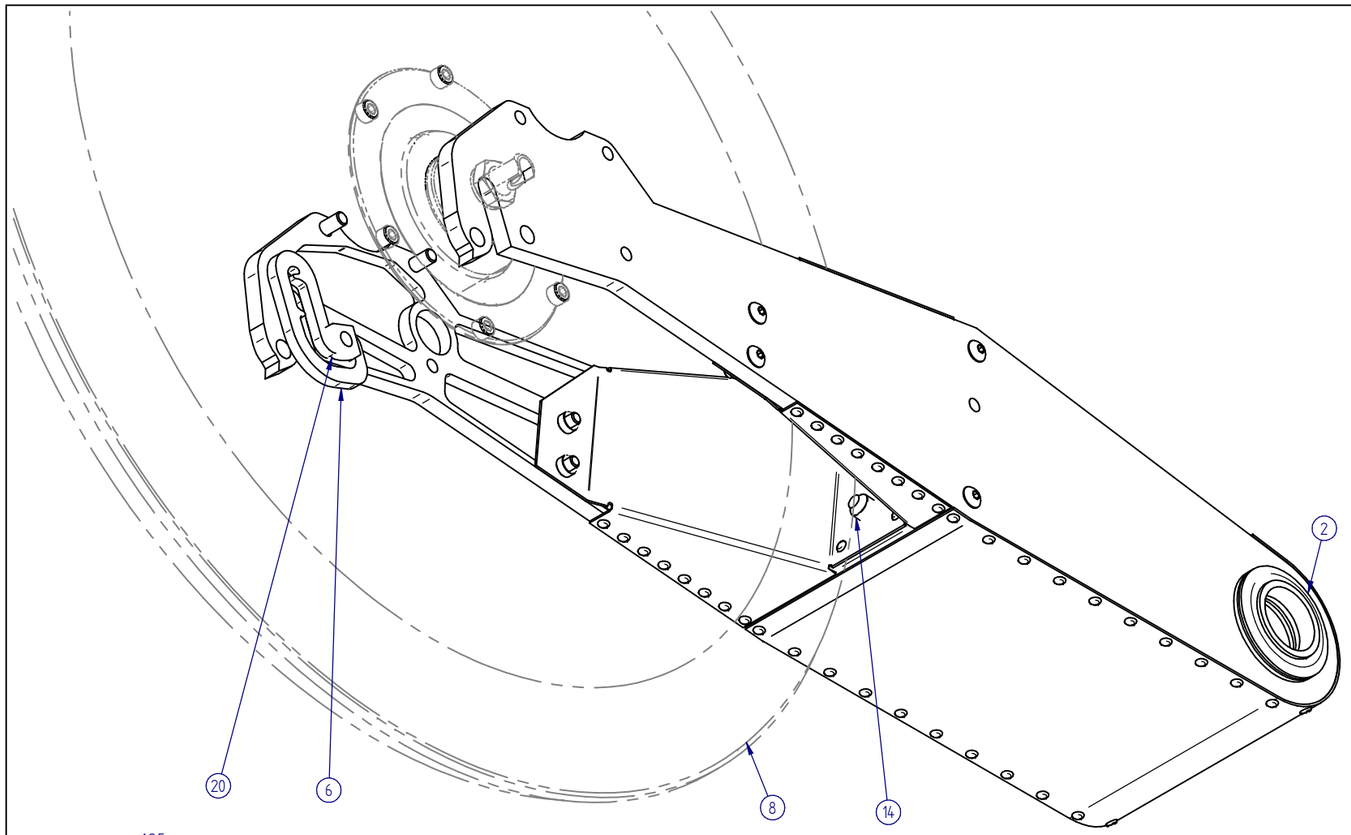

1:2.5

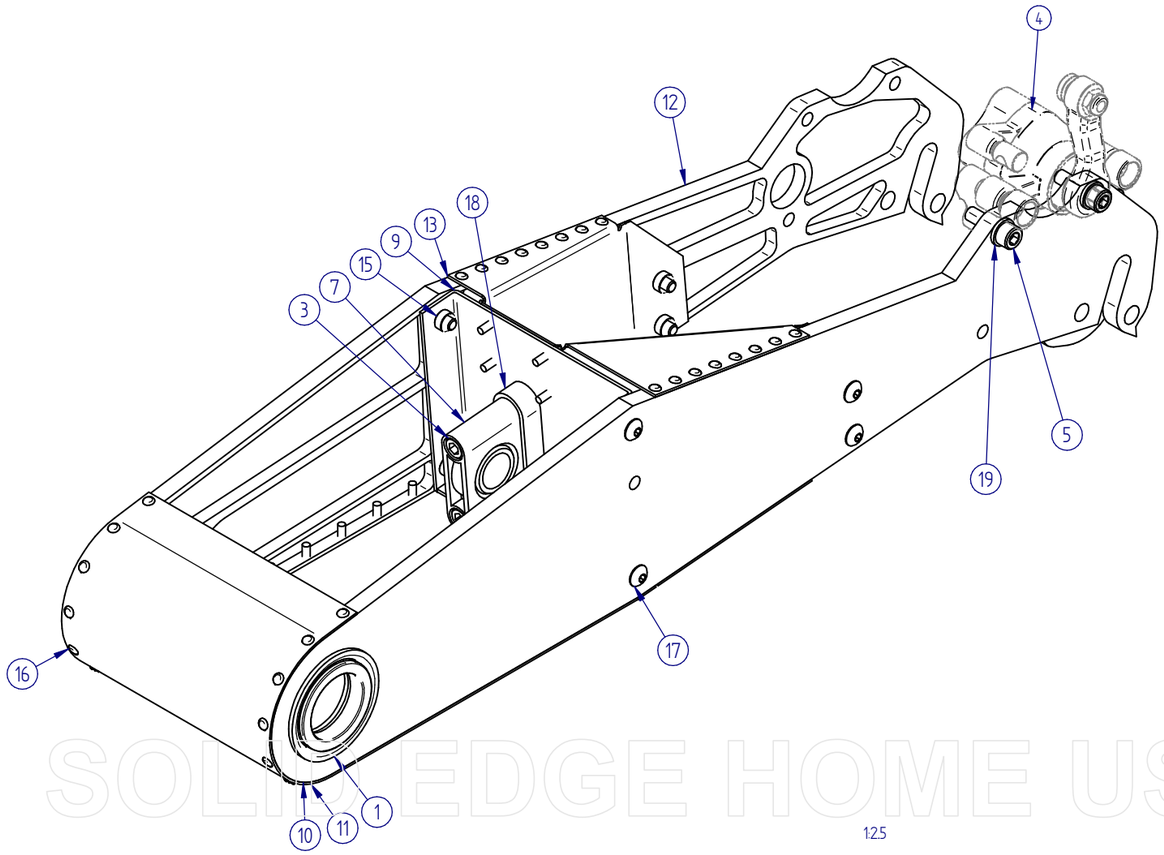

1:2.5

Item	Title	Document Number	Material	Qty	Mass (Item)	Mass (Qty)
	Rear Suspension assembly, right	UIS_MTVR-ASM001			5872,1 g	5872,1 g
1	Ball bearing, cycle, fork, bottom	A118SAK_BOT	Steel	1	52,7 g	52,7 g
2	Ball bearing, cycle, fork, top	A118SAK TOP	Steel	1	83,4 g	83,4 g
3	Bolt	DIN912 M6x45	A4 80	2	13,4 g	26,7 g
4	Brake caliper assy, minimoto	Unspecified		1	288,3 g	288,3 g
5	Hexagon Socket Head Cap Screws, din912	DIN 912 M6x20	A4	2	7,6 g	15,3 g
6	hub motor torque arm, "e"	UIS_MTVR-PSM0300	Stainless Steel, 316	1	41,0 g	41,0 g
7	Polymer bearing, spherical Ø16	IGUS ESTM-16-1	Nylon, general purpose	1	16,7 g	16,7 g
8	Rear motor & wheel assembly	UIS_MTVR_ASM002		1	4238,3 g	4238,3 g
9	Rear suspension, damper bearing holder	UIS_MTVR-PSM0201	Aluminum, 5050	1	58,6 g	58,6 g
10	Rear suspension, inside, left	UIS_MTVR-PAR0112	Aluminum, 6061-T6	1	376,6 g	376,6 g
11	Rear suspension, inside, left	UIS_MTVR-PSM0200	Aluminum, 5050	1	100,1 g	100,1 g
12	Rear suspension, inside, right	UIS_MTVR-PAR0113	Aluminum, 6061-T6	1	376,7 g	376,7 g
13	Rear suspension, profiled stiffener	UIS_MTVR-PSM0202	Aluminum, 5050	1	86,2 g	86,2 g
14	Rivet nut, thin plate	MINOFF M6-008-4MM-Z	Stainless steel	2	2,7 g	5,3 g
15	Rivet nut, thin plate	MINOFF M5-008-4MM-Z	Stainless steel	8	1,4 g	11,1 g
16	Rivet Ø3,2	Rivet	SS 316	70	0,6 g	38,9 g
17	Screw UNI ISO 7380 M5 x 16		Steel	8	3,3 g	26,7 g
18	Suspension bearing reinforcement	UIS_MTVR-PAR0301	Aluminum, 6061-T6	1	25,1 g	25,1 g
19	Washer	DIN 125 M6	A4	2	1,0 g	2,0 g
20	Wedge nut, hand grinded to add draft	Square nut	Aluminum, 5050	1	2,3 g	2,3 g

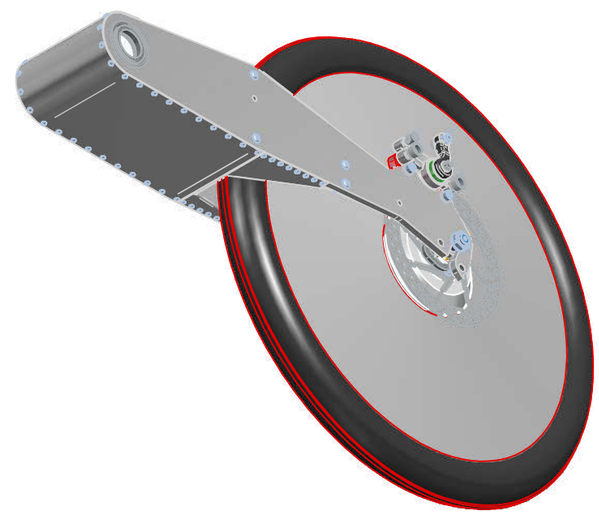

1:6

Weight	Volume
5831.3 g	8671.4 cm^3
Material specification	

Rear Suspension assembly, right

Unless otherwise noted:

All edges to be deburred
All dimensions in mm
Surface roughness, Ra in um:
Dimension tolerances according to ISO 2768-1 class:

Sheet size	Projection	Scale
A3		1:1 unless noted

UIS_MTVR-ASM001-11-B

Sheet: 2 of 2

Velomobile:Redefined
Per H. Sørensen
University of Stavanger

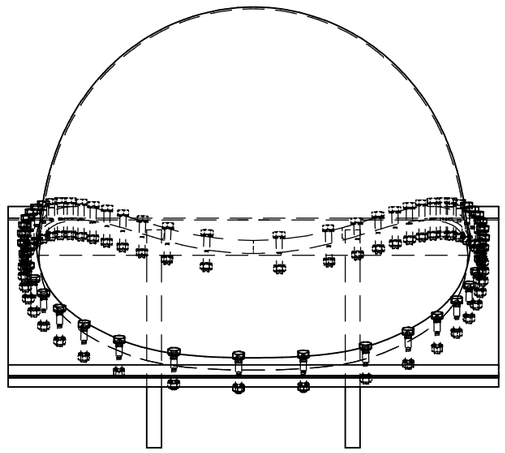

1:10

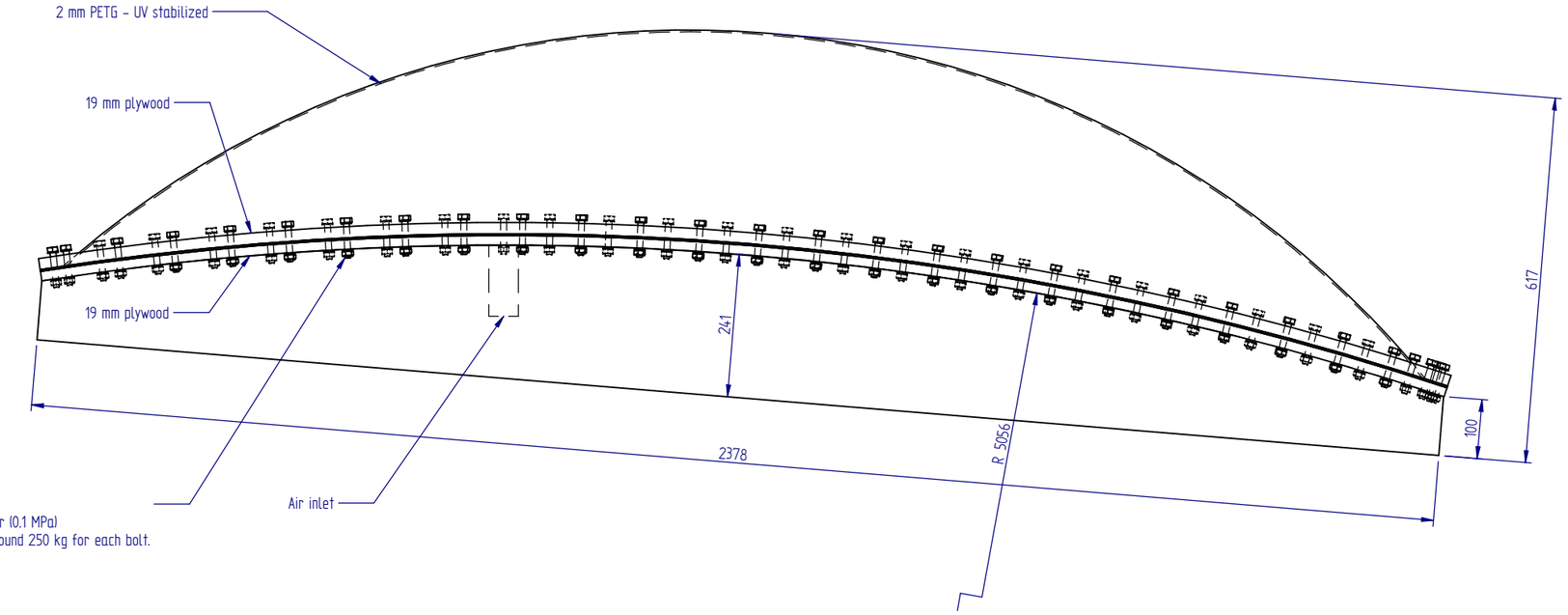

Spacing and size of bolts depend on blow pressure.
Illustration shows 100 mm between M10 bolts suitable for 1 bar (0.1 MPa)
This result in approx 13 ton of total force on blow mold or around 250 kg for each bolt.

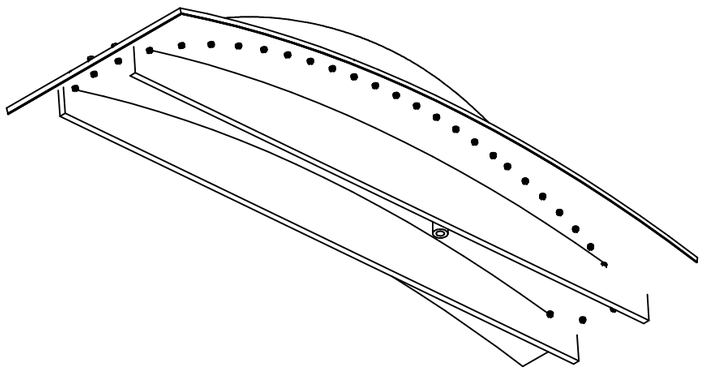

120

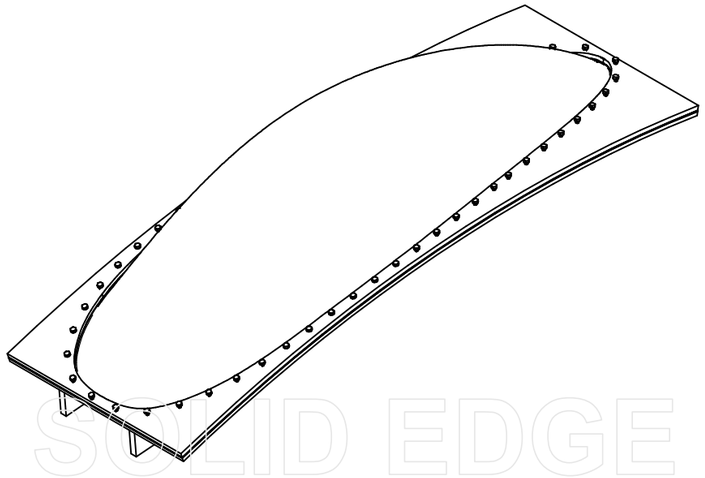

120

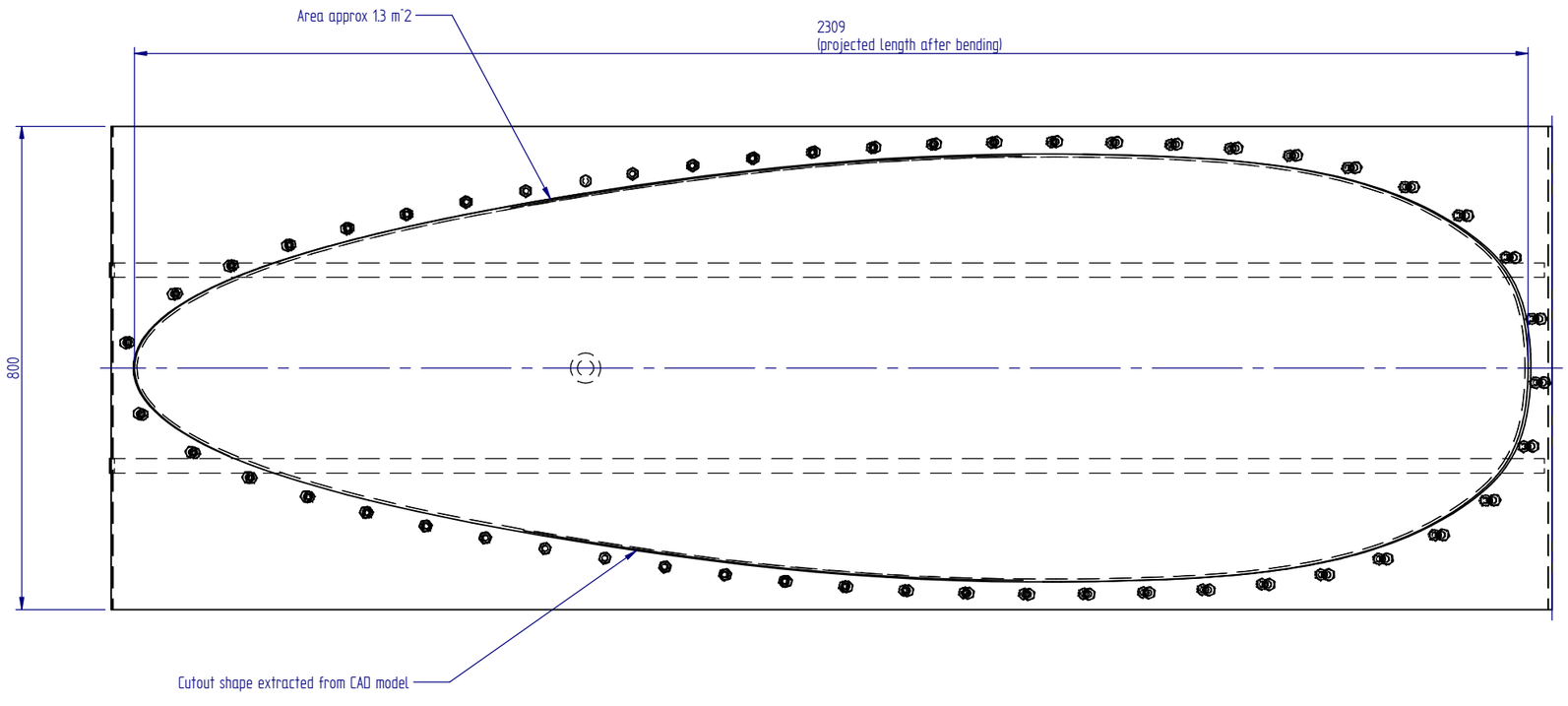

3D last edited: 07.06.2014	3D doc. number: UIS_MTVR-ASM301	Blow thermoforming of canopy	Sheet size A3 / Projection / Scale 1:1 unless noted
3D filename: Canopy production-00.asm			UIS_MTVR-ASM301-00-A
Finish	Density	Unless otherwise noted:	Sheet: 1 of 1
Weight 0,000 g	Volume 0,0 cm^3	All edges to be deburred All dimensions in mm Surface roughness, Ra in um: Dimension tolerances according to ISO 2768-1 class:	Velomobile:Redefined University of Stavanger
Material specification			

Hub dimensions necessary for building wheels: GM minimotor (Front hub)

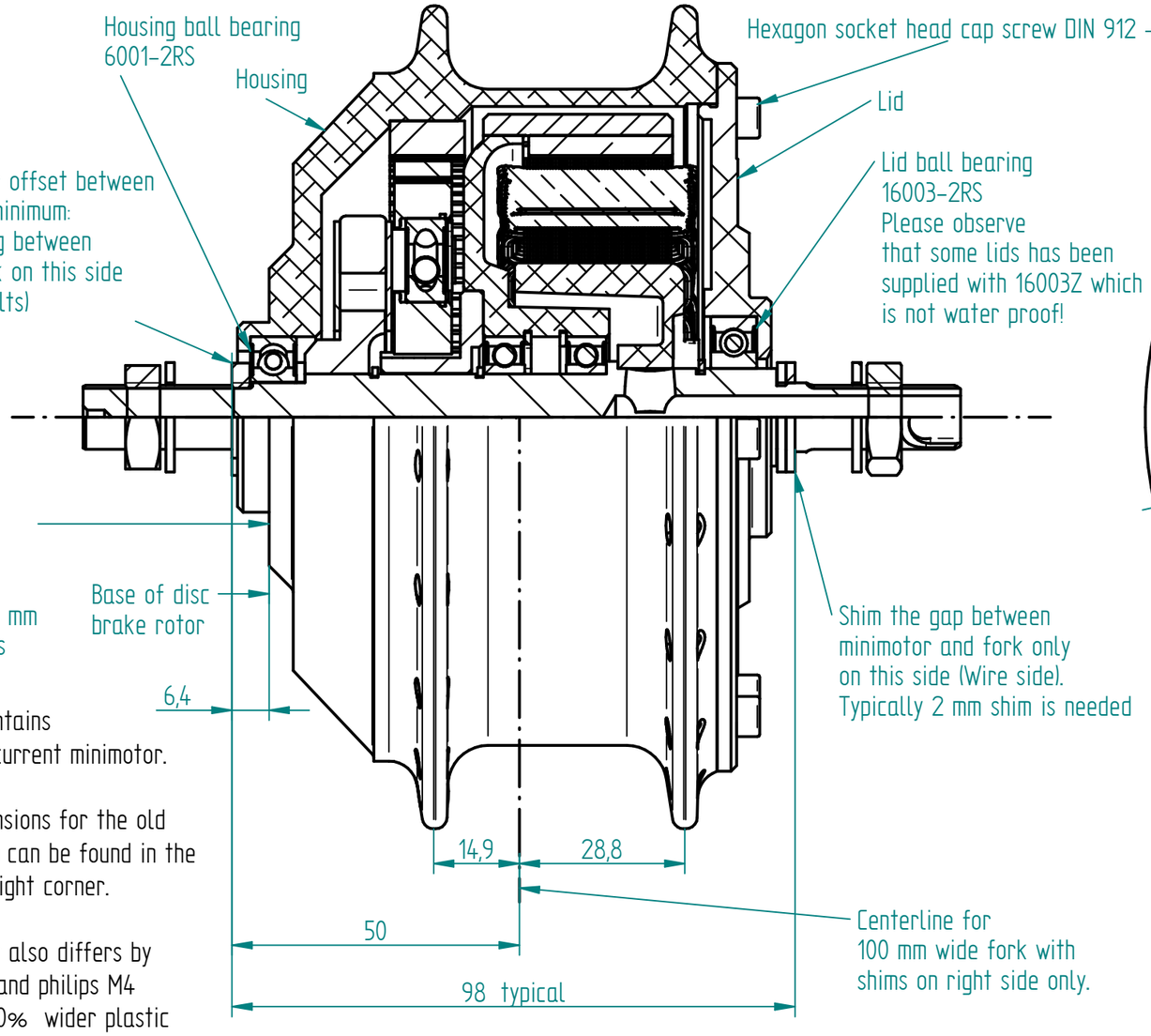

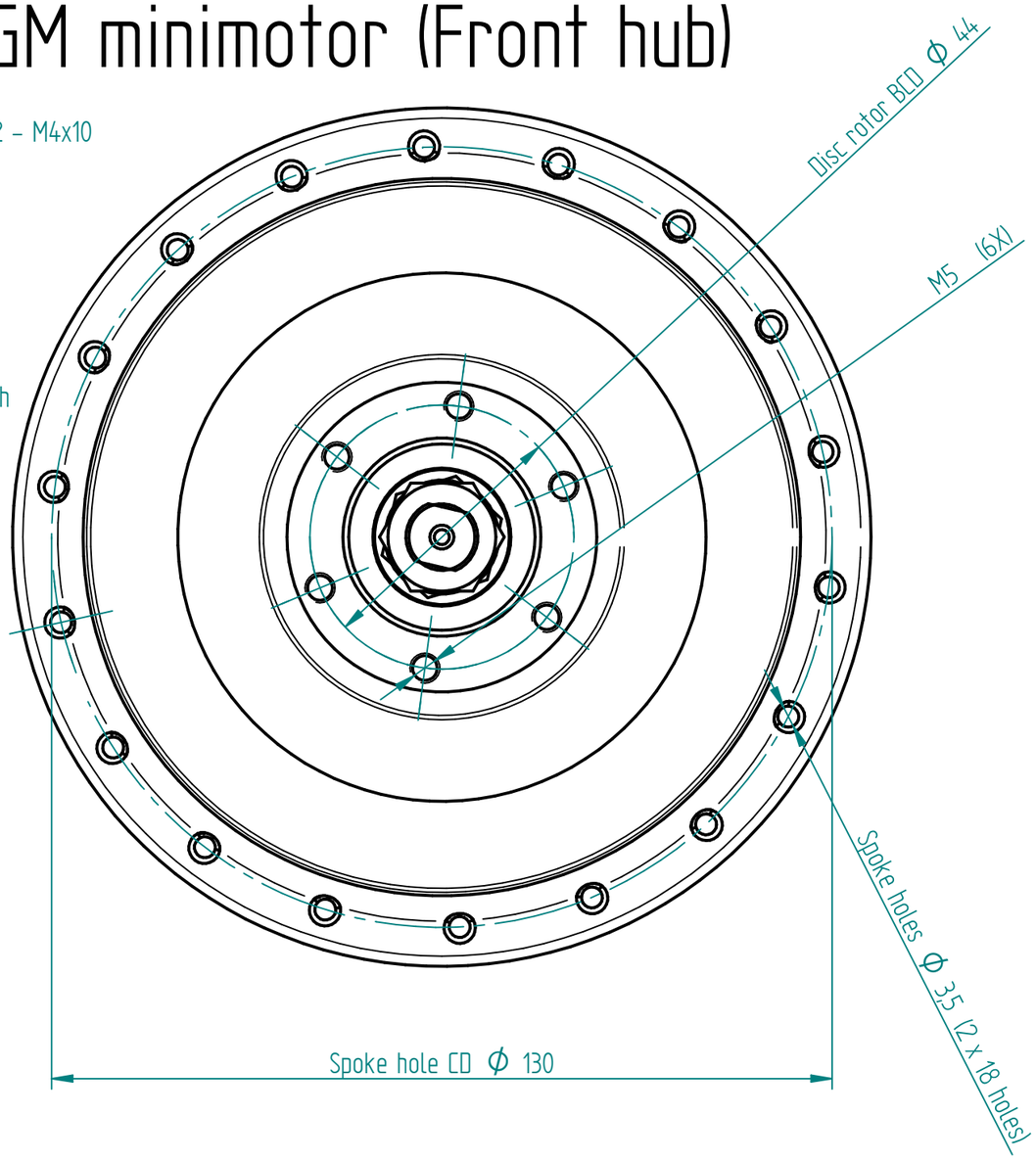

The illustrations contains dimensions for the current minimotor.

Spoke related dimensions for the old black minimotor hub can be found in the table in the lower right corner.

The black minimotor also differs by using 6003 bearing and philips M4 screws on lid and 20% wider plastic planet gears. Both old and new motor/gear assy will however fit either housing.

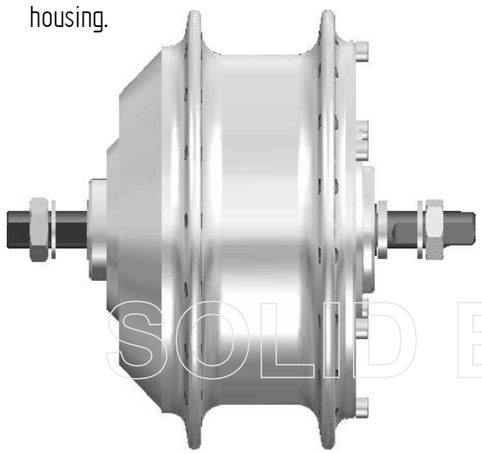

Data for use with Spocalc.xls (http://www.sheldonbrown.com/rinard/spocalc.htm)

S is the Spoke hole diameter, usually 2.4mm.
d is the diameter of the circle through the centers of the spoke holes.
W is the hub width from the center of the wheel to the center of the flange.
F/R indicates whether the hub is for a front or rear wheel.
OLD is the Over Lock Nut dimension, or frame spacing.
cogs is the number of cogs the hub accepts.

	Left Flange		Right Flange					
S, mm	dL, mm	WL, mm	dR, mm	WR, mm	F/R	cogs	OLD, mm	**Select a Hub:** select a cell in this column, then choose "Enter Front Hub Dims" or "Enter Rear Hub Dims" from the "Tools" menu. **Hub**
3,0	121,0	24,3	121,0	26,2	F		100	GM Minimotor old black front
3,5	130,0	14,9	130,0	28,7	F		100	GM Minimotor new aluminium front

BUS_BAT:V[0..16],TEMP[1..4]

C4x and D2x near connector
C5x near IC pins

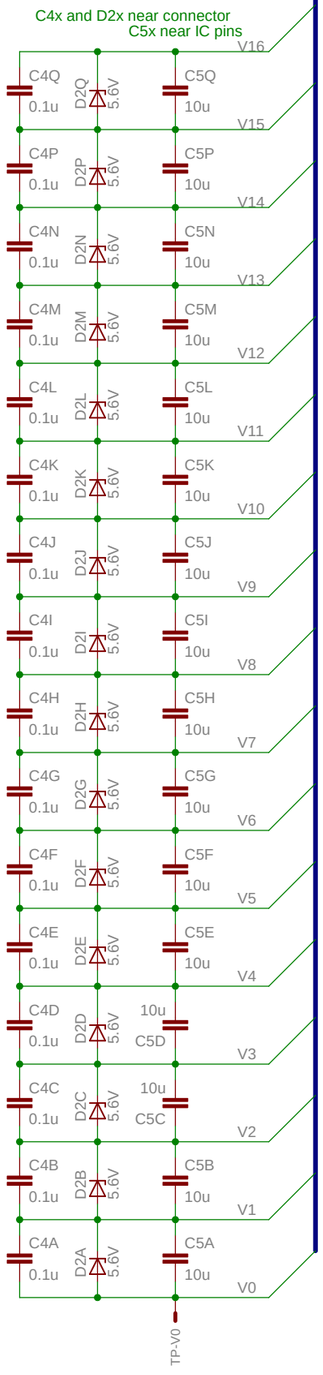

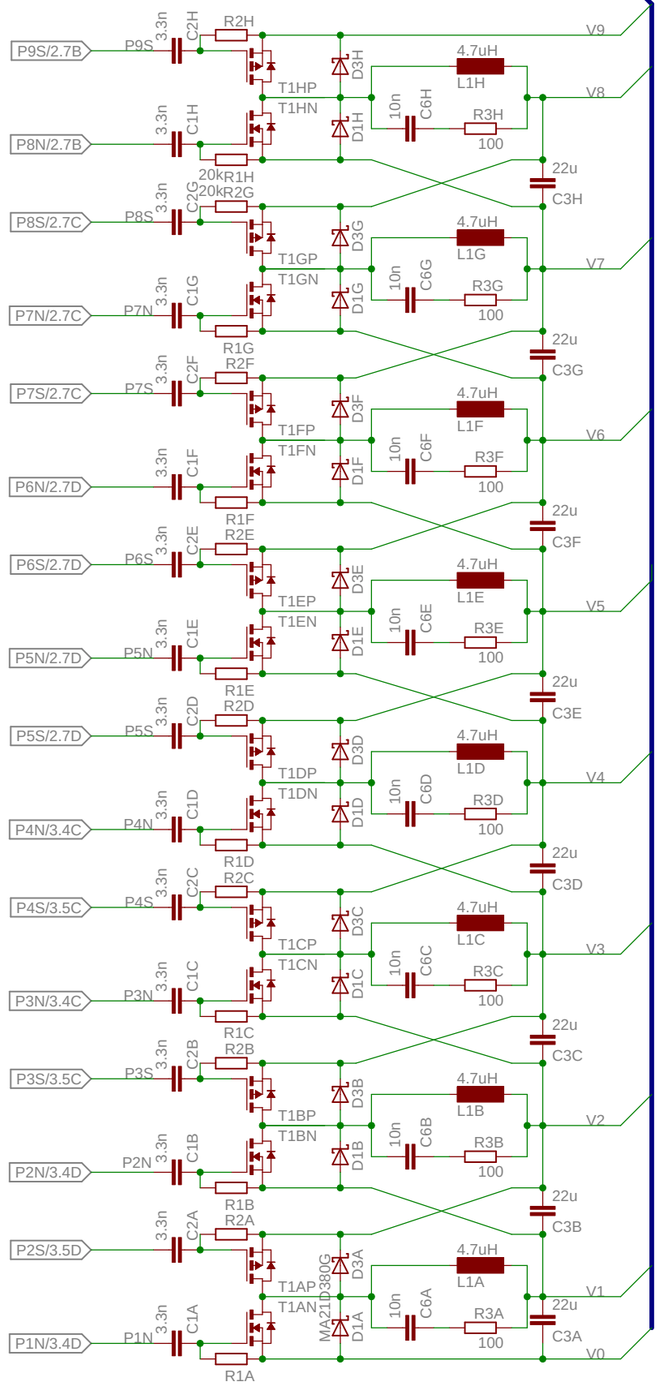

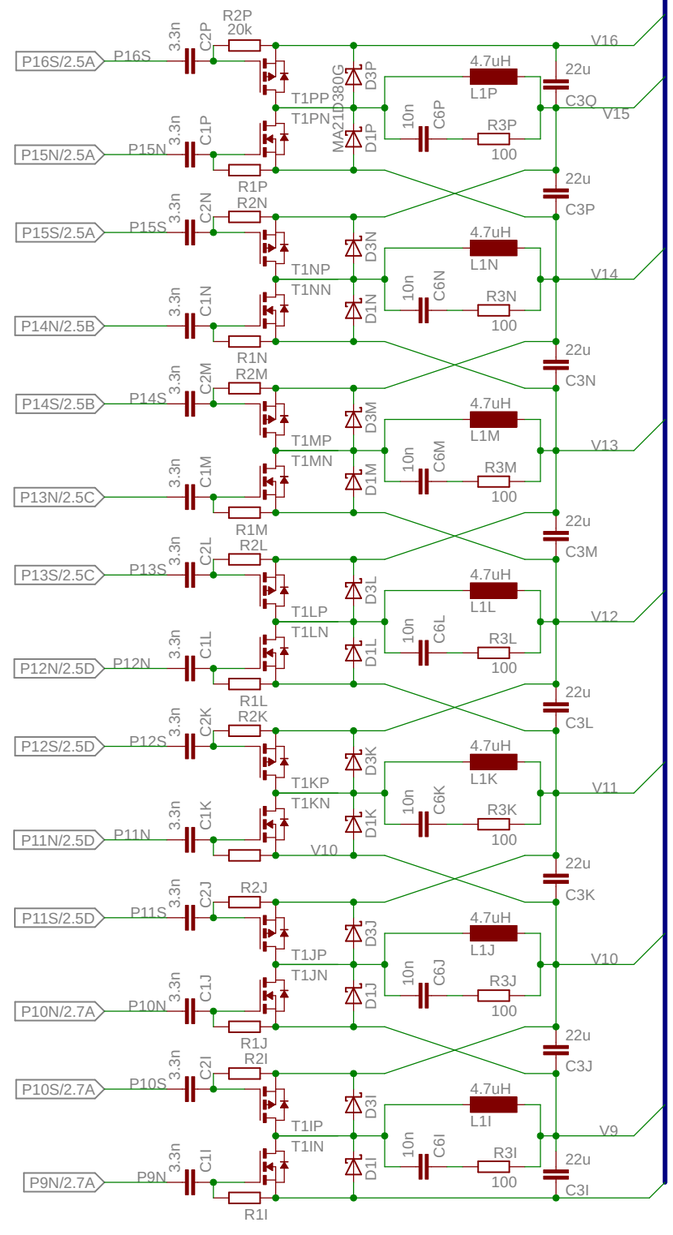

FID1
FID2
FID4

	TBMS-2.311UIS
	09.06.2014 19:21:04
	Sheet: 1/3

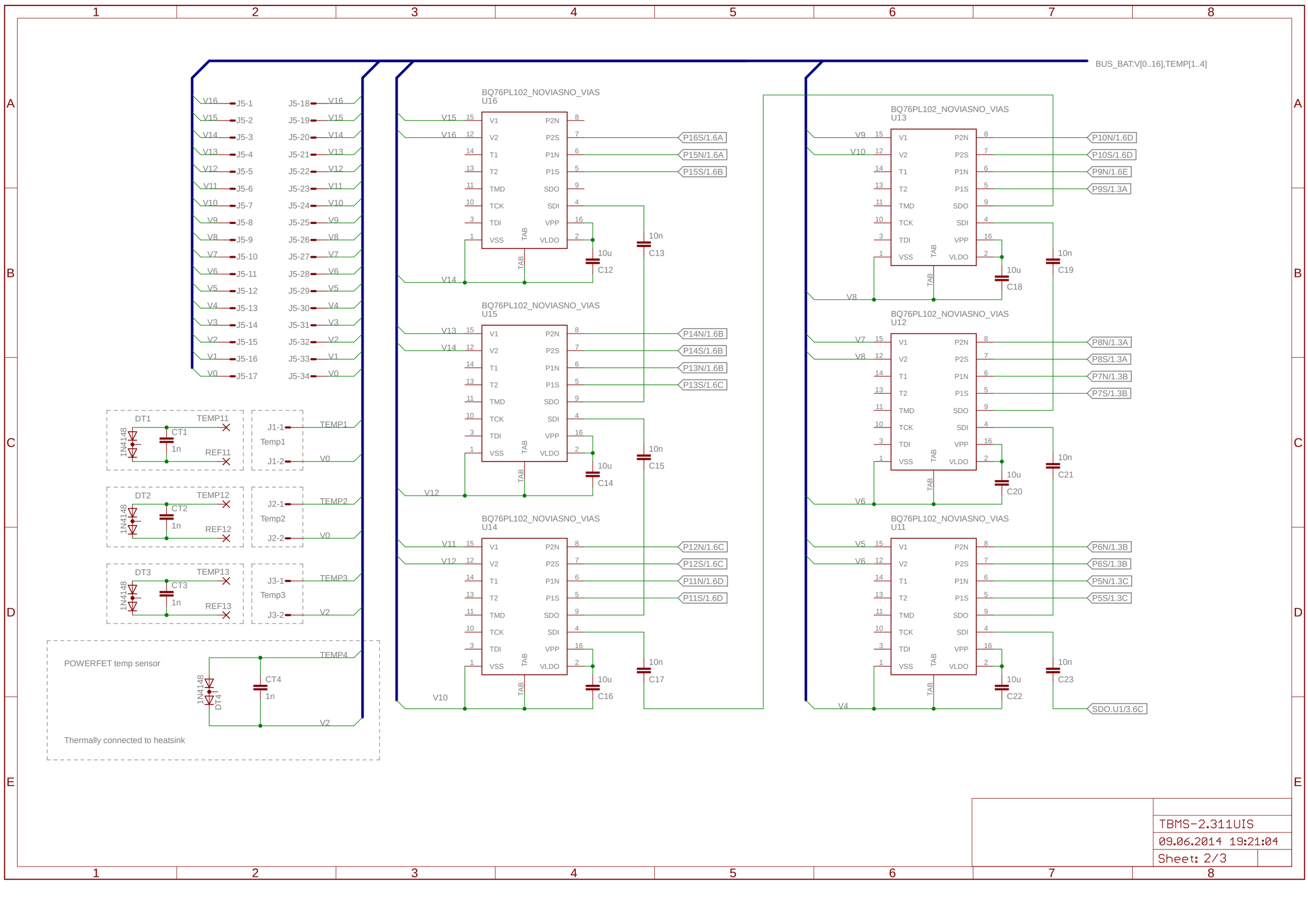

	TBMS-2.311UIS
	09.06.2014 19:21:04
	Sheet: 2/3

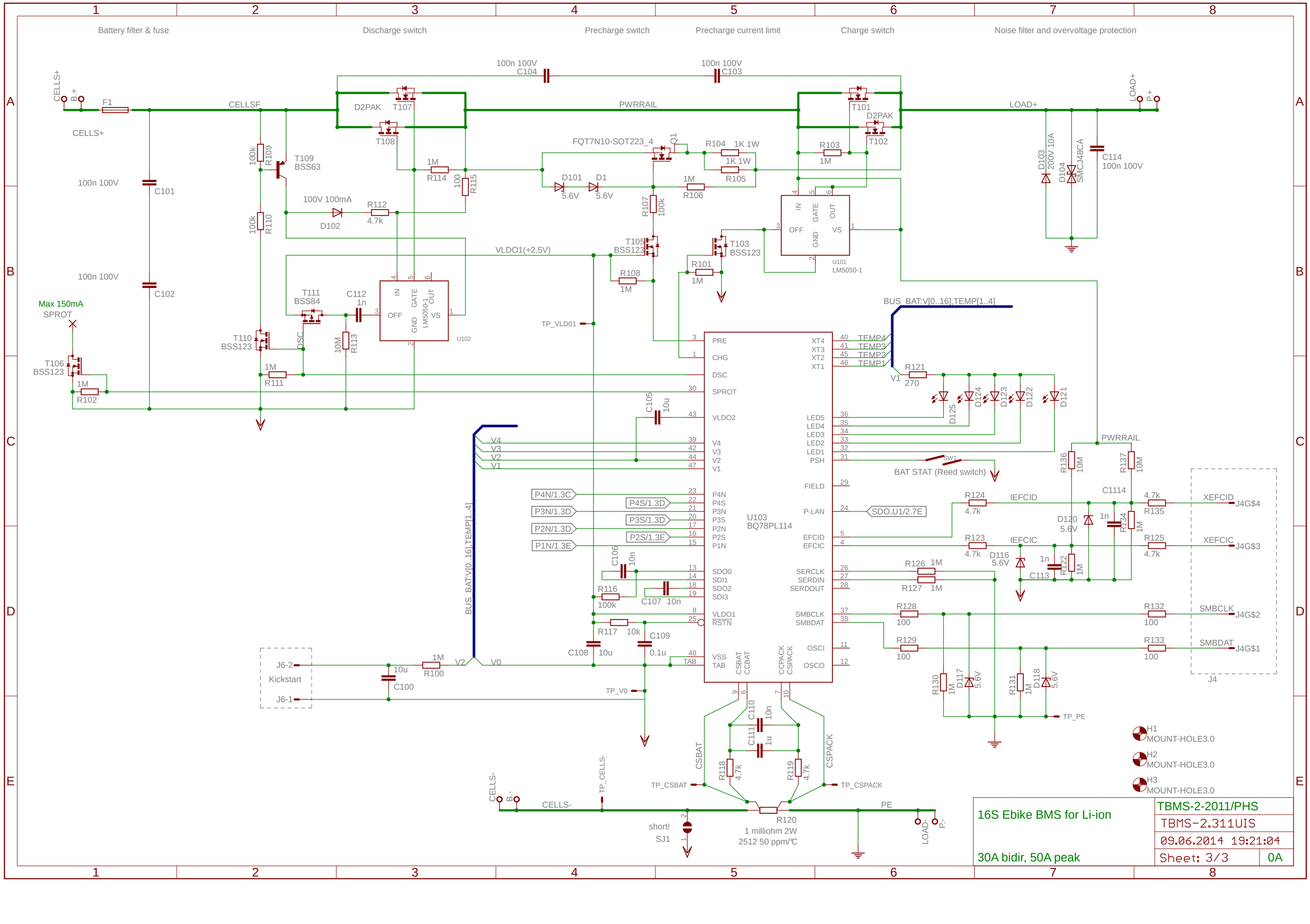
1
2
3
4
5
6
7
8
Battery filter & fuse
Discharge switch
Precharge switch
Precharge current limit
Charge switch
Noise filter and overvoltage protection
A
B
C
D
E
CELLS+
B+
F1
CELLS+
CELLSF
100n 100V
C101
100n 100V
C102
Max 150mA
SPROT
T106
BSS123
1M
R102
100k
R109
T109
BSS63
100k
R110
100V 100mA
D102
R112
4.7k
D2PAK
T107
T108
100n 100V
C104
100n 100V
C103
PWRRAIL
1M
R114
100
R115
FQT7N10-SOT223_4
Q1
R104
1K 1W
1K 1W
R105
D101
5.6V
D1
5.6V
1M
R106
R107
100k
T105
BSS123
VLDO1(+2.5V)
R108
1M
T103
BSS123
R101
1M
T101
D2PAK
T102
R103
1M
LOAD+
P+
LOAD+
D103
200V 10A
D104
SMCJ48CA
C114
100n 100V
IN
GATE
OUT
OFF
GND
VS
U101
LM5050-1
T111
BSS84
C112
1n
T110
BSS123
DSC
10M
R113
1M
R111
IN
GATE
OUT
OFF
GND
VS
LM5050-1
U102
TP_VLD01
BUS_BAT:V[0..16],TEMP[1..4]
PRE
CHG
DSC
SPROT
VLDO2
C105
10u
V4
V3
V2
V1
P4N/1.3C
P3N/1.3D
P2N/1.3D
P1N/1.3E
P4S/1.3D
P3S/1.3D
P2S/1.3E
P4N
P4S
P3N
P3S
P2N
P2S
P1N
U103
BQ78PL114
SDO0
SDI1
SDO2
SDI3
VLDO1
RSTN
VSS
TAB
CSBAT
CCBAT
CCPACK
CSPACK
OSCI
OSCO
XT4
XT3
XT2
XT1
LED5
LED4
LED3
LED2
LED1
PSH
FIELD
P-LAN
EFCID
EFCIC
SERCLK
SERDIN
SERDOUT
SMBCLK
SMBDAT
TEMP4
TEMP3
TEMP2
TEMP1
R121
V1
270
D125
D124
D123
D122
D121
SW1
BAT STAT (Reed switch)
SDO.U1/2.7E
PWRRAIL
R136
10M
R137
10M
C1114
4.7k
R124
4.7k
IEFCID
R123
4.7k
IEFCIC
D120
5.6V
1n
R134
1M
R135
4.7k
R125
4.7k
D116
5.6V
1n
C113
R122
1M
R126
1M
R127
1M
R128
100
R132
100
SMBCLK
R129
100
R133
100
SMBDAT
R130
1M
D117
5.6V
R131
1M
D118
5.6V
TP_PE
XEFCID
J4G$4
XEFCIC
J4G$3
SMBCLK
J4G$2
SMBDAT
J4G$1
J4
J6-2
Kickstart
J6-1
1M
R100
10u
C100
V2
V0
TP_V0
C108
10u
C109
0.1u
R116
100k
C106
10n
C107
10n
R117
10k
C110
10n
C111
1u
CSBAT
CSPACK
R118
4.7k
R119
4.7k
TP_CSBAT
TP_CSPACK
CELLS-
B-
TP_CELLS-
CELLS-
short!
SJ1
R120
1 milliohm 2W
2512 50 ppm/℃
PE
LOAD-
P-
H1
MOUNT-HOLE3.0
H2
MOUNT-HOLE3.0
H3
MOUNT-HOLE3.0
16S Ebike BMS for Li-ion
30A bidir, 50A peak
TBMS-2-2011/PHS
TBMS-2.311UIS
09.06.2014 19:21:04
Sheet: 3/3
0A

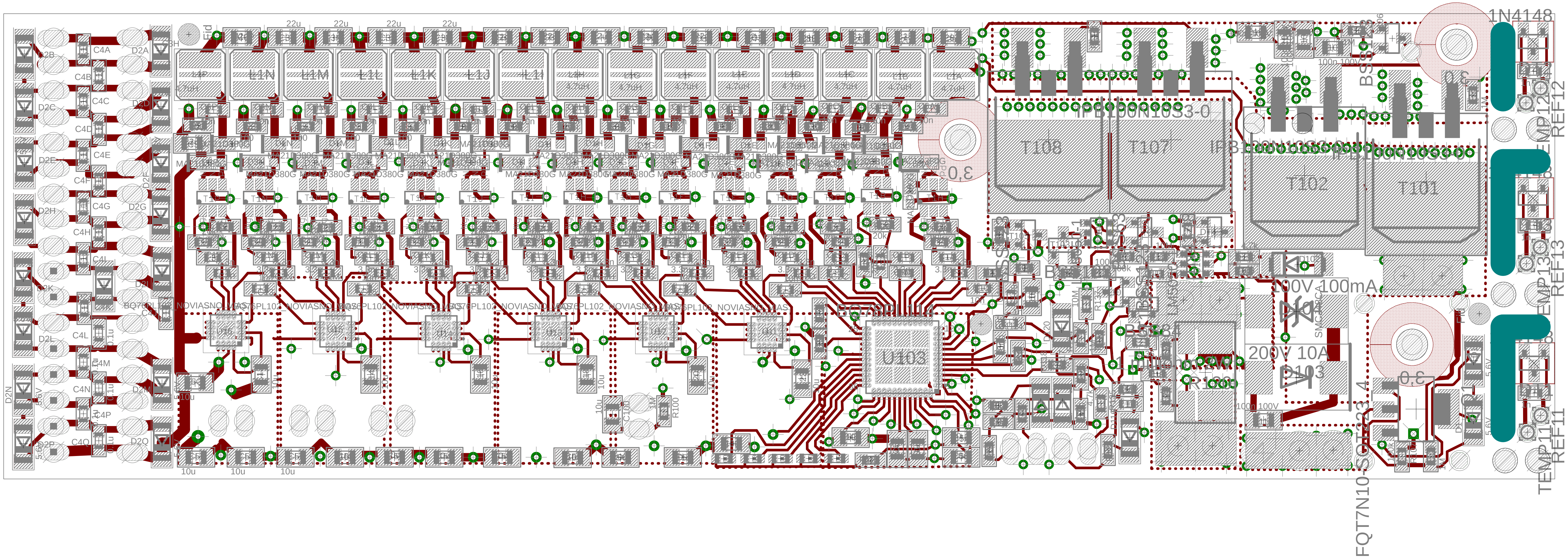

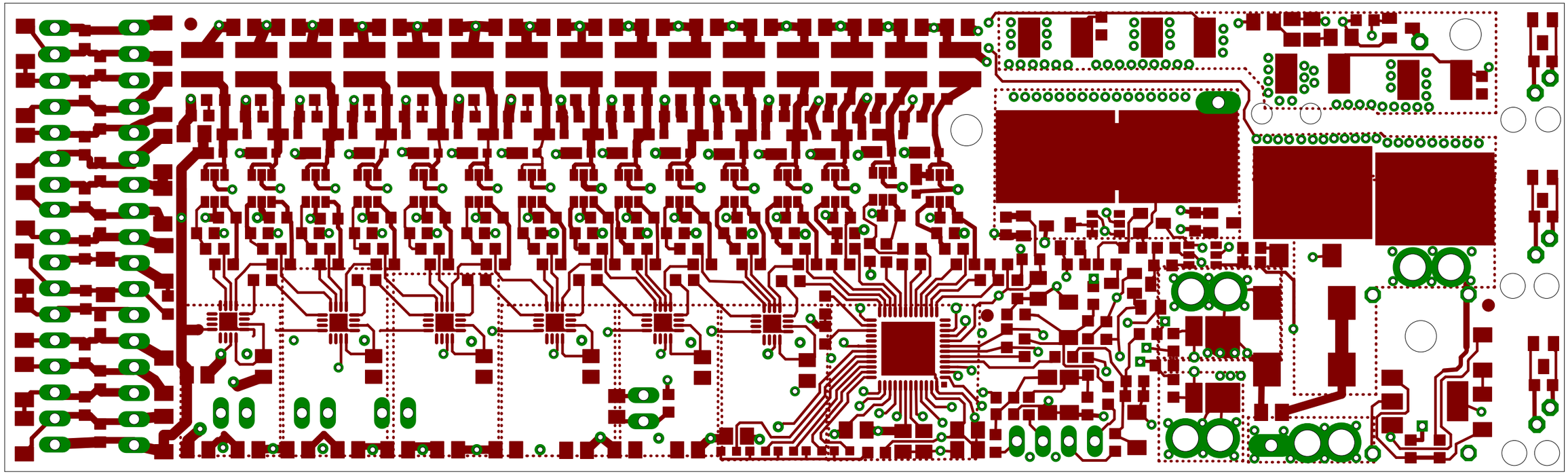

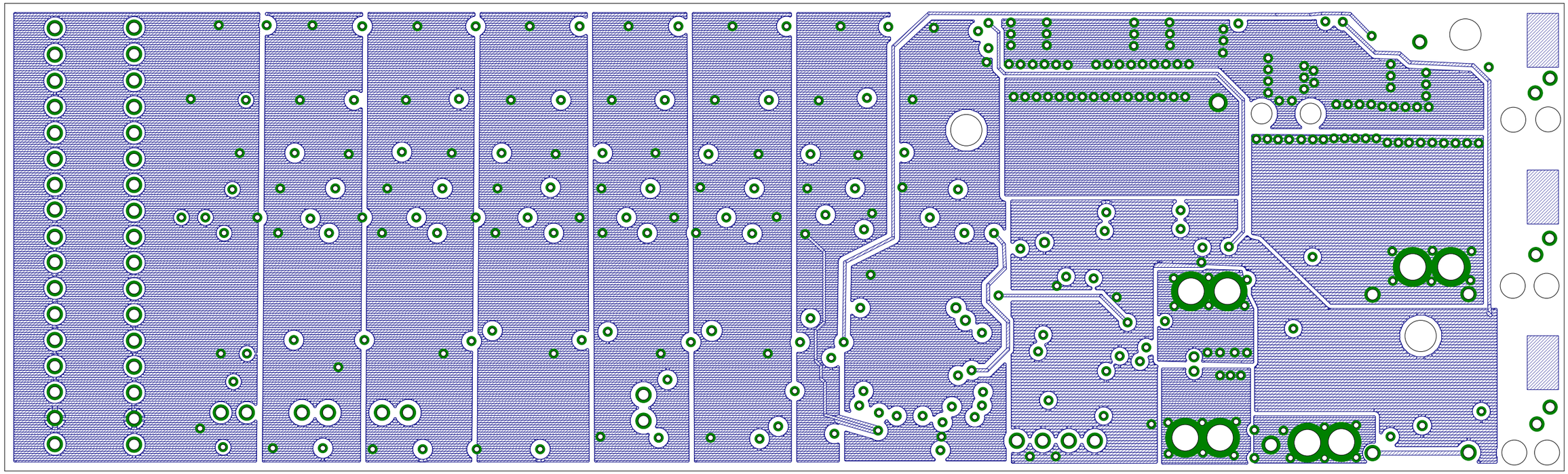

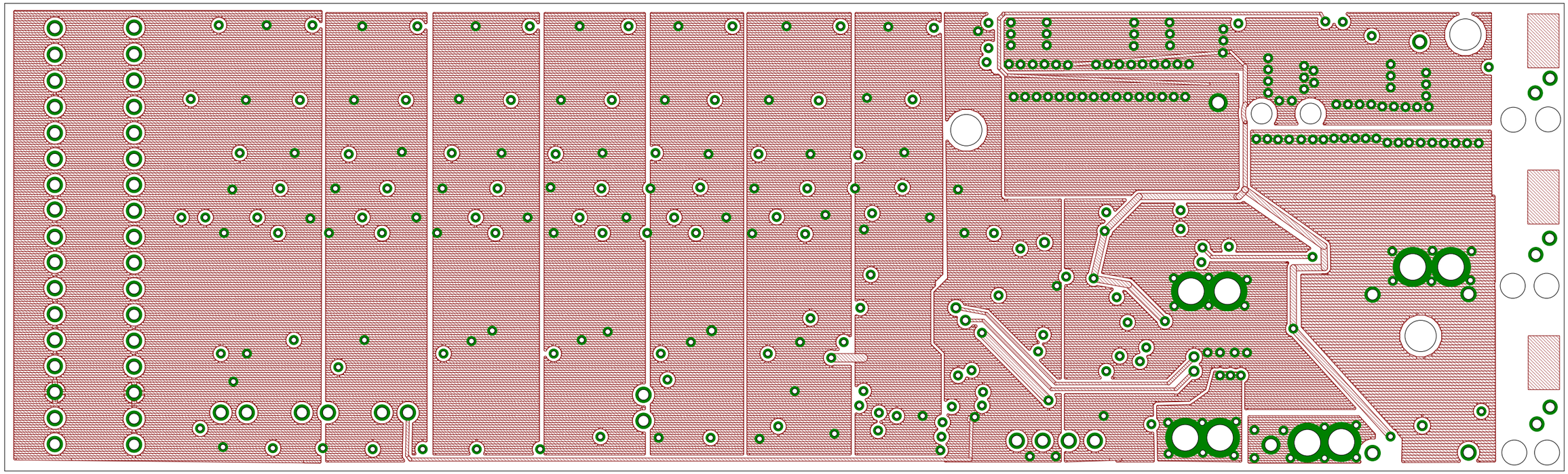

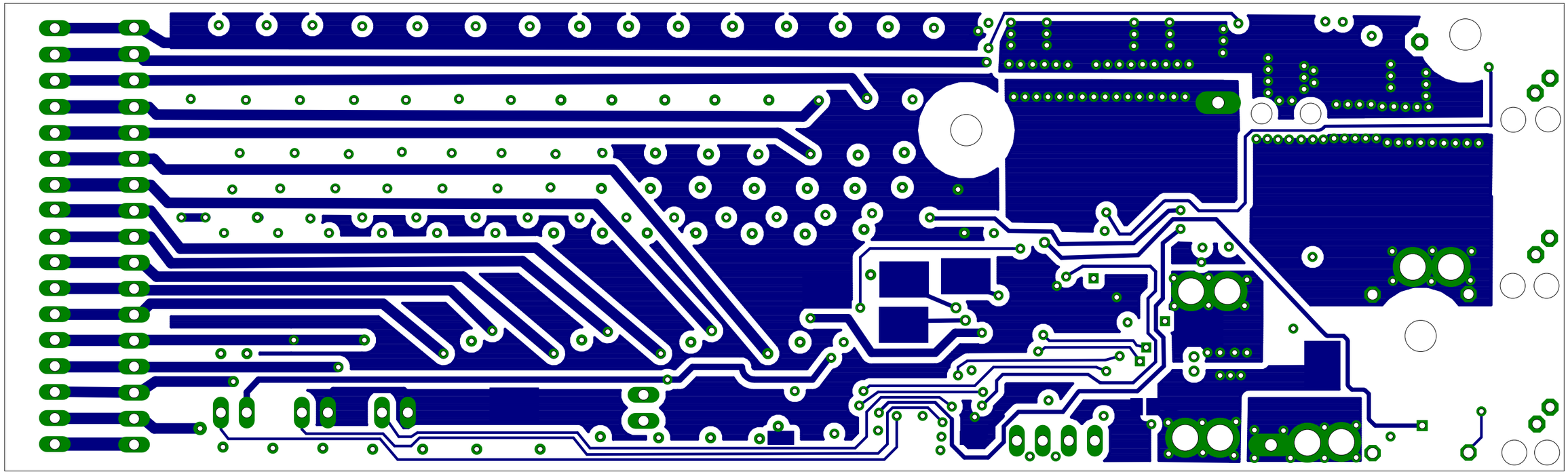

Appendix C

Flow simulations

Two different types of flow simulations has been performed within this thesis work. The major work has been on reducing aerodynamic drag of the velomobile body by iterative redesigning of the 3D geometry based on CFD drag calculation of preceding design. Also a single simulation of ventilation flow has been performed to find base values of ventilation mass and volume flow. This was necessary for evaluating if ventilation is sufficient for the expected heat flow in the cabin of the velomobile. Also a ventilation simulation involving flow over human body was tried. This failed due to too complex 3D model of human body, even after several modification to simplify geometry.

References: Background in CFD [1], base information on aerodynamics of vehicles [2], and ultra-streamlining of land vehicles [3].

Simulations has been performed using the following:

Software:

Caedium Professional 5.2 from Symscape, a unified CFD simulation environment based on a port of OpenFOAM 2.1 to windows. Models has been constructed in Solid Edge versions ST4, ST5 and ST6 from Siemens. OS has been Windows 8.0 64-bit

Hardware:

Software has been running on a home built PC workstation with X79 motherboard, Intel i7 3920k 6-core CPU and 32 Gbyte RAM. Graphics coprocessor has been NVIDIA GeForce GTX770 with 2 Gbyte RAM and 1536 shader cores capable of working as CFD coprocessors. 3Tbyte 7200 RPM SATA disk.

Initial parameters:

The automatic meshing in Caedium use three parameters that can be applied to each entity (surfaces and volume), namely;

- *Growth rate* - the mesh element growth rate moving away from geometric entity
- *Max element size* - Maximum size of element
- *Resolution* - The number of mesh intervals on an entity

The surface mesh edge size is the smallest of either edge length/resolution or max element size

The volume mesh edge size is the smallest of either maximum edge (or bounding box diagonal if no edge exists) / resolution or max element size. Wind tunnel surfaces has been set to:

- Growth rate 1.2
- max element size not limited (1e9 m)
- resolution 5 (minimum five elements per surface edge)

Surface mesh settings for velomobile body surfaces varies from run to run, see table 1. Most of the simulation runs use the following settings:

- growth rate 1.1
- max element size 0.02 m
- resolution 5

Simulation is for air as fluid with density 1.205 kg/m^3 with 10 m/s initial velocity in direction of vehicle axis and wind tunnel axis. Wind tunnel road surface set to linear velocity of 10 m/s to simulate constant speed of vehicle at 36 km/h with no wind.

Body iterations start with VELO14 and continue up to VELO23. Ventilation simulation was performed on a modified VELO17 body (WT17-07).

Table 1 on the following page give an overview of all the VELO CFD simulations and the drag results. The table 1 columns contains the following information:

GEOMETRY: Name of base model, i.e., VELO14 to VELO23

A: Frontal area of half model [m^2]

Change...: Comment on what has been changed from preceding simulation

3D (STEP): Filename of the STEP file containing the 3D-model of 1/2 of vehicle

.SYM: Simulation file. This can be opened using free Caedium software[1].

Growth: *Growth rate* - the mesh element growth rate moving away from geometric entity

Max: Maximum length of a 2D mesh edge

Res: The minimum number of mesh elements on a model edge

Min E. r.: The ratio of the shortest to longest edge in 2D mesh elements. Cannot exceed 1, cells with lower than 0.2 in E ratio is often indicative of bad mesh [4]

Min Vol r.: The ratio of the shortest to longest edge in 3D mesh elements. Cannot exceed 1, cells with Vol ratio less than 0.01 should be investigated [4]

Min y^+: The minimum y^+ value found on the volume cells attached to the VELO*n* surface.

Max y^+: The maximum y^+ value found on the volume cells attached to the VELO*n* surface. For suitable accuracy meshing has been refined if this value exceeded 300.

Elements: The number of cells in the volume mesh

Drag: The fluid drag force on 1/2 VELO body along X axis [N]

Lift: The lift on 1/2 VELO body along Y axis caused by fluid flow [N]

$C_dA/2$: The C_dA calculated from drag and area on simulated 1/2 model of vehicle

C_dA: Two times the calculated C_dA representative for the 1/1vehicle

Cd: Calculated drag coefficient for the 1/1 vehicle

[1] When used as a viewer the Caedium software is free and can be downloaded from www.sysmscape.com/product/downloads It is available for Windows, MAC and Linux platforms.

Base model	*FrontA*	*Comment on model*	*CAD file*	*Data file*	*Finest mesh settings*		
Geometry	**A [m^3]**	**Changed from previous simulation**	**3D (STEP)**	**.SYM (results)**	**Growth**	**Max [m]**	**Res**
VELO14	0,3992	Base model	WT14	WT14-04	1,1	0.001	35
VELO14	0,3992	finer mesh	WT14	WT14-05	1,1	0,007	35
VELO14	0,3992	finer mesh	WT14	WT14-06	1,1	0,005	35
VELO14	0,3992	fluent verification	WT14	Fluent			
VELO15	0,3788	streaml. ang. vel. on wheel	WT15	WT15-02	1,1	0,002	26
VELO15	0,3788	no angular velocity	WT15	WT15-04	1,1	0,002	26
VELO16	0,3261	Added wheel carrier rear	WT16-04	WT16-04	1,1	0,02	1
VELO16	0,3261	Refined geometry	WT16-04	WT16-041	1,1	0,01	1
VELO16	0,3261	Refined geometry	WT16-04	WT16-042	1,1	0,005	1
VELO17	0,3264	With ventilation	WT17-07	WT17-07	1,1	0,01	1
VELO17	0,3264	Refined mesh	WT17-07	WT17-071	1,1	0,01	2
VELO17	0,3264	Refined mesh	WT17-07	WT17-072	1,1	0,007	2
VELO17	0,3264	Refined geometry	WT17-08	WT17-08	1,1	0,02	1
VELO17	0,3264	Refined mesh	WT17-08	WT17-08	1,1	0,02	5
VELO17	0,3264	Refined geometry, mesh	WT17-09	WT17-091	1,3	0,005	5
VELO18	0,3268	Streamlined	WT18-03	WT18-03	1,1	0,02	1
VELO18	0,3268	Refined mesh	WT18-03	WT18-03	1,1	0,02	5
VELO18	0,3268	Refined geometry	WT18-04	WT18-04	1,1	0,02	1
VELO18	0,3268	Refined geometry, mesh	WT18-05	WT18-05	1,2	0,01	1
VELO18	0,3268	Refined mesh	WT18-05	WT18-051	1,1	0,005	1
VELO 19	0,3289	Added ventilation ports	WT19-00	WT19-00	1,2	0,01	1
VELO 19	0,3289	Merged surfaces	WT19-00	WT19-001	1,2	0,02	1
VELO 19	0,3289	Refined mesh	WT19-00	WT19-002	1,2	0,01	1
VELO20	0,3289	Added person in cabin	WT20-00				
VELO21	0,3254	Streamlined underside, plugged vent	WT21-00	WT21-00	1,2	0,02	1
VELO21	0,3254	refined mesh	WT21-00	WT21-001	1,1	0,02	1
VELO21	0,3254	refined mesh	WT21-00	WT21-002	1,1	0,015	1
VELO22	0,3232	Flat underside	WT22-01	WT22-01	1,2	0,02	1
VELO22	0,3232	Rounded canopy edge R=7mm	WT22-02	WT22-02	1,2	unlim.	5
VELO22	0,3232	Rounded canopy edge R=7mm	WT22-02	WT22-021	1,2	0,02	1
VELO23	0,3283	3% camber (front raised 50 mm)	WT23-00	WT23-00	1,2	0,02	1
VELO23	0,3283	refined mesh	WT23-00	WT23-001	1,2	0,015	1
VELO23	0,3283	refined mesh	WT23-00	WT23-002	1,1	0,015	1
VELO23	0,3283	refined mesh, adj. relax f.	WT23-00	WT23-003	1,1	0,012	1
VELO23	0,3283	refined mesh, adj. relax f.	WT23-00	WT23-004	1,1	0,005	26

Data file	*Mesh quality*				*Tetmesh*
.SYM (results)	**min E r.**	**min Vol r.**	**min y+**	**max y+**	**elements**
WT14-04	0,168	0,104	0,974	141	2 158 585
WT14-05		0,035	0	120	4 166 290
WT14-06	0,196	0,062	1,18	106	7 604 731
Fluent			0,0076	19,1	
WT15-02	0,178	0,035	3,42	231	938 658
WT15-04	0,178	0,035	3,42	231	
WT16-04	0,37	0,145	4,12	271	594 990
WT16-041	0,39	0,144	2,74	166	2 025 928
WT16-042	0,12	0,013	0,82	96,9	7 821 153
WT17-07	0,11	0,0033			
WT17-071	0,11	0,0033			2 121 498
WT17-072	0,12	failed vol mesh			
WT17-08	0,125	failed vol mesh			
WT17-08	?	failed vol mesh			
WT17-091	0,112	0,104	2,42	285	751 370
WT18-03	0,06	Stretched surface cells			
WT18-03	0,012	Stretched surface cells			
WT18-04	0,197	failed vol mesh			
WT18-05	0,155	0,122	0,484	167	1 224 251
WT18-051	0,152	0,05	0,12	98,5	7 657 831
WT19-00	0,153	0,074	0,78		1 307 728
WT19-001	0,167	0,105	2	270	307 403
WT19-002	0,194	0,137	0,2	159	1 264 938
WT21-00	0,092	0,099	0,12	316	461 835
WT21-001	0,125	0,073	0,12	306	679 887
WT21-002	0,125	0,072	0,12	222	1 037 107
WT22-01	0,118	failed vol mesh			
WT22-02	0,158	0,137	7,79	834	101 266
WT22-021	0,19	0,109	0	285	313 035
WT23-00	0,191	0,101	0,13	312	392 073
WT23-001	0,187	0,109	0,129	233	629 066
WT23-002	0,189	0,108	0,131	211	1 016 721
WT23-003	0,185	0,078	0,131	158	1 778 174
WT23-004	0,168	0,05	0,13	113	8 363 506

Data file					
.SYM (results)	Drag [N]	Lift [N]	CdA	Cd	Comments
WT14-04	14,5	5,7	0,48	0,603	Simplest geometry that fit
WT14-05	13,3	5,5	0,44	0,553	For verification
WT14-06	13,5	5,3	0,45	0,561	For verification
Fluent	13,2	8,5	0,44	0,549	Base case
WT15-02	10	-2,2	0,33	0,438	Not needed, see txt
WT15-04	12	-1,8	0,40	0,526	
WT16-04	9,7	0,2	0,32	0,494	
WT16-041	9,2	-1,25	0,31	0,468	
WT16-042	8,8	-1,1	0,29	0,448	
WT17-07			NA		Did not finish
WT17-071			NA		Did not finish
WT17-072			NA		Did not finish
WT17-08			NA		Did not finish
WT17-08			NA		Did not finish
WT17-091	9,8	0,2	0,33	0,498	
WT18-03			NA		Did not finish
WT18-03			NA		Did not finish
WT18-04			NA		Did not finish
WT18-05	8,5	-0,8	0,28	0,432	Strange osc in residuals
WT18-051	7,3	0,2	0,24	0,371	did not help on residuals
WT19-00			NA		Did not finish
WT19-001	9,25	-2,2	0,31	0,467	
WT19-002	8,25	-0,5	0,27	0,416	
			NA		Meshing failed, complex 3D model human body
WT21-00			NA		Too high y+ (limit 300)
WT21-001	8,5	8,75	0,28	0,434	Accepted, less than 2% above limit, and only few cells
WT21-002	8,2	-9,2	0,27	0,418	
WT22-01			NA	0,000	Did not finish
WT22-02	9	-9	0,30	0,462	Much too high y+
WT22-021	8	-6	0,27	0,411	
WT23-00	8,25	-8	0,27	0,417	Too high y+ (limit 300)
WT23-001	8	-8	0,27	0,404	
WT23-002	7,2	-7,5	0,24	0,364	
WT23-003	6,5	-5	0,22	0,329	Changed to less agressive relaxation factors
WT23-004	6	0	0,20	0,303	Tuned relaxation, many iterations

Table 1 - summary of CFD results

VELO14

First body used in simulation. Half body has a frontal area of 0.3992 m^2 as shown in Figure A.

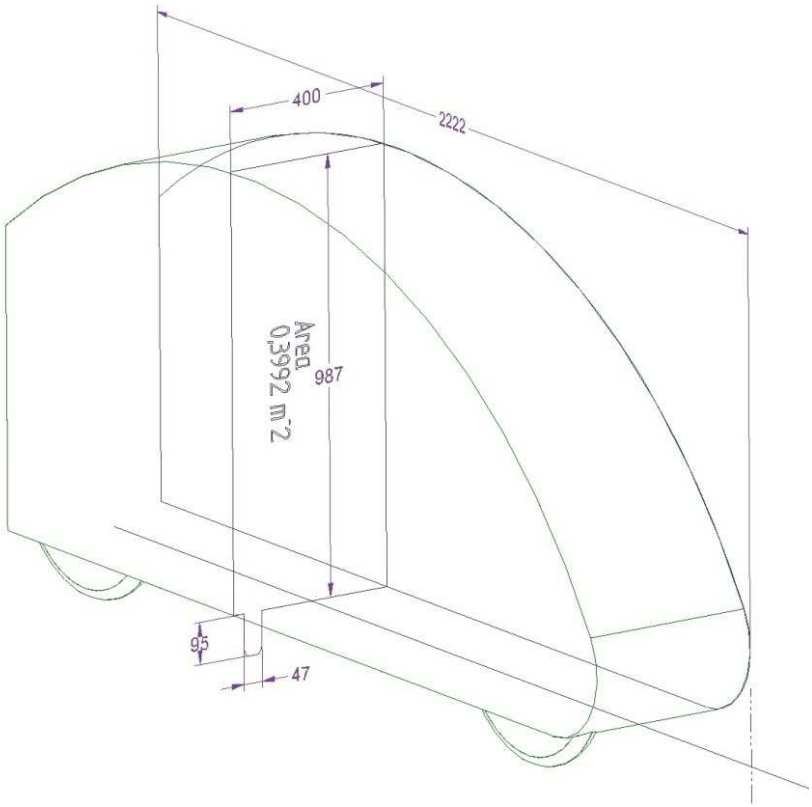

Figure A

The CFD model is actually a wind tunnel (WT) 22 m long, 6 m tall and 3 m (half body) wide where the velo14 body is subtracted from the WT. Velo's origo, the riders hip point, is located 6 m downstream in WT, as illustrated in Figure B:

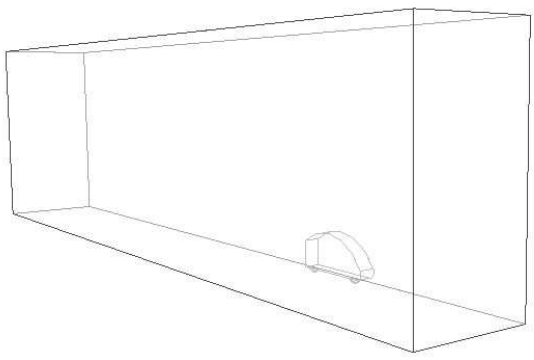

Figure B

Figure C shows an initial mesh with max element size 0.01 m on VELO14 body. It was subsequently doubled in element size and made more coarse to reduce simulation time. A total of four different simulation runs were done on VELO14, the last was done as a verification in

ANSYS Fluent which is a different software package. This was done by *Morten Kjeldsen* who has worked as professor at *NTNU* and is an expert in Fluent [5].

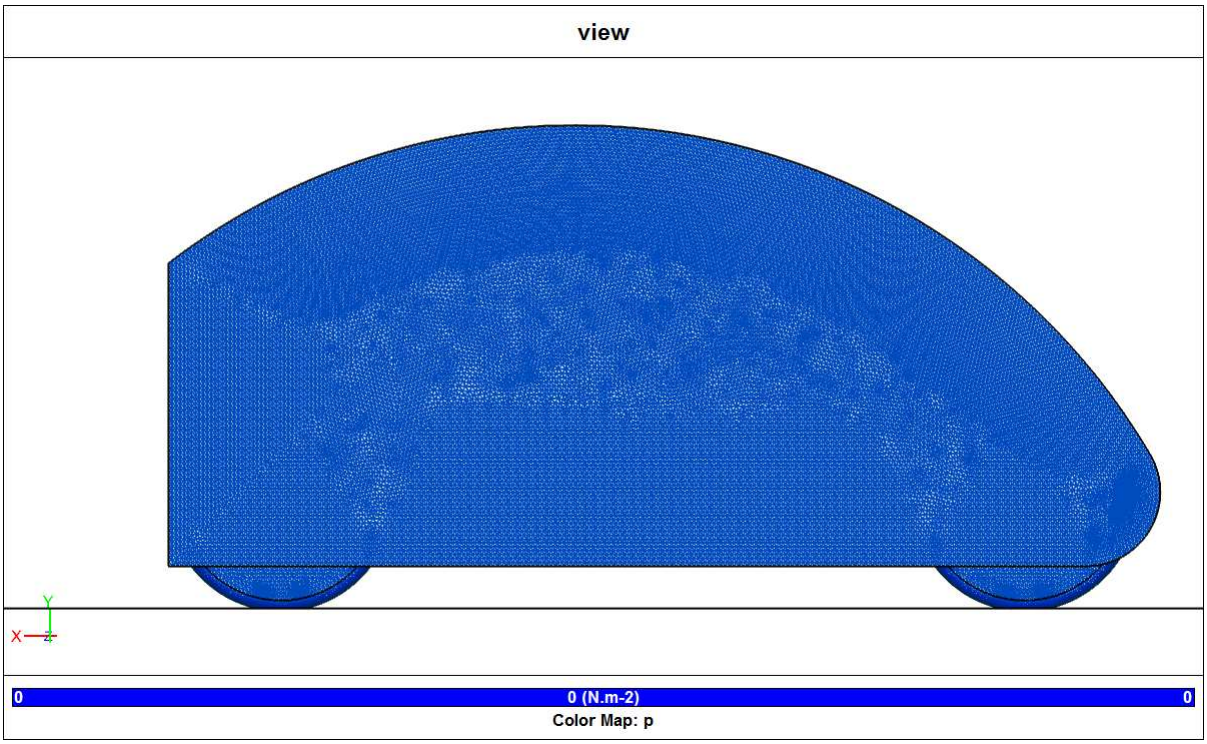

Figure C

To check the mesh quality an E ratio plot was done as shown in Figure D. Values between 0 (infinite)and 1 (no) indicate state of cell elongation ratio. Almost entire surface is above 0.5 and lowest E Ratio value is 0.168. This is favourable, acceptable is 0.1 , even less if it involves only very few and small cells.

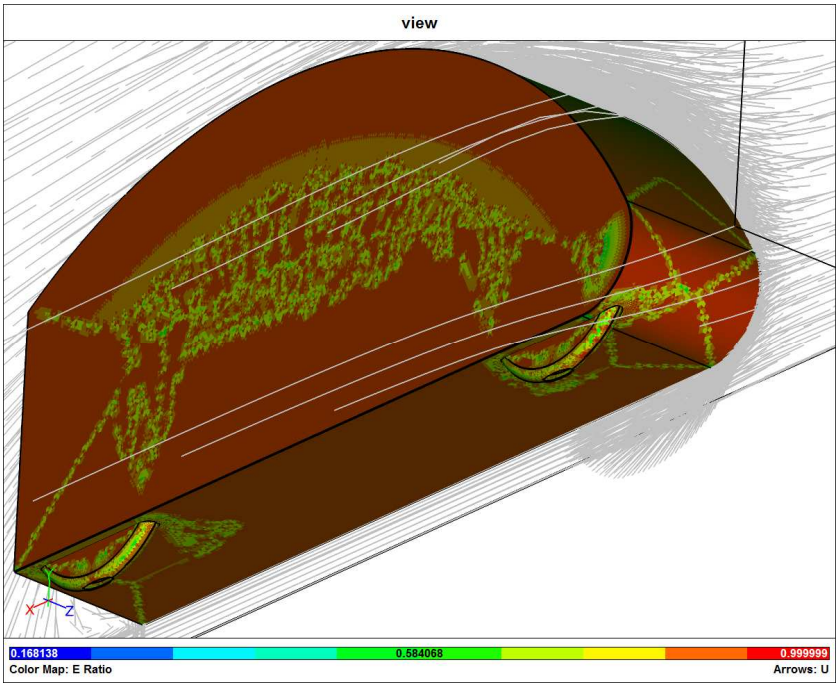

Figure D

To check for the mesh suitability for the CFD simulation a y+ plot, showing indication of how well the boundary layer model match the grid resolution. It should ideally be between 3 and 300. Figure E show values down to 1.079 so a more detailed view is needed.

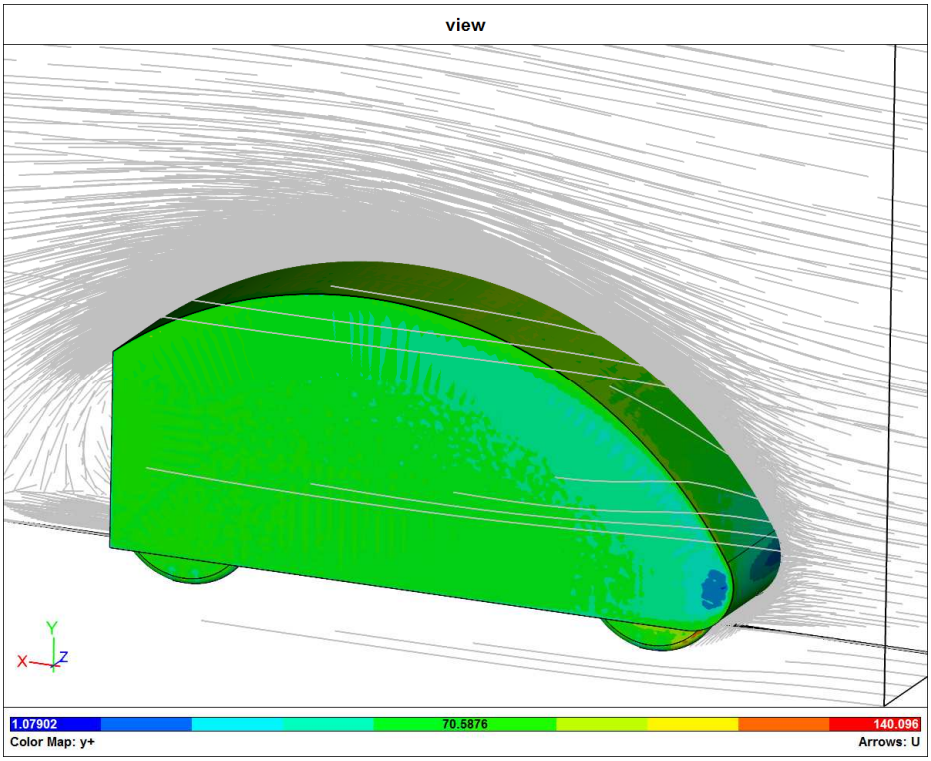

Figure E

In Figure F only surface grid cells having y+ values less than 15 is shown. One area in front at the stagnation point, and two larger areas in the turbulent area behind vehicle.

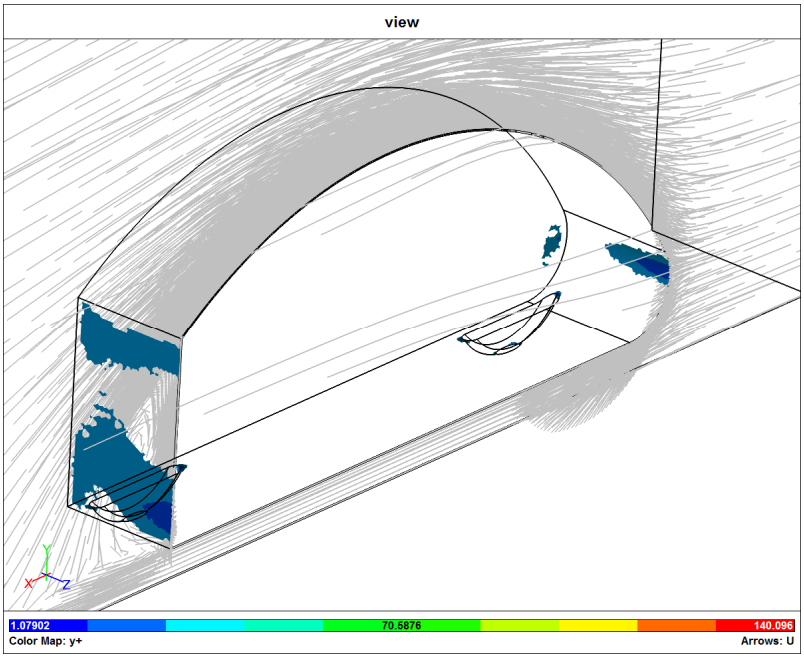

Figure F

As the areas with low y+ are not important now, the grid was deemed to be of sufficient quality and a complete simulation run was performed.

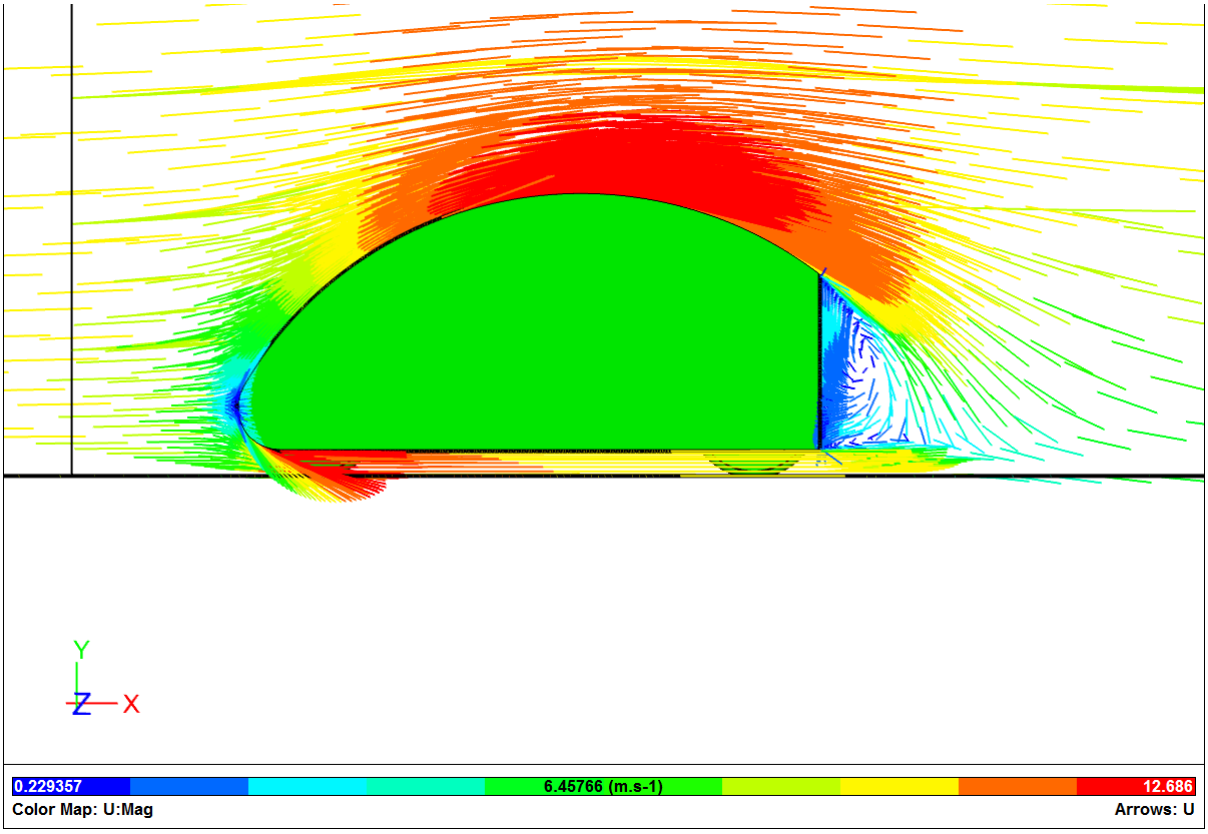

Figure G

The u plot is shown in Figure G taken from side of vehicle. It is easy to se turbulent area behind vehicle.

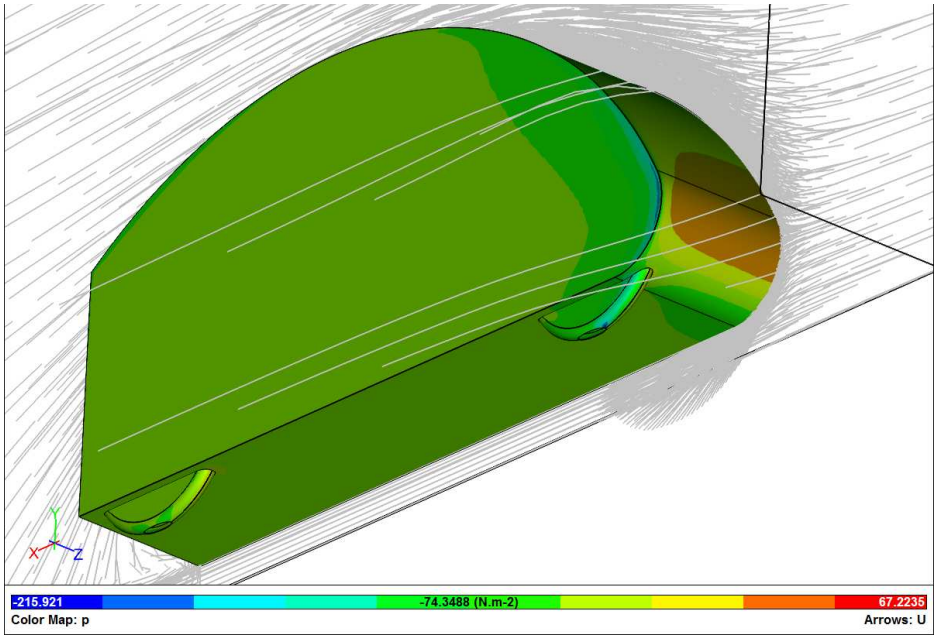

Figure H

Figure H shows pressure plot on the surface of vehicle. Pressure build up in front as expected.

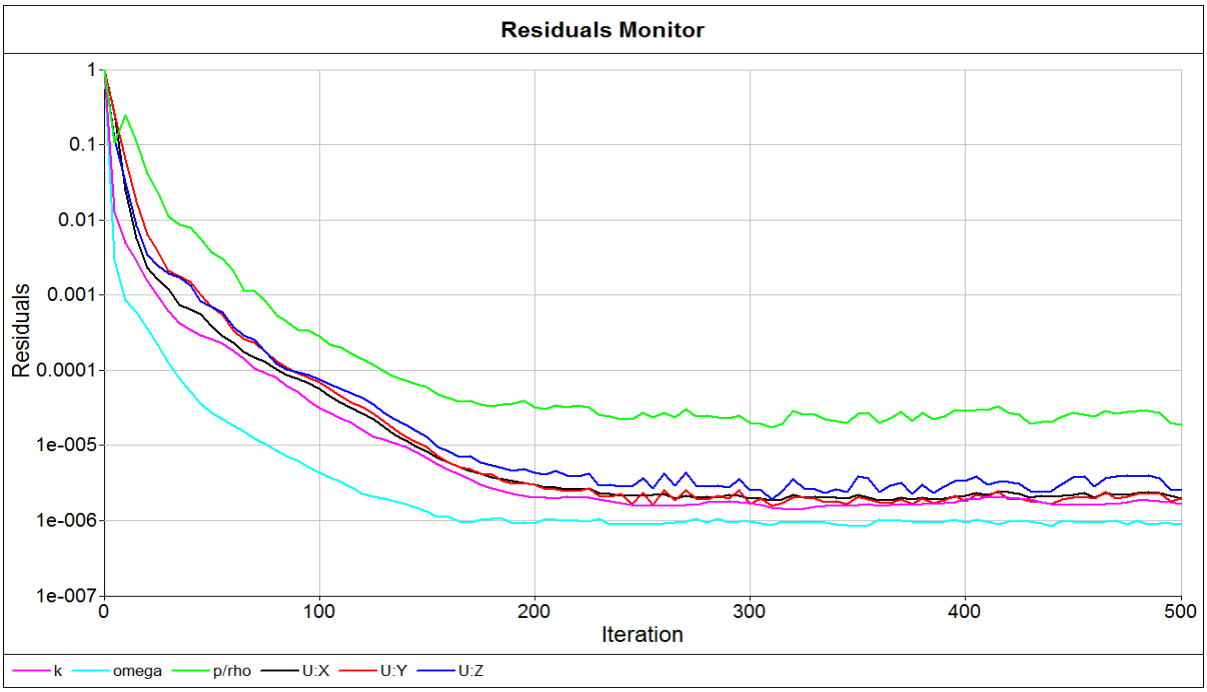

Figure I

Figure I show residuals during the simulation run. It shows good convergence of the problem as defined.

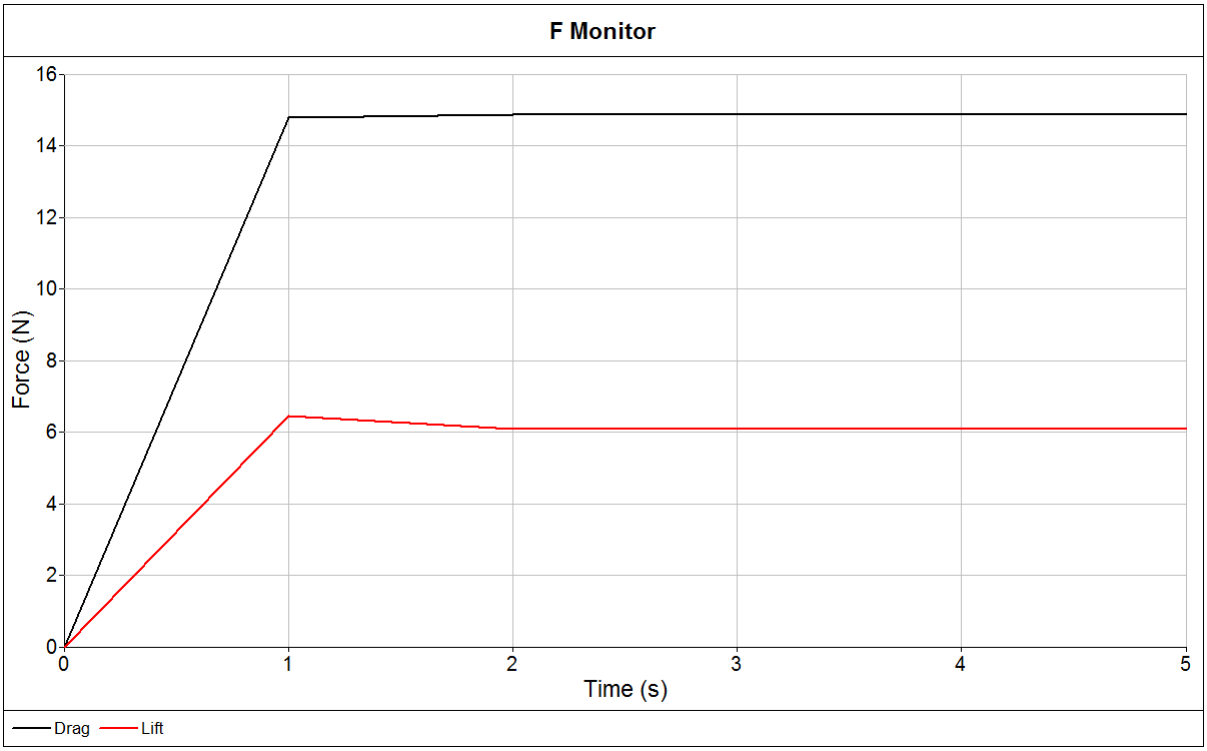

Figure J

The next figure, Figure J, show drag is very high, 14.5 N for half body, 29 N for full body. Power is equal to Force times velocity resulting in 290 W drag loss for velomobile at *v* = 10 m/s.

Air drag is given by:

$F = C_d A \frac{1}{2} \rho v^2$, where ρ is air density. Using the value for ρ from simulation (1.205 kg/m^3) the simulation give CdA of:

$$C_d A = \frac{2F}{\rho v^2} = 2 \frac{29\ N}{120.5 \frac{kg}{ms^2}} = 0.481\ m^2$$

With frontal area of 0.3992 m^2 for half body, the calculated dimensionless VELO14 C_d is 0.603

A verification simulation in FLUENT of the same VELO14 model resulted in 13.2 N drag and 8.5 N lift. As can be seen from screenshots, the resolution is quite high. The screenshots also include comprehensive description so the pictures speak for themselves:

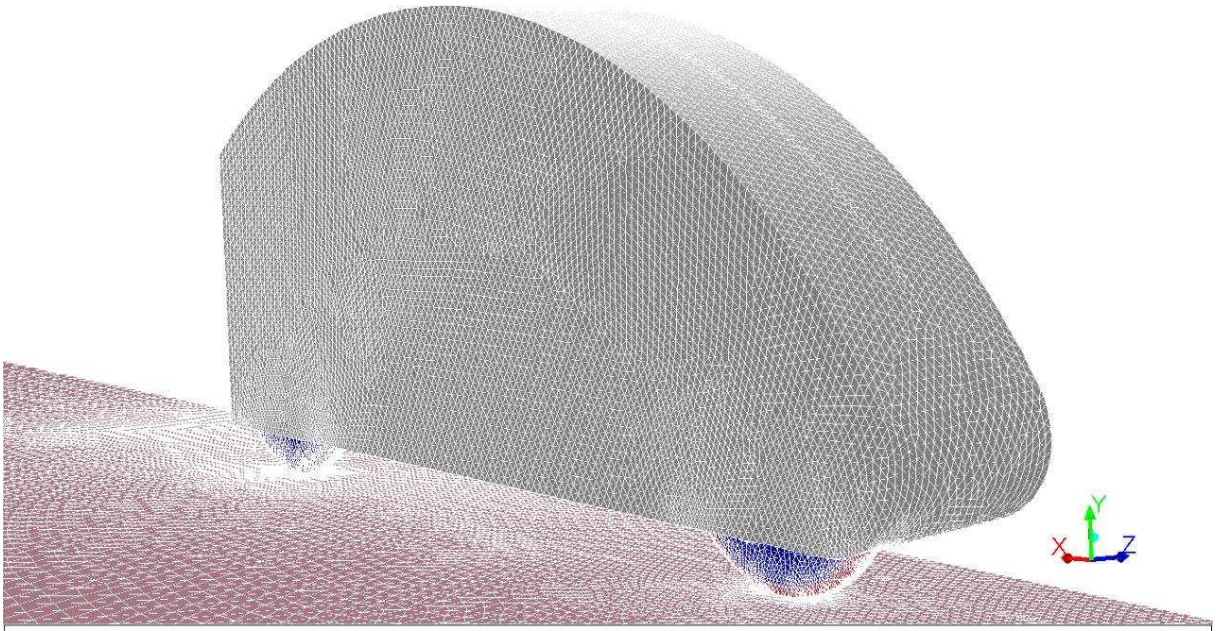

Mesh

May 30, 2014
ANSYS Fluent 14.5 (3d, dp, pbns, sstkw)

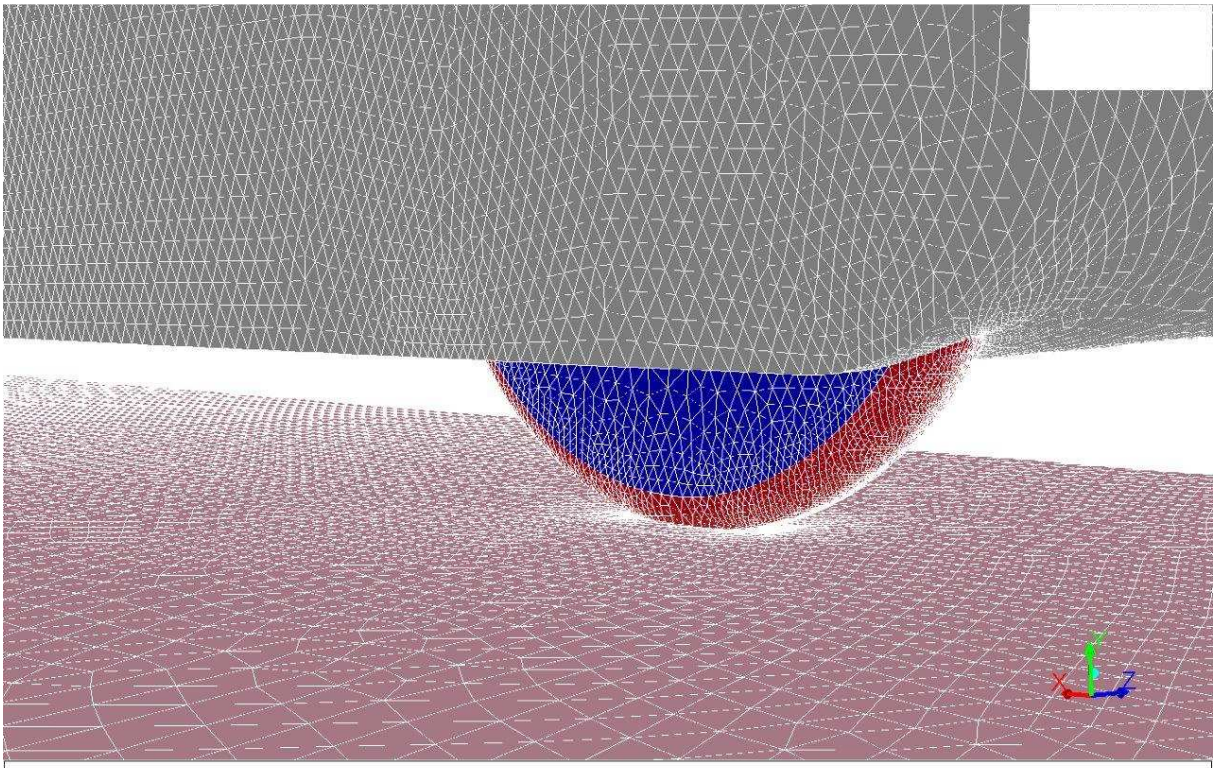

Mesh

May 30, 2014
ANSYS Fluent 14.5 (3d, dp, pbns, sstkw)

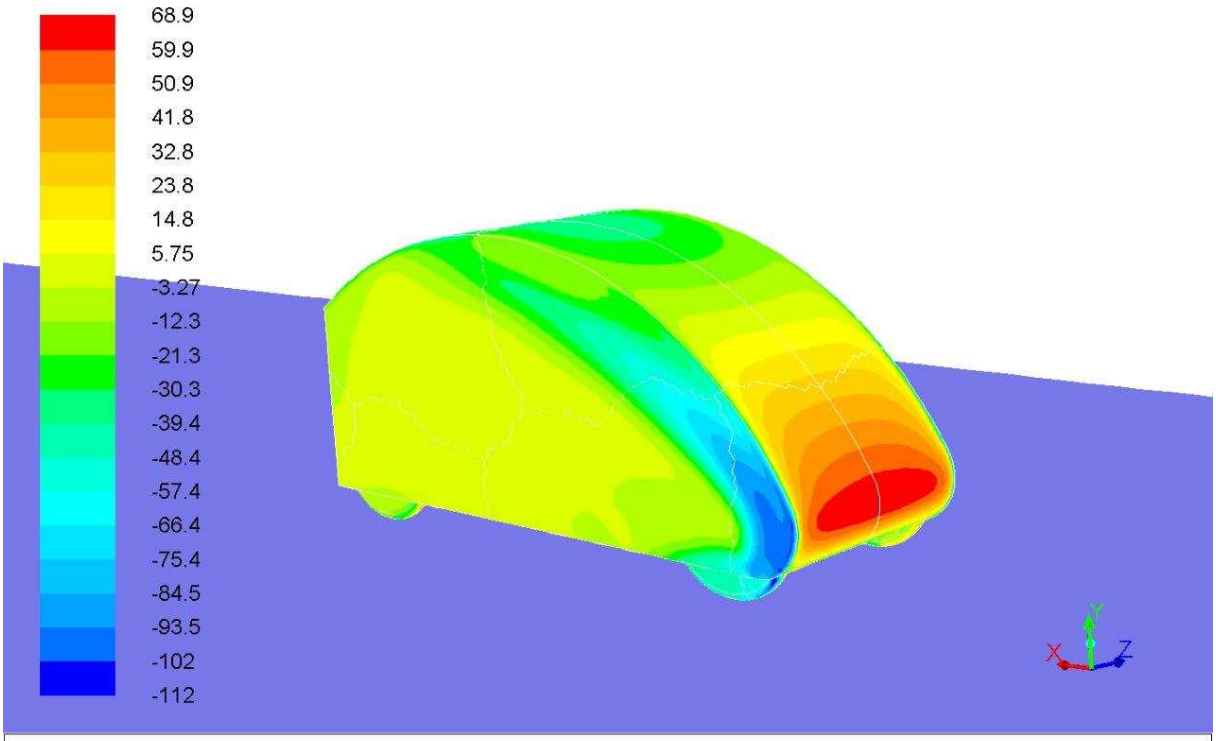

Contours of Static Pressure (pascal)

Flow Design Bureau AS
May 30, 2014
ANSYS Fluent 14.5 (3d, dp, pbns, sstkw)

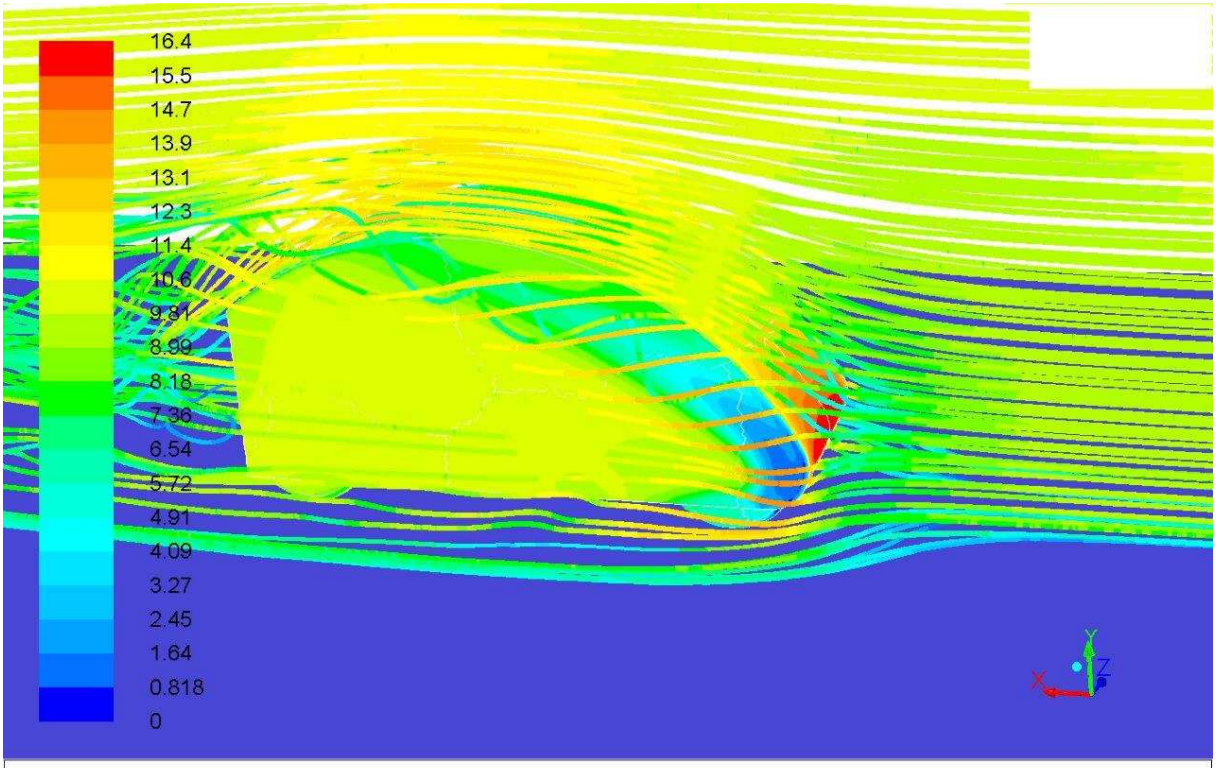

Pathlines Colored by Velocity Magnitude (m/s)

May 30, 2014
ANSYS Fluent 14.5 (3d, dp, pbns, sstkw)

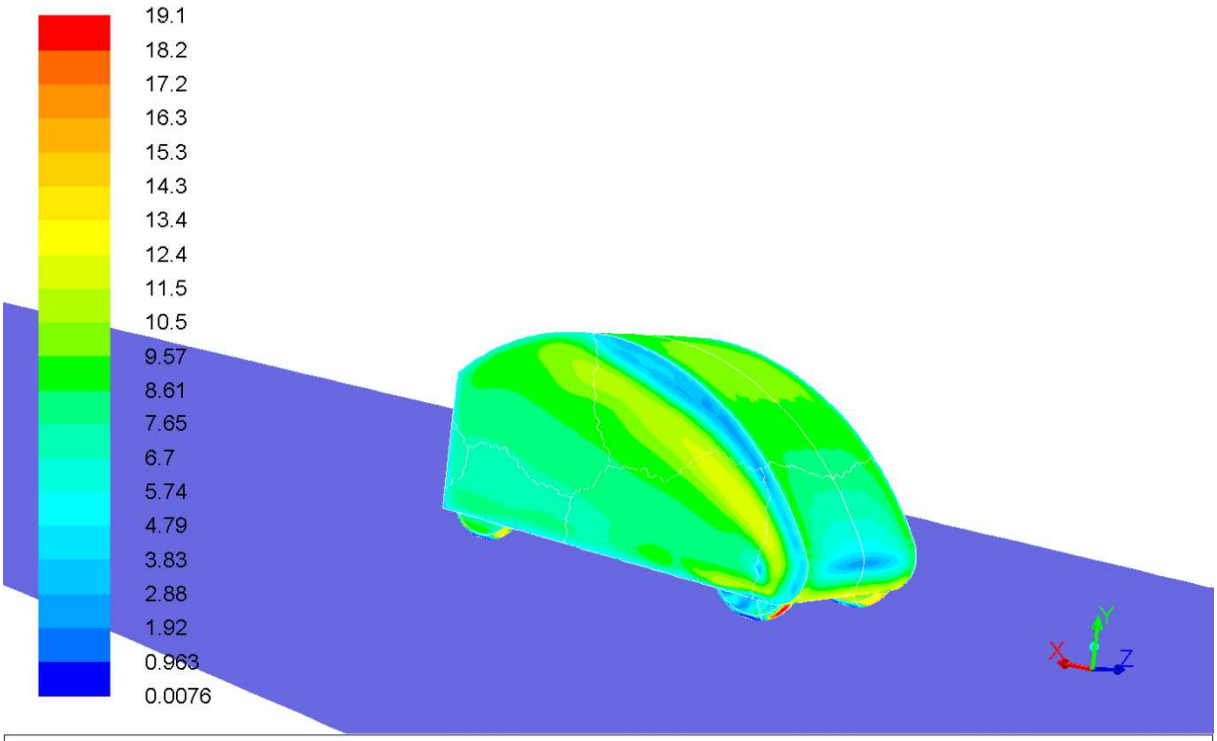
19.1
18.2
17.2
16.3
15.3
14.3
13.4
12.4
11.5
10.5
9.57
8.61
7.65
6.7
5.74
4.79
3.83
2.88
1.92
0.963
0.0076
Y
X
Z
Contours of Wall Yplus
Flow Design Bureau AS
May 30, 2014
ANSYS Fluent 14.5 (3d, dp, pbns, sstkw)

The result from FLUENT was a bit lower drag than from the first simulation run and motivated to two consecutive simulations within Caedium with higher resolution. The first one increased resolution from 2M to 4M cells. Then drag became 13.3 N, very close to the FLUENT result. A final 7.6M cells simulation run resulted in drag increasing again to 13.5 N.

VELO15

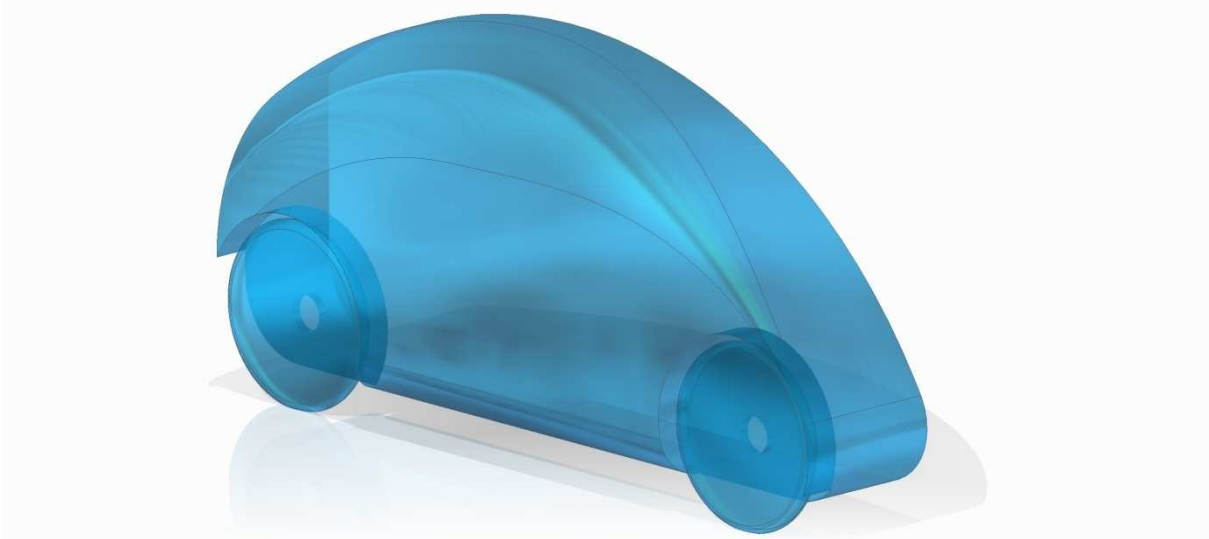

Figure K

VELO 15 differs from VELO 14 in having wheel cavities and a much rounder shape as shown in Figure K. Mesh is shown in Figure L with details of wheel in Figure M

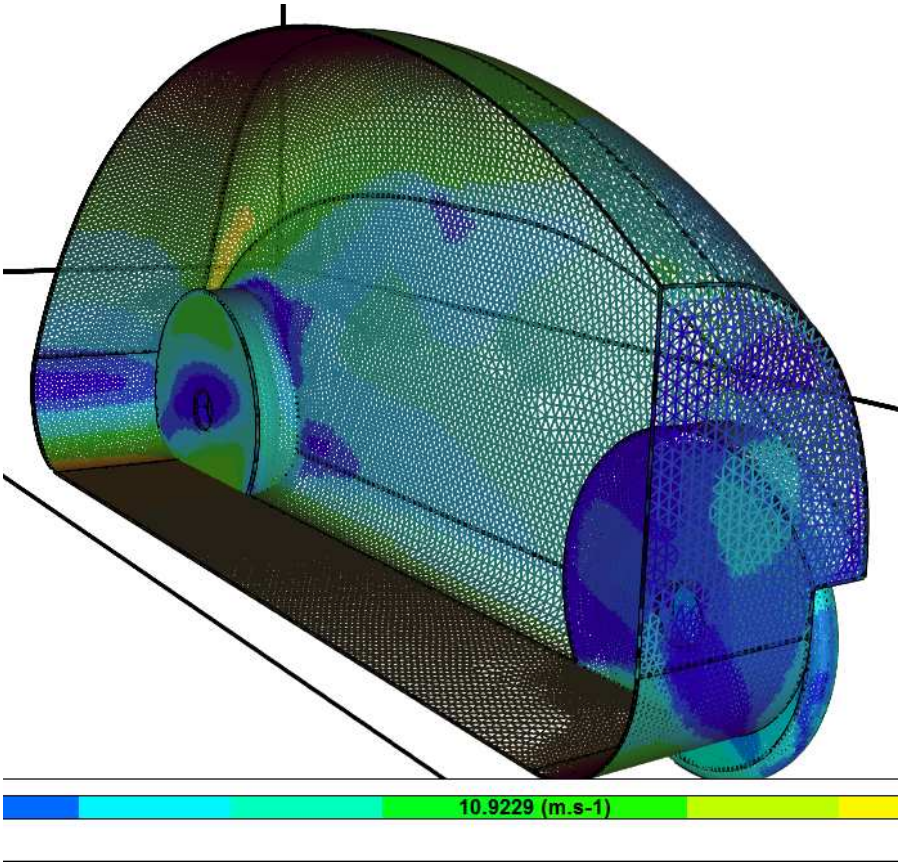

Figure L

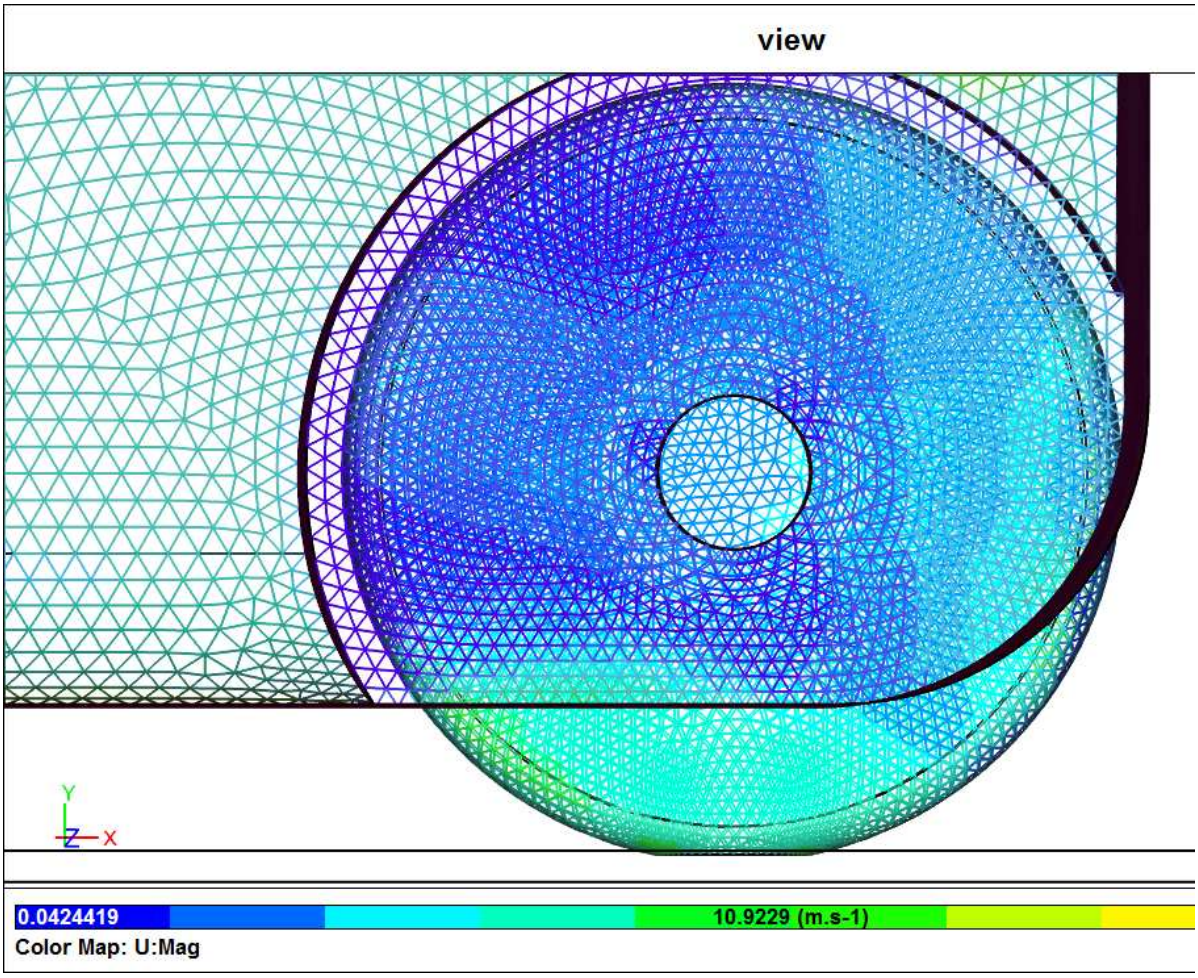

Figure M

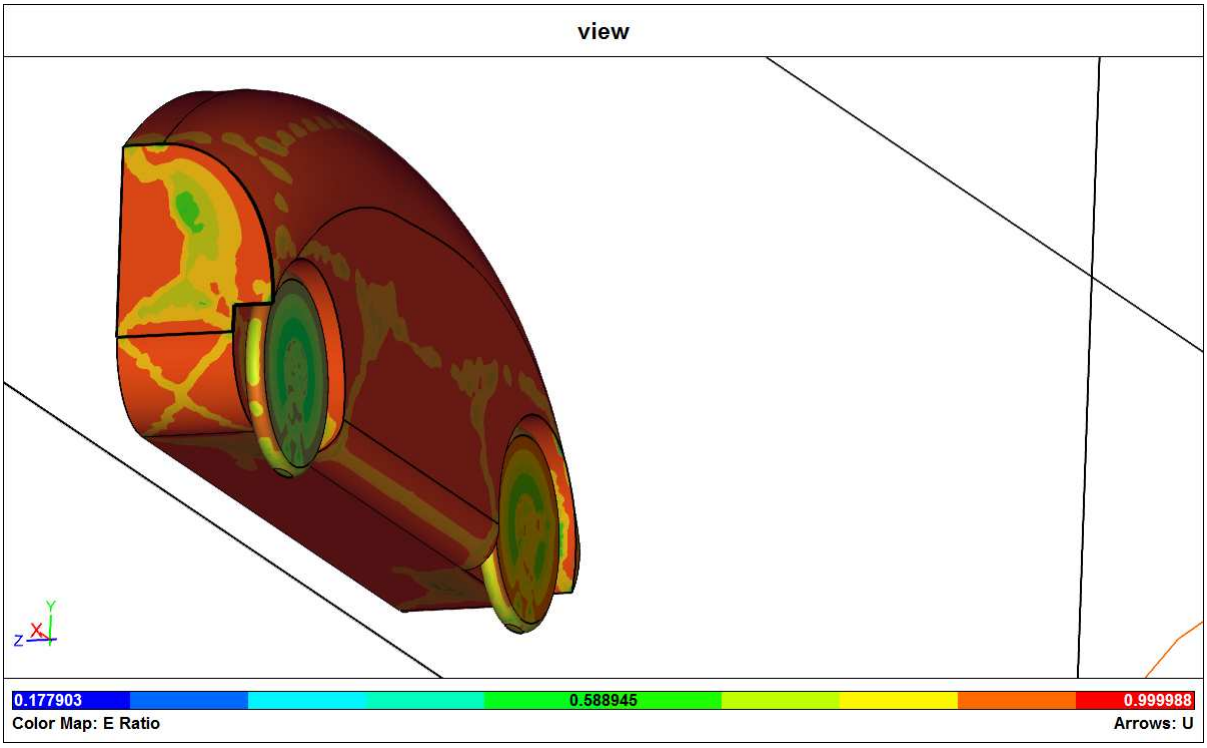

Figure N

In Figure N the quality of surface mesh is inspected by plotting E ratio.

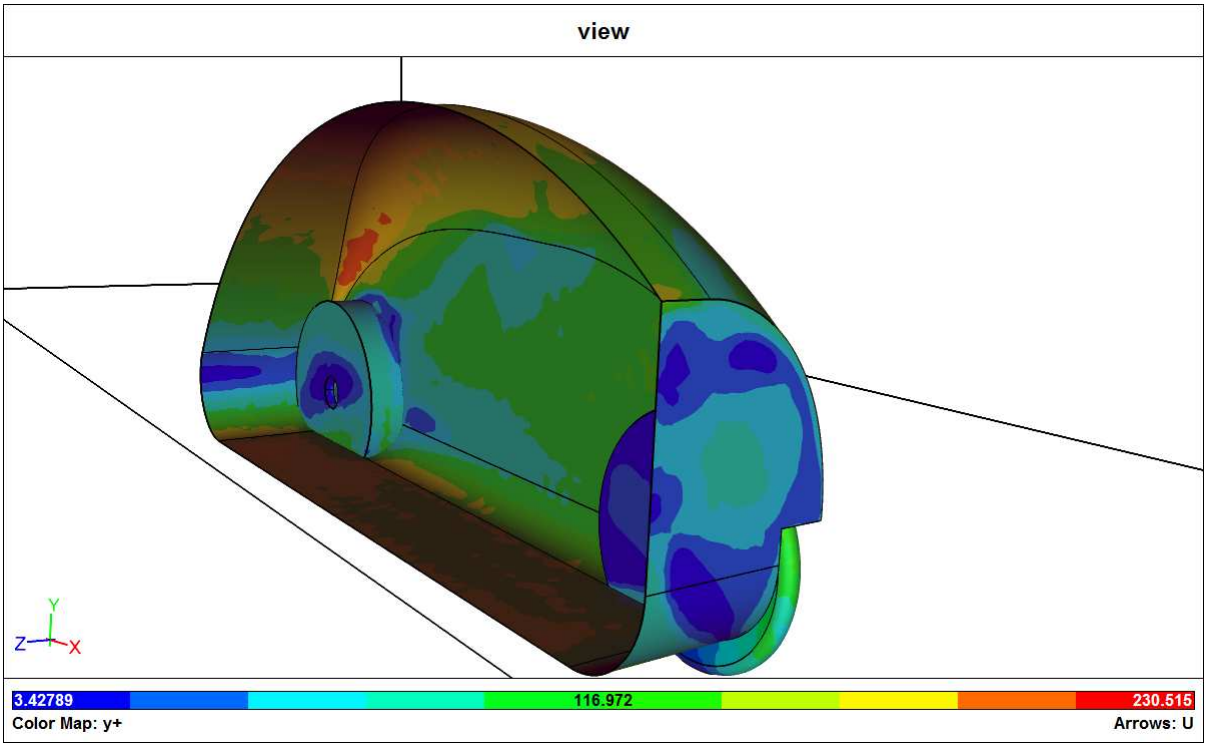

Figure O

Y+ is within recommended range, 3-300, as shown in Figure O. A volume mesh control was performed, with a plot of surfaces in the volume mesh having Vol ratio less than 0.1 in Figure P.

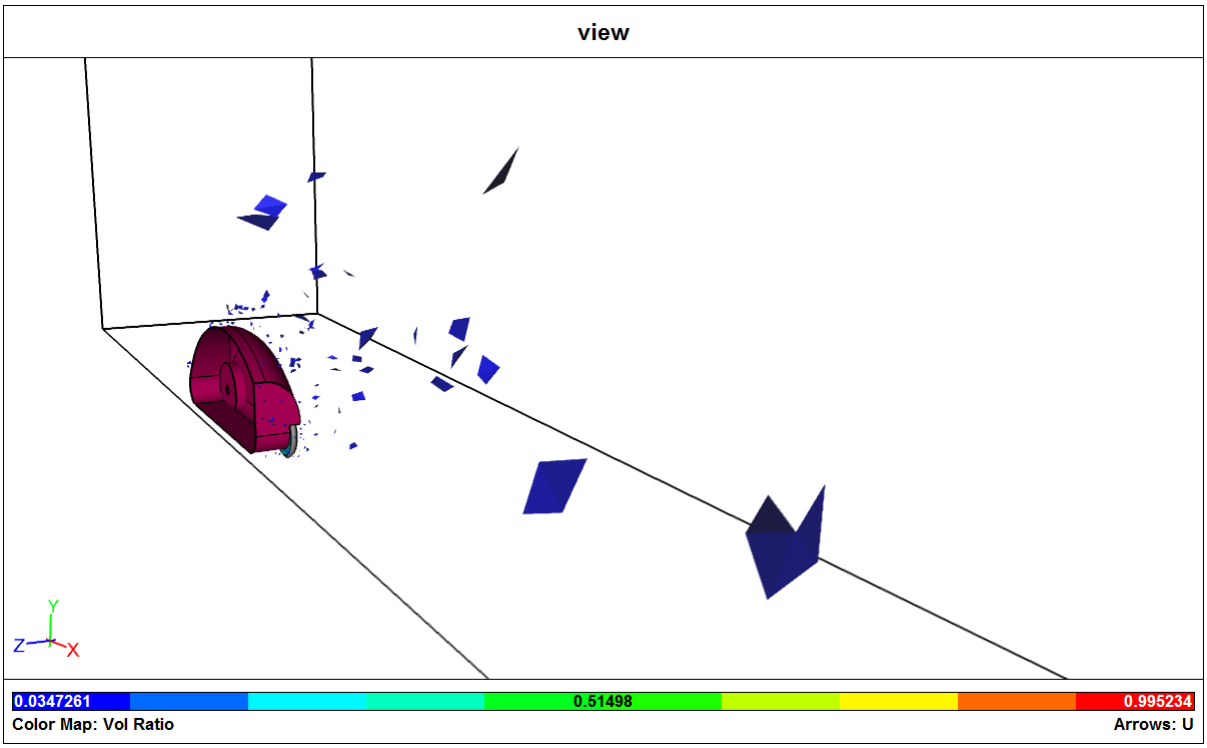

Figure P

Initially, a simulation run was performed with rotational surfaces on the wheels matching ground speed of 10 m/s. The drag result is shown Figure Q.

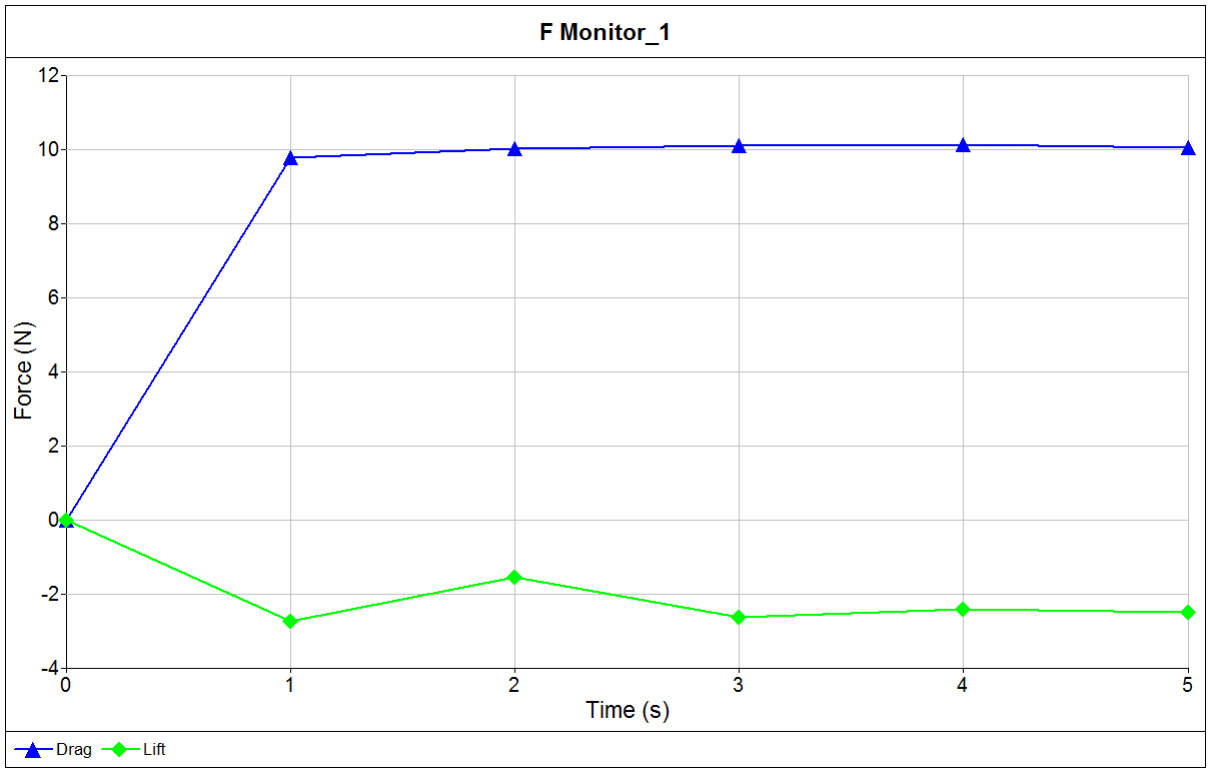

Figure Q

It was then compared to a second run with no rotation on wheels shown in Figure R

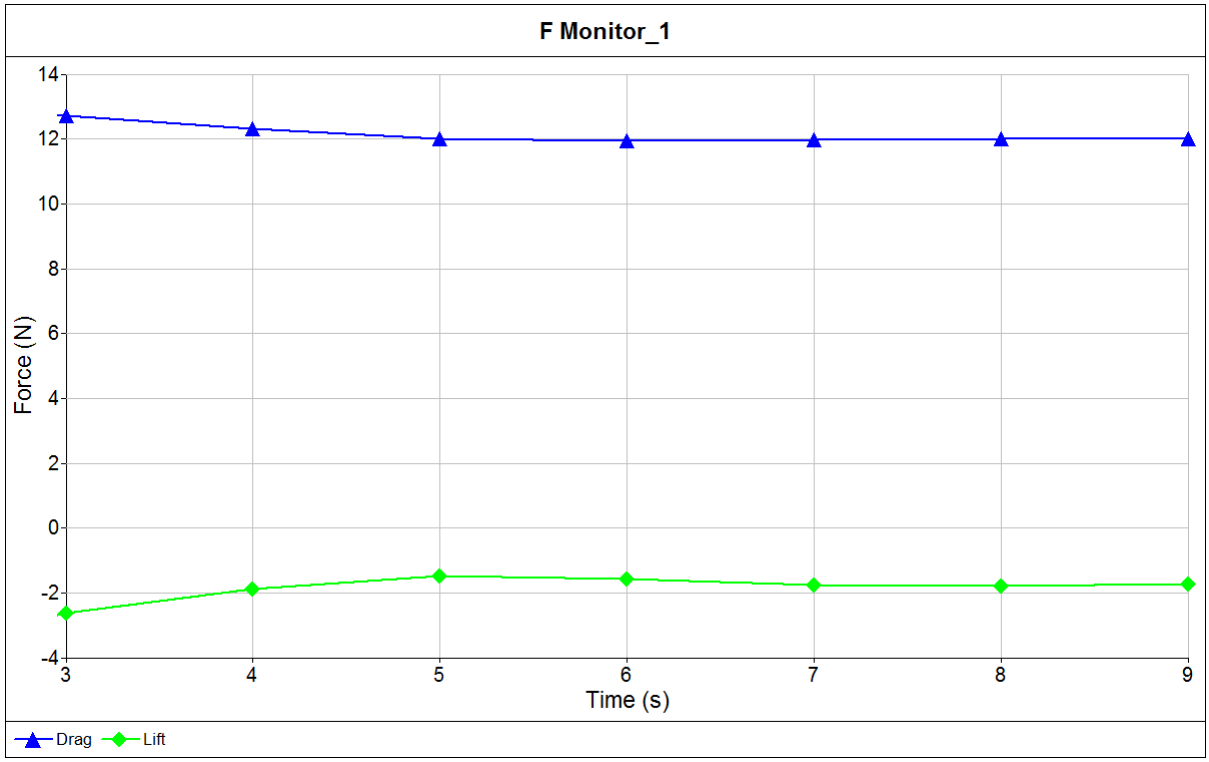

Figure R

The increase in drag can be said to be consistent with information from [3]. In his book he writes that they found lower drag on rotating wheels but no practical difference in simulations and wind tunnel testing of drag with and without rotating wheels. This was due to decrease in drag with rotating wheels was compensated by increase of drag due to air pumping effect. In their application (solar cars) they used wheel fairings having a closed volume around the wheel where wheel spinning acted as an air pump increasing drag on wheel rotation. The VELO 15 simulation does not take into account energy required to keep wheel rotating, missing air pump drag.

Residuals show good convergence, as shown in Figure S

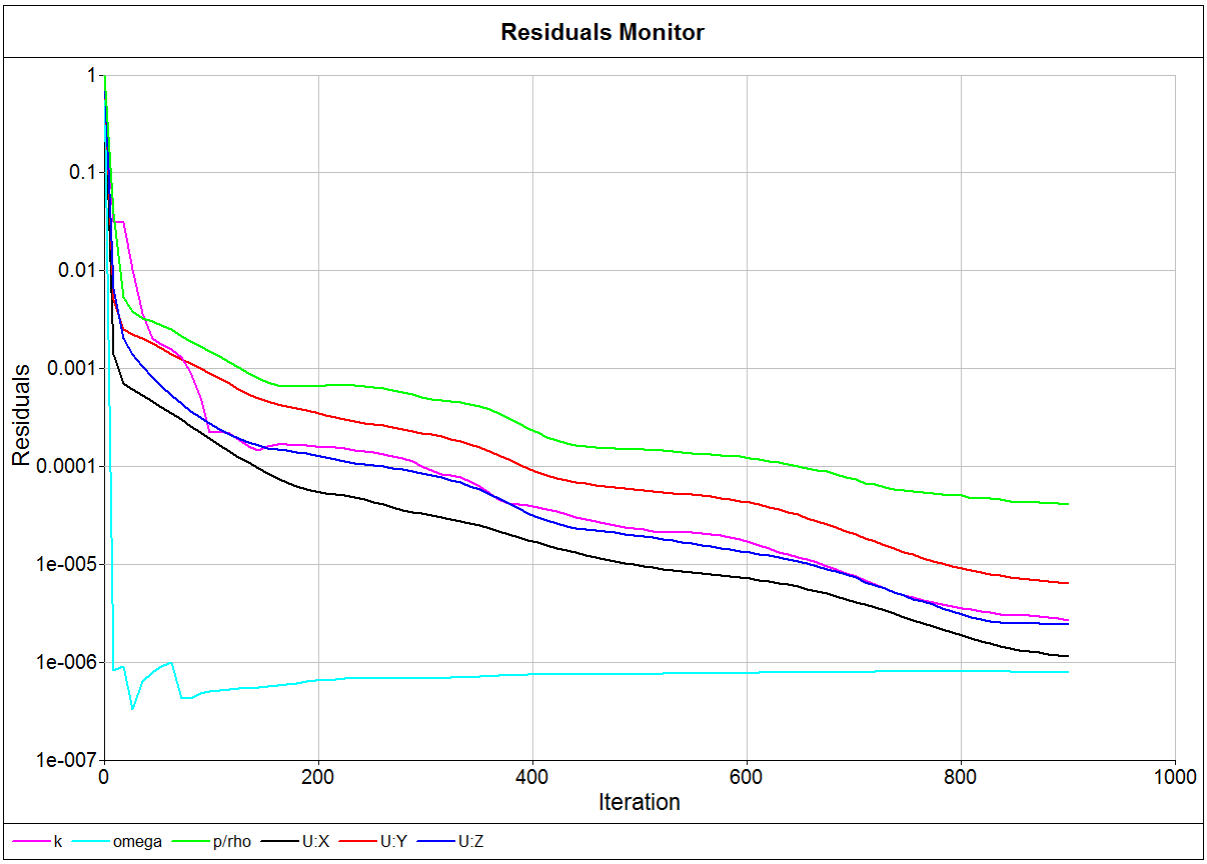

Figure S

VELO 16

A new design iteration having closer resemblance to design model can be seen in Figure T. Initially some problems were caused by sliver surfaces in the model as seen in centre of Figure U.

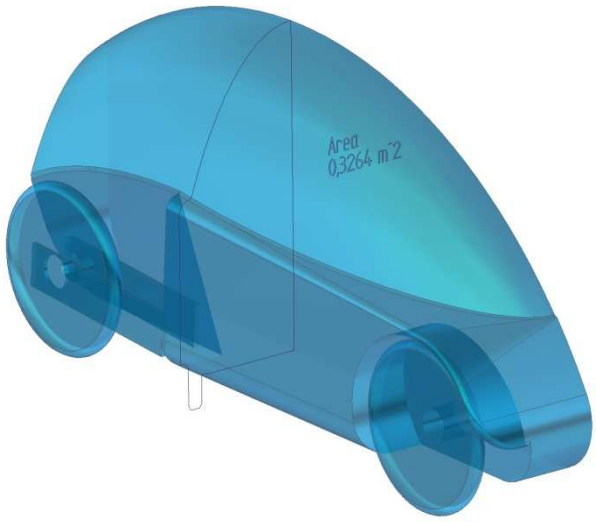

Figure T

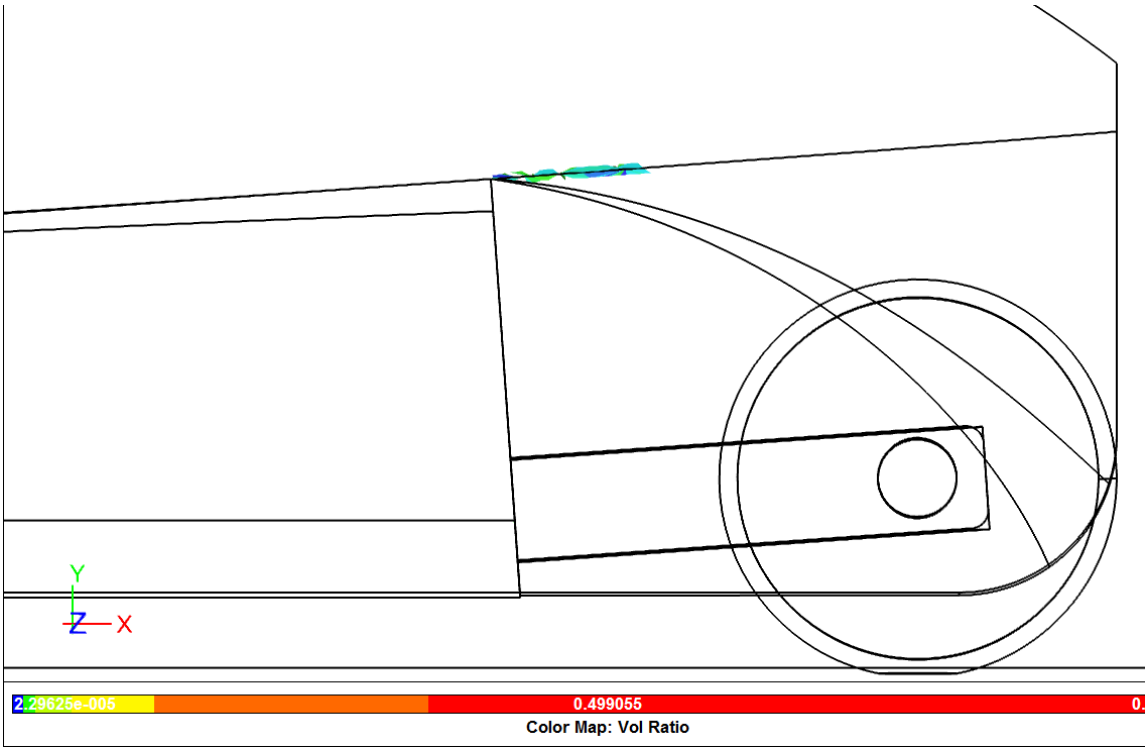

Figure U

Adding a 7 mm chamfer to the edge between canopy and rear side made the meshing algorithm work its magic resulting in a nice surface mesh as shown in Figure V. Altough nice, it was not nice

enough, causing the volume mesh to fail. After closer examination some very sharp corners were found on certain surfaces, as indicated by some cells having an E ratio < 0.1. Slightly altering these surfaces improved the E ratio, as evident in Figure W.

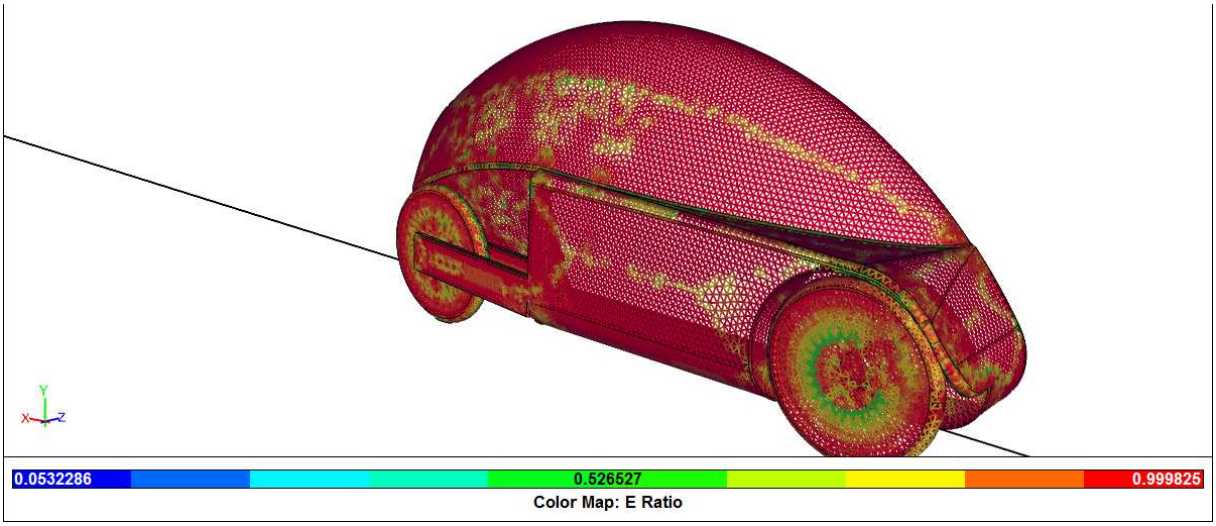

Figure V

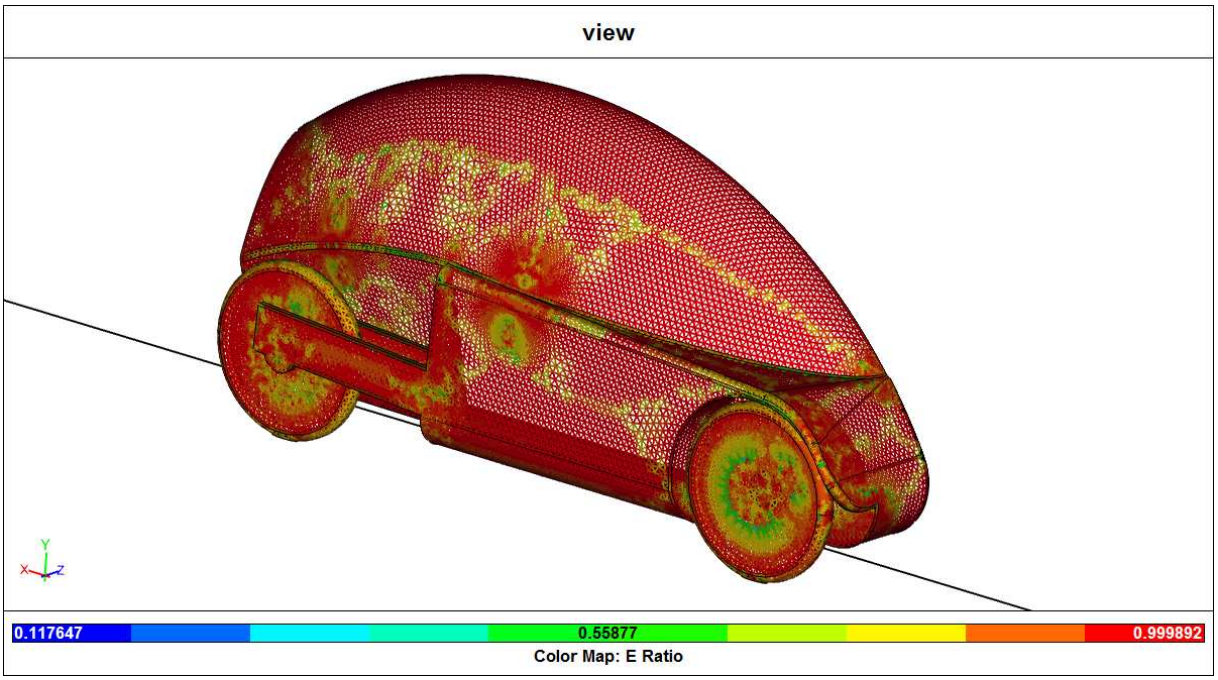

Figure W

Three different meshes were used. WT16-04 had a drag of 9.7 N with 0.59M cells. WT16-041 had 2M cells and gave a drag of 9.2 N. Finally WT16-042 with 7.8M cells gave a drag of 8.8 N and the first simulation run where the velomobile body is having less air resistance than a race cyclist. Mesh details can be seen in Figure X.

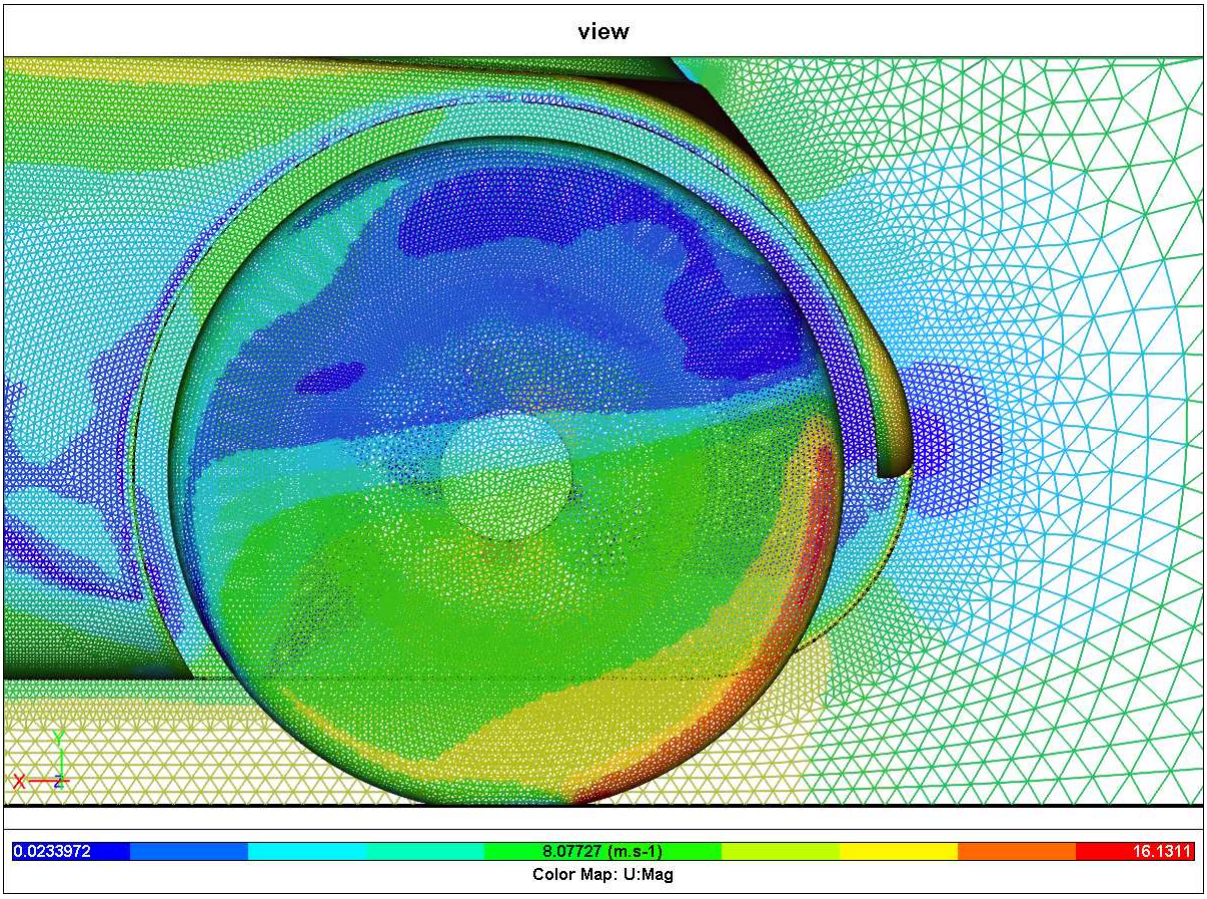

Figure X

The high resolution used in the last simulations takes too much time for efficient development so reducing the resolution and still achieving reasonable results was consequently adopted by changing meshing parameters.

VELO17

The next iteration is identical to VELO16 but has an internal channel for simulating ventilation. Inlet is at stagnation point in front and exit is at upper rear edge of canopy, see Figure Y

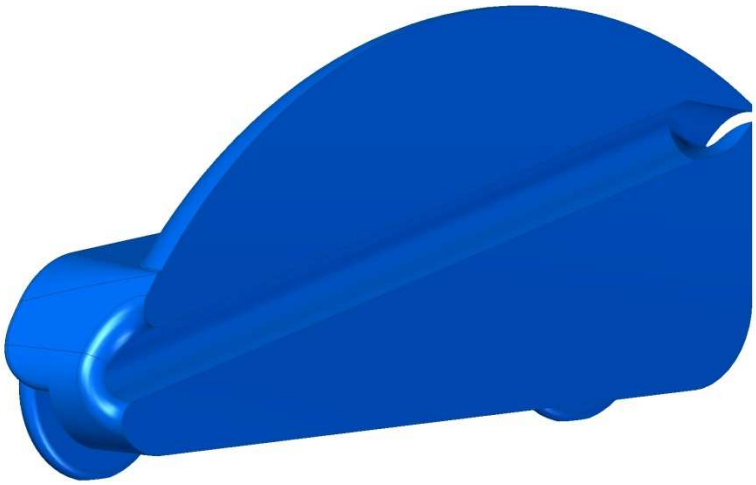

Figure Y

Inlet has a rounding radius of 50mm while ventilation shaft has an inner diameter of 150 mm. Coefficient of pressure, C_p is shown in Figure Z and the velocity in Figure AA

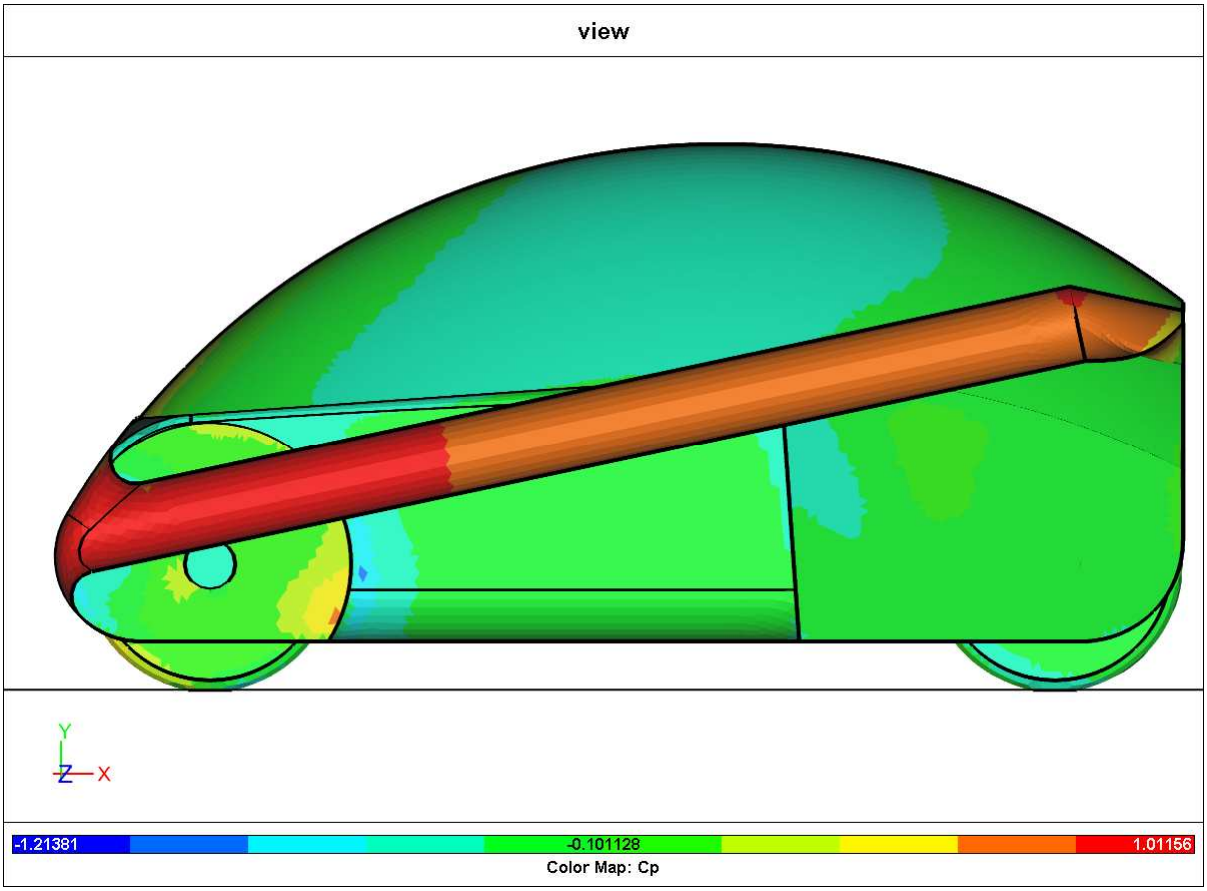

Figure Z

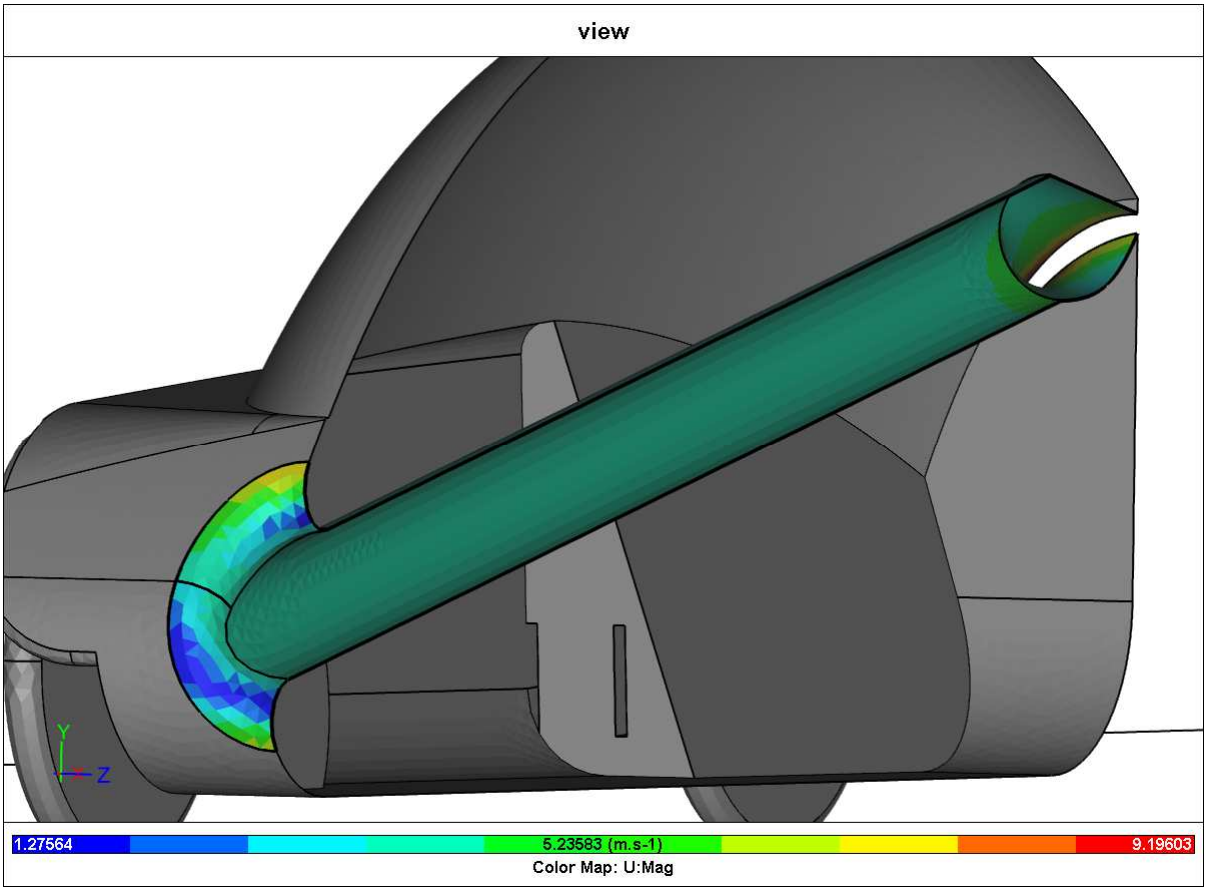

Figure AA

VELO18

The first attempt on making the body as initially planned was VELO18, with a classic boat tail look with associations from a 1930's era *Auburn Speedster*. Having slim wheel housings for each rear wheel, drag is reduced by gradually reducing centre cross section from all sides. It took several tries before meshing succeded. Line length inspection was an important tool for finetuning 3D model to have suitable surfaces for the mesher, see Figure BB.

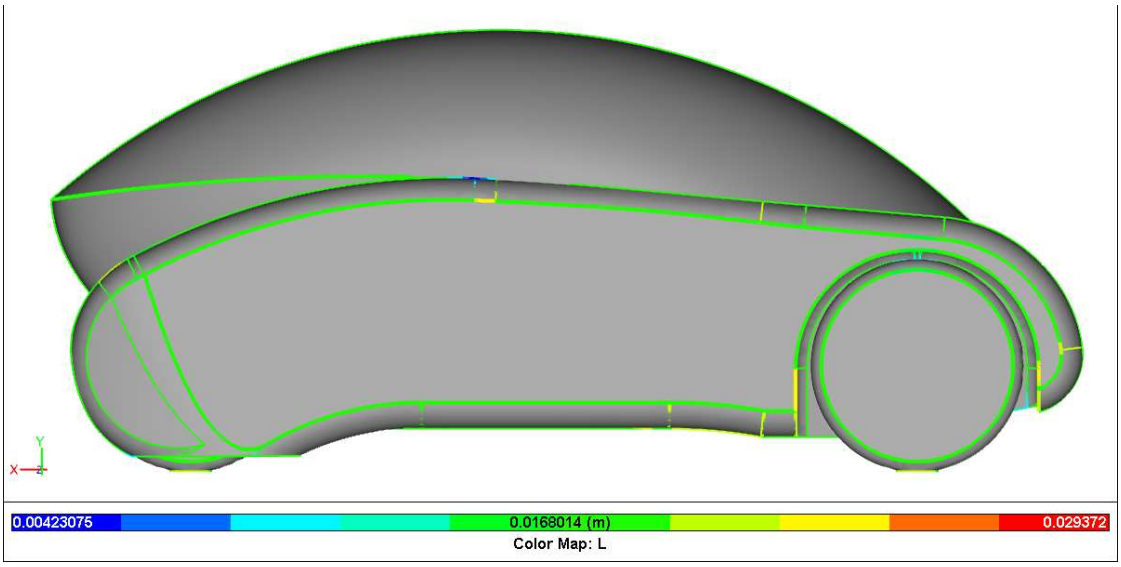

Figure BB

The front was more aggressive since it was much easier to model, see Figure Å and Figure DD.

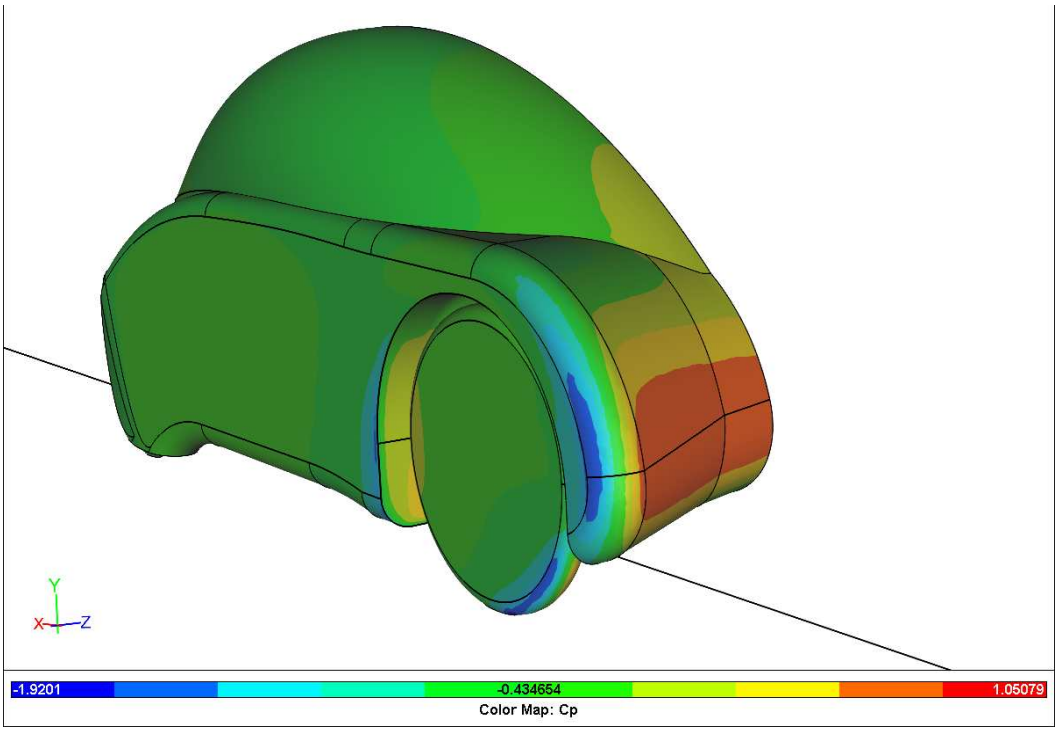

Figure Å

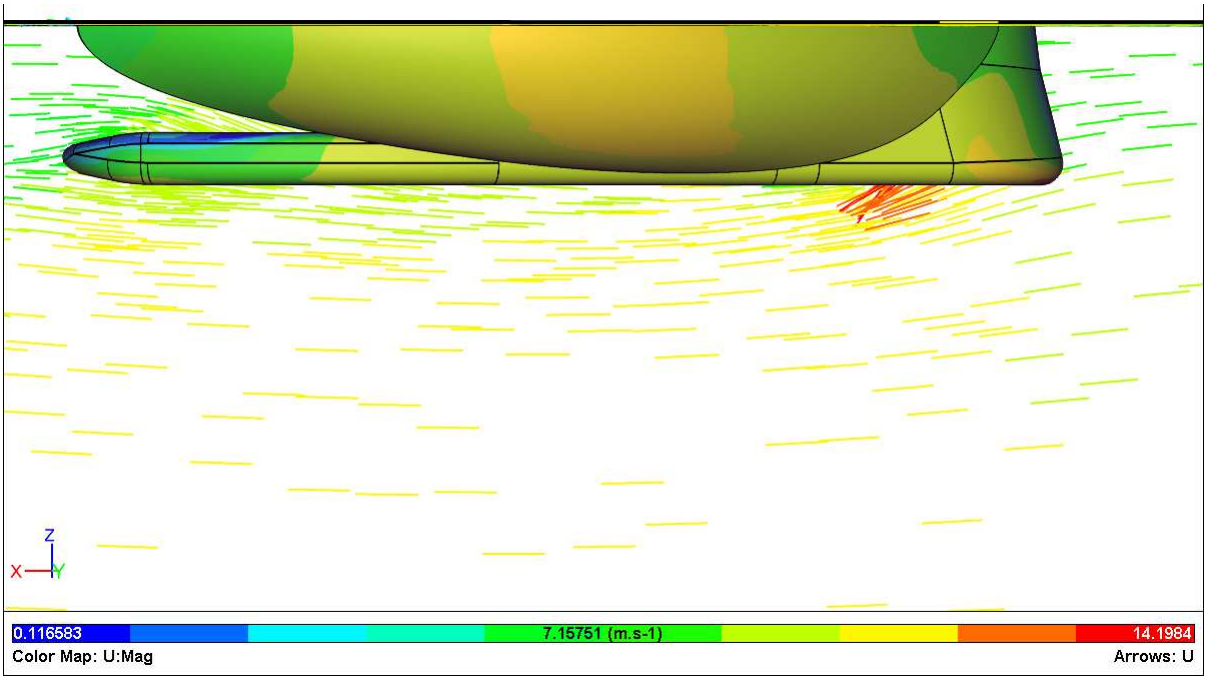

Figure DD

There are still some turbulence that can be avoided. The merging of flow over and under does not merge where it ideally should, at the edge of the canopy. The air flows merge at the low velocity zone underneath the edge, see Figure EE

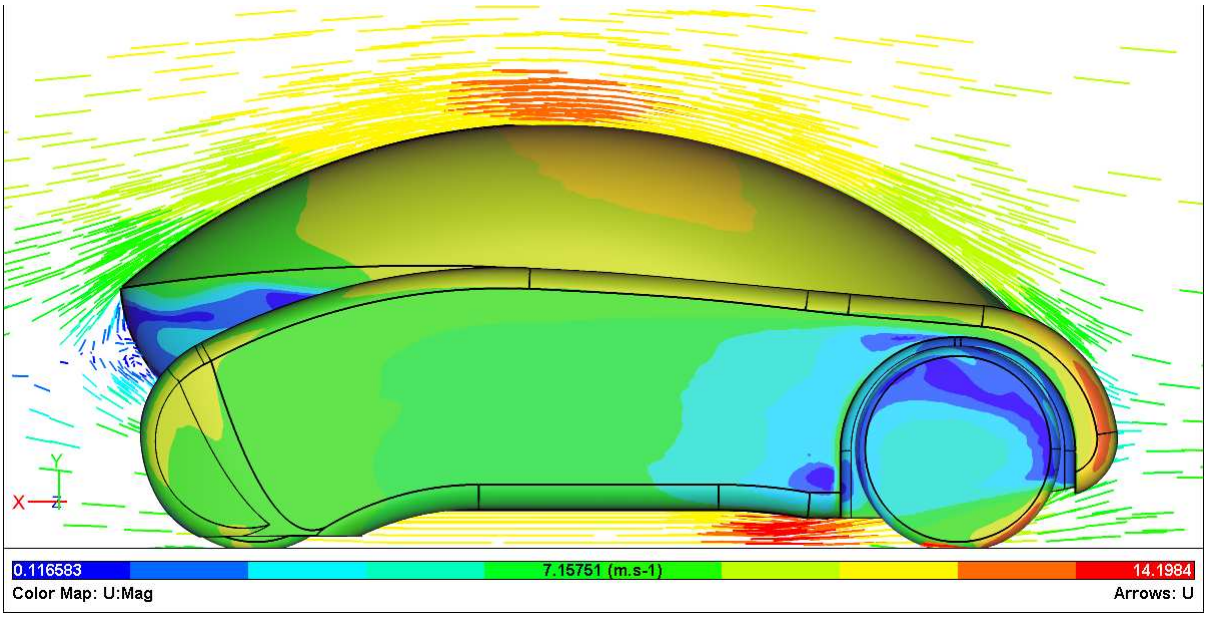

Figure EE

Some strange fluctuations showed up in the residuals, and a finer mesh was tried but the fluctuations on the residuals were still there, as shown in Figure FF.

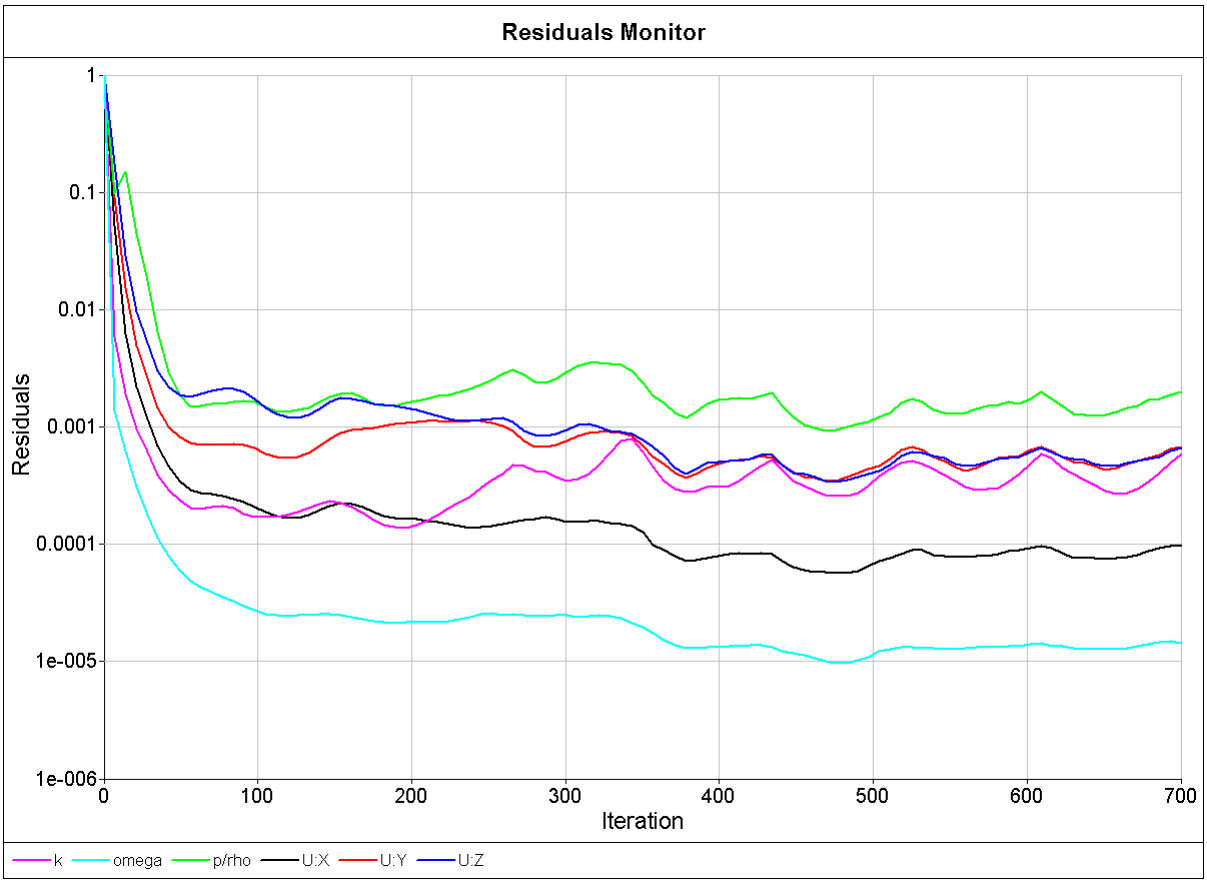

Figure FF

Still, the results converged, lowering drag to 7.3 N, the lowest so far, see Figure GG.

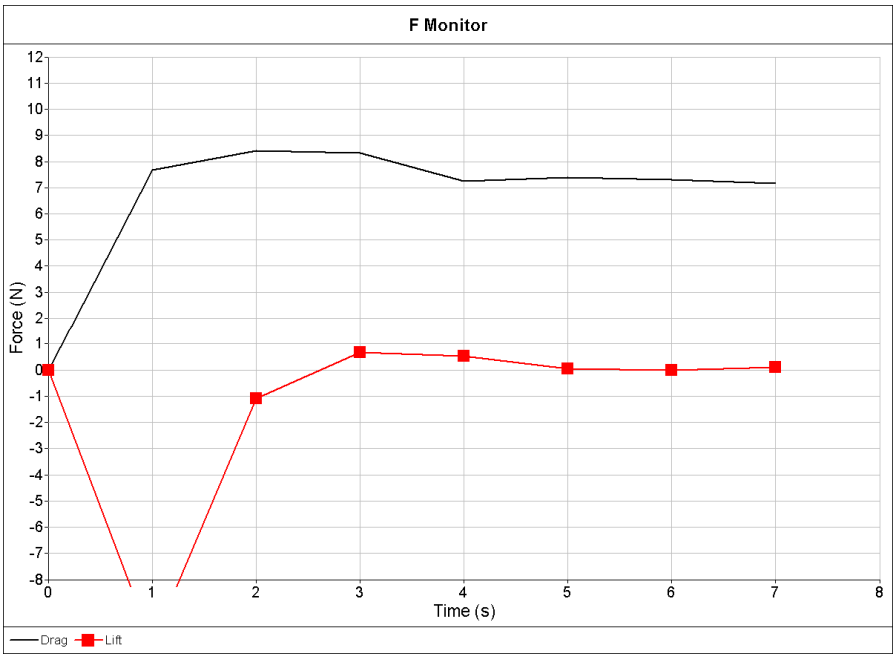

Figure GG

VELO19

The addition of ventilation port to VELO18 is VELO19. The ventilation geometry is slightly different from VELO17 due to different rear end. The ressure plot and the velocity plot indicates less ventilation flow, see Figure EE and Figure II.

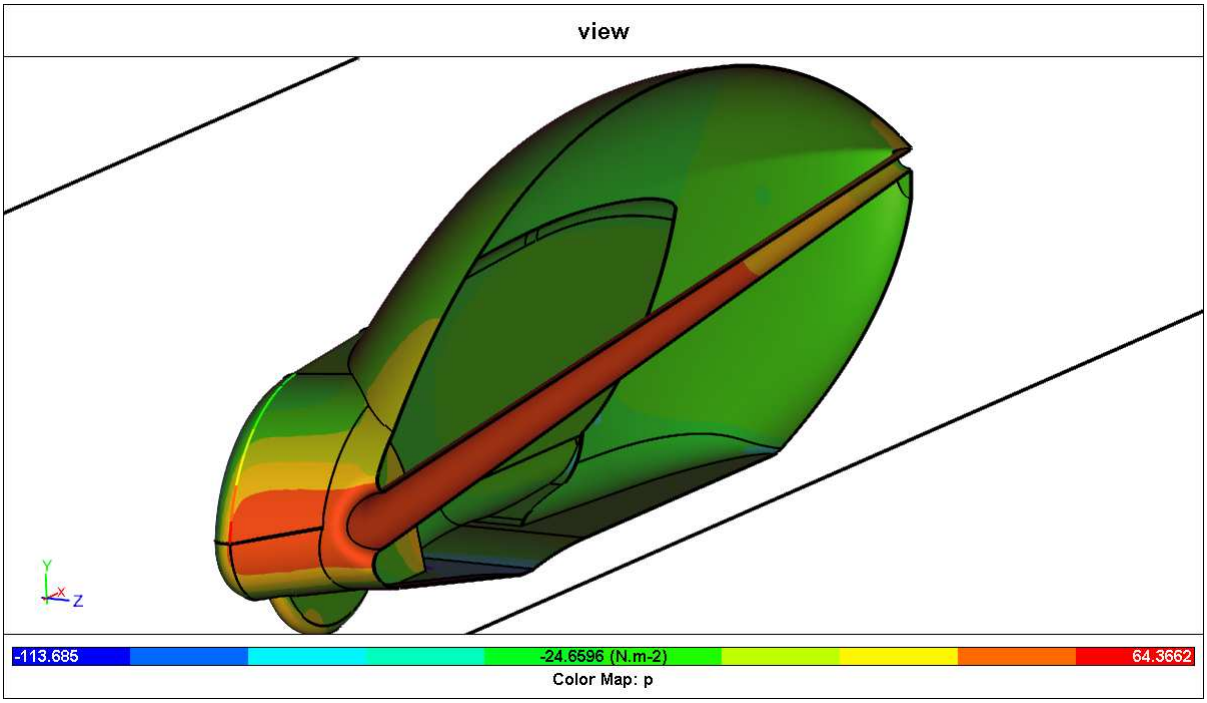

Figure EE

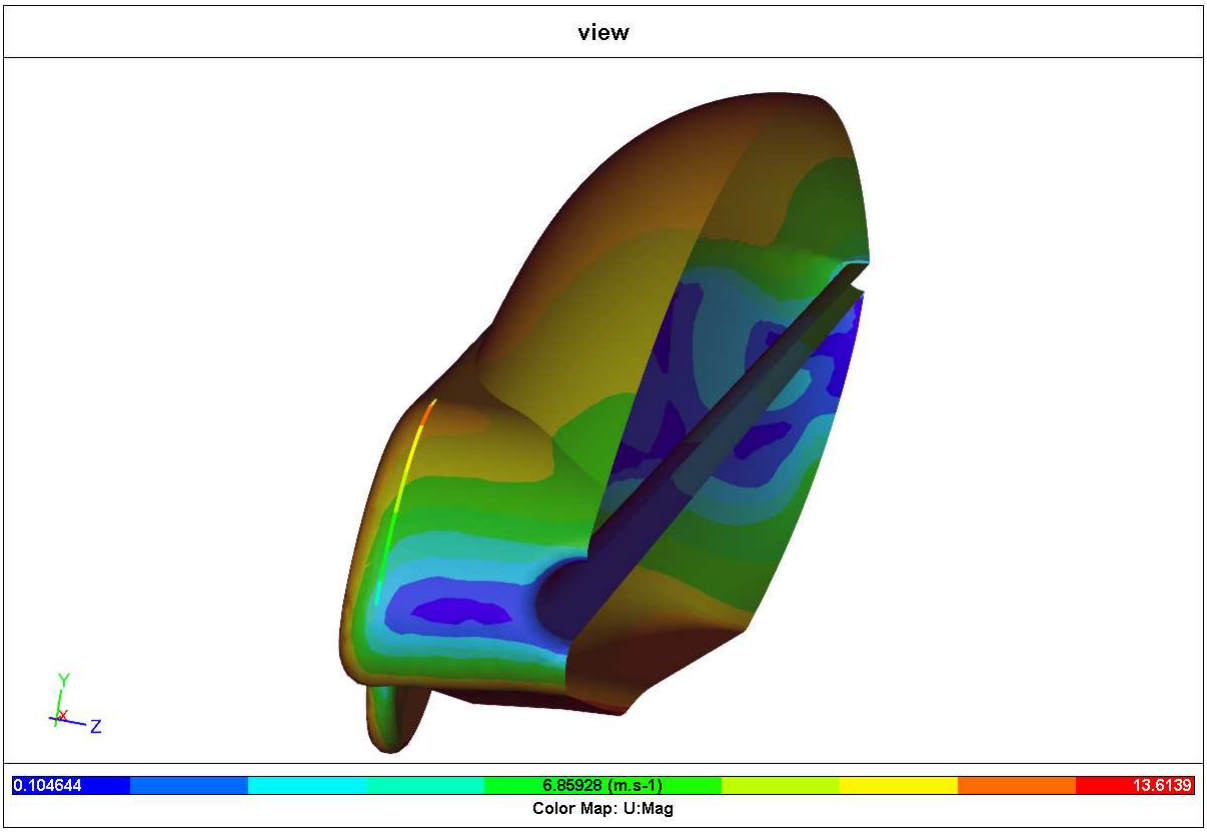

Figure II

VELO20

Cooling of the cyclist is important. VELO20 is a thin walled version of VELO19 with a cyclist added, see Figure JJ.

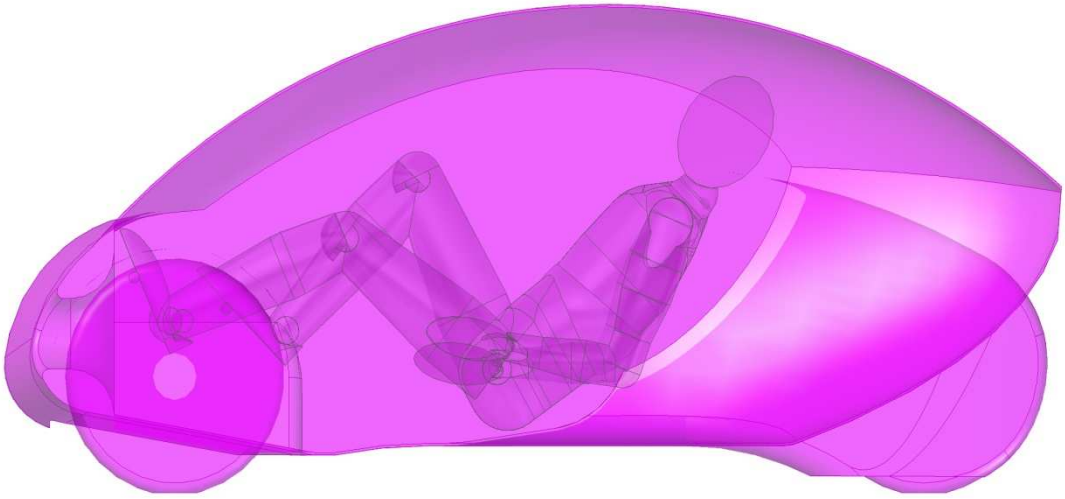

Figure JJ

To find air velocity over body helps evaluating the cooling efficiency of the ventilation. Unfortunately the meshing program never completed a valid volume mesh despite several tries. It was then decided to not complete this simulation.

VELO21

This iteration used VELO19 with a modified underbody to try to make it as smooth as possible. The aim was to try to move the merging area for air flow behind the canopy higher. As can be seen from the flow vectors in the velocity plot Figure KK , this did not fully succeed.

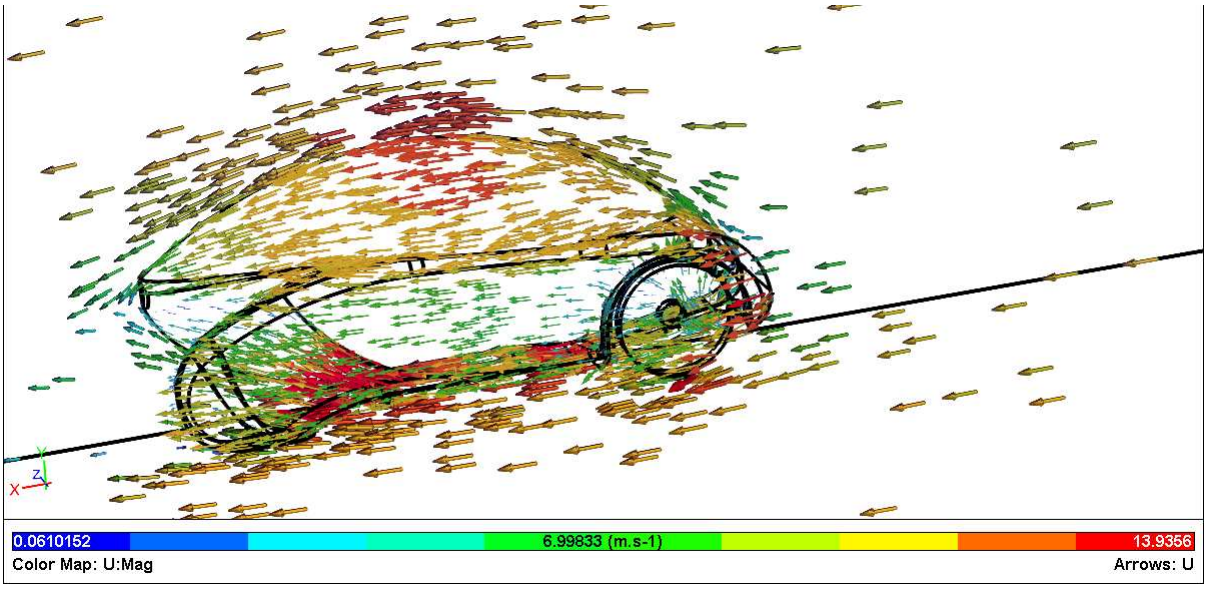

Figure KK

Also the rather high velocity visible in red pointing upwards in Figure KK between the main body and the rear wheel extension is problematic and need to be adressed. Simulation ran smooth, as shown in the force and residuals monitors Figure II and Figure MM.

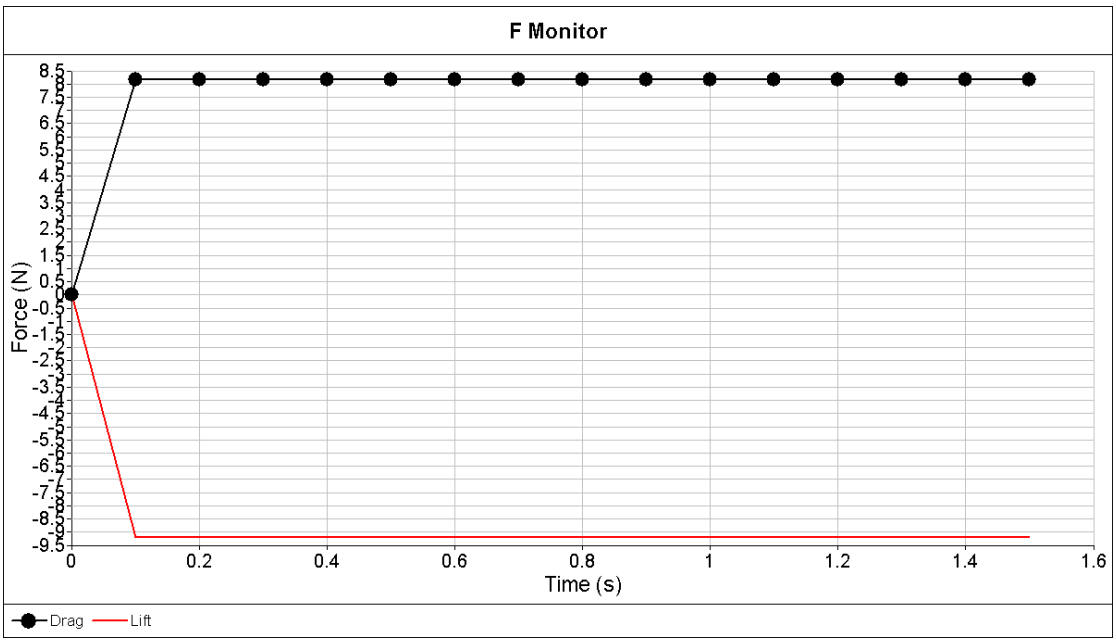

Figure II

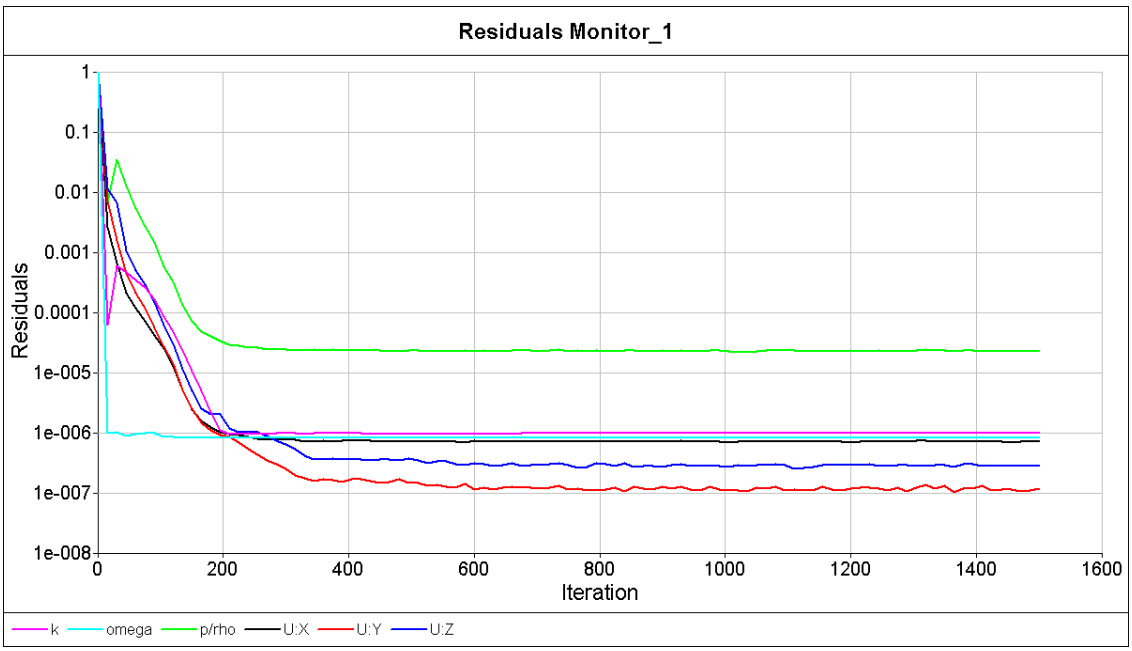

Figure MM

The relatively high forces was disappointing, especially the lift.

Data in table 1 accumulated from the previous simulations indicate that both drag and lift requires a finer mesh for accurate results. The best would be to use same meshing parameters for easier comparison. Unfortunately the meshing software requires fine tuning of the settings for each consecutive iteration to make a successful mesh.

VELO22

To try to reduce drag further some details were improved, like rounding the joint between canopy and overbody. But the rear airstream joining area still stays too low, see Figure NN.

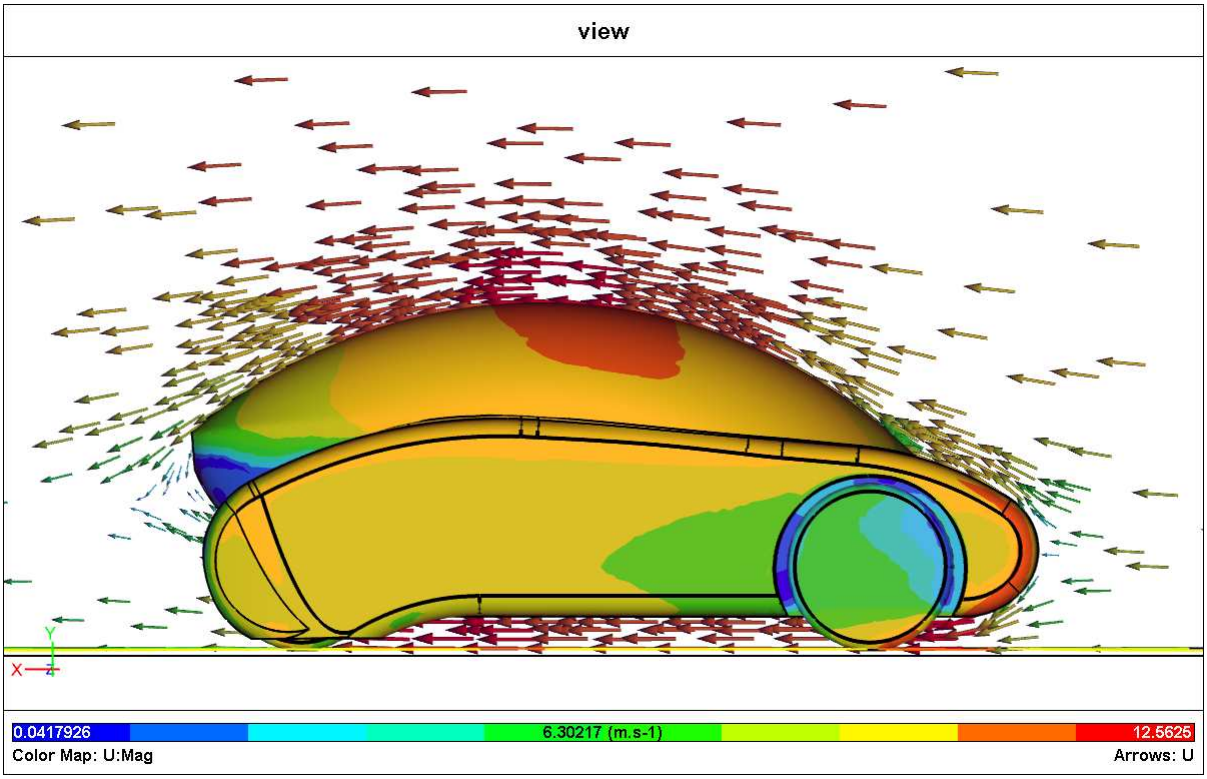

Figure NN

VELO23

In chapter three in Tamai's book [3], it is suggested to have a slight angle on the bottom of the vehicle to have a continously increasing airspeed maintaining laminar flow over a longer distance, suggesting 2-4 % angle from ground plane. But the ultra streamlined vehicles mentioned in his book have much higher ground clearance, between 180 and 300 mm (table 3.3.3)., while the veloquad use 100 mm. But to try to reduce drag further the front wheel is lowered 50 mm resulting in 150 mm ground clearance in front. This resulted in 3% angle on VELO23.

Velocity contours from front and with flow vectors are shown in Figure LL, and velocity contours from the rear show the flow line on the inside of the rear wheel cover in Figure MM. The last figure also shows clearly the angle towards ground.

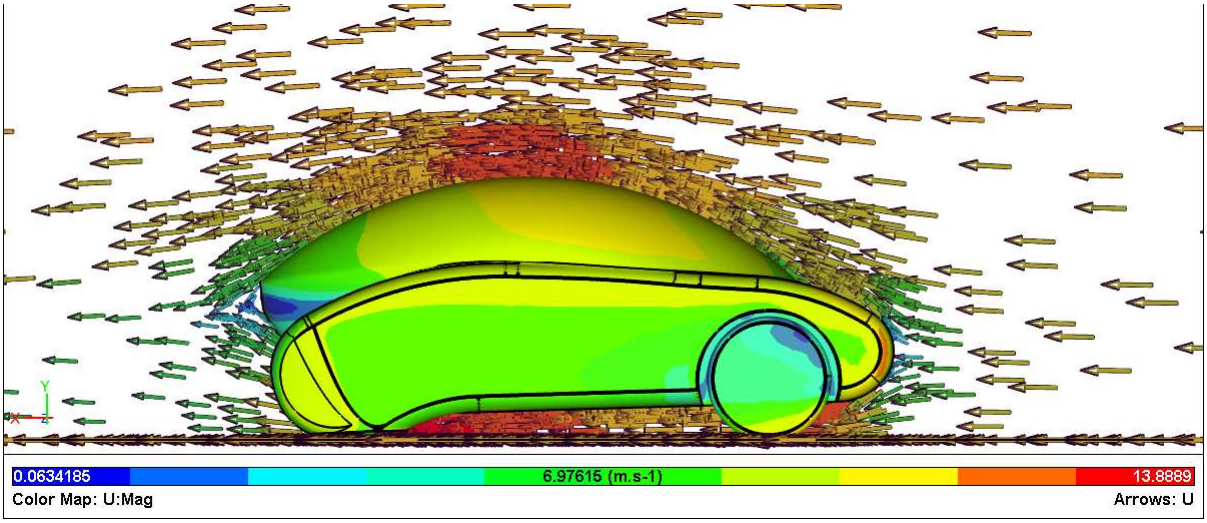

Figure LL

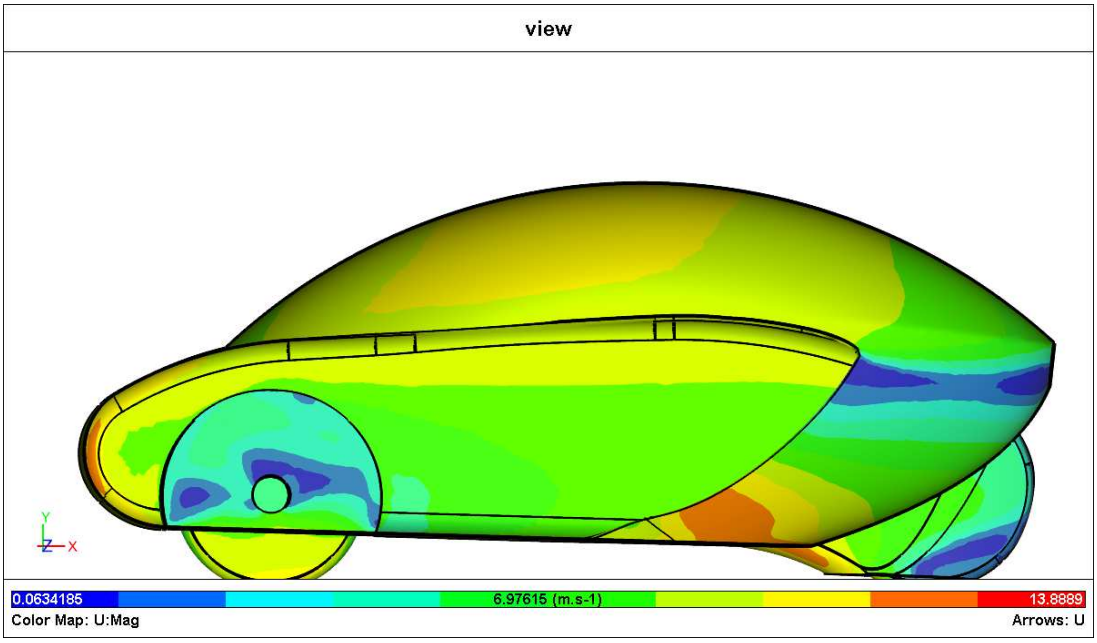

Figure MM

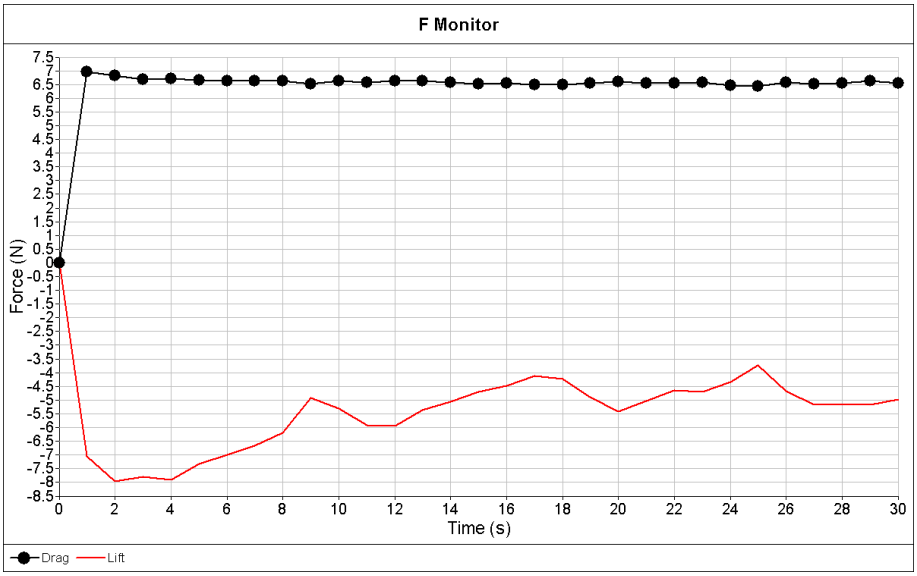

Figure QQ

As shows in Figure QQ, the drag is starting to get low. The primary target is CdA of less than 0.3 m^2 which has been achieved. The secondary target is to get CdA to less than 0.2 m^2. This is not achieved yet, but the design is not far away. It should be achievable with fine tuning current body.

For further reduction of drag, a wall shear stress plot of the veloquad surface give some indications on where too focus. The three plots Figure OO, Figure PP, and Figure TT show τ, or shear stress..

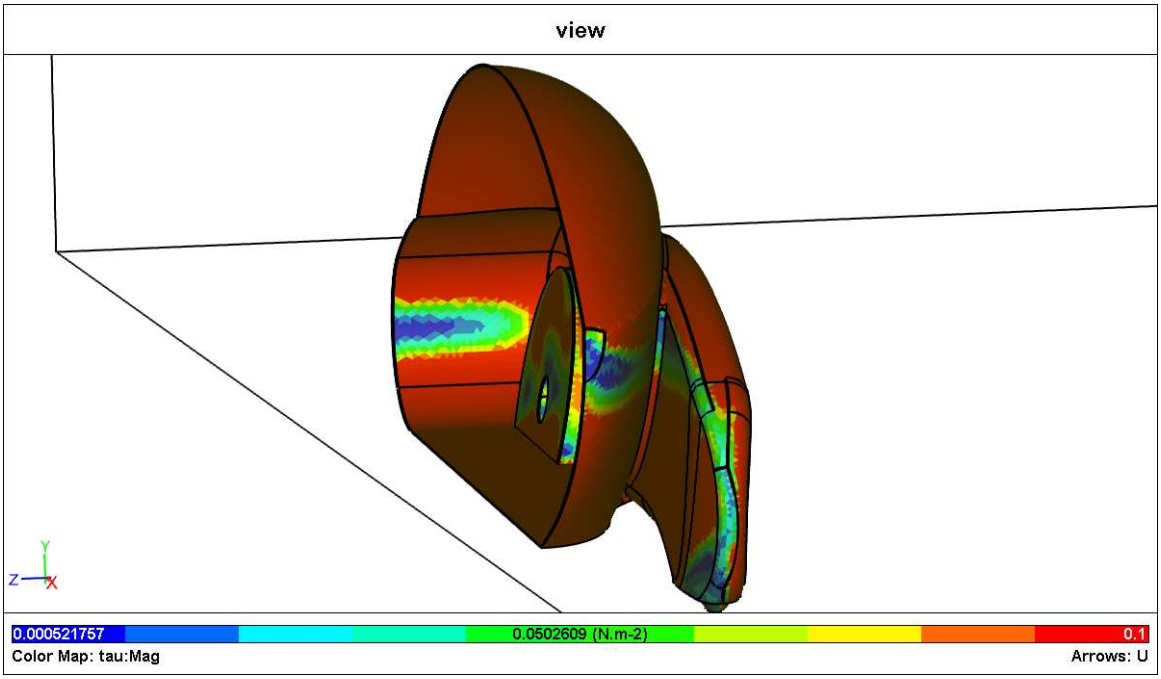

Figure OO

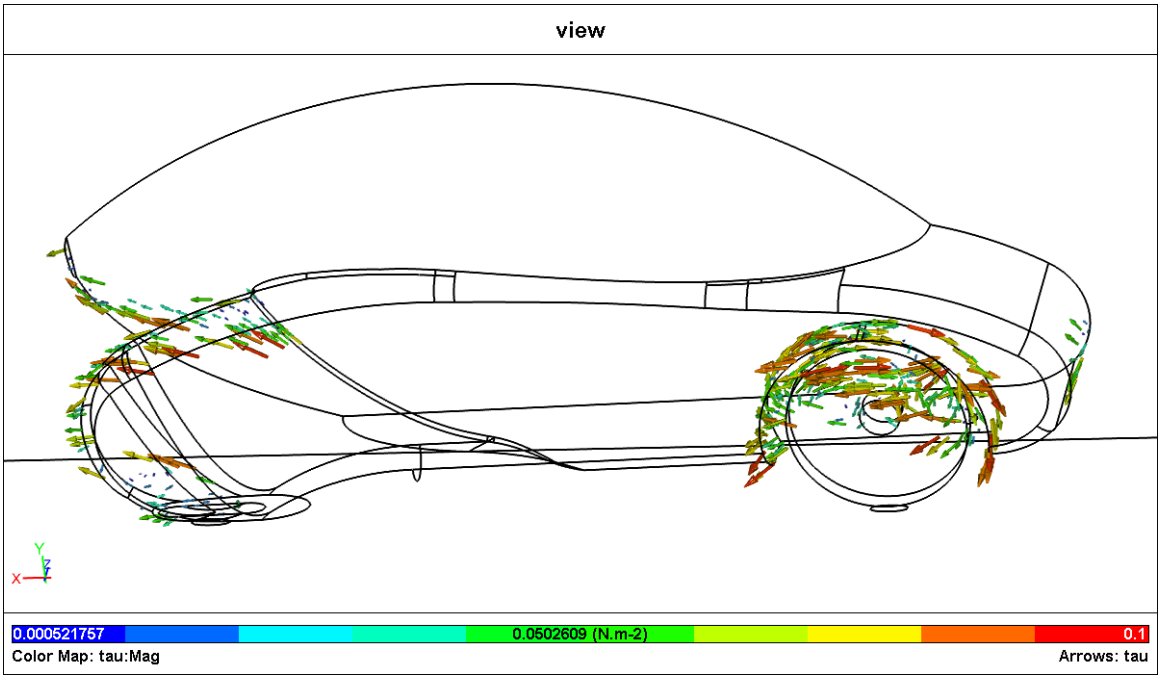

Figure PP

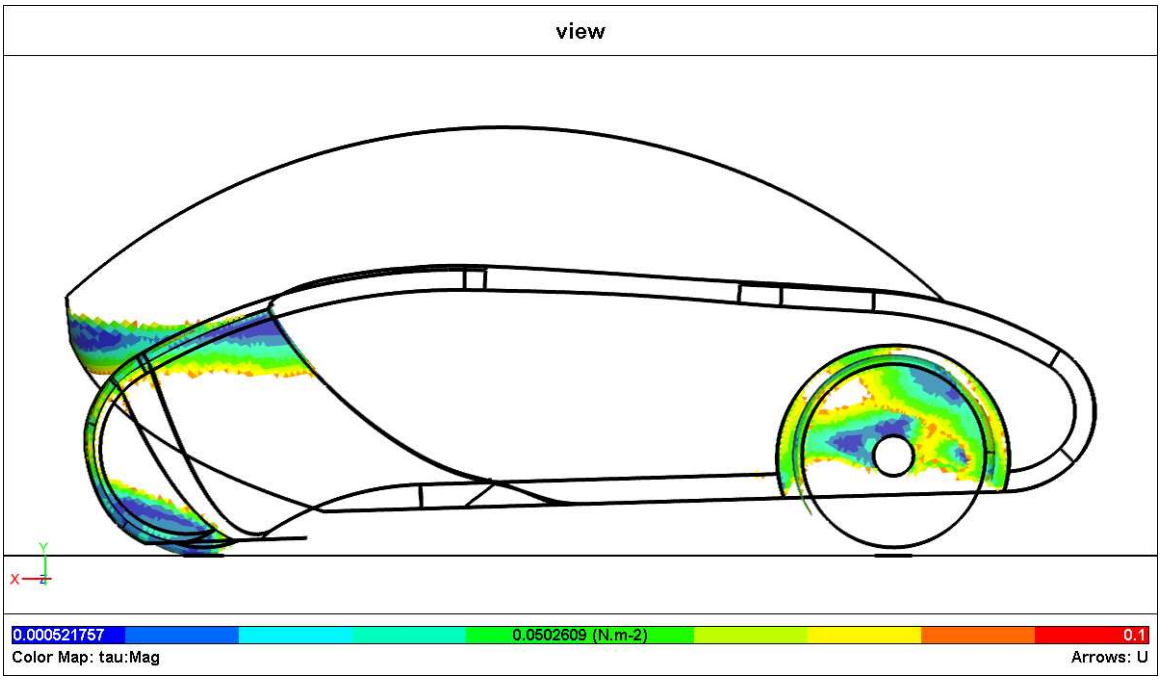

Figure TT

References:

1. Versteeg, H. and W. Malalasekera, *An Introduction to Computational Fluid Dynamics:The Finite Volume Method*. 2nd ed. 2007: Prentice Hall. 520.
2. Hucho, W.-H., et al., *Aerodynamics of Road Vehicles*. Fourth Edition ed. 1998: SAE International. 918.
3. Tamai, G., *The Leading Edge - Aerodynamic Design of Ultra-streamlined Land Vehicles*. 1999, Cambridge, MA, USA: Bentley Publishers.
4. Sysmcape. *How to check for skewed elements in surface mesh*. 2014 2014-06-12].
5. Kjeldsen, M., *Verification run of VELO14 in FLuent using k-omega SST*, P.H. Sørensen, Editor. 2014.

Project

Author	Per Hassel Sørensen
Subject	Intrusion strength
Prepared for	Master thesis
First Saved	Tuesday, June 10, 2014
Last Saved	Tuesday, June 10, 2014
Product Version	13.0 Release

Contents

Report Not Finalized

Not all objects described below are in a finalized state. As a result, data may be incomplete, obsolete or in error. View first state problem. To finalize this report, edit objects as needed and solve the analyses.

Units

TABLE 1

Unit System	Metric (mm, kg, N, s, mV, mA) Degrees rad/s Celsius
Angle	Degrees
Rotational Velocity	rad/s
Temperature	Celsius

Model (B4)

Geometry

TABLE 2
Model (B4) > Geometry

Object Name	*Geometry*
State	Fully Defined
Definition	
Source	C:\Data\CAD\Projects\UiS_velo\Velo20\Top-assy_V20-00.asm
Type	Solid Edge
Length Unit	Meters
Element Control	Program Controlled
Display Style	Part Color
Bounding Box	

Length X	400.8 mm
Length Y	1010.5 mm
Length Z	732.6 mm
Properties	
Volume	3.1465e+006 mm³
Mass	24.7 kg
Scale Factor Value	1.
Statistics	
Bodies	3
Active Bodies	3
Nodes	41866
Elements	18841
Mesh Metric	None
Preferences	
Import Solid Bodies	Yes
Import Surface Bodies	Yes
Import Line Bodies	No
Parameter Processing	Yes
Personal Parameter Key	DS
CAD Attribute Transfer	No
Named Selection Processing	No
Material Properties Transfer	No
CAD Associativity	Yes
Import Coordinate Systems	No
Reader Save Part File	No
Import Using Instances	Yes
Do Smart Update	No
Attach File Via Temp File	Yes
Temporary Directory	C:\Users\per\AppData\Local\Temp
Analysis Type	3-D
Mixed Import Resolution	None
Enclosure and Symmetry Processing	Yes

TABLE 3
Model (B4) > Geometry > Parts

Object Name	*Velo_suspension_rear.asm:1,Collision_test_support-00.par:1*	*Velo_suspension_rear.asm:1,Door_section-00.par:1*	*Car_fender-00.par:1*
State	Meshed		
Graphics Properties			
Visible	Yes		
Transparency	1		
Definition			
Suppressed	No		
Stiffness Behavior	Flexible		
Coordinate System	Default Coordinate System		
Reference Temperature	By Environment		
Material			

Assignment	Structural Steel		
Nonlinear Effects	Yes		
Thermal Strain Effects	Yes		
Bounding Box			
Length X	300. mm	120. mm	100. mm
Length Y	63.512 mm	1010.5 mm	180. mm
Length Z	476.11 mm	732.6 mm	180. mm
Properties			
Volume	85412 mm³	5.282e+005 mm³	2.5329e+006 mm³
Mass	0.67048 kg	4.1464 kg	19.883 kg
Centroid X	-256.81 mm	-393.11 mm	-455.05 mm
Centroid Y	93.363 mm	-358.06 mm	-375.15 mm
Centroid Z	234.17 mm	200.16 mm	111.02 mm
Moment of Inertia Ip1	33775 kg·mm²	4.7679e+005 kg·mm²	80109 kg·mm²
Moment of Inertia Ip2	38907 kg·mm²	1.3907e+005 kg·mm²	56472 kg·mm²
Moment of Inertia Ip3	5280.8 kg·mm²	3.4271e+005 kg·mm²	56472 kg·mm²
Statistics			
Nodes	7137	28377	6352
Elements	3536	13964	1341
Mesh Metric	None		

Coordinate Systems

TABLE 4
Model (B4) > Coordinate Systems > Coordinate System

Object Name	*Global Coordinate System*
State	Fully Defined
Definition	
Type	Cartesian
Coordinate System ID	0.
Origin	
Origin X	0. mm
Origin Y	0. mm
Origin Z	0. mm
Directional Vectors	
X Axis Data	[1. 0. 0.]
Y Axis Data	[0. 1. 0.]
Z Axis Data	[0. 0. 1.]

Connections

TABLE 5
Model (B4) > Connections

Object Name	*Connections*
State	Fully Defined
Auto Detection	
Generate Automatic Connection On Refresh	Yes
Transparency	
Enabled	Yes

TABLE 6
Model (B4) > Connections > Contacts

Object Name	*Contacts*
State	Fully Defined
Definition	
Connection Type	Contact
Scope	
Scoping Method	Geometry Selection
Geometry	All Bodies
Auto Detection	
Tolerance Type	Slider
Tolerance Slider	0.
Tolerance Value	3.2772 mm
Face/Face	Yes
Face/Edge	No
Edge/Edge	No
Priority	Include All
Group By	Bodies
Search Across	Bodies

TABLE 7
Model (B4) > Connections > Contacts > Contact Regions

Object Name	*Contact Region*	*Contact Region 2*
State	Fully Defined	
Scope		
Scoping Method	Geometry Selection	
Contact	3 Faces	1 Face
Target	3 Faces	2 Faces
Contact Bodies	Velo_suspension_rear.asm:1,Collision_test_support-00.par:1	Velo_suspension_rear.asm:1,Door_section-00.par:1
Target Bodies	Velo_suspension_rear.asm:1,Door_section-00.par:1	Car_fender-00.par:1
Definition		
Type	Bonded	
Scope Mode	Automatic	
Behavior	Symmetric	
Suppressed	No	
Advanced		
Formulation	Pure Penalty	
Normal	Program Controlled	

Stiffness	
Update Stiffness	Never
Pinball Region	Program Controlled

Mesh

TABLE 8
Model (B4) > Mesh

Object Name	*Mesh*
State	Solved
Defaults	
Physics Preference	Mechanical
Relevance	0
Sizing	
Use Advanced Size Function	Off
Relevance Center	Medium
Element Size	Default
Initial Size Seed	Active Assembly
Smoothing	Medium
Transition	Fast
Span Angle Center	Coarse
Minimum Edge Length	2.0087e-002 mm
Inflation	
Use Automatic Inflation	None
Inflation Option	Smooth Transition
Transition Ratio	0.272
Maximum Layers	5
Growth Rate	1.2
Inflation Algorithm	Pre
View Advanced Options	No
Advanced	
Shape Checking	Standard Mechanical
Element Midside Nodes	Program Controlled
Straight Sided Elements	No
Number of Retries	Default (4)
Extra Retries For Assembly	Yes
Rigid Body Behavior	Dimensionally Reduced
Mesh Morphing	Disabled
Defeaturing	
Pinch Tolerance	Please Define
Generate Pinch on Refresh	No
Automatic Mesh Based Defeaturing	On
Defeaturing Tolerance	Default
Statistics	
Nodes	41866
Elements	18841
Mesh Metric	None

Static Structural (B5)

TABLE 9
Model (B4) > Analysis

Object Name	*Static Structural (B5)*
State	Not Solved
Definition	
Physics Type	Structural
Analysis Type	Static Structural
Solver Target	Mechanical APDL
Options	
Environment Temperature	22. °C
Generate Input Only	No

TABLE 10
Model (B4) > Static Structural (B5) > Analysis Settings

Object Name	*Analysis Settings*
State	Fully Defined
Restart Analysis	
Restart Type	Program Controlled
Load Step	1
Substep	6
Time	0.925 s
Step Controls	
Number Of Steps	1.
Current Step Number	1.
Step End Time	1. s
Auto Time Stepping	Program Controlled
Solver Controls	
Solver Type	Program Controlled
Weak Springs	Program Controlled
Large Deflection	On
Inertia Relief	Off
Restart Controls	
Generate Restart Points	Program Controlled
Retain Files After Full Solve	No
Nonlinear Controls	
Force Convergence	Program Controlled
Moment Convergence	Program Controlled
Displacement Convergence	Program Controlled
Rotation Convergence	Program Controlled
Line Search	Program Controlled
Stabilization	Off
Output Controls	
Calculate Stress	Yes
Calculate Strain	Yes
Calculate Contact	No
Calculate Results At	All Time Points
Analysis Data Management	
Solver Files Directory	C:\Data\FEM\UIS_VELO_FEM\Door collision\door1_files\dp0\SYS\MECH\
Future Analysis	None
Scratch Solver Files Directory	
Save MAPDL db	No

Delete Unneeded Files	Yes
Nonlinear Solution	Yes
Solver Units	Active System
Solver Unit System	nmm

TABLE 11
Model (B4) > Static Structural (B5) > Loads

Object Name	*Fixed Support*	*Force*	*Displacement*
State	Fully Defined	Suppressed	Fully Defined
Scope			
Scoping Method	Geometry Selection		
Geometry	3 Faces	1 Face	
Definition			
Type	Fixed Support	Force	Displacement
Suppressed	No	Yes	No
Define By		Vector	Components
Magnitude		8000. N (ramped)	
Direction		Defined	
Coordinate System			Global Coordinate System
X Component			50. mm (ramped)
Y Component			Free
Z Component			Free

FIGURE 1
Model (B4) > Static Structural (B5) > Force

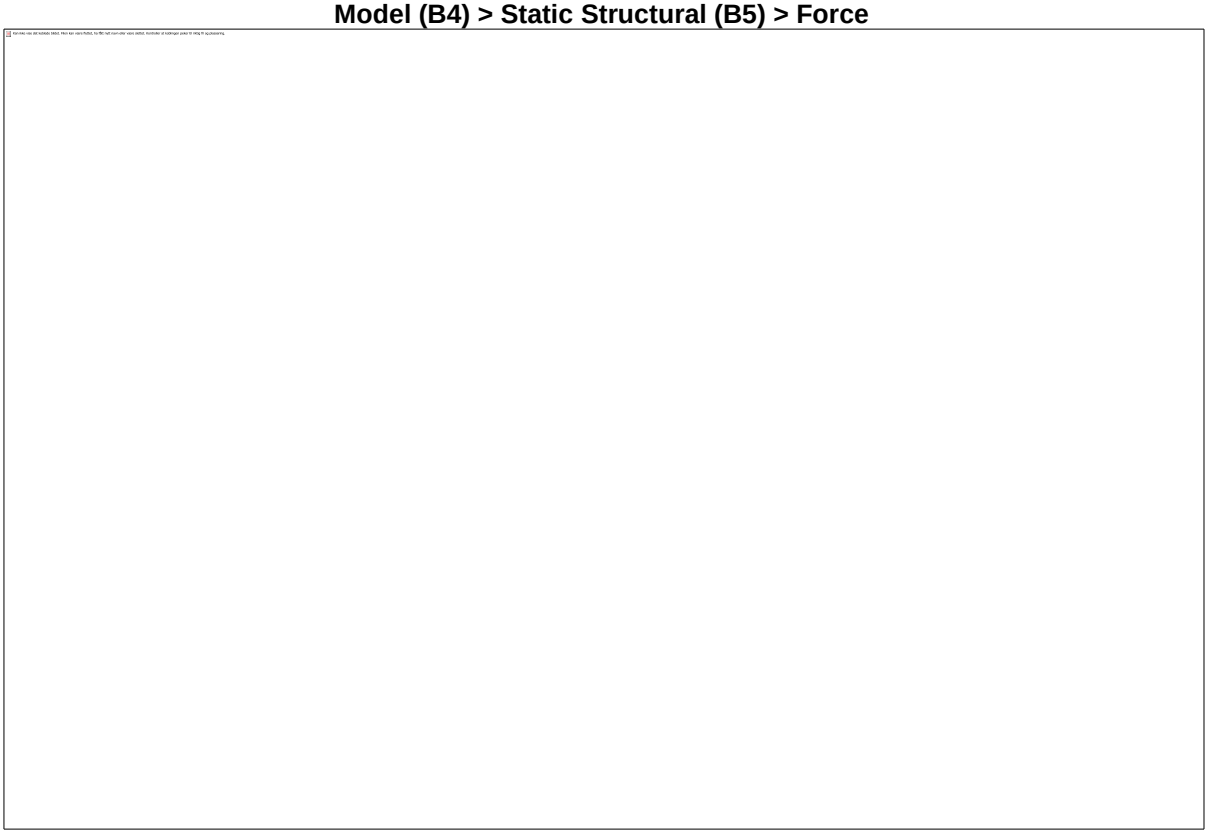

FIGURE 2
Model (B4) > Static Structural (B5) > Displacement

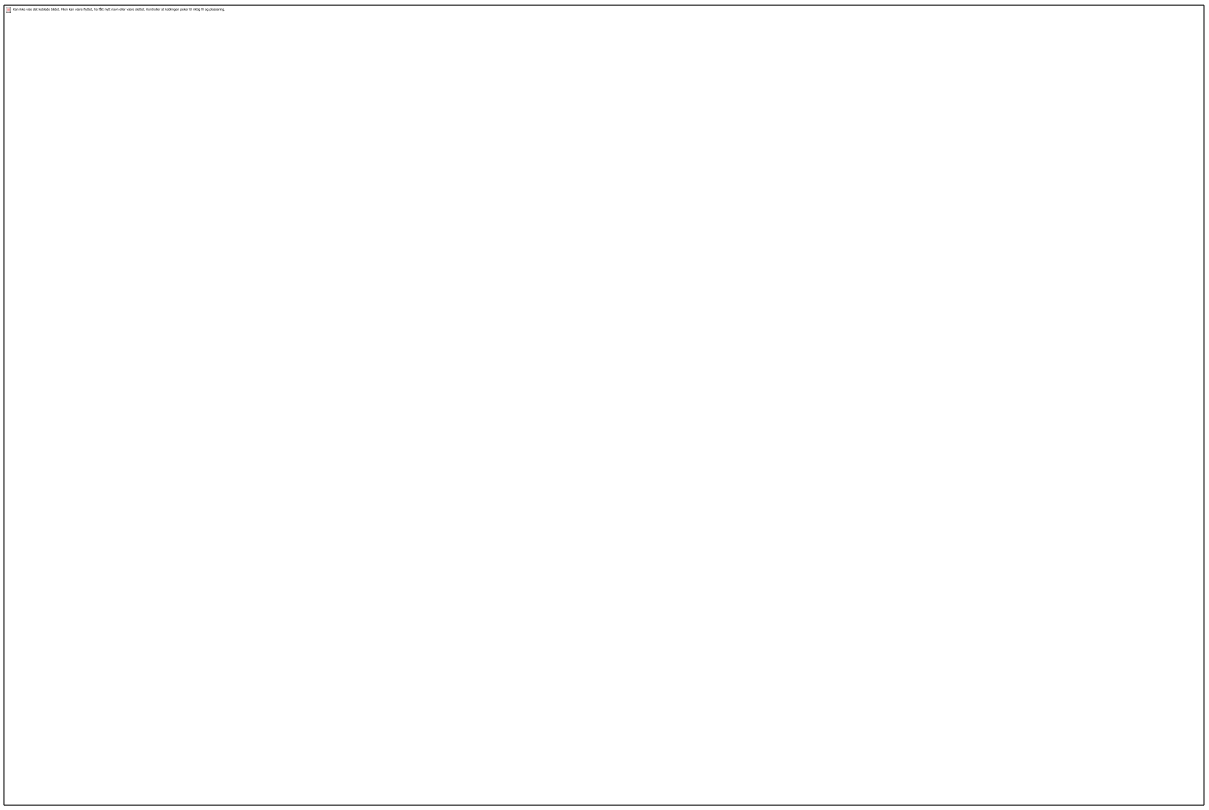

Solution (B6)

TABLE 12
Model (B4) > Static Structural (B5) > Solution

Object Name	*Solution (B6)*
State	Solve Failed
Adaptive Mesh Refinement	
Max Refinement Loops	1.
Refinement Depth	2.
Information	
Status	Solve Required, Restart Available

TABLE 13
Model (B4) > Static Structural (B5) > Solution (B6) > Solution Information

Object Name	*Solution Information*
State	Solve Failed
Solution Information	
Solution Output	Solver Output
Newton-Raphson Residuals	0
Update Interval	2.5 s
Display Points	All

TABLE 14
Model (B4) > Static Structural (B5) > Solution (B6) > Results

Object Name	*Total Deformation*	*Equivalent Stress*	*Directional Deformation*
State	Solve Failed		
Scope			
Scoping	Geometry Selection		

Method			
Geometry	All Bodies		
Definition			
Type	Total Deformation	Equivalent (von-Mises) Stress	Directional Deformation
By	Time		
Display Time	Last		
Calculate Time History	Yes		
Identifier			
Orientation			X Axis
Coordinate System			Global Coordinate System
Results			
Minimum	0. mm	0.20706 MPa	-2.4837 mm
Maximum	50.793 mm	11047 MPa	50.72 mm
Minimum Occurs On	Velo_suspension_rear.asm:1,Collision_test_support-00.par:1	Car_fender-00.par:1	Velo_suspension_rear.asm:1,Door_section-00.par:1
Maximum Occurs On	Velo_suspension_rear.asm:1,Door_section-00.par:1		
Minimum Value Over Time			
Minimum	0. mm	1.9937e-002 MPa	-2.4837 mm
Maximum	0. mm	0.33125 MPa	-0.59476 mm
Maximum Value Over Time			
Minimum	12.521 mm	1708.3 MPa	12.502 mm
Maximum	50.793 mm	11047 MPa	50.72 mm
Information			
Time	1. s		
Load Step	1		
Substep	999999		
Iteration Number	184		
Integration Point Results			
Display Option		Averaged	

FIGURE 3
Model (B4) > Static Structural (B5) > Solution (B6) > Total Deformation

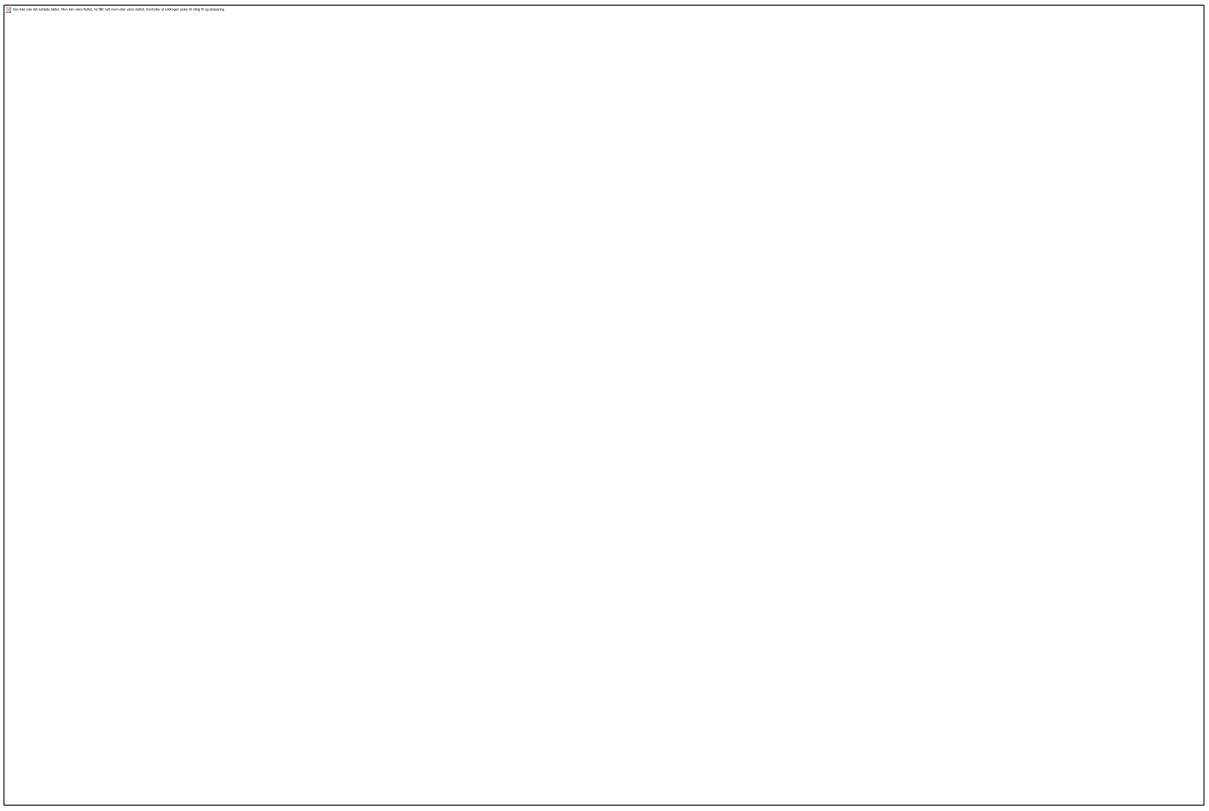

TABLE 15
Model (B4) > Static Structural (B5) > Solution (B6) > Total Deformation

Time [s]	Minimum [mm]	Maximum [mm]
0.25	0.	12.521
0.35		17.527
0.45		22.533
0.6		30.119
0.825		41.817
0.925		46.911
1.		50.793

FIGURE 4
Model (B4) > Static Structural (B5) > Solution (B6) > Equivalent Stress

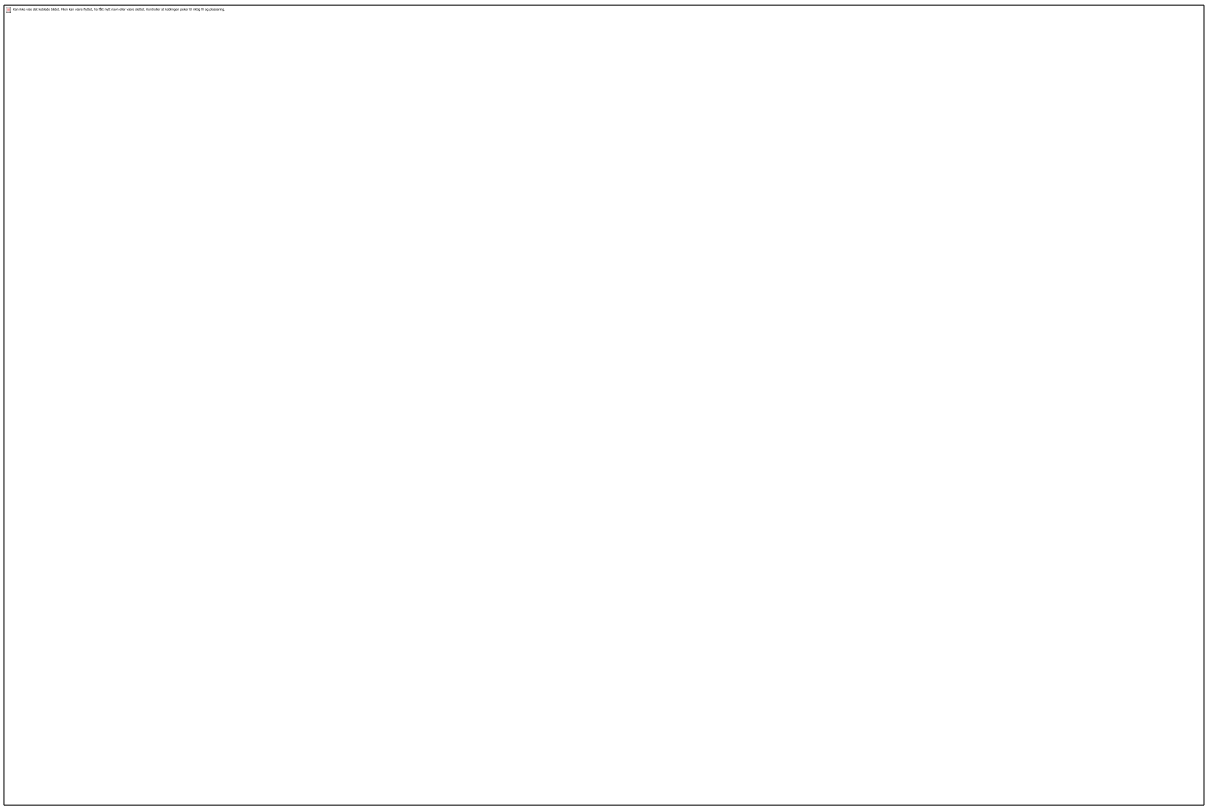

TABLE 16
Model (B4) > Static Structural (B5) > Solution (B6) > Equivalent Stress

Time [s]	Minimum [MPa]	Maximum [MPa]
0.25	1.9937e-002	1708.3
0.35	3.7277e-002	2638.4
0.45	4.1413e-002	3798.5
0.6	8.3043e-002	5720.5
0.825	0.28863	8679.8
0.925	0.33125	9983.6
1.	0.20706	11047

FIGURE 5
Model (B4) > Static Structural (B5) > Solution (B6) > Directional Deformation

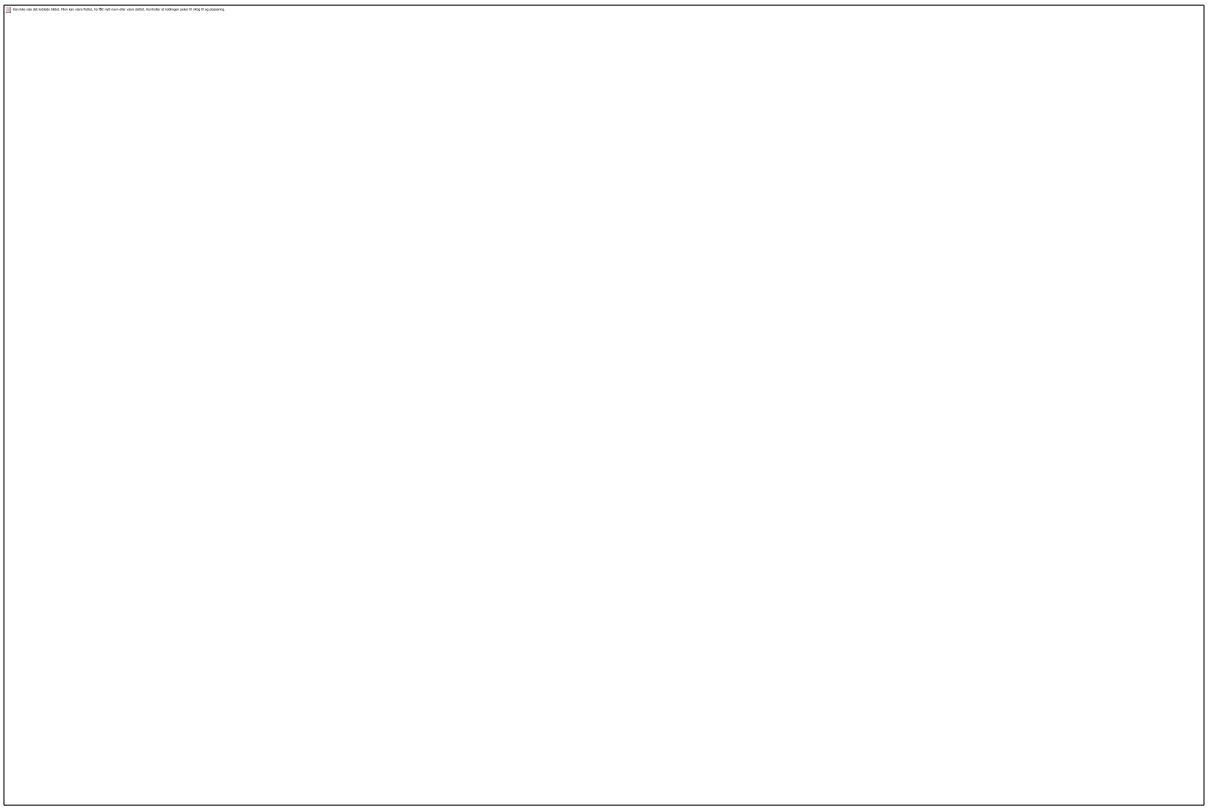

TABLE 17
Model (B4) > Static Structural (B5) > Solution (B6) > Directional Deformation

Time [s]	Minimum [mm]	Maximum [mm]
0.25	-0.81866	12.502
0.35	-0.59476	17.502
0.45	-0.83075	22.503
0.6	-1.289	30.08
0.825	-2.0571	41.768
0.925	-2.3871	46.855
1.	-2.4837	50.72

FIGURE 6
Model (B4) > Static Structural (B5) > Solution (B6) > Directional Deformation > Figure

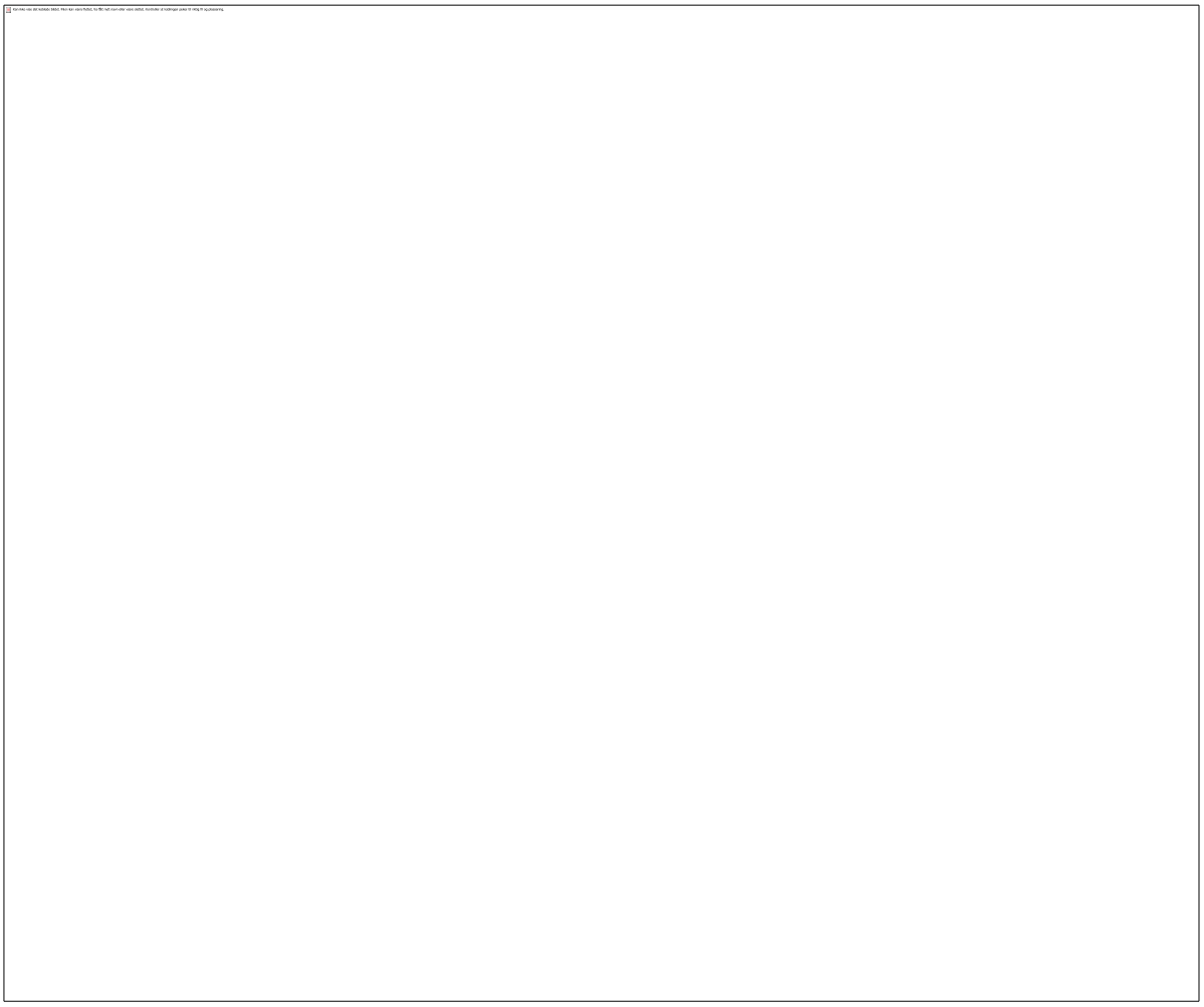

TABLE 18
Model (B4) > Static Structural (B5) > Solution (B6) > Probes

Object Name	*Force Reaction*
State	Solve Failed
Definition	
Type	Force Reaction
Location Method	Boundary Condition
Boundary Condition	Fixed Support
Orientation	Global Coordinate System
Options	
Result Selection	All
Display Time	End Time
Results	
X Axis	-7348. N
Y Axis	0.13013 N
Z Axis	-8.8006e-003 N
Total	7348. N
Maximum Value Over Time	
X Axis	-1771.6 N
Y Axis	0.13013 N
Z Axis	1.8069e-004 N
Total	7751.6 N
Minimum Value Over Time	

X Axis	-7751.6 N
Y Axis	-2.6199e-004 N
Z Axis	-3.3671e-002 N
Total	1771.6 N
Information	
Time	1. s
Load Step	1
Substep	999999
Iteration Number	184

FIGURE 7
Model (B4) > Static Structural (B5) > Solution (B6) > Force Reaction

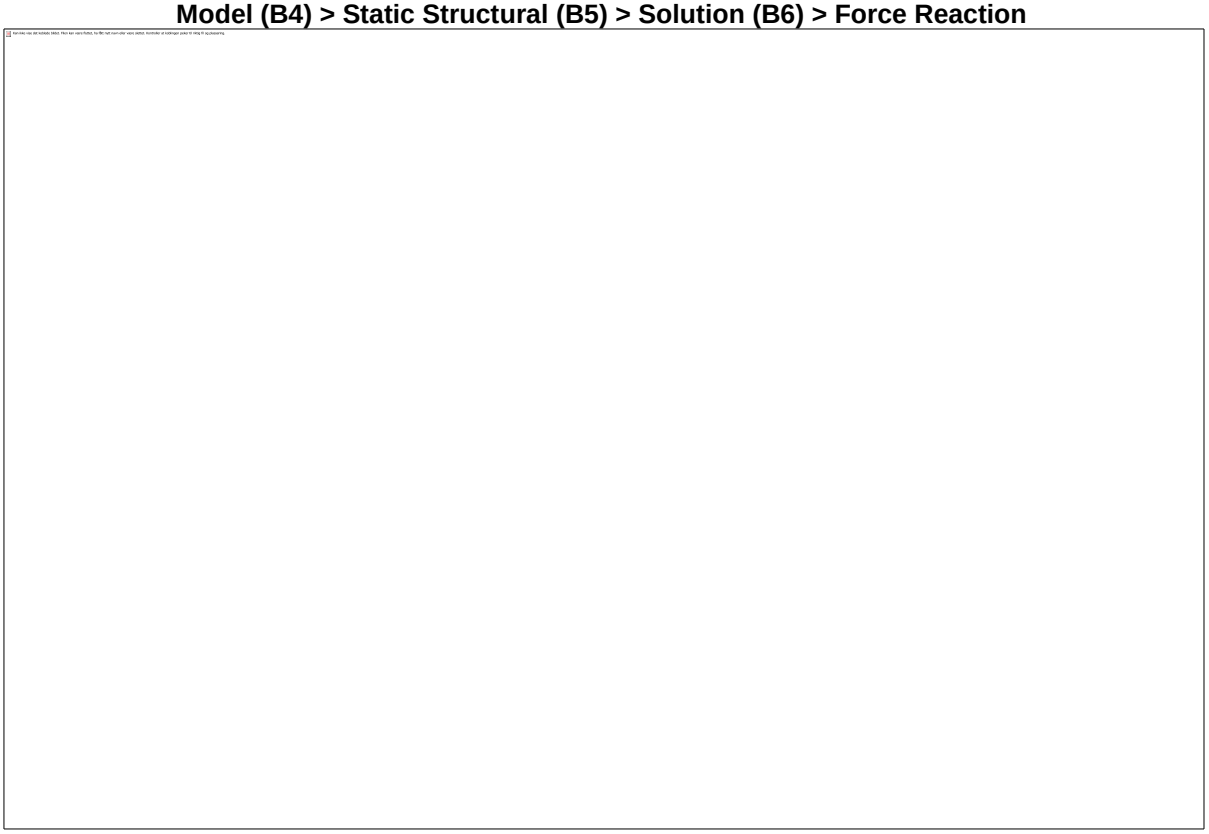

Material Data

Structural Steel

TABLE 19
Structural Steel > Constants

Density	7.85e-006 kg mm^-3
Coefficient of Thermal Expansion	1.2e-005 C^-1
Specific Heat	4.34e+005 mJ kg^-1 C^-1
Thermal Conductivity	6.05e-002 W mm^-1 C^-1
Resistivity	1.7e-004 ohm mm

TABLE 20
Structural Steel > Compressive Ultimate Strength

Compressive Ultimate Strength MPa
0

TABLE 21
Structural Steel > Compressive Yield Strength

Compressive Yield Strength MPa
250

TABLE 22
Structural Steel > Tensile Yield Strength

Tensile Yield Strength MPa
250

TABLE 23
Structural Steel > Tensile Ultimate Strength

Tensile Ultimate Strength MPa
460

TABLE 24
Structural Steel > Isotropic Secant Coefficient of Thermal Expansion

Reference Temperature C
22

TABLE 25
Structural Steel > Alternating Stress Mean Stress

Alternating Stress MPa	Cycles	Mean Stress MPa
3999	10	0
2827	20	0
1896	50	0
1413	100	0
1069	200	0
441	2000	0
262	10000	0
214	20000	0
138	1.e+005	0
114	2.e+005	0
86.2	1.e+006	0

TABLE 26
Structural Steel > Strain-Life Parameters

Strength Coefficient MPa	Strength Exponent	Ductility Coefficient	Ductility Exponent	Cyclic Strength Coefficient MPa	Cyclic Strain Hardening Exponent
920	-0.106	0.213	-0.47	1000	0.2

TABLE 27
Structural Steel > Isotropic Elasticity

Temperature C	Young's Modulus MPa	Poisson's Ratio	Bulk Modulus MPa	Shear Modulus MPa
	2.e+005	0.3	1.6667e+005	76923

TABLE 28
Structural Steel > Isotropic Relative Permeability

Relative Permeability
10000

Project

First Saved	Wednesday, June 11, 2014
Last Saved	Wednesday, June 11, 2014
Product Version	13.0 Release

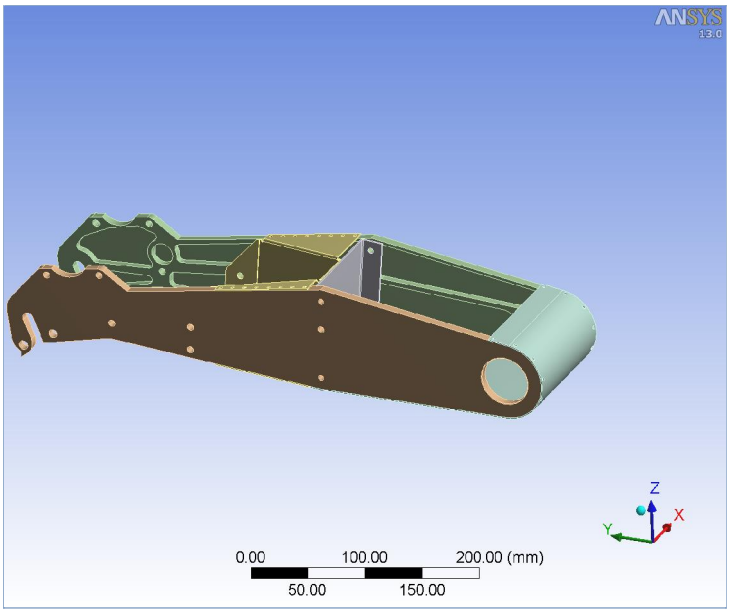

Contents

Units

TABLE 1

Unit System	Metric (mm, kg, N, s, mV, mA) Degrees rad/s Celsius
Angle	Degrees
Rotational Velocity	rad/s
Temperature	Celsius

Model (B4)

Geometry

TABLE 2
Model (B4) > Geometry

Object Name	*Geometry*
State	Fully Defined
Definition	
Source	C:\Data\CAD\Projects\UiS_velo\3D_design\Assy_new\Rear_suspension_assy_right-11.asm
Type	Solid Edge
Length Unit	Meters
Element Control	Program Controlled
Display Style	Part Color
Bounding Box	
Length X	120. mm
Length Y	514.7 mm
Length Z	140.74 mm
Properties	
Volume	3.9196e+005 mm³
Mass	1.0857 kg
Scale Factor Value	1.
Statistics	
Bodies	7
Active Bodies	7
Nodes	969968
Elements	575377
Mesh Metric	None
Preferences	
Import Solid Bodies	Yes
Import Surface Bodies	Yes
Import Line Bodies	No
Parameter Processing	Yes
Personal Parameter Key	DS
CAD Attribute Transfer	No
Named Selection Processing	No
Material Properties Transfer	No
CAD Associativity	Yes
Import Coordinate Systems	No
Reader Save Part File	No
Import Using Instances	Yes
Do Smart Update	No
Attach File Via Temp File	Yes
Temporary Directory	C:\Users\per\AppData\Local\Temp
Analysis Type	3-D
Mixed Import Resolution	None
Enclosure and Symmetry Processing	Yes

TABLE 3
Model (B4) > Geometry > Parts

Object Name	*ESTM_16_1.par:2*	*Suspension_rod_bearing_reinforcement-00.par:1*	*Rear_suspension_structural_parts Right-00.asm:1,Rear-wheel-inside_left-01.par:1*	*Rear_suspension_structural_parts Right-00.asm:1,Rear-wheel-inside-right-02.par:1*	*Rear_suspension_structural_ 00.asm:1,Rear_Suspension_arn 00.psm:1*
State	Meshed				
Graphics Properties					
Visible	Yes				
Transparency	1				
Definition					
Suppressed	No				
Stiffness Behavior	Flexible				
Coordinate	Default Coordinate System				

System					
Reference Temperature	By Environment				
Material					
Assignment	Aluminum Alloy				
Nonlinear Effects	Yes				
Thermal Strain Effects	Yes				
Bounding Box					
Length X	13. mm	17. mm	8. mm		120. mm
Length Y	38.327 mm	15.468 mm	514.7 mm		222.8 mm
Length Z	52.824 mm	64.343 mm	140.74 mm		74.618 mm
Properties					
Volume	13693 mm³	9258.2 mm³	1.3885e+005 mm³	1.389e+005 mm³	37292 mm³
Mass	3.7928e-002 kg	2.5645e-002 kg	0.38462 kg	0.38475 kg	0.1033 kg
Centroid X	-1.2 mm		68.262 mm	-45.453 mm	11.304 mm
Centroid Y	-294.08 mm	-273.77 mm	-234.59 mm	-234.52 mm	-407.65 mm
Centroid Z	12.297 mm	7.7034 mm	16.267 mm	16.277 mm	-10.099 mm
Moment of Inertia Ip1	4.169 kg·mm²	8.6784 kg·mm²	228.65 kg·mm²	228.76 kg·mm²	570.54 kg·mm²
Moment of Inertia Ip2	11.112 kg·mm²	9.1361 kg·mm²	9043.3 kg·mm²	9049.9 kg·mm²	166.25 kg·mm²
Moment of Inertia Ip3	8.1179 kg·mm²	0.81272 kg·mm²	8819.1 kg·mm²	8825.6 kg·mm²	649.49 kg·mm²
Statistics					
Nodes	913899	839	9080	9149	18511
Elements	548430	418	4565	4595	8804
Mesh Metric	None				

TABLE 4
Model (B4) > Geometry > Parts

Object Name	*Rear_suspension_structural_parts Right-00.asm:1,Rear_Suspension_arm_diagonal_bracket-01.psm:1*	*Rear_suspension_structural_parts Right-00.asm:1,Rear_Suspension_arm_damper_plate-02.psm:1*
State	Meshed	
Graphics Properties		
Visible	Yes	
Transparency	1	
Definition		
Suppressed	No	
Stiffness Behavior	Flexible	
Coordinate System	Default Coordinate System	
Reference Temperature	By Environment	
Material		
Assignment	Aluminum Alloy	
Nonlinear Effects	Yes	
Thermal Strain Effects	Yes	
Bounding Box		
Length X	119.8 mm	103.8 mm
Length Y	133.93 mm	28.046 mm
Length Z	95.887 mm	94.912 mm
Properties		
Volume	32134 mm³	21836 mm³
Mass	8.9011e-002 kg	6.0486e-002 kg
Centroid X	8.9933 mm	11.54 mm
Centroid Y	-225. mm	-272.98 mm
Centroid Z	20.128 mm	17.252 mm
Moment of Inertia Ip1	186.61 kg·mm²	54.498 kg·mm²
Moment of Inertia Ip2	222. kg·mm²	129.94 kg·mm²
Moment of Inertia Ip3	255.72 kg·mm²	79.27 kg·mm²
Statistics		
Nodes	13749	4741
Elements	6342	2223
Mesh Metric	None	

Coordinate Systems

TABLE 5
Model (B4) > Coordinate Systems > Coordinate System

Object Name	*Global Coordinate System*
State	Fully Defined
Definition	
Type	Cartesian
Coordinate System ID	0.
Origin	
Origin X	0. mm
Origin Y	0. mm
Origin Z	0. mm
Directional Vectors	
X Axis Data	[1. 0. 0.]
Y Axis Data	[0. 1. 0.]
Z Axis Data	[0. 0. 1.]

Connections

TABLE 6
Model (B4) > Connections

Object Name	*Connections*
State	Fully Defined
Auto Detection	
Generate Automatic Connection On Refresh	Yes

Transparency	
Enabled	Yes

TABLE 7
Model (B4) > Connections > Contacts

Object Name	*Contacts*
State	Fully Defined
Definition	
Connection Type	Contact
Scope	
Scoping Method	Geometry Selection
Geometry	All Bodies
Auto Detection	
Tolerance Type	Slider
Tolerance Slider	0.
Tolerance Value	1.3673 mm
Face/Face	Yes
Face/Edge	No
Edge/Edge	No
Priority	Include All
Group By	Bodies
Search Across	Bodies

TABLE 8
Model (B4) > Connections > Contacts > Contact Regions

Object Name	*Bonded - ESTM_16_1.par:2 To Suspension_rod_bearing_reinforcement-00.par:1*	*Bonded - Suspension_rod_bearing_reinforcement-00.par:1 To Rear_suspension_structural_parts Right-00.asm:1,Rear_Suspension_arm_damper_plate-02.psm:1*	*Bonded - Rear_suspension_structural_parts Right-00.asm:1,Rear-wheel-inside_left-01.par:1 To Rear_suspension_structural_parts Right-00.asm:1,Rear_Suspension_arm_lower_plate-00.psm:1*	*Bonded - Rear_suspensior 00.asm:1,Rear-wheel-in Rear_suspension_stru 00.asm:1,Rear_Suspensior 01.psi*
State	Fully Defined			
Scope				
Scoping Method	Geometry Selection			
Contact	5 Faces	3 Faces	6 Faces	3 Fac
Target	5 Faces	3 Faces	5 Faces	4 Fac
Contact Bodies	ESTM_16_1.par:2	Suspension_rod_bearing_reinforcement-00.par:1	Rear_suspension_structural_parts Right-(	
Target Bodies	Suspension_rod_bearing_reinforcement-00.par:1	Rear_suspension_structural_parts Right-00.asm:1,Rear_Suspension_arm_damper_plate-02.psm:1	Rear_suspension_structural_parts Right-00.asm:1,Rear_Suspension_arm_lower_plate-00.psm:1	Rear_suspension_stri 00.asm:1,Rear_Suspensior 01.psi
Definition				
Type	Bonded			
Scope Mode	Automatic			
Behavior	Symmetric			
Suppressed	No			
Advanced				
Formulation	Pure Penalty			
Normal Stiffness	Program Controlled			
Update Stiffness	Never			
Pinball Region	Program Controlled			

TABLE 9
Model (B4) > Connections > Contacts > Contact Regions

Object Name	*Bonded - Rear_suspension_structural_parts Right-00.asm:1,Rear-wheel-inside-right-02.par:1 To Rear_suspension_structural_parts Right-00.asm:1,Rear_Suspension_arm_lower_plate-00.psm:1*	*Bonded - Rear_suspension_structural_parts Right-00.asm:1,Rear-wheel-inside-right-02.par:1 To Rear_suspension_structural_parts Right-00.asm:1,Rear_Suspension_arm_diagonal_bracket-01.psm:1*	*Bonded - Rear_suspension_structural_parts Right-00.asm:1,Rear-wheel-inside-right-02.par:1 To Rear_suspension_structural_parts Right-00.asm:1,Rear_Suspension_arm_damper_plate-02.psm:1*	*Bonded - Rear_ 00.asm:1,Rea 00.psm:1 To I 00.asm:1,Rear_*
State	Fully Defined			
Scope				
Scoping Method	Geometry Selection			
Contact	6 Faces	3 Faces	1 Face	
Target	5 Faces	7 Faces		
Contact Bodies	Rear_suspension_structural_parts Right-00.asm:1,Rear-wheel-inside-right-02.par:1			Rear_susper
Target Bodies	Rear_suspension_structural_parts Right-00.asm:1,Rear_Suspension_arm_lower_plate-00.psm:1	Rear_suspension_structural_parts Right-00.asm:1,Rear_Suspension_arm_diagonal_bracket-01.psm:1	Rear_suspension_structural_parts Right-00.asm:1,Rear_Suspension_arm_damper_plate-02.psm:1	Rear_susp 00.asm:1,Rear_
Definition				
Type	Bonded			
Scope Mode	Automatic			
Behavior	Symmetric			
Suppressed	No			
Advanced				
Formulation	Pure Penalty			
Normal Stiffness	Program Controlled			
Update Stiffness	Never			
Pinball Region	Program Controlled			

TABLE 10
Model (B4) > Connections > Contacts > Contact Regions

Object Name	*Bonded - Rear_suspension_structural_parts Right-00.asm:1,Rear_Suspension_arm_diagonal_bracket-01.psm:1 To Rear_suspension_structural_parts Right-00.asm:1,Rear_Suspension_arm_damper_plate-02.psm:1*
State	Fully Defined
Scope	

Scoping Method	Geometry Selection
Contact	5 Faces
Target	4 Faces
Contact Bodies	Rear_suspension_structural_parts Right-00.asm:1,Rear_Suspension_arm_diagonal_bracket-01.psm:1
Target Bodies	Rear_suspension_structural_parts Right-00.asm:1,Rear_Suspension_arm_damper_plate-02.psm:1
Definition	
Type	Bonded
Scope Mode	Automatic
Behavior	Symmetric
Suppressed	No
Advanced	
Formulation	Pure Penalty
Normal Stiffness	Program Controlled
Update Stiffness	Never
Pinball Region	Program Controlled

Mesh

TABLE 11
Model (B4) > Mesh

Object Name	*Mesh*
State	Solved
Defaults	
Physics Preference	Mechanical
Relevance	0
Sizing	
Use Advanced Size Function	Off
Relevance Center	Coarse
Element Size	Default
Initial Size Seed	Active Assembly
Smoothing	Medium
Transition	Fast
Span Angle Center	Coarse
Minimum Edge Length	8.939e-002 mm
Inflation	
Use Automatic Inflation	None
Inflation Option	Smooth Transition
Transition Ratio	0.272
Maximum Layers	5
Growth Rate	1.2
Inflation Algorithm	Pre
View Advanced Options	No
Advanced	
Shape Checking	Standard Mechanical
Element Midside Nodes	Program Controlled
Straight Sided Elements	No
Number of Retries	Default (4)
Extra Retries For Assembly	Yes
Rigid Body Behavior	Dimensionally Reduced
Mesh Morphing	Disabled
Defeaturing	
Pinch Tolerance	Please Define
Generate Pinch on Refresh	No
Automatic Mesh Based Defeaturing	On
Defeaturing Tolerance	Default
Statistics	
Nodes	969968
Elements	575377
Mesh Metric	None

FIGURE 1
Model (B4) > Mesh > Figure

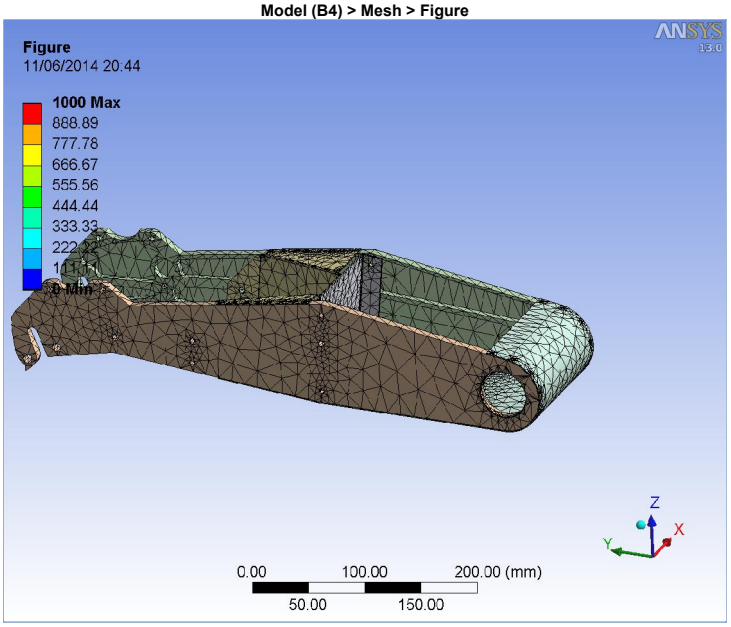

Static Structural (B5)

TABLE 12
Model (B4) > Analysis

Object Name	*Static Structural (B5)*
State	Solved
Definition	
Physics Type	Structural
Analysis Type	Static Structural
Solver Target	Mechanical APDL
Options	
Environment Temperature	22. °C
Generate Input Only	No

TABLE 13
Model (B4) > Static Structural (B5) > Analysis Settings

Object Name	*Analysis Settings*
State	Fully Defined
Step Controls	
Number Of Steps	1.
Current Step Number	1.
Step End Time	1. s
Auto Time Stepping	Program Controlled
Solver Controls	
Solver Type	Program Controlled
Weak Springs	Program Controlled
Large Deflection	Off
Inertia Relief	Off
Restart Controls	
Generate Restart Points	Program Controlled
Retain Files After Full Solve	No
Nonlinear Controls	
Force Convergence	Program Controlled
Moment Convergence	Program Controlled
Displacement Convergence	Program Controlled
Rotation Convergence	Program Controlled
Line Search	Program Controlled
Stabilization	Off
Output Controls	
Calculate Stress	Yes
Calculate Strain	Yes
Calculate Contact	No
Calculate Results At	All Time Points
Analysis Data Management	
Solver Files Directory	C:\Users\per\AppData\Local\Temp\WB_CFDGURU1_6944_2\unsaved_project_files\dp0\SYS\MECH\
Future Analysis	None
Scratch Solver Files Directory	
Save MAPDL db	No
Delete Unneeded Files	Yes
Nonlinear Solution	No
Solver Units	Active System
Solver Unit System	nmm

TABLE 14
Model (B4) > Static Structural (B5) > Loads

Object Name	*Fixed Support*	*Fixed Support 2*	*Remote Force*
State	Fully Defined		
Scope			
Scoping Method	Geometry Selection		
Geometry	2 Faces	1 Face	2 Faces
Coordinate System			Global Coordinate System
X Coordinate			0. mm
Y Coordinate			0. mm
Z Coordinate			-250. mm
Location			Defined
Definition			
Type	Fixed Support		Remote Force
Suppressed	No		
Define By			Components
X Component			0. N (ramped)
Y Component			0. N (ramped)
Z Component			800. N (ramped)
Behavior			Deformable
Advanced			
Pinball Region			All

FIGURE 2
Model (B4) > Static Structural (B5) > Remote Force

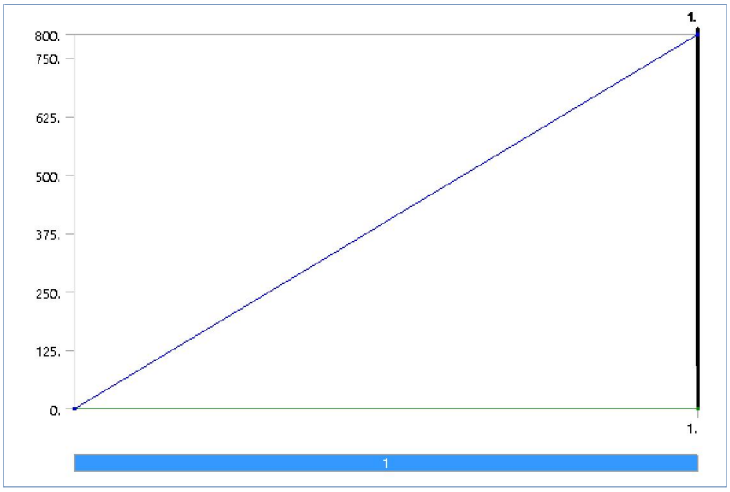

Solution (B6)

TABLE 15
Model (B4) > Static Structural (B5) > Solution

Object Name	*Solution (B6)*
State	Solved
Adaptive Mesh Refinement	
Max Refinement Loops	1.
Refinement Depth	2.
Information	
Status	Done

TABLE 16
Model (B4) > Static Structural (B5) > Solution (B6) > Solution Information

Object Name	*Solution Information*
State	Solved
Solution Information	
Solution Output	Solver Output
Newton-Raphson Residuals	0
Update Interval	2.5 s
Display Points	All

TABLE 17
Model (B4) > Static Structural (B5) > Solution (B6) > Results

Object Name	*Equivalent Stress*
State	Solved
Scope	
Scoping Method	Geometry Selection
Geometry	All Bodies
Definition	
Type	Equivalent (von-Mises) Stress
By	Time
Display Time	Last
Calculate Time History	Yes
Identifier	
Integration Point Results	
Display Option	Averaged
Results	
Minimum	0. MPa
Maximum	128.16 MPa
Minimum Occurs On	ESTM_16_1.par:2
Maximum Occurs On	Rear_suspension_structural_parts Right-00.asm:1,Rear_Suspension_arm_diagonal_bracket-01.psm:1
Information	
Time	1. s
Load Step	1
Substep	1
Iteration Number	1

FIGURE 3
Model (B4) > Static Structural (B5) > Solution (B6) > Equivalent Stress > Figure

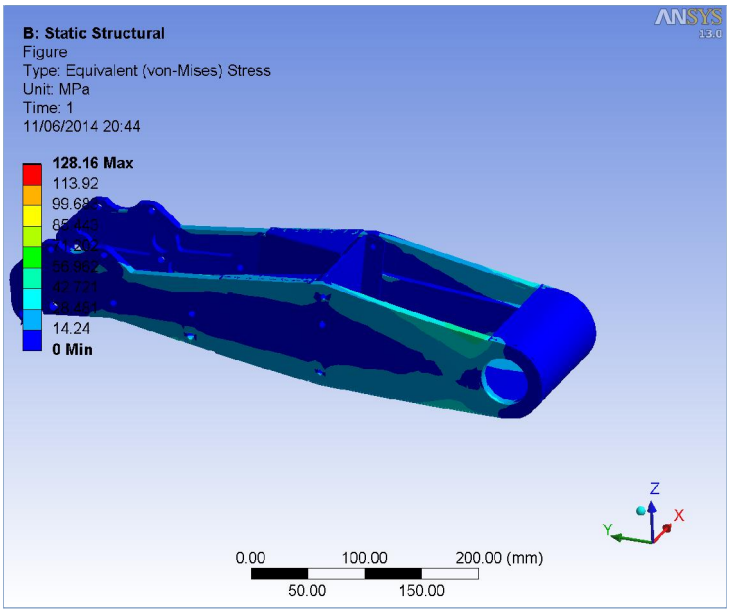

Material Data

Aluminum Alloy

TABLE 18
Aluminum Alloy > Constants

Density	2.77e-006 kg mm^-3
Coefficient of Thermal Expansion	2.3e-005 C^-1
Specific Heat	8.75e+005 mJ kg^-1 C^-1

TABLE 19
Aluminum Alloy > Compressive Ultimate Strength

Compressive Ultimate Strength MPa
0

TABLE 20
Aluminum Alloy > Compressive Yield Strength

Compressive Yield Strength MPa
280

TABLE 21
Aluminum Alloy > Tensile Yield Strength

Tensile Yield Strength MPa
280

TABLE 22
Aluminum Alloy > Tensile Ultimate Strength

Tensile Ultimate Strength MPa
310

TABLE 23
Aluminum Alloy > Isotropic Secant Coefficient of Thermal Expansion

Reference Temperature C
22

TABLE 24
Aluminum Alloy > Isotropic Thermal Conductivity

Thermal Conductivity W mm^-1 C^-1	Temperature C
0.114	-100
0.144	0
0.165	100
0.175	200

TABLE 25
Aluminum Alloy > Alternating Stress R-Ratio

Alternating Stress MPa	Cycles	R-Ratio
275.8	1700	-1
241.3	5000	-1
206.8	34000	-1
172.4	1.4e+005	-1
137.9	8.e+005	-1
117.2	2.4e+006	-1
89.63	5.5e+007	-1
82.74	1.e+008	-1
170.6	50000	-0.5
139.6	3.5e+005	-0.5
108.6	3.7e+006	-0.5
87.91	1.4e+007	-0.5
77.57	5.e+007	-0.5
72.39	1.e+008	-0.5
144.8	50000	0
120.7	1.9e+005	0
103.4	1.3e+006	0
93.08	4.4e+006	0

86.18	1.2e+007	0
72.39	1.e+008	0
74.12	3.e+005	0.5
70.67	1.5e+006	0.5
66.36	1.2e+007	0.5
62.05	1.e+008	0.5

TABLE 26
Aluminum Alloy > Isotropic Resistivity

Resistivity ohm mm	Temperature C
2.43e-005	0
2.67e-005	20
3.63e-005	100

TABLE 27
Aluminum Alloy > Isotropic Elasticity

Temperature C	Young's Modulus MPa	Poisson's Ratio	Bulk Modulus MPa	Shear Modulus MPa
	71000	0.33	69608	26692

TABLE 28
Aluminum Alloy > Isotropic Relative Permeability

Relative Permeability
1

Project

Author	Per Hassel Sørensen
Subject	800 N vertical load plus 800 N sideways remote load on rear wheel carrier incl. motor axle and some fasteners - increased rounding
Prepared for	VELOMOBILE: redefined thesis
First Saved	Wednesday, June 11, 2014
Last Saved	Thursday, June 12, 2014
Product Version	13.0 Release

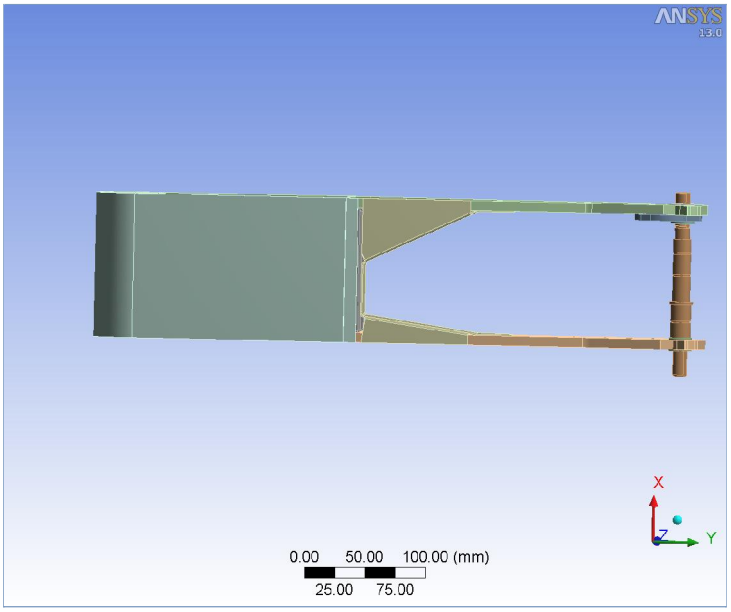

Contents

Units

TABLE 1

Unit System	Metric (mm, kg, N, s, mV, mA) Degrees rad/s Celsius
Angle	Degrees
Rotational Velocity	rad/s
Temperature	Celsius

Model (B4)

Geometry

TABLE 2
Model (B4) > Geometry

Object Name	*Geometry*
State	Fully Defined
Definition	
Source	C:\Data\CAD\Projects\UiS_velo\3D_design\Assy_new\Rear_suspension_assy_right-11.asm
Type	Solid Edge
Length Unit	Meters
Element Control	Program Controlled
Display Style	Part Color
Bounding Box	
Length X	152.6 mm
Length Y	514.7 mm
Length Z	140.74 mm
Properties	
Volume	4.2148e+005 mm³
Mass	1.3183 kg
Scale Factor Value	1.
Statistics	
Bodies	13
Active Bodies	13
Nodes	964187
Elements	567270
Mesh Metric	None
Preferences	
Import Solid Bodies	Yes
Import Surface Bodies	Yes
Import Line Bodies	No
Parameter Processing	Yes
Personal Parameter Key	DS
CAD Attribute Transfer	No
Named Selection Processing	No
Material Properties Transfer	No
CAD Associativity	Yes
Import Coordinate Systems	No
Reader Save Part File	No
Import Using Instances	Yes
Do Smart Update	No
Attach File Via Temp File	Yes
Temporary Directory	C:\Users\per\AppData\Local\Temp
Analysis Type	3-D
Mixed Import Resolution	None
Enclosure and Symmetry Processing	Yes

TABLE 3
Model (B4) > Geometry > Parts

Object Name	*ESTM_16_1.par:2*	*Suspension_rod_bearing_reinforcement-00.par:1*	*Rear_suspension_structural_parts Right-00.asm:1,Rear-wheel-inside_left-01.par:1*	*Rear_suspension_structural_parts Right-00.asm:1,Rear-wheel-inside-right-02.par:1*	*Rear_suspension_structural_ 00.asm:1,Rear_Suspension_arn 00.psm:1*
State	Meshed				
Graphics Properties					
Visible	Yes				
Transparency	1				
Definition					
Suppressed	No				

Stiffness Behavior	Flexible				
Coordinate System	Default Coordinate System				
Reference Temperature	By Environment				
Material					
Assignment	Aluminum Alloy				
Nonlinear Effects	Yes				
Thermal Strain Effects	Yes				
Bounding Box					
Length X	13. mm	17. mm	8. mm		120. mm
Length Y	38.327 mm	15.551 mm	514.7 mm		222.8 mm
Length Z	52.824 mm	65.269 mm	140.74 mm		74.618 mm
Properties					
Volume	13693 mm³	9417.4 mm³	1.3885e+005 mm³	1.389e+005 mm³	37549 mm³
Mass	3.7928e-002 kg	2.6086e-002 kg	0.38462 kg	0.38475 kg	0.10401 kg
Centroid X	-1.2 mm		68.262 mm	-45.453 mm	11.304 mm
Centroid Y	-294.08 mm	-273.73 mm	-234.59 mm	-234.52 mm	-407.64 mm
Centroid Z	12.297 mm	7.1872 mm	16.267 mm	16.277 mm	-10.094 mm
Moment of Inertia Ip1	4.169 kg·mm²	9.0879 kg·mm²	228.65 kg·mm²	228.76 kg·mm²	574.59 kg·mm²
Moment of Inertia Ip2	11.112 kg·mm²	9.5525 kg·mm²	9043.3 kg·mm²	9049.9 kg·mm²	168.78 kg·mm²
Moment of Inertia Ip3	8.1179 kg·mm²	0.82701 kg·mm²	8819.1 kg·mm²	8825.6 kg·mm²	655.43 kg·mm²
Statistics					
Nodes	891711	1061	11277	11309	7200
Elements	535243	531	5605	5610	988
Mesh Metric	None				

TABLE 4
Model (B4) > Geometry > Parts

Object Name	*Rear_suspension_structural_parts Right-00.asm:1,Rear_Suspension_arm_diagonal_bracket-02.psm:1*	*Rear_suspension_structural_parts Right-00.asm:1,Rear_Suspension_arm_damper_plate-03.psm:1*	*Torque_arm-02.psm:1*	*Rear_motor_and_wheel_assy-00.asm:1,Minimotor2Rear_ST6.asm:1,Minimotor stator subassy.asm:1,Washer_id12od19t1.5.par:2*
State	Meshed			
Graphics Properties				
Visible	Yes			
Transparency	1			
Definition				
Suppressed	No			
Stiffness Behavior	Flexible			
Coordinate System	Default Coordinate System			
Reference Temperature	By Environment			
Material				
Assignment	Aluminum Alloy		Structural Ste	
Nonlinear Effects	Yes			
Thermal Strain Effects	Yes			
Bounding Box				
Length X	119.8 mm	103.8 mm	5. mm	1.5 mm
Length Y	133.93 mm	28.13 mm	59.321 mm	24.618 mm
Length Z	95.643 mm	95.846 mm	68.954 mm	24.618 mm
Properties				
Volume	32345 mm³	21031 mm³	5103.8 mm³	255.65 mm³
Mass	8.9594e-002 kg	5.8255e-002 kg	4.0065e-002 kg	2.0068e-003 kg
Centroid X	9.0019 mm	11.504 mm	60.804 mm	-39.746 mm
Centroid Y	-224.39 mm	-272.52 mm	-8.3783 mm	2.4389e-008 mm
Centroid Z	20.398 mm	18.766 mm	-8.8864 mm	-9.5468e-009 mm
Moment of Inertia Ip1	188.04 kg·mm²	50.679 kg·mm²	3.9651 kg·mm²	6.3674e-002 kg·mm²
Moment of Inertia Ip2	223.44 kg·mm²	124.78 kg·mm²	17.047 kg·mm²	6.3674e-002 kg·mm²
Moment of Inertia Ip3	260.67 kg·mm²	77.234 kg·mm²	13.249 kg·mm²	0.1266 kg·mm²
Statistics				
Nodes	22530	8552	1566	682
Elements	11294	4074	214	76
Mesh Metric	None			

TABLE 5
Model (B4) > Geometry > Parts

Object Name	*Rear_motor_and_wheel_assy-00.asm:1,Minimotor2Rear_ST6.asm:1,Rear_motor_spacer-00.par:1*	*Rear_motor_and_wheel_assy-00.asm:1,Washer_id12od19t1.5.par:1*	*Rear_motor_and_wheel_assy-00.asm:1,Washer_id12od19t1.5.par:2*
State	Meshed		
Graphics Properties			
Visible	Yes		
Transparency	1		
Definition			
Suppressed	No		
Stiffness Behavior	Flexible		
Coordinate System	Default Coordinate System		
Reference Temperature	By Environment		
Material			
Assignment	Structural Steel		
Nonlinear			

Effects	Yes		
Thermal Strain Effects	Yes		
Bounding Box			
Length X	2.5 mm	1.5 mm	
Length Y	25.914 mm	19.706 mm	
Length Z	25.914 mm	19.706 mm	
Properties			
Volume	493.15 mm³	255.65 mm³	
Mass	3.8712e-003 kg	2.0068e-003 kg	
Centroid X	57.054 mm	-49.246 mm	72.054 mm
Centroid Y	-1.7344e-008 mm	9.9238e-010 mm	-2.6172e-008 mm
Centroid Z	1.9223e-008 mm	-2.6172e-008 mm	-9.9236e-010 mm
Moment of Inertia Ip1	0.13472 kg·mm²	6.3674e-002 kg·mm²	
Moment of Inertia Ip2	0.26541 kg·mm²	6.3674e-002 kg·mm²	
Moment of Inertia Ip3	0.13472 kg·mm²	0.1266 kg·mm²	
Statistics			
Nodes	991	682	
Elements	138	76	
Mesh Metric	None		

Coordinate Systems

TABLE 6
Model (B4) > Coordinate Systems > Coordinate System

Object Name	*Global Coordinate System*
State	Fully Defined
Definition	
Type	Cartesian
Coordinate System ID	0.
Origin	
Origin X	0. mm
Origin Y	0. mm
Origin Z	0. mm
Directional Vectors	
X Axis Data	[1. 0. 0.]
Y Axis Data	[0. 1. 0.]
Z Axis Data	[0. 0. 1.]

Connections

TABLE 7
Model (B4) > Connections

Object Name	*Connections*
State	Fully Defined
Auto Detection	
Generate Automatic Connection On Refresh	Yes
Transparency	
Enabled	Yes

TABLE 8
Model (B4) > Connections > Contacts

Object Name	*Contacts*
State	Fully Defined
Definition	
Connection Type	Contact
Scope	
Scoping Method	Geometry Selection
Geometry	All Bodies
Auto Detection	
Tolerance Type	Slider
Tolerance Slider	0.
Tolerance Value	1.3875 mm
Face/Face	Yes
Face/Edge	No
Edge/Edge	No
Priority	Include All
Group By	Bodies
Search Across	Bodies

TABLE 9
Model (B4) > Connections > Contacts > Contact Regions

Object Name	*Bonded - ESTM_16_1.par:2 To Suspension_rod_bearing_reinforcement-00.par:1*	*Bonded - Rear_suspension_structural_parts Right-00.asm:1,Rear-wheel-inside_left-01.par:1 To Rear_suspension_structural_parts Right-00.asm:1,Rear_Suspension_arm_lower_plate-00.psm:1*	*Bonded - Rear_suspension_structural_parts Right-00.asm:1,Rear-wheel-inside-right-02.par:1 To Rear_suspension_structural_parts Right-00.asm:1,Rear_Suspension_arm_lower_plate-00.psm:1*	*Bonded - Suspension_rod_bearing_reir To Rear_suspension_struc 00.asm:1,Rear_Suspension_ 03.psm:1*
State	Fully Defined			
Scope				
Scoping Method	Geometry Selection			
Contact	5 Faces	6 Faces		
Target	5 Faces			3 Faces
Contact Bodies	ESTM_16_1.par:2	Rear_suspension_structural_parts Right-00.asm:1,Rear-wheel-inside_left-01.par:1	Rear_suspension_structural_parts Right-00.asm:1,Rear-wheel-inside-right-02.par:1	Suspension_rod_bearing_reir
Target Bodies	Suspension_rod_bearing_reinforcement-00.par:1	Rear_suspension_structural_parts Right-00.asm:1,Rear_Suspension_arm_lower_plate-00.psm:1		Rear_suspension_structu 00.asm:1,Rear_Suspension_ 03.psm:1
Definition				
Type	Bonded			
Scope Mode	Automatic			

Behavior	Symmetric
Suppressed	No
Advanced	
Formulation	Pure Penalty
Normal Stiffness	Program Controlled
Update Stiffness	Never
Pinball Region	Program Controlled

TABLE 10
Model (B4) > Connections > Contacts > Contact Regions

Object Name	*Bonded - Rear_suspension_structural_parts Right-00.asm:1,Rear-wheel-inside_left-01.par:1 To Rear_suspension_structural_parts Right-00.asm:1,Rear_Suspension_arm_damper_plate-03.psm:1*	*Bonded - Rear_suspension_structural_parts Right-00.asm:1,Rear-wheel-inside-right-02.par:1 To Rear_suspension_structural_parts Right-00.asm:1,Rear_Suspension_arm_diagonal_bracket-02.psm:1*	*Bonded - Rear_suspension_structural_parts Right-00.asm:1,Rear-wheel-inside-right-02.par:1 To Rear_suspension_structural_parts Right-00.asm:1,Rear_Suspension_arm_damper_plate-03.psm:1*	*Bonded - R 00.asm:1,Re 00.psm:1 To 00.asm:1,Rea*
State	Fully Defined			
Scope				
Scoping Method	Geometry Selection			
Contact	1 Face	3 Faces	1 Face	
Target	3 Faces	7 Faces	2 Faces	
Contact Bodies	Rear_suspension_structural_parts Right-00.asm:1,Rear-wheel-inside_left-01.par:1	Rear_suspension_structural_parts Right-00.asm:1,Rear-wheel-inside-right-02.par:1		Rear_sus 00.asm:1,Re
Target Bodies	Rear_suspension_structural_parts Right-00.asm:1,Rear_Suspension_arm_damper_plate-03.psm:1	Rear_suspension_structural_parts Right-00.asm:1,Rear_Suspension_arm_diagonal_bracket-02.psm:1	Rear_suspension_structural_parts Ri	
Definition				
Type	Bonded			
Scope Mode	Automatic			
Behavior	Symmetric			
Suppressed	No			
Advanced				
Formulation	Pure Penalty			
Normal Stiffness	Program Controlled			
Update Stiffness	Never			
Pinball Region	Program Controlled			

TABLE 11
Model (B4) > Connections > Contacts > Contact Regions

Object Name	*Bonded - Rear_suspension_structural_parts Right-00.asm:1,Rear-wheel-inside_left-01.par:1 To Torque_arm-02.psm:1*	*Bonded - Rear_suspension_structural_parts Right-00.asm:1,Rear-wheel-inside_left-01.par:1 To Rear_motor_and_wheel_assy-00.asm:1,Minimotor2Rear_ST6.asm:1,Minimotor stator subassy.asm:1,Minimotor axle.par:1*	*Bonded - Rear_suspension_structural_parts Right-00.asm:1,Rear-wheel-inside-right-02.par:1 To Rear_motor_and_wheel_assy-00.asm:1,Minimotor2Rear_ST6.asm:1,Minimotor stator subassy.asm:1,Washer_id12od19t1.5.par:2*	*Bonded - Rear_suspension_s Right-00.asm:1,Rear-wheel-insi To Rear_motor_and_wh 00.asm:1,Minimotor2Rear_ST6. stator subassy.asm:1,Minimo*
State	Fully Defined			
Scope				
Scoping Method	Geometry Selection			
Contact	1 Face	3 Faces	1 Face	3 Faces
Target	1 Face	2 Faces	1 Face	
Contact Bodies	Rear_suspension_structural_parts Right-00.asm:1,Rear-wheel-inside_left-01.par:1		Rear_suspension_structural_parts Right-00.asm:1,Rear-wheel-inside-right	
Target Bodies	Torque_arm-02.psm:1	Rear_motor_and_wheel_assy-00.asm:1,Minimotor2Rear_ST6.asm:1,Minimotor stator subassy.asm:1,Minimotor axle.par:1	Rear_motor_and_wheel_assy-00.asm:1,Minimotor2Rear_ST6.asm:1,Minimotor stator subassy.asm:1,Washer_id12od19t1.5.par:2	Rear_motor_and_wheel_
Definition				
Type	Bonded			
Scope Mode	Automatic			
Behavior	Symmetric			
Suppressed	No			
Advanced				
Formulation	Pure Penalty			
Normal Stiffness	Program Controlled			
Update Stiffness	Never			
Pinball Region	Program Controlled			

TABLE 12
Model (B4) > Connections > Contacts > Contact Regions

Object Name	*Bonded - Torque_arm-02.psm:1 To Rear_motor_and_wheel_assy-00.asm:1,Minimotor2Rear_ST6.asm:1,Rear_motor_spacer-00.par:1*	*Bonded - Rear_motor_and_wheel_assy-00.asm:1,Minimotor2Rear_ST6.asm:1,Minimotor stator subassy.asm:1,Washer_id12od19t1.5.par:2 To Rear_motor_and_wheel_assy-00.asm:1,Minimotor2Rear_ST6.asm:1,Minimotor stator subassy.asm:1,Minimotor axle.par:1*	*Bonded - Rear_motor_and_wheel_assy-00.asm:1,Minimotor2Rear_ST6.asm:1,Minimotor stator subassy.asm:1,Minimotor axle.par:1 To Rear_motor_and_wheel_assy-00.asm:1,Minimotor2Rear_ST6.asm:1,Rear_motor_space 00.par:1*
State	Fully Defined		
Scope			
Scoping Method	Geometry Selection		
Contact	1 Face	2 Faces	4 Faces
Target	1 Face	2 Faces	
Contact Bodies	Torque_arm-02.psm:1	Rear_motor_and_wheel_assy-00.asm:1,Minimotor2Rear_ST6.asm:1,Minimotor stator	Rear_motor_and_wheel_assy-00.asm:1,Minimotor2Rear_ST6.asm:1,Minimotor stator subassy.asm:1,Minimotor axle.par:1

		subassy.asm:1,Washer_id12od19t1.5.par:2	
Target Bodies	Rear_motor_and_wheel_assy-00.asm:1,Minimotor2Rear_ST6.asm:1,Rear_motor_spacer-00.par:1	Rear_motor_and_wheel_assy-00.asm:1,Minimotor2Rear_ST6.asm:1,Minimotor stator subassy.asm:1,Minimotor axle.par:1	Rear_motor_and_wheel_assy-00.asm:1,Minimotor2Rear_ST6.asm:1,Rear_motor_spacer-00.par:1
Definition			
Type	Bonded		
Scope Mode	Automatic		
Behavior	Symmetric		
Suppressed	No		
Advanced			
Formulation	Pure Penalty		
Normal Stiffness	Program Controlled		
Update Stiffness	Never		
Pinball Region	Program Controlled		

TABLE 13
Model (B4) > Connections > Contacts > Contact Regions

Object Name	*Contact Region 21*	*Contact Region 22*
State	Fully Defined	
Scope		
Scoping Method	Geometry Selection	
Contact	3 Faces	4 Faces
Target	1 Face	
Contact Bodies	Rear_motor_and_wheel_assy-00.asm:1,Minimotor2Rear_ST6.asm:1,Minimotor stator subassy.asm:1,Minimotor axle.par:1	
Target Bodies	Rear_motor_and_wheel_assy-00.asm:1,Washer_id12od19t1.5.par:1	Rear_motor_and_wheel_assy-00.asm:1,Washer_id12od19t1.5.par:2
Definition		
Type	Bonded	
Scope Mode	Automatic	
Behavior	Symmetric	
Suppressed	No	
Advanced		
Formulation	Pure Penalty	
Normal Stiffness	Program Controlled	
Update Stiffness	Never	
Pinball Region	Program Controlled	

Mesh

TABLE 14
Model (B4) > Mesh

Object Name	*Mesh*
State	Solved
Defaults	
Physics Preference	Mechanical
Relevance	0
Sizing	
Use Advanced Size Function	Off
Relevance Center	Medium
Element Size	Default
Initial Size Seed	Active Assembly
Smoothing	Medium
Transition	Fast
Span Angle Center	Coarse
Minimum Edge Length	8.939e-002 mm
Inflation	
Use Automatic Inflation	None
Inflation Option	Smooth Transition
Transition Ratio	0.272
Maximum Layers	5
Growth Rate	1.2
Inflation Algorithm	Pre
View Advanced Options	No
Advanced	
Shape Checking	Standard Mechanical
Element Midside Nodes	Program Controlled
Straight Sided Elements	No
Number of Retries	Default (4)
Extra Retries For Assembly	Yes
Rigid Body Behavior	Dimensionally Reduced
Mesh Morphing	Disabled
Defeaturing	
Pinch Tolerance	Please Define
Generate Pinch on Refresh	No
Automatic Mesh Based Defeaturing	On
Defeaturing Tolerance	Default
Statistics	
Nodes	964187
Elements	567270
Mesh Metric	None

TABLE 15
Model (B4) > Mesh > Mesh Controls

Object Name	*Face Sizing*
State	Fully Defined
Scope	
Scoping Method	Geometry Selection
Geometry	11 Faces
Definition	
Suppressed	No
Type	Element Size
Element Size	0.2 mm

Behavior	Soft

FIGURE 1
Model (B4) > Mesh > Figure

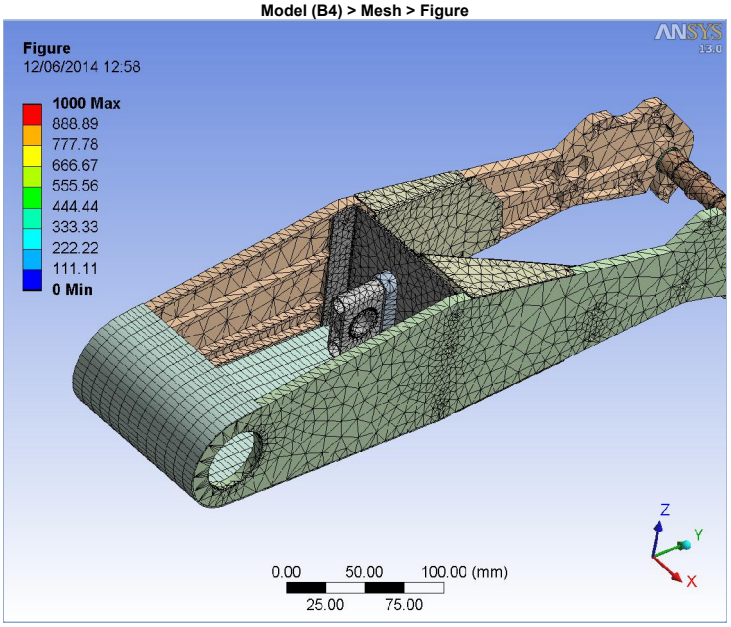

Static Structural (B5)

TABLE 16
Model (B4) > Analysis

Object Name	*Static Structural (B5)*
State	Solved
Definition	
Physics Type	Structural
Analysis Type	Static Structural
Solver Target	Mechanical APDL
Options	
Environment Temperature	22. °C
Generate Input Only	No

TABLE 17
Model (B4) > Static Structural (B5) > Analysis Settings

Object Name	*Analysis Settings*
State	Fully Defined
Step Controls	
Number Of Steps	1.
Current Step Number	1.
Step End Time	1. s
Auto Time Stepping	Program Controlled
Solver Controls	
Solver Type	Program Controlled
Weak Springs	Program Controlled
Large Deflection	Off
Inertia Relief	Off
Restart Controls	
Generate Restart Points	Program Controlled
Retain Files After Full Solve	No
Nonlinear Controls	
Force Convergence	Program Controlled
Moment Convergence	Program Controlled
Displacement Convergence	Program Controlled
Rotation Convergence	Program Controlled
Line Search	Program Controlled
Stabilization	Off
Output Controls	
Calculate Stress	Yes
Calculate Strain	Yes
Calculate Contact	No
Calculate Results At	All Time Points
Analysis Data Management	
Solver Files Directory	C:\Data\FEM\UIS_VELO_FEM\Wheel carrier-005_files\dp0\SYS\MECH\
Future Analysis	None
Scratch Solver Files Directory	
Save MAPDL db	No
Delete Unneeded Files	Yes
Nonlinear Solution	No
Solver Units	Active System
Solver Unit System	nmm

FIGURE 2
Model (B4) > Static Structural (B5) > Figure

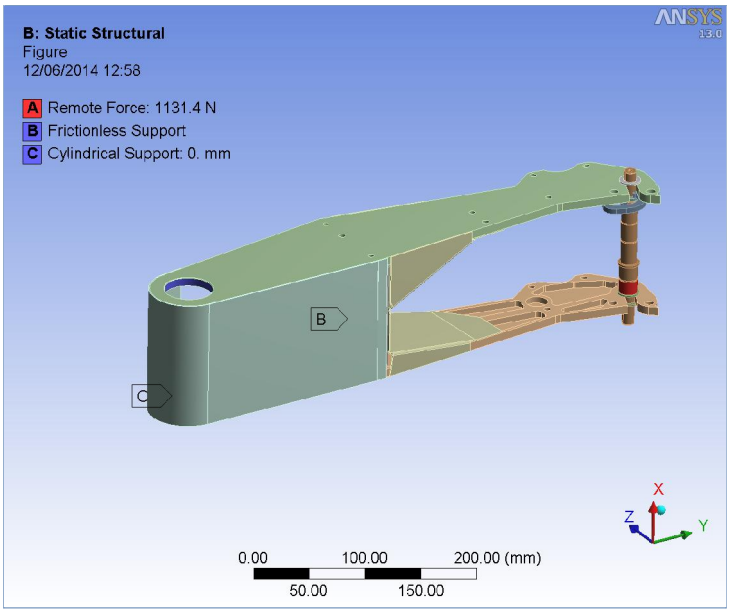

TABLE 18
Model (B4) > Static Structural (B5) > Loads

Object Name	*Remote Force*	*Frictionless Support*	*Cylindrical Support*
State	Fully Defined		
Scope			
Scoping Method	Geometry Selection		
Geometry	2 Faces		
Coordinate System	Global Coordinate System		
X Coordinate	0. mm		
Y Coordinate	0. mm		
Z Coordinate	-250. mm		
Location	Defined		
Definition			
Type	Remote Force	Frictionless Support	Cylindrical Support
Define By	Components		
X Component	800. N (ramped)		
Y Component	0. N (ramped)		
Z Component	800. N (ramped)		
Suppressed	No		
Behavior	Deformable		
Radial			Fixed
Axial			Fixed
Tangential			Free
Advanced			
Pinball Region	All		

FIGURE 3
Model (B4) > Static Structural (B5) > Remote Force

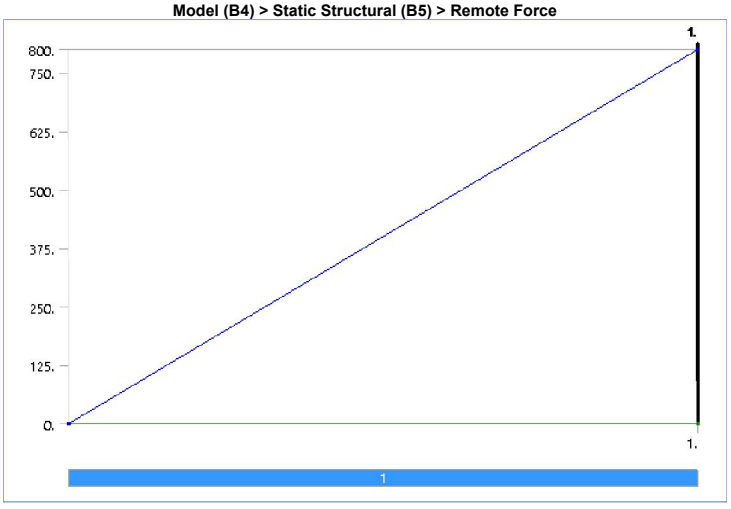

Solution (B6)

TABLE 19
Model (B4) > Static Structural (B5) > Solution

Object Name	*Solution (B6)*
State	Solved
Adaptive Mesh Refinement	
Max Refinement Loops	1.
Refinement Depth	2.
Information	
Status	Done

TABLE 20
Model (B4) > Static Structural (B5) > Solution (B6) > Solution Information

Object Name	*Solution Information*
State	Solved
Solution Information	
Solution Output	Solver Output
Newton-Raphson Residuals	0
Update Interval	2.5 s
Display Points	All

TABLE 21
Model (B4) > Static Structural (B5) > Solution (B6) > Results

Object Name	*Equivalent Stress*	*Directional Deformation*	*Directional Deformation 2*	*Equivalent Stre*
State	Solved			
Scope				
Scoping Method	Geometry Selection			
Geometry	All Bodies			6 Bodies
Definition				
Type	Equivalent (von-Mises) Stress	Directional Deformation		Equivalent (von-Mis
By	Time			
Display Time	Last			
Calculate Time History	Yes			
Identifier				
Orientation		Z Axis	X Axis	
Coordinate System		Global Coordinate System		
Integration Point Results				
Display Option	Averaged			Averaged
Results				
Minimum	0. MPa	-1.1941 mm	-0.22146 mm	1.5556e-002 I
Maximum	2517.4 MPa	2.3015 mm	3.6164 mm	2517.4 MP
Minimum Occurs On	ESTM_16_1.par:2	Rear_motor_and_wheel_assy-00.asm:1,Minimotor2Rear_ST6.asm:1,Minimotor stator subassy.asm:1,Minimotor axle.par:1	Rear_suspension_structural_parts Right-00.asm:1,Rear-wheel-ir	
Maximum Occurs On	Rear_suspension_structural_parts Right-00.asm:1,Rear_Suspension_arm_diagonal_bracket-02.psm:1	Rear_motor_and_wheel_assy-00.asm:1,Minimotor2Rear_ST6.asm:1,Minimotor stator subassy.asm:1,Minimotor axle.par:1	Rear_suspension_structural_parts Right-00.asm:1,Rear-wheel-inside-right-02.par:1	Rear_suspension_structu 00.asm:1,Rear_Suspension_ar 02.psm:1
Information				
Time	1. s			
Load Step	1			
Substep	1			
Iteration Number	1			

FIGURE 4
Model (B4) > Static Structural (B5) > Solution (B6) > Equivalent Stress > Figure

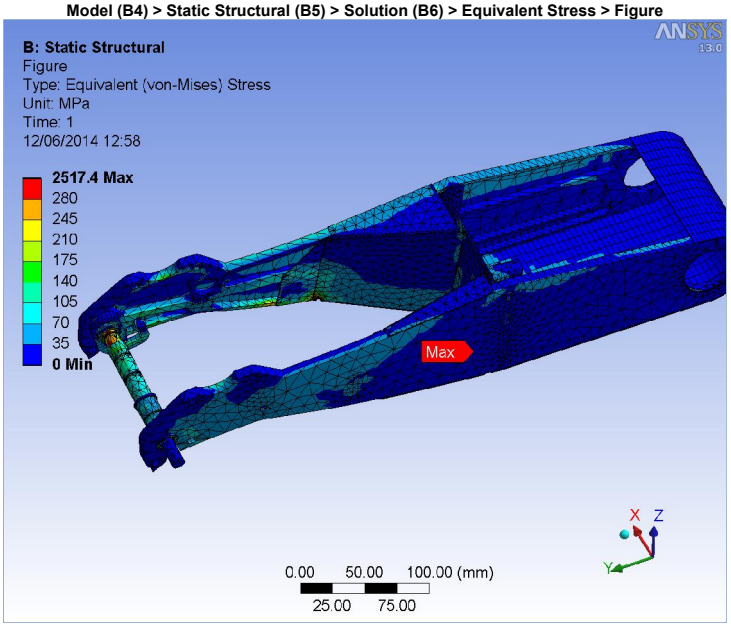

FIGURE 5
Model (B4) > Static Structural (B5) > Solution (B6) > Directional Deformation > Figure

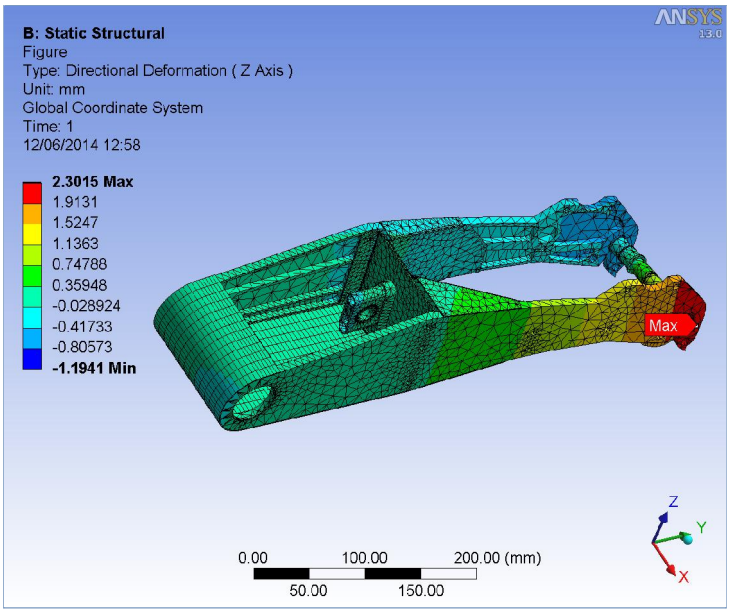

FIGURE 6
Model (B4) > Static Structural (B5) > Solution (B6) > Directional Deformation 2 > Figure

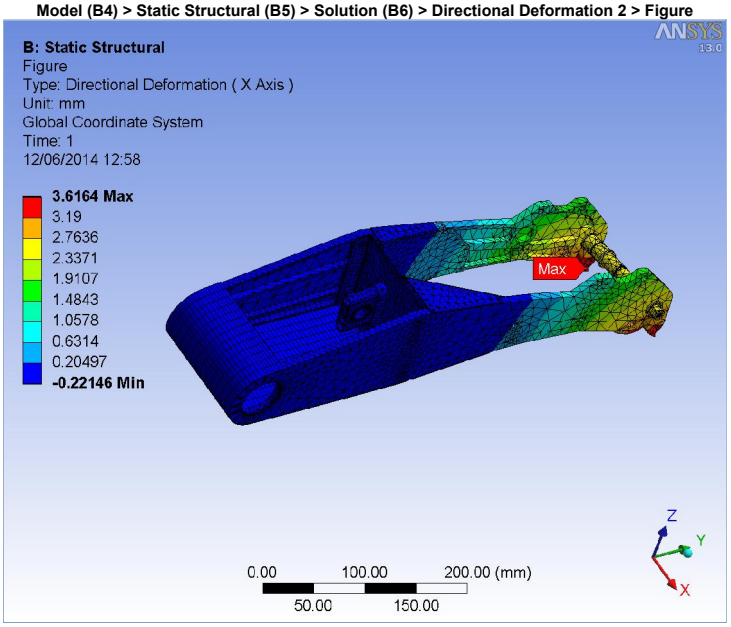

FIGURE 7
Model (B4) > Static Structural (B5) > Solution (B6) > Equivalent Stress 2 > Figure

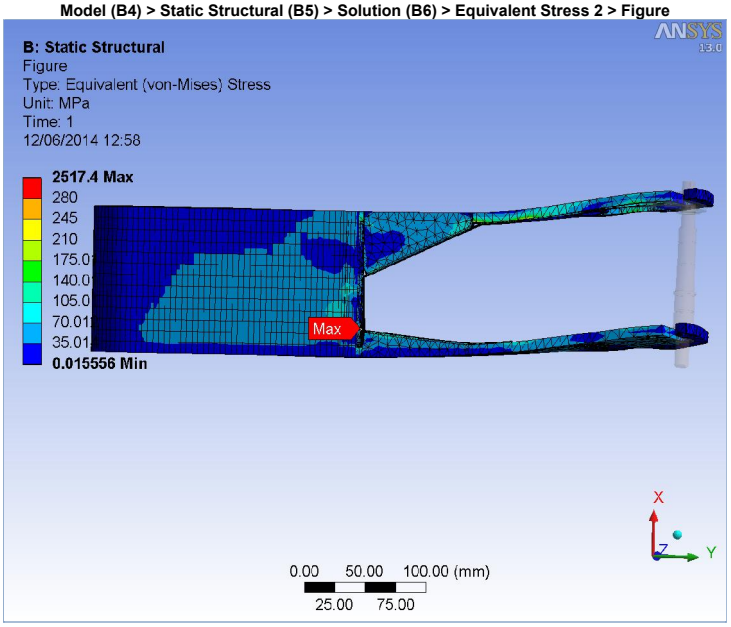

TABLE 22
Model (B4) > Static Structural (B5) > Solution (B6) > Probes

Object Name	*Force Reaction*
State	Solved
Definition	
Type	Force Reaction
Location Method	Boundary Condition
Boundary Condition	Frictionless Support
Orientation	Global Coordinate System
Options	
Result Selection	All
Display Time	End Time
Results	
X Axis	1557.7 N
Y Axis	1764.1 N
Z Axis	-2146.5 N
Total	3185.3 N
Maximum Value Over Time	
X Axis	1557.7 N
Y Axis	1764.1 N
Z Axis	-2146.5 N
Total	3185.3 N
Minimum Value Over Time	
X Axis	1557.7 N
Y Axis	1764.1 N
Z Axis	-2146.5 N
Total	3185.3 N
Information	
Time	1. s
Load Step	1
Substep	1
Iteration Number	1

Material Data

Aluminum Alloy

TABLE 23
Aluminum Alloy > Constants

Density	2.77e-006 kg mm^-3
Coefficient of Thermal Expansion	2.3e-005 C^-1
Specific Heat	8.75e+005 mJ kg^-1 C^-1

TABLE 24
Aluminum Alloy > Compressive Ultimate Strength

Compressive Ultimate Strength MPa
0

TABLE 25
Aluminum Alloy > Compressive Yield Strength

Compressive Yield Strength MPa
280

TABLE 26
Aluminum Alloy > Tensile Yield Strength

Tensile Yield Strength MPa
280

TABLE 27
Aluminum Alloy > Tensile Ultimate Strength

Tensile Ultimate Strength MPa
310

TABLE 28
Aluminum Alloy > Isotropic Secant Coefficient of Thermal Expansion

Reference Temperature C
22

TABLE 29
Aluminum Alloy > Isotropic Thermal Conductivity

Thermal Conductivity W mm^-1 C^-1	Temperature C
0.114	-100
0.144	0
0.165	100
0.175	200

TABLE 30
Aluminum Alloy > Alternating Stress R-Ratio

Alternating Stress MPa	Cycles	R-Ratio
275.8	1700	-1
241.3	5000	-1
206.8	34000	-1
172.4	1.4e+005	-1
137.9	8.e+005	-1
117.2	2.4e+006	-1
89.63	5.5e+007	-1
82.74	1.e+008	-1
170.6	50000	-0.5
139.6	3.5e+005	-0.5
108.6	3.7e+006	-0.5
87.91	1.4e+007	-0.5
77.57	5.e+007	-0.5
72.39	1.e+008	-0.5
144.8	50000	0
120.7	1.9e+005	0

103.4	1.3e+006	0
93.08	4.4e+006	0
86.18	1.2e+007	0
72.39	1.e+008	0
74.12	3.e+005	0.5
70.67	1.5e+006	0.5
66.36	1.2e+007	0.5
62.05	1.e+008	0.5

TABLE 31
Aluminum Alloy > Isotropic Resistivity

Resistivity ohm mm	Temperature C
2.43e-005	0
2.67e-005	20
3.63e-005	100

TABLE 32
Aluminum Alloy > Isotropic Elasticity

Temperature C	Young's Modulus MPa	Poisson's Ratio	Bulk Modulus MPa	Shear Modulus MPa
	71000	0.33	69608	26692

TABLE 33
Aluminum Alloy > Isotropic Relative Permeability

Relative Permeability
1

Structural Steel

TABLE 34
Structural Steel > Constants

Density	7.85e-006 kg mm^-3
Coefficient of Thermal Expansion	1.2e-005 C^-1
Specific Heat	4.34e+005 mJ kg^-1 C^-1
Thermal Conductivity	6.05e-002 W mm^-1 C^-1
Resistivity	1.7e-004 ohm mm

TABLE 35
Structural Steel > Compressive Ultimate Strength

Compressive Ultimate Strength MPa
0

TABLE 36
Structural Steel > Compressive Yield Strength

Compressive Yield Strength MPa
250

TABLE 37
Structural Steel > Tensile Yield Strength

Tensile Yield Strength MPa
250

TABLE 38
Structural Steel > Tensile Ultimate Strength

Tensile Ultimate Strength MPa
460

TABLE 39
Structural Steel > Isotropic Secant Coefficient of Thermal Expansion

Reference Temperature C
22

TABLE 40
Structural Steel > Alternating Stress Mean Stress

Alternating Stress MPa	Cycles	Mean Stress MPa
3999	10	0
2827	20	0
1896	50	0
1413	100	0
1069	200	0
441	2000	0
262	10000	0
214	20000	0
138	1.e+005	0
114	2.e+005	0
86.2	1.e+006	0

TABLE 41
Structural Steel > Strain-Life Parameters

Strength Coefficient MPa	Strength Exponent	Ductility Coefficient	Ductility Exponent	Cyclic Strength Coefficient MPa	Cyclic Strain Hardening Exponent
920	-0.106	0.213	-0.47	1000	0.2

TABLE 42
Structural Steel > Isotropic Elasticity

Temperature C	Young's Modulus MPa	Poisson's Ratio	Bulk Modulus MPa	Shear Modulus MPa
	2.e+005	0.3	1.6667e+005	76923

TABLE 43
Structural Steel > Isotropic Relative Permeability

Relative Permeability
10000

Project

Author	Per Hassel Sørensen
Subject	Vertical load on rear wheel carrier
Prepared for	VELOMOBILE: redefined thesis
First Saved	Wednesday, June 11, 2014
Last Saved	Thursday, June 12, 2014
Product Version	13.0 Release

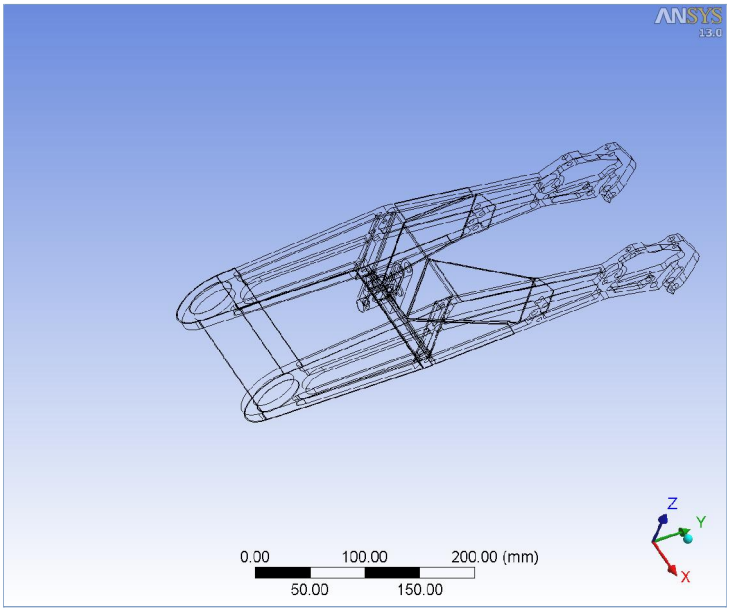

Contents

Units

TABLE 1

Unit System	Metric (mm, kg, N, s, mV, mA) Degrees rad/s Celsius
Angle	Degrees
Rotational Velocity	rad/s
Temperature	Celsius

Model (B4)

Geometry

TABLE 2
Model (B4) > Geometry

Object Name	*Geometry*
State	Fully Defined
Definition	
Source	C:\Data\CAD\Projects\UiS_velo\3D_design\Assy_new\Rear_suspension_assy_right-11.asm
Type	Solid Edge
Length Unit	Meters
Element Control	Program Controlled
Display Style	Part Color
Bounding Box	
Length X	120. mm
Length Y	514.7 mm
Length Z	140.74 mm
Properties	
Volume	3.9178e+005 mm³
Mass	1.0852 kg
Scale Factor Value	1.
Statistics	
Bodies	7
Active Bodies	7
Nodes	945082
Elements	558577
Mesh Metric	None
Preferences	
Import Solid Bodies	Yes
Import Surface Bodies	Yes
Import Line Bodies	No
Parameter Processing	Yes
Personal Parameter Key	DS
CAD Attribute Transfer	No
Named Selection Processing	No
Material Properties Transfer	No
CAD Associativity	Yes
Import Coordinate Systems	No
Reader Save Part File	No
Import Using Instances	Yes
Do Smart Update	No
Attach File Via Temp File	Yes
Temporary Directory	C:\Users\per\AppData\Local\Temp
Analysis Type	3-D
Mixed Import Resolution	None
Enclosure and Symmetry Processing	Yes

TABLE 3
Model (B4) > Geometry > Parts

Object Name	*ESTM_16_1.par:2*	*Suspension_rod_bearing_reinforcement-00.par:1*	*Rear_suspension_structural_parts Right-00.asm:1,Rear-wheel-inside_left-01.par:1*	*Rear_suspension_structural_parts Right-00.asm:1,Rear-wheel-inside-right-02.par:1*	*Rear_suspension_structural_ 00.asm:1,Rear_Suspension_arn 00.psm:1*
State	Meshed				
Graphics Properties					
Visible	Yes				
Transparency	1				
Definition					
Suppressed	No				

Stiffness Behavior	Flexible				
Coordinate System	Default Coordinate System				
Reference Temperature	By Environment				
Material					
Assignment	Aluminum Alloy				
Nonlinear Effects	Yes				
Thermal Strain Effects	Yes				
Bounding Box					
Length X	13. mm	17. mm	8. mm		120. mm
Length Y	38.327 mm	15.551 mm	514.7 mm		222.8 mm
Length Z	52.824 mm	65.269 mm	140.74 mm		74.618 mm
Properties					
Volume	13693 mm³	9417.4 mm³	1.3885e+005 mm³	1.389e+005 mm³	37549 mm³
Mass	3.7928e-002 kg	2.6086e-002 kg	0.38462 kg	0.38475 kg	0.10401 kg
Centroid X	-1.2 mm		68.262 mm	-45.453 mm	11.304 mm
Centroid Y	-294.08 mm	-273.73 mm	-234.59 mm	-234.52 mm	-407.64 mm
Centroid Z	12.297 mm	7.1872 mm	16.267 mm	16.277 mm	-10.094 mm
Moment of Inertia Ip1	4.169 kg·mm²	9.0879 kg·mm²	228.65 kg·mm²	228.76 kg·mm²	574.59 kg·mm²
Moment of Inertia Ip2	11.112 kg·mm²	9.5525 kg·mm²	9043.3 kg·mm²	9049.9 kg·mm²	168.78 kg·mm²
Moment of Inertia Ip3	8.1179 kg·mm²	0.82701 kg·mm²	8819.1 kg·mm²	8825.6 kg·mm²	655.43 kg·mm²
Statistics					
Nodes	891511	1061	11298	11232	7268
Elements	535077	531	5616	5549	975
Mesh Metric	None				

TABLE 4
Model (B4) > Geometry > Parts

Object Name	*Rear_suspension_structural_parts Right-00.asm:1,Rear_Suspension_arm_diagonal_bracket-02.psm:1*	*Rear_suspension_structural_parts Right-00.asm:1,Rear_Suspension_arm_damper_plate-03.psm:1*
State	Meshed	
Graphics Properties		
Visible	Yes	
Transparency	1	
Definition		
Suppressed	No	
Stiffness Behavior	Flexible	
Coordinate System	Default Coordinate System	
Reference Temperature	By Environment	
Material		
Assignment	Aluminum Alloy	
Nonlinear Effects	Yes	
Thermal Strain Effects	Yes	
Bounding Box		
Length X	119.8 mm	103.8 mm
Length Y	133.93 mm	28.13 mm
Length Z	95.643 mm	95.846 mm
Properties		
Volume	32336 mm³	21031 mm³
Mass	8.9571e-002 kg	5.8255e-002 kg
Centroid X	8.9358 mm	11.504 mm
Centroid Y	-224.54 mm	-272.52 mm
Centroid Z	20.395 mm	18.766 mm
Moment of Inertia Ip1	187.92 kg·mm²	50.679 kg·mm²
Moment of Inertia Ip2	223.57 kg·mm²	124.78 kg·mm²
Moment of Inertia Ip3	259.91 kg·mm²	77.234 kg·mm²
Statistics		
Nodes	14101	8611
Elements	6711	4118
Mesh Metric	None	

Coordinate Systems

TABLE 5
Model (B4) > Coordinate Systems > Coordinate System

Object Name	*Global Coordinate System*
State	Fully Defined
Definition	
Type	Cartesian
Coordinate System ID	0.
Origin	
Origin X	0. mm
Origin Y	0. mm
Origin Z	0. mm
Directional Vectors	
X Axis Data	[1. 0. 0.]
Y Axis Data	[0. 1. 0.]
Z Axis Data	[0. 0. 1.]

Connections

TABLE 6
Model (B4) > Connections

Object Name	*Connections*

State	Fully Defined
Auto Detection	
Generate Automatic Connection On Refresh	Yes
Transparency	
Enabled	Yes

TABLE 7
Model (B4) > Connections > Contacts

Object Name	*Contacts*
State	Fully Defined
Definition	
Connection Type	Contact
Scope	
Scoping Method	Geometry Selection
Geometry	All Bodies
Auto Detection	
Tolerance Type	Slider
Tolerance Slider	0.
Tolerance Value	1.3673 mm
Face/Face	Yes
Face/Edge	No
Edge/Edge	No
Priority	Include All
Group By	Bodies
Search Across	Bodies

TABLE 8
Model (B4) > Connections > Contacts > Contact Regions

Object Name	*Bonded - ESTM_16_1.par:2 To Suspension_rod_bearing_reinforcement-00.par:1*	*Bonded - Rear_suspension_structural_parts Right-00.asm:1,Rear-wheel-inside_left-01.par:1 To Rear_suspension_structural_parts Right-00.asm:1,Rear_Suspension_arm_lower_plate-00.psm:1*	*Bonded - Rear_suspension_structural_parts Right-00.asm:1,Rear-wheel-inside-right-02.par:1 To Rear_suspension_structural_parts Right-00.asm:1,Rear_Suspension_arm_lower_plate-00.psm:1*	*Contact Regio*
State	Fully Defined			
Scope				
Scoping Method	Geometry Selection			
Contact	5 Faces	6 Faces		
Target	5 Faces			3 Faces
Contact Bodies	ESTM_16_1.par:2	Rear_suspension_structural_parts Right-00.asm:1,Rear-wheel-inside_left-01.par:1	Rear_suspension_structural_parts Right-00.asm:1,Rear-wheel-inside-right-02.par:1	Suspension_rod_bearing_00.par:1
Target Bodies	Suspension_rod_bearing_reinforcement-00.par:1	Rear_suspension_structural_parts Right-00.asm:1,Rear_Suspension_arm_lower_plate-00.psm:1		Rear_suspension_structu 00.asm:1,Rear_Suspension_a 03.psm:1
Definition				
Type	Bonded			
Scope Mode	Automatic			
Behavior	Symmetric			
Suppressed	No			
Advanced				
Formulation	Pure Penalty			
Normal Stiffness	Program Controlled			
Update Stiffness	Never			
Pinball Region	Program Controlled			

TABLE 9
Model (B4) > Connections > Contacts > Contact Regions

Object Name	*Contact Region 6*	*Contact Region 7*	*Contact Region 8*	*Contact Region 9*	
State	Fully Defined				
Scope					
Scoping Method	Geometry Selection				
Contact	1 Face	3 Faces	1 Face	3 Faces	
Target	3 Faces	7 Faces	2 Faces	3 Faces	
Contact Bodies	Rear_suspension_structural_parts Right-00.asm:1,Rear-wheel-inside_left-01.par:1	Rear_suspension_structural_parts Right-00.asm:1,Rear-wheel-inside-right-02.par:1		Rear_suspension_structural_parts Right-00.asm:1,Rear_Suspension_arm_lower_plate-00.psm:1	Re 00.asm:
Target Bodies	Rear_suspension_structural_parts Right-00.asm:1,Rear_Suspension_arm_damper_plate-03.psm:1	Rear_suspension_structural_parts Right-00.asm:1,Rear_Suspension_arm_diagonal_bracket-02.psm:1	Rear_suspension_structural_parts Right-00.asm:1,Rear_Sus		
Definition					
Type	Bonded				
Scope Mode	Automatic				
Behavior	Symmetric				
Suppressed	No				
Advanced					
Formulation	Pure Penalty				
Normal Stiffness	Program Controlled				
Update Stiffness	Never				
Pinball Region	Program Controlled				

Mesh

TABLE 10
Model (B4) > Mesh

Object Name	*Mesh*
State	Solved

Defaults	
Physics Preference	Mechanical
Relevance	0
Sizing	
Use Advanced Size Function	Off
Relevance Center	Medium
Element Size	Default
Initial Size Seed	Active Assembly
Smoothing	Medium
Transition	Fast
Span Angle Center	Coarse
Minimum Edge Length	8.939e-002 mm
Inflation	
Use Automatic Inflation	None
Inflation Option	Smooth Transition
Transition Ratio	0.272
Maximum Layers	5
Growth Rate	1.2
Inflation Algorithm	Pre
View Advanced Options	No
Advanced	
Shape Checking	Standard Mechanical
Element Midside Nodes	Program Controlled
Straight Sided Elements	No
Number of Retries	Default (4)
Extra Retries For Assembly	Yes
Rigid Body Behavior	Dimensionally Reduced
Mesh Morphing	Disabled
Defeaturing	
Pinch Tolerance	Please Define
Generate Pinch on Refresh	No
Automatic Mesh Based Defeaturing	On
Defeaturing Tolerance	Default
Statistics	
Nodes	945082
Elements	558577
Mesh Metric	None

FIGURE 1
Model (B4) > Mesh > Figure

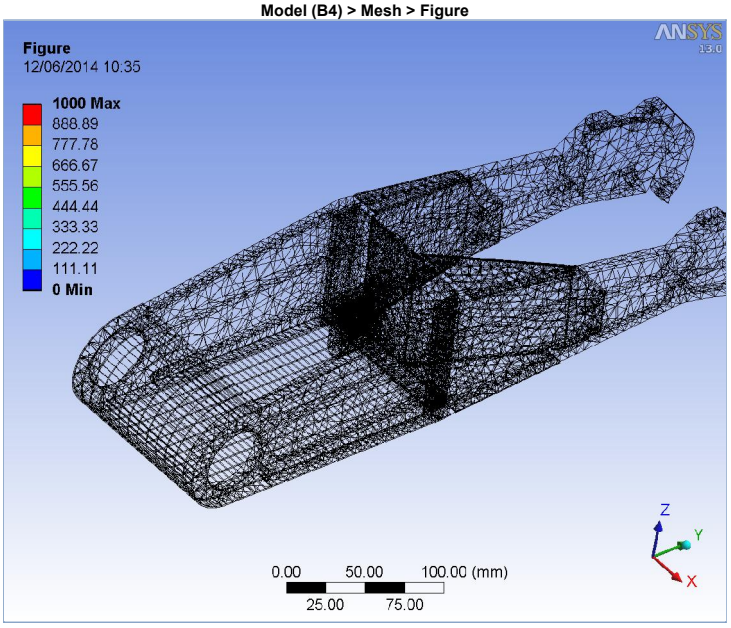

Static Structural (B5)

TABLE 11
Model (B4) > Analysis

Object Name	*Static Structural (B5)*
State	Solved
Definition	
Physics Type	Structural
Analysis Type	Static Structural
Solver Target	Mechanical APDL
Options	
Environment Temperature	22. °C
Generate Input Only	No

TABLE 12
Model (B4) > Static Structural (B5) > Analysis Settings

Object Name	*Analysis Settings*
State	Fully Defined
Step Controls	
Number Of Steps	1.
Current Step Number	1.
Step End Time	1. s
Auto Time Stepping	Program Controlled
Solver Controls	

Solver Type	Program Controlled
Weak Springs	Program Controlled
Large Deflection	Off
Inertia Relief	Off
Restart Controls	
Generate Restart Points	Program Controlled
Retain Files After Full Solve	No
Nonlinear Controls	
Force Convergence	Program Controlled
Moment Convergence	Program Controlled
Displacement Convergence	Program Controlled
Rotation Convergence	Program Controlled
Line Search	Program Controlled
Stabilization	Off
Output Controls	
Calculate Stress	Yes
Calculate Strain	Yes
Calculate Contact	No
Calculate Results At	All Time Points
Analysis Data Management	
Solver Files Directory	C:\Data\FEM\UIS_VELO_FEM\Wheel carrier-003_files\dp0\SYS\MECH\
Future Analysis	None
Scratch Solver Files Directory	
Save MAPDL db	No
Delete Unneeded Files	Yes
Nonlinear Solution	No
Solver Units	Active System
Solver Unit System	nmm

TABLE 13
Model (B4) > Static Structural (B5) > Loads

Object Name	*Remote Force*	*Frictionless Support*	*Cylindrical Support*
State	Fully Defined		
Scope			
Scoping Method	Geometry Selection		
Geometry	2 Faces		
Coordinate System	Global Coordinate System		
X Coordinate	0. mm		
Y Coordinate	0. mm		
Z Coordinate	-250. mm		
Location	Defined		
Definition			
Type	Remote Force	Frictionless Support	Cylindrical Support
Define By	Components		
X Component	0. N (ramped)		
Y Component	0. N (ramped)		
Z Component	800. N (ramped)		
Suppressed	No		
Behavior	Deformable		
Radial			Fixed
Axial			Fixed
Tangential			Free
Advanced			
Pinball Region	All		

FIGURE 2
Model (B4) > Static Structural (B5) > Remote Force

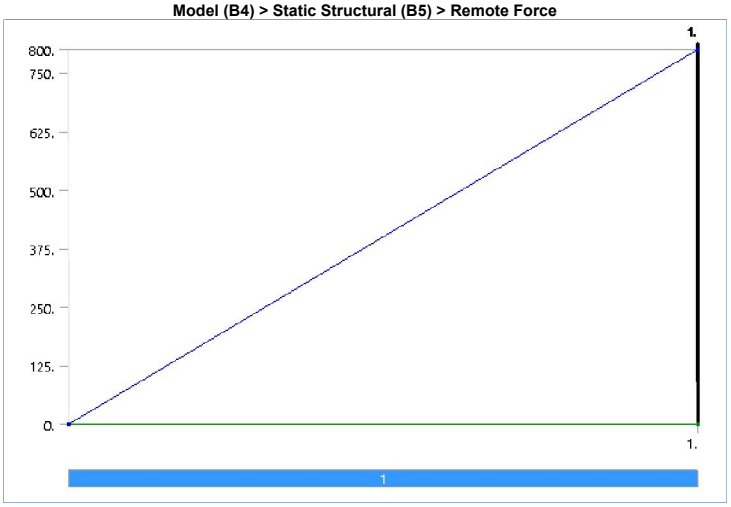

FIGURE 3
Model (B4) > Static Structural (B5) > Figure

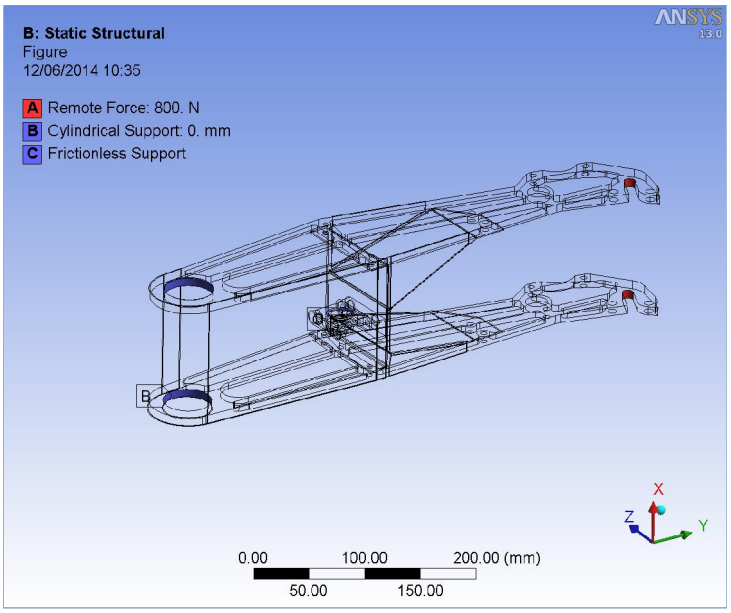

Solution (B6)

TABLE 14
Model (B4) > Static Structural (B5) > Solution

Object Name	*Solution (B6)*
State	Solved
Adaptive Mesh Refinement	
Max Refinement Loops	1.
Refinement Depth	2.
Information	
Status	Done

TABLE 15
Model (B4) > Static Structural (B5) > Solution (B6) > Solution Information

Object Name	*Solution Information*
State	Solved
Solution Information	
Solution Output	Solver Output
Newton-Raphson Residuals	0
Update Interval	2.5 s
Display Points	All

TABLE 16
Model (B4) > Static Structural (B5) > Solution (B6) > Results

Object Name	*Equivalent Stress*	*Directional Deformation*	*Directional Deformation 2*
State	Solved		
Scope			
Scoping Method	Geometry Selection		
Geometry	All Bodies		
Definition			
Type	Equivalent (von-Mises) Stress	Directional Deformation	
By	Time		
Display Time	Last		
Calculate Time History	Yes		
Identifier			
Orientation		Z Axis	X Axis
Coordinate System		Global Coordinate System	
Integration Point Results			
Display Option	Averaged		
Results			
Minimum	0. MPa	-4.3379e-002 mm	-0.16042 mm
Maximum	94.257 MPa	0.76918 mm	0.31453 mm
Minimum Occurs On	ESTM_16_1.par:2		Rear_suspension_structural_parts Right-00.asm:1,Rear-wheel-inside_left-01.par:1
Maximum Occurs On	ESTM_16_1.par:2	Rear_suspension_structural_parts Right-00.asm:1,Rear-wheel-inside-right-02.par:1	
Information			
Time	1. s		
Load Step	1		
Substep	1		
Iteration Number	1		

FIGURE 4
Model (B4) > Static Structural (B5) > Solution (B6) > Equivalent Stress > Figure

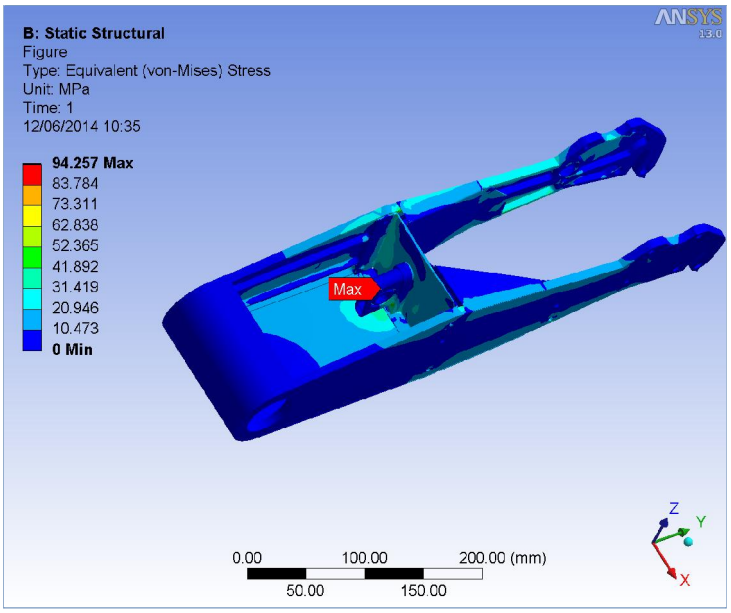

FIGURE 5
Model (B4) > Static Structural (B5) > Solution (B6) > Directional Deformation > Figure

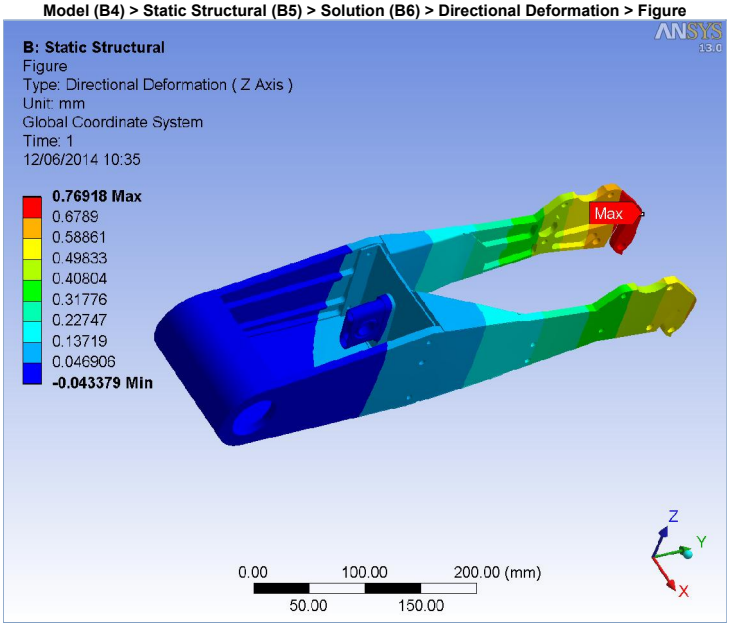

FIGURE 6
Model (B4) > Static Structural (B5) > Solution (B6) > Directional Deformation 2 > Figure

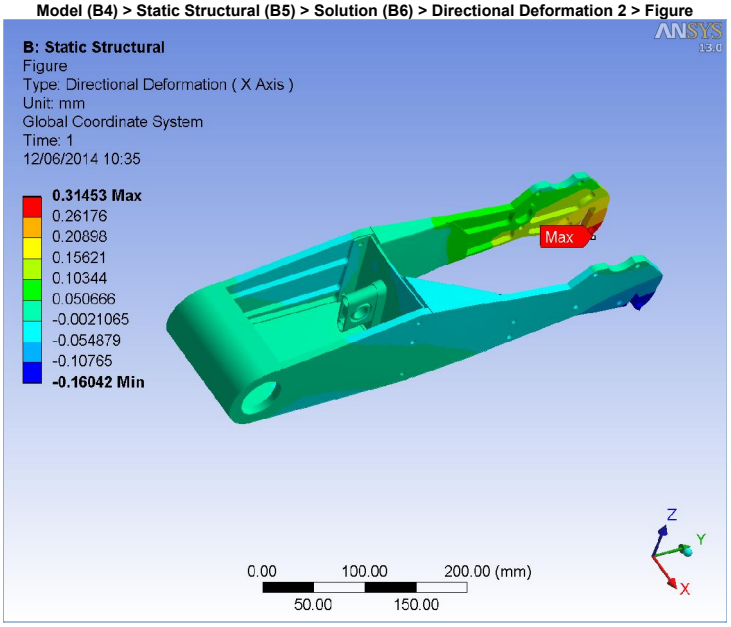

TABLE 17
Model (B4) > Static Structural (B5) > Solution (B6) > Fatigue Tools

Object Name	*Fatigue Tool*
State	Solved
Materials	
Fatigue Strength Factor (Kf)	1.
Loading	
Type	Ratio
Loading Ratio	0.
Scale Factor	1.
Definition	
Display Time	End Time
Options	
Analysis Type	Stress Life
Mean Stress Theory	None
Stress Component	Equivalent (Von Mises)
Life Units	
Units Name	cycles
1 cycle is equal to	1. cycles

FIGURE 7
Model (B4) > Static Structural (B5) > Solution (B6) > Fatigue Tool

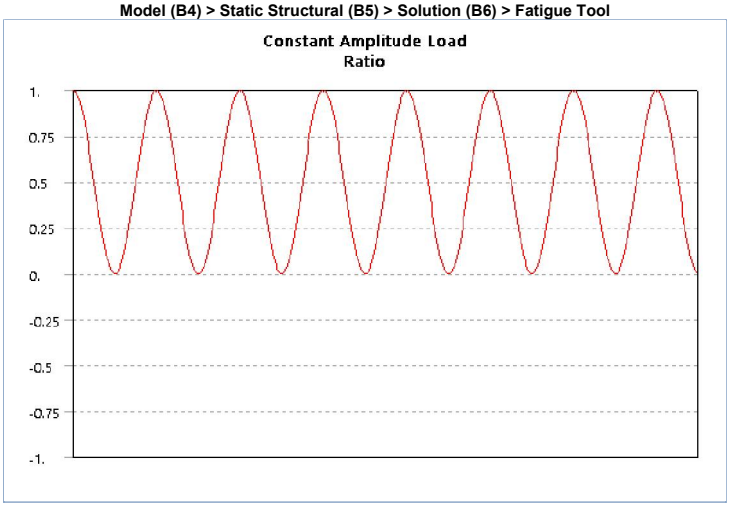

FIGURE 8
Model (B4) > Static Structural (B5) > Solution (B6) > Fatigue Tool

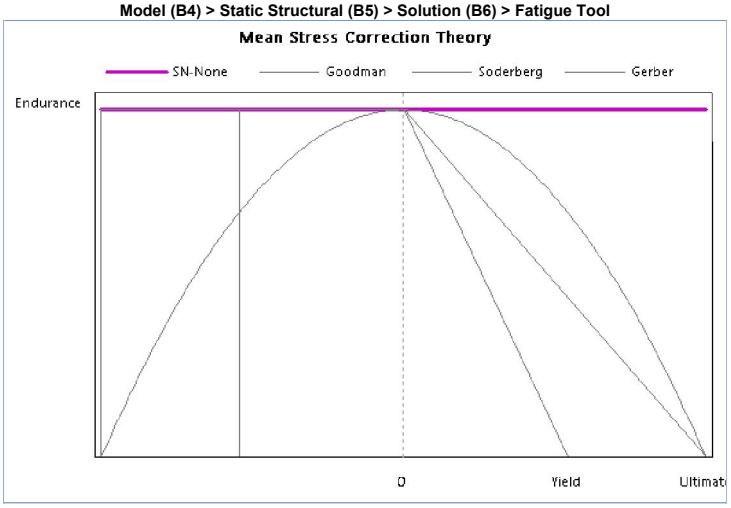

TABLE 18
Model (B4) > Static Structural (B5) > Solution (B6) > Fatigue Tool > Results

Object Name	*Life*
State	Solved
Scope	
Scoping Method	Geometry Selection
Geometry	All Bodies
Definition	
Type	Life
Identifier	
Results	
Minimum	1.e+008 cycles
Minimum Occurs On	ESTM_16_1.par:2

TABLE 19
Model (B4) > Static Structural (B5) > Solution (B6) > Probes

Object Name	*Force Reaction*
State	Solved
Definition	
Type	Force Reaction
Location Method	Boundary Condition
Boundary Condition	Frictionless Support

Orientation	Global Coordinate System
Options	
Result Selection	All
Display Time	End Time
Results	
X Axis	5.6945 N
Y Axis	1431. N
Z Axis	-2234.4 N
Total	2653.4 N
Maximum Value Over Time	
X Axis	5.6945 N
Y Axis	1431. N
Z Axis	-2234.4 N
Total	2653.4 N
Minimum Value Over Time	
X Axis	5.6945 N
Y Axis	1431. N
Z Axis	-2234.4 N
Total	2653.4 N
Information	
Time	1. s
Load Step	1
Substep	1
Iteration Number	1

Material Data

Aluminum Alloy

TABLE 20
Aluminum Alloy > Constants

Density	2.77e-006 kg mm^-3
Coefficient of Thermal Expansion	2.3e-005 C^-1
Specific Heat	8.75e+005 mJ kg^-1 C^-1

TABLE 21
Aluminum Alloy > Compressive Ultimate Strength

Compressive Ultimate Strength MPa
0

TABLE 22
Aluminum Alloy > Compressive Yield Strength

Compressive Yield Strength MPa
280

TABLE 23
Aluminum Alloy > Tensile Yield Strength

Tensile Yield Strength MPa
280

TABLE 24
Aluminum Alloy > Tensile Ultimate Strength

Tensile Ultimate Strength MPa
310

TABLE 25
Aluminum Alloy > Isotropic Secant Coefficient of Thermal Expansion

Reference Temperature C
22

TABLE 26
Aluminum Alloy > Isotropic Thermal Conductivity

Thermal Conductivity W mm^-1 C^-1	Temperature C
0.114	-100
0.144	0
0.165	100
0.175	200

TABLE 27
Aluminum Alloy > Alternating Stress R-Ratio

Alternating Stress MPa	Cycles	R-Ratio
275.8	1700	-1
241.3	5000	-1
206.8	34000	-1
172.4	1.4e+005	-1
137.9	8.e+005	-1
117.2	2.4e+006	-1
89.63	5.5e+007	-1
82.74	1.e+008	-1
170.6	50000	-0.5
139.6	3.5e+005	-0.5
108.6	3.7e+006	-0.5
87.91	1.4e+007	-0.5
77.57	5.e+007	-0.5
72.39	1.e+008	-0.5
144.8	50000	0
120.7	1.9e+005	0
103.4	1.3e+006	0
93.08	4.4e+006	0
86.18	1.2e+007	0
72.39	1.e+008	0
74.12	3.e+005	0.5
70.67	1.5e+006	0.5
66.36	1.2e+007	0.5

62.05	1.e+008	0.5

TABLE 28
Aluminum Alloy > Isotropic Resistivity

Resistivity ohm mm	Temperature C
2.43e-005	0
2.67e-005	20
3.63e-005	100

TABLE 29
Aluminum Alloy > Isotropic Elasticity

Temperature C	Young's Modulus MPa	Poisson's Ratio	Bulk Modulus MPa	Shear Modulus MPa
	71000	0.33	69608	26692

TABLE 30
Aluminum Alloy > Isotropic Relative Permeability

Relative Permeability
1

Project

Author	Per Hassel Sørensen
Subject	Torque arm 'G' - 5 mm
Prepared for	Master thesis
First Saved	Saturday, June 14, 2014
Last Saved	Sunday, June 15, 2014
Product Version	13.0 Release

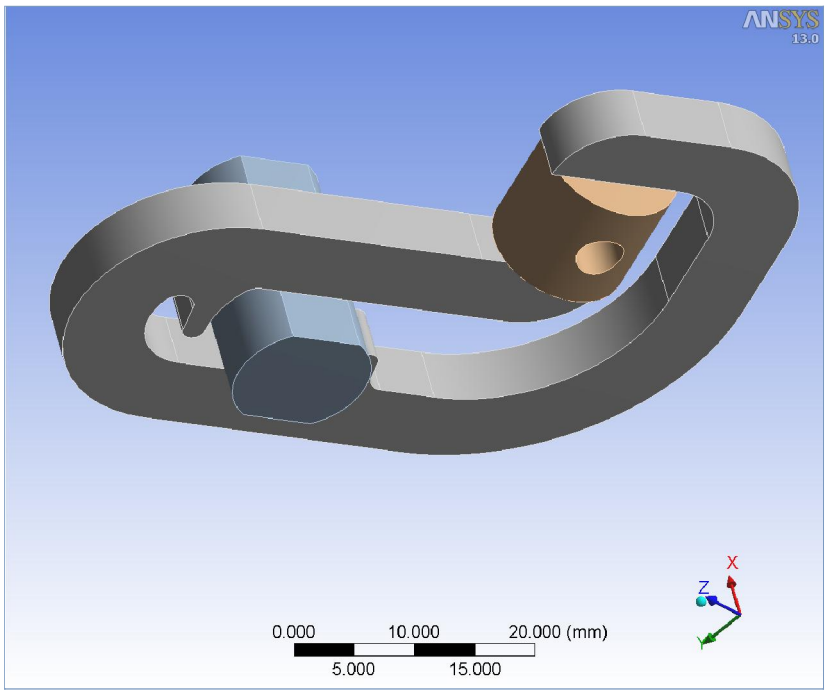

Contents

Units

TABLE 1

Unit System	Metric (mm, kg, N, s, mV, mA) Degrees rad/s Celsius
Angle	Degrees
Rotational Velocity	rad/s
Temperature	Celsius

Model (B4)

Geometry

TABLE 2
Model (B4) > Geometry

Object Name	*Geometry*
State	Fully Defined
Definition	
Source	C:\Data\CAD\Projects\UiS_velo\3D_design\Assy_new\Rear_suspension_assy_right-11.asm
Type	Solid Edge
Length Unit	Meters
Element Control	Program Controlled
Display Style	Part Color
Bounding Box	
Length X	20. mm
Length Y	59.321 mm
Length Z	68.954 mm
Properties	
Volume	8223.8 mm³
Mass	6.4557e-002 kg
Scale Factor Value	1.
Statistics	
Bodies	3
Active Bodies	3
Nodes	45524
Elements	19308
Mesh Metric	None
Preferences	
Import Solid Bodies	Yes
Import Surface Bodies	Yes
Import Line Bodies	No
Parameter Processing	Yes
Personal Parameter Key	DS
CAD Attribute Transfer	No
Named Selection Processing	No
Material Properties Transfer	No
CAD Associativity	Yes
Import Coordinate Systems	No
Reader Save Part File	No
Import Using Instances	Yes
Do Smart Update	No
Attach File Via Temp File	Yes
Temporary Directory	C:\Users\per\AppData\Local\Temp
Analysis Type	3-D
Mixed Import Resolution	None
Enclosure and Symmetry Processing	Yes

TABLE 3
Model (B4) > Geometry > Parts

Object Name	*Torque_arm-02.psm:1*	*Rear_motor_and_wheel_assy-00.asm:1,Minimotor2Rear_ST6.asm:1,Minimotor axle_modified.par:1*	*FEM_wedgenut.par:1*
State	Meshed		
Graphics Properties			
Visible	Yes		
Transparency	1		
Definition			
Suppressed	No		
Stiffness Behavior	Flexible		
Coordinate System	Default Coordinate System		
Reference Temperature	By Environment		
Material			
Assignment	Structural Steel		
Nonlinear Effects	Yes		
Thermal Strain Effects	Yes		
Bounding Box			
Length X	5. mm	20. mm	12. mm
Length Y	59.321 mm	13.611 mm	14.617 mm
Length Z	68.954 mm	14.629 mm	15.184 mm
Properties			
Volume	5098.3 mm³	2034.4 mm³	1091.1 mm³
Mass	4.0021e-002 kg	1.597e-002 kg	8.5652e-003 kg
Centroid X	60.804 mm	63.304 mm	60.804 mm
Centroid Y	-8.3599 mm	4.3759e-014 mm	-23.68 mm
Centroid Z	-8.8833 mm	-6.0645e-014 mm	-12.484 mm
Moment of Inertia Ip1	3.9588 kg·mm²	0.67899 kg·mm²	0.18377 kg·mm²
Moment of Inertia Ip2	17.033 kg·mm²	0.26166 kg·mm²	0.16041 kg·mm²
Moment of Inertia Ip3	13.241 kg·mm²	0.64692 kg·mm²	0.17101 kg·mm²
Statistics			
Nodes	17987	15669	11868
Elements	8877	3328	7103
Mesh Metric	None		

Coordinate Systems

TABLE 4
Model (B4) > Coordinate Systems > Coordinate System

Object Name	*Global Coordinate System*
State	Fully Defined
Definition	
Type	Cartesian
Coordinate System ID	0.
Origin	
Origin X	0. mm
Origin Y	0. mm
Origin Z	0. mm
Directional Vectors	
X Axis Data	[1. 0. 0.]
Y Axis Data	[0. 1. 0.]
Z Axis Data	[0. 0. 1.]

Connections

TABLE 5
Model (B4) > Connections

Object Name	*Connections*
State	Fully Defined
Auto Detection	
Generate Automatic Connection On Refresh	No
Transparency	
Enabled	Yes

TABLE 6
Model (B4) > Connections > Contacts

Object Name	*Contacts*
State	Fully Defined
Definition	
Connection Type	Contact
Scope	
Scoping Method	Geometry Selection
Geometry	All Bodies
Auto Detection	
Tolerance Type	Slider
Tolerance Slider	0.
Tolerance Value	0.23283 mm
Face/Face	Yes
Face/Edge	No
Edge/Edge	No
Priority	Include All
Group By	Bodies

Search Across	Bodies

TABLE 7
Model (B4) > Connections > Contacts > Contact Regions

Object Name	*Bonded - Torque_arm-02.psm:1 To Rear_motor_and_wheel_assy-00.asm:1,Minimotor2Rear_ST6.asm:1,Minimotor axle_modified.par:1*	*Rough - FEM_wedgenut.par:1 To Torque_arm-02.psm:1*	*Rough - FEM_wedgenut.par:1 To Torque_arm-02.psm:1*	*Rough - Torque_arm-02.psm:1 To Rear_motor_and_wheel_assy-00.asm:1,Minimotor2Rear_ST6.asm:1,Minimotor axle_modified.par:1*
State	Fully Defined			
Scope				
Scoping Method	Geometry Selection			
Contact	1 Face			
Target	3 Faces	1 Face		3 Faces
Contact Bodies	Torque_arm-02.psm:1	FEM_wedgenut.par:1		Torque_arm-02.psm:1
Target Bodies	Rear_motor_and_wheel_assy-00.asm:1,Minimotor2Rear_ST6.asm:1,Minimotor axle_modified.par:1	Torque_arm-02.psm:1		Rear_motor_and_wheel_assy-00.asm:1,Minimotor2Rear_ST6.asm:1,Minimotor axle_modified.par:1
Definition				
Type	Bonded	Rough		
Scope Mode	Manual			
Behavior	Symmetric			
Suppressed	No			
Advanced				
Formulation	Pure Penalty			
Normal Stiffness	Program Controlled			
Update Stiffness	Never			
Pinball Region	Program Controlled			
Interface Treatment		Add Offset, No Ramping		
Offset		0. mm		
Time Step Controls		None		

FIGURE 1
Model (B4) > Connections > Contacts > Bonded - Torque_arm-02.psm:1 To Rear_motor_and_wheel_assy-00.asm:1,Minimotor2Rear_ST6.asm:1,Minimotor axle_modified.par:1 > Figure
Only bonded contact

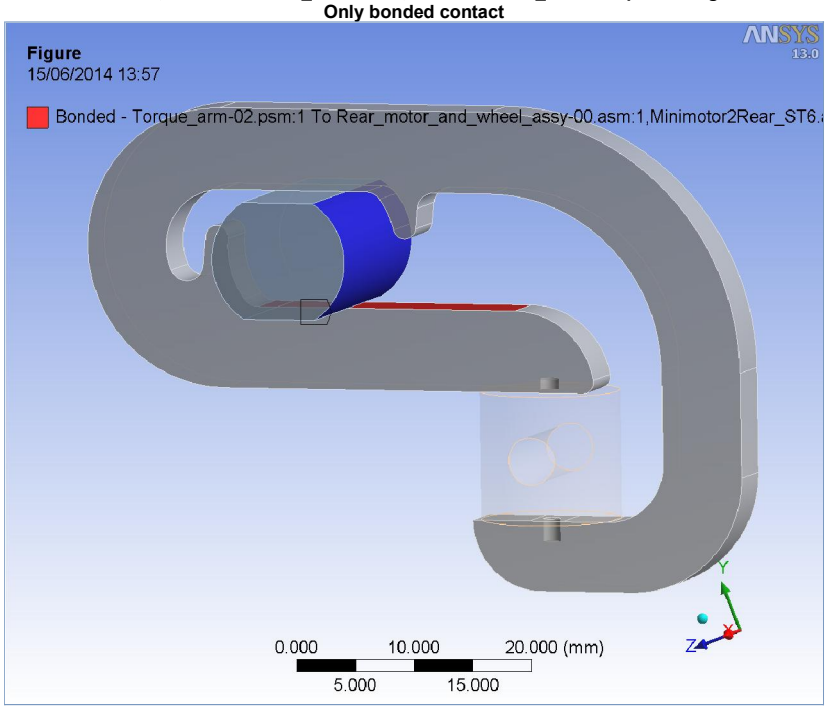

Mesh

TABLE 8
Model (B4) > Mesh

Object Name	*Mesh*
State	Solved
Defaults	
Physics Preference	Mechanical
Relevance	100
Sizing	
Use Advanced Size Function	Off
Relevance Center	Coarse

Element Size	Default
Initial Size Seed	Active Assembly
Smoothing	Medium
Transition	Fast
Span Angle Center	Coarse
Minimum Edge Length	1.4220 mm
Inflation	
Use Automatic Inflation	None
Inflation Option	Smooth Transition
Transition Ratio	0.272
Maximum Layers	5
Growth Rate	1.2
Inflation Algorithm	Pre
View Advanced Options	No
Advanced	
Shape Checking	Standard Mechanical
Element Midside Nodes	Program Controlled
Straight Sided Elements	No
Number of Retries	Default (4)
Extra Retries For Assembly	Yes
Rigid Body Behavior	Dimensionally Reduced
Mesh Morphing	Disabled
Defeaturing	
Pinch Tolerance	Please Define
Generate Pinch on Refresh	No
Automatic Mesh Based Defeaturing	On
Defeaturing Tolerance	Default
Statistics	
Nodes	45524
Elements	19308
Mesh Metric	None

TABLE 9
Model (B4) > Mesh > Mesh Controls

Object Name	*Refinement*
State	Fully Defined
Scope	
Scoping Method	Geometry Selection
Geometry	4 Faces
Definition	
Suppressed	No
Refinement	1

Static Structural (B5)

TABLE 10
Model (B4) > Analysis

Object Name	*Static Structural (B5)*
State	Solved
Definition	
Physics Type	Structural
Analysis Type	Static Structural
Solver Target	Mechanical APDL
Options	
Environment Temperature	22. °C
Generate Input Only	No

TABLE 11
Model (B4) > Static Structural (B5) > Analysis Settings

Object Name	*Analysis Settings*
State	Fully Defined
Step Controls	
Number Of Steps	1.
Current Step Number	1.
Step End Time	1. s
Auto Time Stepping	Program Controlled
Solver Controls	
Solver Type	Program Controlled
Weak Springs	Program Controlled
Large Deflection	On
Inertia Relief	Off
Restart Controls	
Generate Restart Points	Program Controlled
Retain Files After Full Solve	No
Nonlinear Controls	
Force Convergence	Program Controlled
Moment Convergence	Program Controlled
Displacement Convergence	Program Controlled
Rotation Convergence	Program Controlled
Line Search	Program Controlled
Stabilization	Off
Output Controls	
Calculate Stress	Yes

Calculate Strain	Yes
Calculate Contact	Yes
Calculate Results At	All Time Points
Analysis Data Management	
Solver Files Directory	C:\Data\FEM\Torque_arm\Torque_arm-07_files\dp0\SYS\MECH\
Future Analysis	None
Scratch Solver Files Directory	
Save MAPDL db	No
Delete Unneeded Files	Yes
Nonlinear Solution	Yes
Solver Units	Active System
Solver Unit System	nmm

FIGURE 2
Model (B4) > Static Structural (B5) > Figure

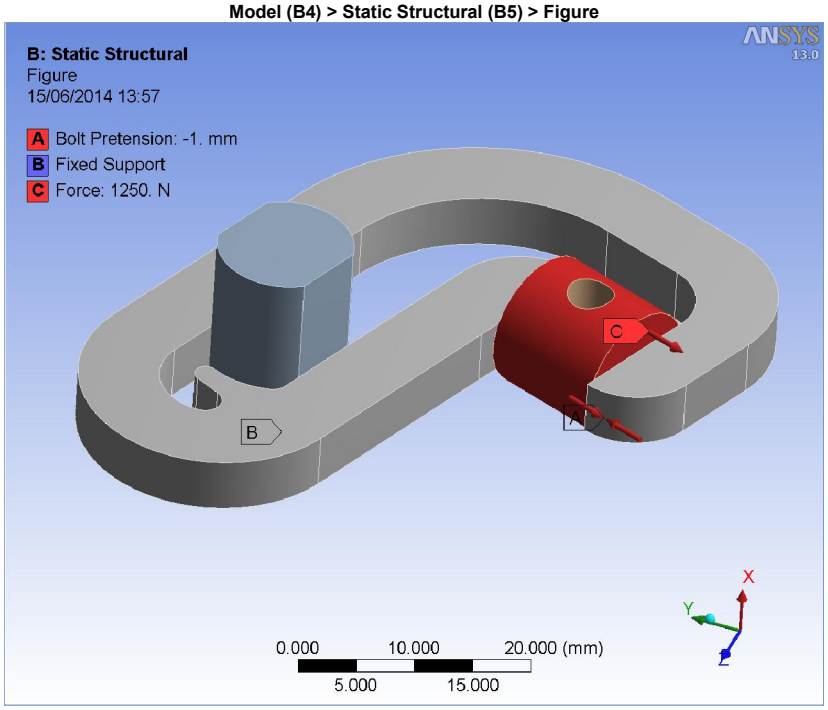

TABLE 12
Model (B4) > Static Structural (B5) > Loads

Object Name	*Fixed Support*	*Force*
State	Fully Defined	
Scope		
Scoping Method	Geometry Selection	
Geometry	1 Face	
Definition		
Type	Fixed Support	Force
Suppressed	No	
Define By		Vector
Magnitude		1250. N (ramped)
Direction		Defined

FIGURE 3
Model (B4) > Static Structural (B5) > Force

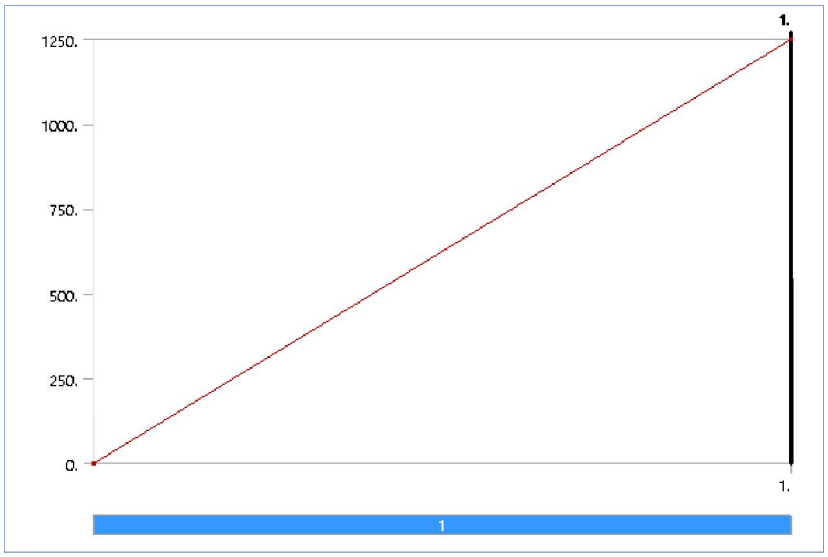

TABLE 13
Model (B4) > Static Structural (B5) > Bolt Pretension

Object Name	*Bolt Pretension*
State	Fully Defined
Scope	
Scoping Method	Geometry Selection
Geometry	1 Face
Definition	
Type	Bolt Pretension
Suppressed	No
Define By	Adjustment
Preadjustment	-1. mm

TABLE 14
Model (B4) > Static Structural (B5) > Bolt Pretension

Steps	Define By	Preload [N]	Adjustment [mm]
1.	Adjustment	N/A	-1.

FIGURE 4
Model (B4) > Static Structural (B5) > Figure 2

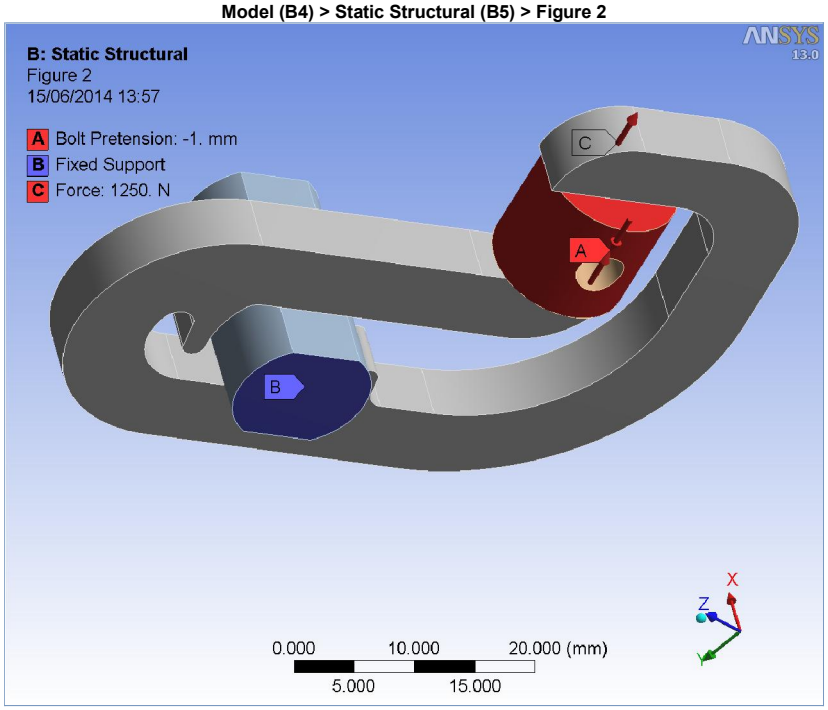

Solution (B6)

TABLE 15
Model (B4) > Static Structural (B5) > Solution

Object Name	*Solution (B6)*
State	Solved
Adaptive Mesh Refinement	
Max Refinement Loops	1.
Refinement Depth	2.

Information	
Status	Done

TABLE 16
Model (B4) > Static Structural (B5) > Solution (B6) > Solution Information

Object Name	*Solution Information*
State	Solved
Solution Information	
Solution Output	Solver Output
Newton-Raphson Residuals	0
Update Interval	2.5 s
Display Points	All

TABLE 17
Model (B4) > Static Structural (B5) > Solution (B6) > Results

Object Name	*Equivalent Stress 2*	*Total Deformation*
State	Solved	
Scope		
Scoping Method	Geometry Selection	
Geometry	1 Body	All Bodies
Definition		
Type	Equivalent (von-Mises) Stress	Total Deformation
By	Time	
Display Time	Last	
Calculate Time History	Yes	
Identifier		
Integration Point Results		
Display Option	Averaged	
Results		
Minimum	5.3311e-003 MPa	0. mm
Maximum	1237.7 MPa	1.1281 mm
Minimum Occurs On		Rear_motor_and_wheel_assy-00.asm:1,Minimotor2Rear_ST6.asm:1,Minimotor axle_modified.par:1
Maximum Occurs On		Torque_arm-02.psm:1
Information		
Time	1. s	
Load Step	1	
Substep	1	
Iteration Number	19	

FIGURE 5
Model (B4) > Static Structural (B5) > Solution (B6) > Equivalent Stress 2 > Figure

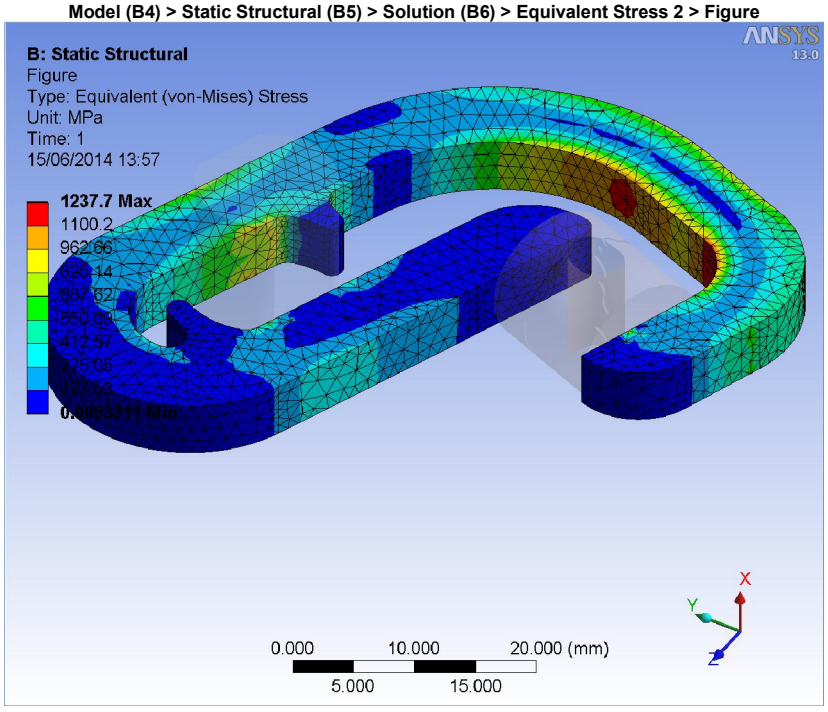

FIGURE 6
Model (B4) > Static Structural (B5) > Solution (B6) > Total Deformation > Figure

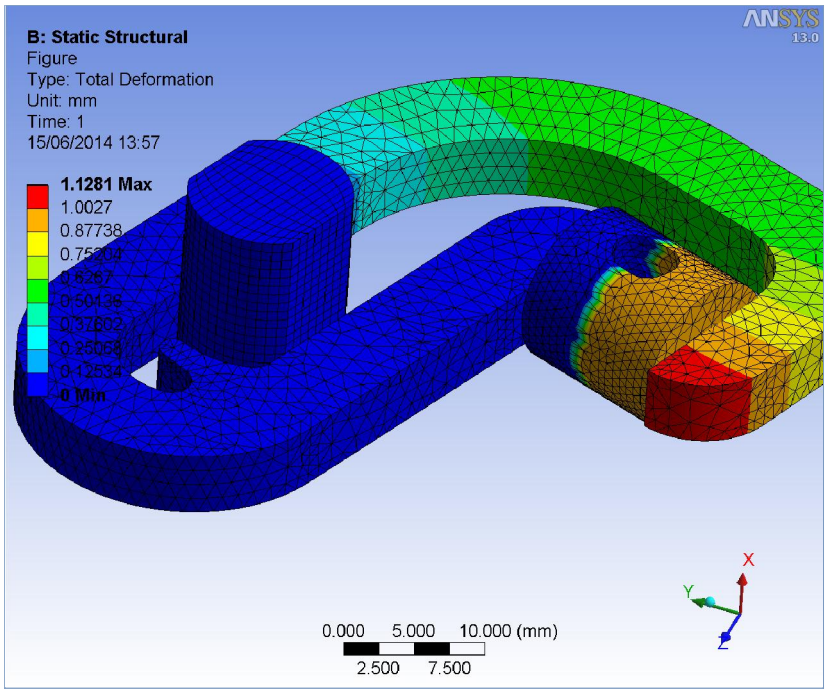

TABLE 18
Model (B4) > Static Structural (B5) > Solution (B6) > Probes

Object Name	*Moment Reaction*
State	Solved
Definition	
Type	Moment Reaction
Location Method	Boundary Condition
Boundary Condition	Fixed Support
Orientation	Global Coordinate System
Summation	Centroid
Options	
Result Selection	All
Display Time	End Time
Results	
X Axis	25862 N·mm
Y Axis	3389.6 N·mm
Z Axis	8709.4 N·mm
Total	27499 N·mm
Maximum Value Over Time	
X Axis	25862 N·mm
Y Axis	3389.6 N·mm
Z Axis	8709.4 N·mm
Total	27499 N·mm
Minimum Value Over Time	
X Axis	25862 N·mm
Y Axis	3389.6 N·mm
Z Axis	8709.4 N·mm
Total	27499 N·mm
Information	
Time	1. s
Load Step	1
Substep	1
Iteration Number	19

Material Data

Structural Steel

TABLE 19
Structural Steel > Constants

Density	7.85e-006 kg mm^-3
Coefficient of Thermal Expansion	1.2e-005 C^-1
Specific Heat	4.34e+005 mJ kg^-1 C^-1
Thermal Conductivity	6.05e-002 W mm^-1 C^-1
Resistivity	1.7e-004 ohm mm

TABLE 20
Structural Steel > Compressive Ultimate Strength

Compressive Ultimate Strength MPa
0

TABLE 21
Structural Steel > Compressive Yield Strength

Compressive Yield Strength MPa
250

TABLE 22
Structural Steel > Tensile Yield Strength

Tensile Yield Strength MPa
250

TABLE 23
Structural Steel > Tensile Ultimate Strength

Tensile Ultimate Strength MPa
460

TABLE 24
Structural Steel > Isotropic Secant Coefficient of Thermal Expansion

Reference Temperature C
22

TABLE 25
Structural Steel > Alternating Stress Mean Stress

Alternating Stress MPa	Cycles	Mean Stress MPa
3999	10	0
2827	20	0
1896	50	0
1413	100	0
1069	200	0
441	2000	0
262	10000	0
214	20000	0
138	1.e+005	0
114	2.e+005	0
86.2	1.e+006	0

TABLE 26
Structural Steel > Strain-Life Parameters

Strength Coefficient MPa	Strength Exponent	Ductility Coefficient	Ductility Exponent	Cyclic Strength Coefficient MPa	Cyclic Strain Hardening Exponent
920	-0.106	0.213	-0.47	1000	0.2

TABLE 27
Structural Steel > Isotropic Elasticity

Temperature C	Young's Modulus MPa	Poisson's Ratio	Bulk Modulus MPa	Shear Modulus MPa
	2.e+005	0.3	1.6667e+005	76923

TABLE 28
Structural Steel > Isotropic Relative Permeability

Relative Permeability
10000

EcoDesigner Report

Date : 6/15/2014

Company Information:

- *Company Name:* VELOMOBILE redefined
- *Address:*
- *Prepared By Name:* Per Hassel SÃ¸rensen
- *Title:*
- *Email Address:*
- *Phone Number:*

Assembly/Part Information:

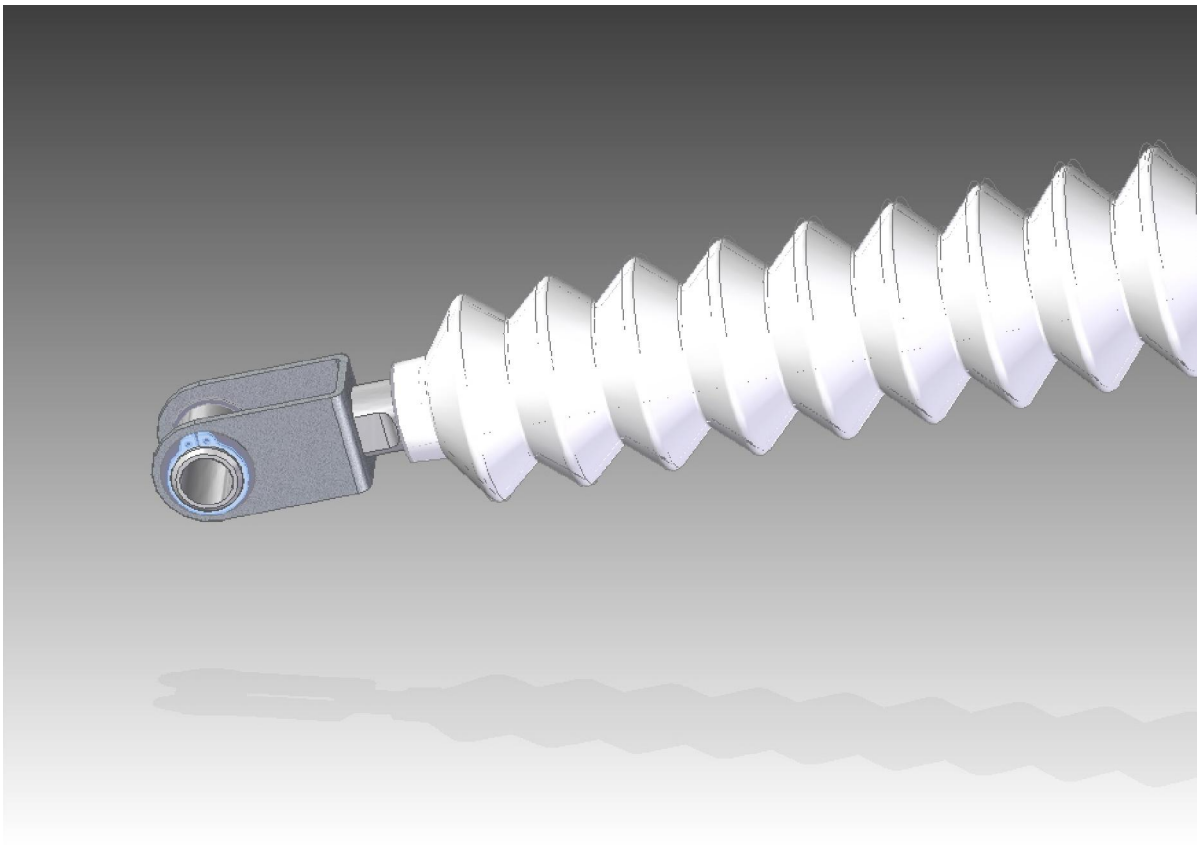

- *Assembly/Part Name:* Hydropneumatic_suspension_piston_separate-00.asm
- *Volume:* 0 cm3
- *Mass:* 0.207 kg

Screening Life Cycle Analysis:

- *Analysis Method:* ReCiPe Endpoint (I)
- *Analysis Type:* Damage Assessment
- *Functional Unit:* 1
- *LCA Software used:*

Environmental Impact:

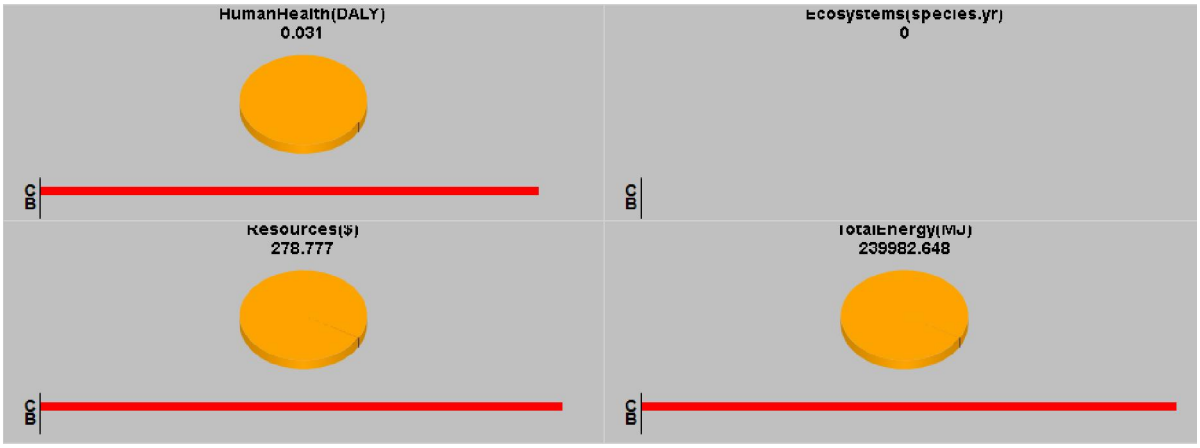

1. HumanHealth (DALY) : Total Result => Current = 0.031, Baseline = 0
   - Material = 0.002
   - Manufacturing = 0.007
   - Transportation = 0
   - Use Phase = 99.991
   - End of Life = 0
2. Ecosystems (species.yr) : Total Result => Current = 0, Baseline = 0
   - Material = 0.002
   - Manufacturing = 0.007
   - Transportation = 0
   - Use Phase = 99.99
   - End of Life = 0
3. Resources ($) : Total Result => Current = 278.777, Baseline = 0
   - Material = 0.008
   - Manufacturing = 0.007
   - Transportation = 0
   - Use Phase = 99.985
   - End of Life = 0
4. TotalEnergy (MJ) : Total Result => Current = 239982.648, Baseline = 0
   - Material = 0.003
   - Manufacturing = 0.009
   - Transportation = 0
   - Use Phase = 99.988
   - End of Life = 0

Assembly parts information:

1. No.of parts in assembly: 14
2. Analysed Parts Information:

Part Name	Material	Mass (kg)	No. of Instances	Manufacturing Process(es)	Air Transport (km)	Sea Transport (km)	Road Transport (km)	Rail Transport (km)
MCM_16_02_1.par	Nylon, general purpose	0	2	Injection Molding	0	0	0	0
din7 3x15-316.par	Stainless Steel, 304	0.001	1	Average Metal Working	0	0	0	0
RUbber-boot-washer-00.par	Stainless Steel, 316	0.003	1	Stamping	0	0	0	0
DIN 471x16.par	Stainless steel	0.001	4	Stamping	0	0	0	0

Rod_end_screw-00.par	Stainless Steel, 316	0.01	1	Turning	0	0	0	0
Piston_seal-00.par	Polyurethene	0.002	1	Injection Molding	0	0	0	0
Damping_rod_piston-02.par	Nylon, general purpose	0.006	1	(None)	0	0	0	0
Piston_U_flange-00.psm	Stainless Steel, 316	0.032	1	Stamping	0	0	0	0
Rod-hollow-bolt-00.par	Aluminum, 6061-T6	0.006	1	Extrusion Turning	0	0	0	0
V6-404 428849(240).par	Polypropylene, high impact	0.058	1	Blow Molding	0	0	0	0
Damping_rod-02.par	Aluminum, 6061-T6	0.081	1	Anodizing Extrusion Turning	0	0	0	0
Hydropneumatic_suspension_piston_separate-00.asm		0.207			0	5000	0	0

3. Individual Part Environmental Impact Results:

Part Name	Environmental Impact	Material Phase	Manufacturing Phase	Transportation Phase	Use Phase	End of Life Phase	Total Result
MCM_16_02_1.par	HumanHealth (DALY)	0	0	0	100	0	0.003
	Ecosystems (species.yr)	0	0	0	100	0	0
	Resources ($)	0	0	0	100	0	25.339
	TotalEnergy (MJ)	0	0	0	100	0	21814.071
din7 3x15-316.par	HumanHealth (DALY)	0	0	0	100	0	0.003
	Ecosystems (species.yr)	0	0	0	100	0	0
	Resources ($)	0.001	0.001	0	99.998	0	25.34
	TotalEnergy (MJ)	0	0	0	100	0	21814.136
RUbber-boot-washer-00.par	HumanHealth (DALY)	0	0	0	100	0	0.003
	Ecosystems (species.yr)	0	0	0	100	0	0
	Resources ($)	0.004	0	0	99.996	0	25.34
	TotalEnergy (MJ)	0	0	0	100	0	21814.149
DIN 471x16.par	HumanHealth (DALY)	0	0	0	99.999	0	0.003
	Ecosystems (species.yr)	0	0	0	100	0	0
	Resources ($)	0.005	0	0	99.995	0	25.341
	TotalEnergy (MJ)	0	0	0	100	0	21814.165
Rod_end_screw-00.par	HumanHealth (DALY)	0.001	0	0	99.999	0	0.003
	Ecosystems (species.yr)	0.001	0	0	99.999	0	0
	Resources ($)	0.012	0	0	99.988	0	25.343
	TotalEnergy (MJ)	0.001	0	0	99.999	0	21814.315
Piston_seal-00.par	HumanHealth (DALY)	0.001	0	0	99.999	0	0.003
	Ecosystems (species.yr)	0.001	0	0	99.999	0	0
	Resources ($)	0.001	0	0	99.999	0	25.34
	TotalEnergy (MJ)	0.001	0	0	99.999	0	21814.337
Damping_rod_piston-02.par	HumanHealth (DALY)	0.004	0	0	99.996	0	0.003
	Ecosystems (species.yr)	0.004	0	0	99.996	0	0
	Resources ($)	0.003	0	0	99.997	0	25.34
	TotalEnergy (MJ)	0.003	0	0	99.997	0	21814.812
Piston_U_flange-00.psm	HumanHealth (DALY)	0.004	0	0	99.995	0	0.003
	Ecosystems (species.yr)	0.003	0	0	99.997	0	0
	Resources ($)	0.039	0	0	99.96	0	25.35
	TotalEnergy (MJ)	0.003	0	0	99.996	0	21814.898
Rod-hollow-bolt-00.par	HumanHealth (DALY)	0	0.004	0	99.995	0	0.003
	Ecosystems (species.yr)	0	0.005	0	99.995	0	0
	Resources ($)	0	0.005	0	99.995	0	25.341
	TotalEnergy (MJ)	0	0.005	0	99.994	0	21815.299
V6-404 428849(240).par	HumanHealth (DALY)	0.008	0.004	0.001	99.988	0	0.003
	Ecosystems (species.yr)	0.009	0.006	0	99.985	0	0
	Resources ($)	0.019	0.004	0	99.977	0	25.345
	TotalEnergy (MJ)	0.02	0.008	0	99.972	0	21820.164
Damping_rod-02.par	HumanHealth (DALY)	0.002	0.064	0.001	99.933	0	0.003
	Ecosystems (species.yr)	0.003	0.071	0	99.926	0	0
	Resources ($)	0.005	0.068	0	99.927	0	25.358

TotalEnergy (MJ)	0.003	0.08	0	99.916	0	21832.302

4. Skipped Part List:

Part Name	Material	No. of Instances
o-ring 015,47 x 3,53 nbr, 70 shore.par	NBR	2
Rod_glider-00.par	PTFE	2
O-ring 005,23x2,62 NBR 70 shore.par	NBR	1

5. Material Usage Analysis:

Material	Mass(kg)	Percentage (%) mass in assembly
Stainless Steel, 316	0.045	21.74
Aluminum, 6061-T6	0.087	42.03
Stainless steel	0.004	1.93
Polyurethene	0.002	0.97
Stainless Steel, 304	0.001	0.48
NBR	0.002	0.97
PTFE	0.002	0.97
Nylon, general purpose	0.006	2.9
Polypropylene, high impact	0.058	28.02

EcoDesigner Report

Date : 6/11/2014

Company Information:

- *Company Name:*
- *Address:*
- *Prepared By Name:*
- *Title:*
- *Email Address:*
- *Phone Number:*

Assembly/Part Information:

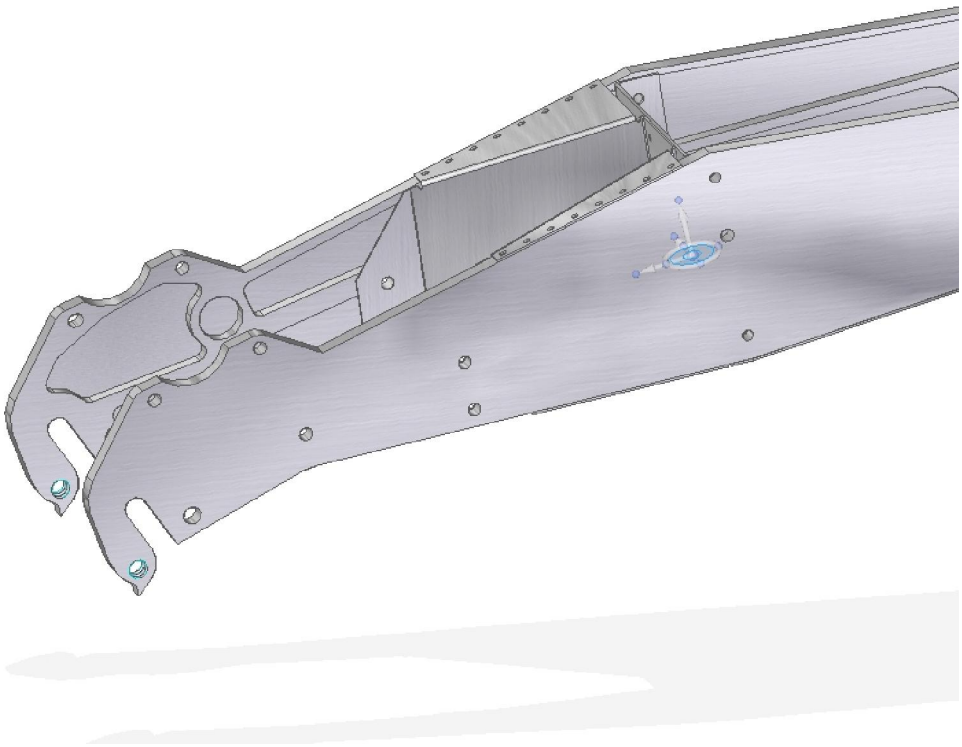

- *Assembly/Part Name:* Rear_suspension_assy_right-11.asm
- *Volume:* 0.009 cm3
- *Mass:* 1.191 kg

Screening Life Cycle Analysis:

- *Analysis Method:* Eco-indicator 99 (I)
- *Analysis Type:* Single Score
- *Functional Unit:* 1
- *LCA Software used:*

Environmental Impact:

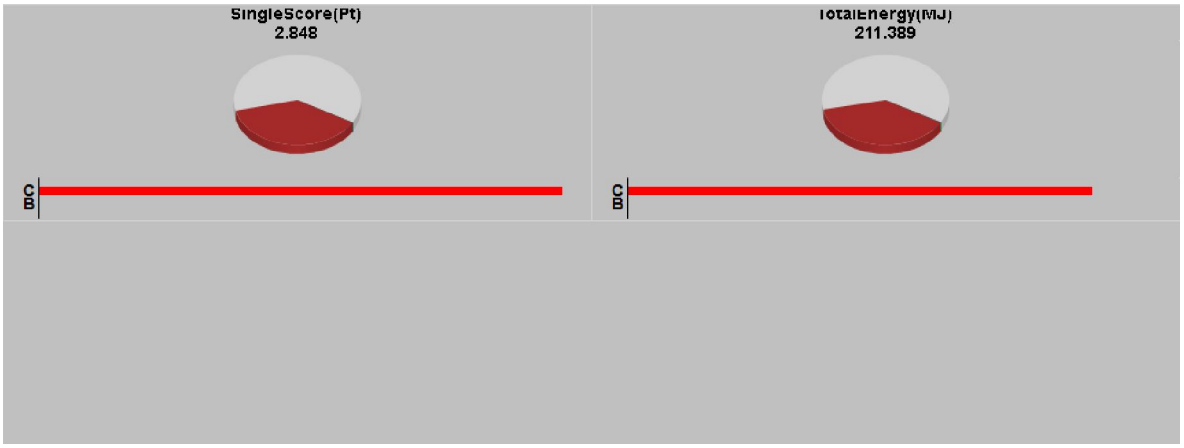

1. SingleScore (Pt) : Total Result => Current = 2.848, Baseline = 0
   - Material = 1.077
   - Manufacturing = 1.77
   - Transportation = 0
   - Use Phase = 0
   - End of Life = 0.001
2. TotalEnergy (MJ) : Total Result => Current = 211.389, Baseline = 0
   - Material = 80.89
   - Manufacturing = 130.311
   - Transportation = 0
   - Use Phase = 0
   - End of Life = 0.187

Assembly parts information:

1. No.of parts in assembly: 12
2. Analysed Parts Information:

Part Name	Material	Mass (kg)	No. of Instances	Manufacturing Process(es)	Air Transport (km)	Sea Transport (km)	Road Transport (km)	Rail Transport (km)
blind rivet Ã‚3.2 L6.par	Aluminum, 5050	0	70	Average Metal working	0	0	0	0
MINARB-M6-012-SS.par	Stainless steel	0.003	2	Deep Drawing	0	0	0	0
MINOFF-M5-008-S-4MM-Z.par	Stainless steel	0.001	8	Deep Drawing	0	0	0	0
ESTM_16_1.par	Nylon, general purpose	0.017	1	Injection Molding	0	0	0	0
Suspension_rod_bearing_reinforcement-00.par	Aluminum, 6061-T6	0.025	1	Casting	0	0	0	0
A118SAK_Bottom.par	Steel	0.053	1	Average Metal Working	0	0	0	0
Rear_Suspension_arm_damper_plate-02.psm	Aluminum, 5050	0.059	1	Stamping	0	0	0	0
A118SAK_Top.par	Steel	0.083	1	Average Metal Working	0	0	0	0
Rear_Suspension_arm_diagonal_bracket-01.psm	Aluminum, 5050	0.086	1	Stamping	0	0	0	0
Rear_Suspension_arm_lower_plate-00.psm	Aluminum, 5050	0.1	1	Stamping	0	0	0	0
Rear-wheel-inside-right-02.par	Aluminum, 6061-T6	0.377	1	Milling	0	0	0	0
Rear-wheel-inside_left-01.par	Aluminum, 6061-T6	0.377	1	Milling	0	0	0	0
Rear_suspension_assy_right-11.asm		1.191			0	0	0	0

3. Individual Part Environmental Impact Results:

Part Name	Environmental Impact	Material Phase	Manufacturing Phase	Transportation Phase	Use Phase	End of Life Phase	Total Result

blind rivet Ã‚3.2 L6.par	SingleScore (Pt)	0	0	0	0	0	0
	TotalEnergy (MJ)	0	0	0	0	0	0
MINARB-M6-012-SS.par	SingleScore (Pt)	0.051	0	0	0	0	0.051
	TotalEnergy (MJ)	0.41	0.023	0	0	0.001	0.433
MINOFF-M5-008-S-4MM-Z.par	SingleScore (Pt)	0.068	0	0	0	0	0.068
	TotalEnergy (MJ)	0.546	0.03	0	0	0.001	0.578
ESTM_16_1.par	SingleScore (Pt)	0.005	0.001	0	0	0	0.006
	TotalEnergy (MJ)	2.076	0.488	0	0	0.003	2.567
Suspension_rod_bearing_reinforcement-00.par	SingleScore (Pt)	0.02	0.003	0	0	0	0.023
	TotalEnergy (MJ)	1.808	0.951	0	0	0.004	2.763
A118SAK_Bottom.par	SingleScore (Pt)	0.05	0.107	0	0	0	0.157
	TotalEnergy (MJ)	1.479	2.254	0	0	0.008	3.741
Rear_Suspension_arm_damper_plate-02.psm	SingleScore (Pt)	0.048	0.001	0	0	0	0.049
	TotalEnergy (MJ)	4.267	0.396	0	0	0.009	4.673
A118SAK_Top.par	SingleScore (Pt)	0.078	0.168	0	0	0	0.246
	TotalEnergy (MJ)	2.315	3.53	0	0	0.013	5.859
Rear_Suspension_arm_diagonal_bracket-01.psm	SingleScore (Pt)	0.069	0.002	0	0	0	0.071
	TotalEnergy (MJ)	6.22	0.578	0	0	0.014	6.811
Rear_Suspension_arm_lower_plate-00.psm	SingleScore (Pt)	0.081	0.002	0	0	0	0.083
	TotalEnergy (MJ)	7.233	0.672	0	0	0.016	7.92
Rear-wheel-inside-right-02.par	SingleScore (Pt)	0.304	0.743	0	0	0	1.047
	TotalEnergy (MJ)	27.268	60.695	0	0	0.059	88.022
Rear-wheel-inside_left-01.par	SingleScore (Pt)	0.304	0.743	0	0	0	1.047
	TotalEnergy (MJ)	27.268	60.695	0	0	0.059	88.022

4. Skipped Part List:

Part Name	Material	No. of Instances

5. Material Usage Analysis:

Material	Mass(kg)	Percentage (%) mass in assembly
Aluminum, 6061-T6	0.779	65.41
Steel	0.136	11.42
Stainless steel	0.014	1.18
Nylon, general purpose	0.017	1.43
Aluminum, 5050	0.245	20.57

EcoDesigner Report

Date : 6/16/2014

Company Information:

- *Company Name:* VELOMOBILE redefined
- *Address:*
- *Prepared By Name:* Per Hassel Sorensen
- *Title:* Part of Master Thesis by
- *Email Address:*
- *Phone Number:*

Assembly/Part Information:

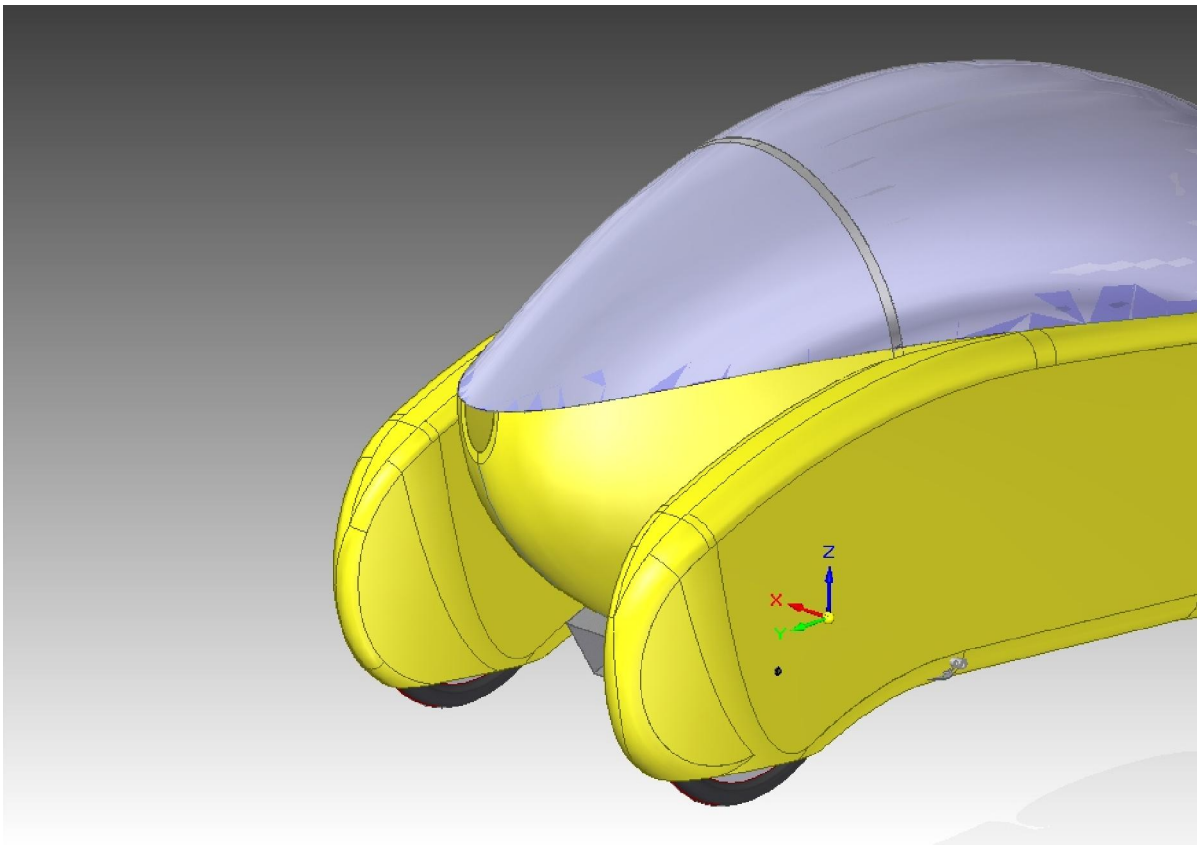

- *Assembly/Part Name:* Velo_for_LCA-00.asm
- *Volume:* 0.026 cm3
- *Mass:* 50.355 kg

Screening Life Cycle Analysis:

- *Analysis Method:* IPCC 2007 GWP 100a
- *Analysis Type:* Selected Impact
- *Functional Unit:* 1
- *LCA Software used:*

Environmental Impact:

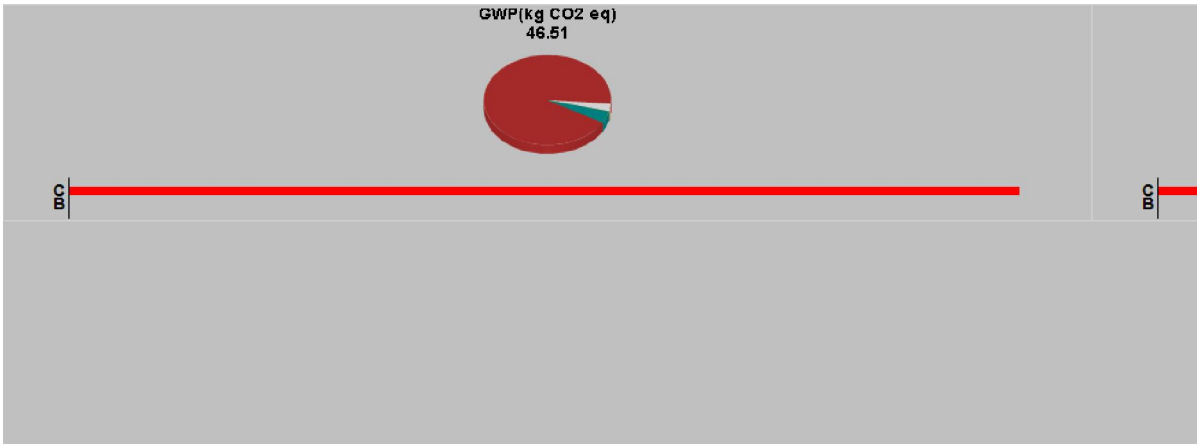

1. GWP (kg CO2 eq) : Total Result => Current = 46.51, Baseline = 0
   - Material = 43.257
   - Manufacturing = 1.262
   - Transportation = 0
   - Use Phase = 0
   - End of Life = 1.991
2. TotalEnergy (MJ) : Total Result => Current = 1116.838, Baseline = 0
   - Material = 1088.915
   - Manufacturing = 20.039
   - Transportation = 0
   - Use Phase = 0
   - End of Life = 7.884

Assembly parts information:

1. No.of parts in assembly: 251
2. Analysed Parts Information:

Part Name	Material	Mass (kg)	No. of Instances	Manufacturing Process(es)	Air Transport (km)	Sea Transport (km)	Road Transport (km)	Rail Transport (km)
NK 12_16_PART1.par	Steel	0	1	(None)	0	0	0	0
61902_2Z_PART3.par	Steel	0	4	(None)	0	0	0	0
I_BIKE_ASSY_QUILT_58_3.par	Steel	0	1	(None)	0	0	0	0
Rectifier housing-01.par	Nylon, general purpose	0	1	(None)	0	0	0	0
TRM_SRF_23.par	Steel	0	1	(None)	0	0	0	0
TRM_SRF_62.par	Steel	0	1	(None)	0	0	0	0
TRM_SRF_48.par	Steel	0	1	(None)	0	0	0	0
TRM_SRF_5.par	Steel	0	1	(None)	0	0	0	0
61902_2Z_PART4.par	Steel	0	4	(None)	0	0	0	0
61902_2Z_PART5.par	Steel	0	40	(None)	0	0	0	0
I_BIKE_ASSY_QUILT_54_3.par	Steel	0	1	(None)	0	0	0	0
TRM_SRF_20.par	Steel	0	1	(None)	0	0	0	0
TRM_SRF_42.par	Steel	0	1	(None)	0	0	0	0
I_BIKE_ASSY_QUILT_24_2.par	Steel	0	1	(None)	0	0	0	0
TRM_SRF_41.par	Steel	0	1	(None)	0	0	0	0
ok-del11.par	Steel	0	2	(None)	0	0	0	0
I_BIKE_ASSY_QUILT_16_3.par	Steel	0	1	(None)	0	0	0	0
NK 12_16_PART2.par	Steel	0	13	(None)	0	0	0	0
TRM_SRF_40.par	Steel	0	1	(None)	0	0	0	0
TRM_SRF_11.par	Steel	0	1	(None)	0	0	0	0
TRM_SRF_37.par	Steel	0	1	(None)	0	0	0	0
TRM_SRF_3.par	Steel	0	1	(None)	0	0	0	0

TRM_SRF_18.par	Steel	0	1	(None)	0	0	0	0
TRM_SRF_38.par	Steel	0	1	(None)	0	0	0	0
TRM_SRF_2.par	Steel	0	1	(None)	0	0	0	0
One-way-roller-spring-00.par	Steel	0	6	(None)	0	0	0	0
I_BIKE_ASSY_QUILT_66_2.par	Nylon, general purpose	0	1	(None)	0	0	0	0
TRM_SRF_54.par	Steel	0	1	(None)	0	0	0	0
original clean_47.par	Steel	0	1	(None)	0	0	0	0
TRM_SRF_14.par	Steel	0	1	(None)	0	0	0	0
TRM_SRF_26.par	Steel	0	1	(None)	0	0	0	0
V4_2-13--_-_ISO7050_C_2.par	Steel	0	2	(None)	0	0	0	0
TRM_SRF_39.par	Steel	0	1	(None)	0	0	0	0
TRM_SRF_0.par	Steel	0	1	(None)	0	0	0	0
DIN 125 M5 A4-00.par	Steel	0	3	(None)	0	0	0	0
16003_2Z_PART5.par	Steel	0	20	(None)	0	0	0	0
TRM_SRF_47.par	Steel	0	1	(None)	0	0	0	0
TRM_SRF_24.par	Steel	0	1	(None)	0	0	0	0
Gyuru_W_DIN_471_8x0.8_A_v9.00.par	Steel	0	6	(None)	0	0	0	0
TRM_SRF_31.par	Steel	0	1	(None)	0	0	0	0
TRM_SRF_63.par	Steel	0	1	(None)	0	0	0	0
TRM_SRF_25.par	Steel	0	1	(None)	0	0	0	0
DIN912 M5x20 T2.par	Steel	0	3	(None)	0	0	0	0
TRM_SRF_34.par	Steel	0	1	(None)	0	0	0	0
Valve_pin.par	Stainless Steel, 304	0	2	(None)	0	0	0	0
TRM_SRF_33.par	Steel	0	1	(None)	0	0	0	0
TRM_SRF_19.par	Steel	0	1	(None)	0	0	0	0
TRM_SRF_35.par	Steel	0	1	(None)	0	0	0	0
Valve_spring-00.par	Stainless steel	0	2	(None)	0	0	0	0
TRM_SRF_27.par	Steel	0	1	(None)	0	0	0	0
Valve_seat-00.par	Brass, yellow brass	0	2	(None)	0	0	0	0
Valve_end-00.par	Brass, yellow brass	0	2	(None)	0	0	0	0
Valve_threads-00.par	Brass, yellow brass	0	2	(None)	0	0	0	0
TRM_SRF_1.par	Steel	0	1	(None)	0	0	0	0
TRM_SRF_17.par	Steel	0	1	(None)	0	0	0	0
crankaxle_fixed.par	Steel	0	1	(None)	0	0	0	0
TRM_SRF_50.par	Steel	0	1	(None)	0	0	0	0
TRM_SRF_6.par	Steel	0	1	(None)	0	0	0	0
TRM_SRF_7.par	Steel	0	1	(None)	0	0	0	0
TRM_SRF_12.par	Steel	0	1	(None)	0	0	0	0
TRM_SRF_30.par	Steel	0	1	(None)	0	0	0	0
TRM_SRF_53.par	Steel	0	1	(None)	0	0	0	0
MCM_16_02_1.par	Nylon, general purpose	0	2	(None)	0	0	0	0
TRM_SRF_46.par	Steel	0	1	(None)	0	0	0	0
TRM_SRF_32.par	Steel	0	1	(None)	0	0	0	0
TRM_SRF_21.par	Steel	0	1	(None)	0	0	0	0
TRM_SRF_16.par	Steel	0	1	(None)	0	0	0	0
TRM_SRF_28.par	Steel	0	1	(None)	0	0	0	0
TRM_SRF_44.par	Steel	0	1	(None)	0	0	0	0
TRM_SRF_55.par	Steel	0	1	(None)	0	0	0	0
TRM_SRF_61.par	Steel	0	1	(None)	0	0	0	0
original clean_36.par	Steel	0	1	(None)	0	0	0	0
TRM_SRF_57.par	Steel	0	1	(None)	0	0	0	0
TRM_SRF_43.par	Steel	0	1	(None)	0	0	0	0
TRM_SRF_10.par	Steel	0	1	(None)	0	0	0	0
blind rivet Ã‚3.2 L6.par	Aluminum, 5050	0	172	(None)	0	0	0	0
I_BIKE_ASSY_QUILT_70_2.par	Steel	0	1	(None)	0	0	0	0
din127 M4 A4.par		0	16	(None)	0	0	0	0

	Stainless Steel, 316							
TRM_SRF_36.par	Steel	0	1	(None)	0	0	0	0
TRM_SRF_29.par	Steel	0	1	(None)	0	0	0	0
TRM_SRF_45.par	Steel	0	1	(None)	0	0	0	0
Final-drivewheel-00.par	Steel	0	1	(None)	0	0	0	0
Washer_DIN_125_1_A_6.4_v9.00.par	Steel	0.001	1	(None)	0	0	0	0
Rivet_DIN_7338_A_M_6_v9.00.par	Steel	0.003	1	(None)	0	0	0	0
Washer_DIN_125_1_A_8.4_v9.50.par	Steel	0.002	1	(None)	0	0	0	0
Screw_ISO_7380_M4x10_v9.00.par	Steel	0.001	2	(None)	0	0	0	0
16003_2Z_PART3.par	Steel	0.001	2	(None)	0	0	0	0
16003_2Z_PART4.par	Steel	0.001	2	(None)	0	0	0	0
Ring_UNI_7435_17_v9.00.par	Steel	0.001	2	(None)	0	0	0	0
din7 3x15-316.par	Stainless Steel, 304	0.001	1	(None)	0	0	0	0
Screw_ISO_7380_M6x16_v9.00.par	Steel	0.005	1	(None)	0	0	0	0
Brake retainer spacer.par	Aluminum, 6061-T6	0.001	1	(None)	0	0	0	0
DIN 471x16.par	Stainless steel	0.001	4	Stamping	0	0	0	0
Short spring.par	Steel	0.011	1	(None)	0	0	0	0
Ring_UNI_7435_15_v9.00.par	Steel	0.001	4	(None)	0	0	0	0
ok-del10.par	Steel	0.002	2	(None)	0	0	0	0
ok-del7.par	Silicone	0.001	2	(None)	0	0	0	0
DIN 71802_cs2_M 6 (10).par	Steel	0.009	1	(None)	0	0	0	0
Nut_DIN_917_M8_Custom.par	Steel	0.01	1	(None)	0	0	0	0
Rear_motor_spacer-00.par	Aluminum, 6061-T6	0.001	2	(None)	0	0	0	0
kula x6.par	Steel	0.001	6	(None)	0	0	0	0
Rivet_UNI_748_H_3x14_v9.50.par	Steel	0.001	6	(None)	0	0	0	0
Washer_ISO_7093_1_2000_8_v9.50.par	Steel	0.006	1	(None)	0	0	0	0
Nut_ISO_4032_1999_M8_v9.50.par	Steel	0.006	1	(None)	0	0	0	0
Rivet_DIN_7338_A_M_6_v9.00_1.par	Steel	0.003	2	(None)	0	0	0	0
ok-del9.par	Steel	0.003	2	(None)	0	0	0	0
valve nut big.par	Brass, yellow brass	0.002	2	(None)	0	0	0	0
valve cap.par	Brass, yellow brass	0.002	2	(None)	0	0	0	0
Screw_DIN_7991_M8x12_v9.00.par	Steel	0.007	1	(None)	0	0	0	0
Ring_UNI_7434_28_v9.00.par	Steel	0.002	4	(None)	0	0	0	0
RUbber-boot-washer-00.par	Stainless Steel, 316	0.003	1	(None)	0	0	0	0
Spring center plug.par	Polyethylene, low density	0.003	1	(None)	0	0	0	0
Rod_end_screw-00.par	Stainless Steel, 316	0.01	1	(None)	0	0	0	0
ok-del4.par	Aluminum, 5050	0.016	2	(None)	0	0	0	0
socket button head cap screw_am_B18.3.4M - 5 x 0.8 x 10 SBHCS --N.par	Steel	0.003	6	(None)	0	0	0	0
Longitudional_fixture_right-00.par	Aluminum, 6061-T6	0.034	1	(None)	0	0	0	0
Piston_seal-00.par	Polyurethene	0.002	1	Injection Molding	0	0	0	0
cs13r_M8_ball.par	Steel	0.019	1	(None)	0	0	0	0
DIN 471x30.par	Stainless steel	0.002	2	(None)	0	0	0	0
Ring_DIN_472_26mm.par	Stainless steel	0.002	2	(None)	0	0	0	0
Nut_M12_thin.par	Steel	0.005	2	(None)	0	0	0	0
16003_2Z_PART1.par	Steel	0.01	2	(None)	0	0	0	0
Wedgenut-00.par	Aluminum, 5050	0.002	2	(None)	0	0	0	0
ok-del3_mirrored.par	Aluminum, 5050	0.021	2	(None)	0	0	0	0
One-way-roller-00.par	Steel	0.002	6	(None)	0	0	0	0
ok-del14.par	Steel	0.006	2	(None)	0	0	0	0
ok-del8.par	Steel	0.006	2	(None)	0	0	0	0

Hubspacer.par	Aluminum, 6061-T6	0.005	1	(None)	0	0	0	0
Front wheel Upper suspension mount right-00.par	Aluminum, 6061-T6	0.05	1	(None)	0	0	0	0
Suspension_rod_bearing_reinforcement-00.par	Aluminum, 6061-T6	0.026	2	(None)	0	0	0	0
61902_2Z_PART2.par	Steel	0.007	4	(None)	0	0	0	0
Brake shield 1.par	Aluminum, 6061-T6	0.053	1	(None)	0	0	0	0
16003_2Z_PART2.par	Steel	0.015	2	(None)	0	0	0	0
Rod-hollow-bolt-00.par	Aluminum, 6061-T6	0.006	1	(None)	0	0	0	0
ok-del12.par	Steel	0.008	2	(None)	0	0	0	0
Washer_id12od19t1.5.par	Steel	0.002	8	(None)	0	0	0	0
ok-del6.par	Steel	0.016	2	(None)	0	0	0	0
Bearing_DIN_625_1_1989_6001_2RS_v9.00.par	Steel	0.016	2	(None)	0	0	0	0
DIN 985 M6 A4.par	Stainless Steel, 316	0.003	2	(None)	0	0	0	0
DIN 71802_cs1__M 6_0.par	Steel	0.017	2	(None)	0	0	0	0
cs13r_M8_joint.par	Steel	0.035	1	(None)	0	0	0	0
Screw_DIN_912_M5x10_v9.00.par	Steel	0.003	12	(None)	0	0	0	0
Schrader_tube_18,5x7.7.par	Brass, yellow brass	0.006	2	(None)	0	0	0	0
Front wheel arm right.par	Aluminum, 6061-T6	0.073	1	(None)	0	0	0	0
61902_2Z_PART1.par	Steel	0.005	4	(None)	0	0	0	0
ok-del13.par	Steel	0.01	4	(None)	0	0	0	0
Damper bushing.par	Polypropylene, high impact	0.009	1	(None)	0	0	0	0
Brake retainer.psm	Steel	0.047	1	(None)	0	0	0	0
Screw_UNI_ISO_7380_M5x10_v9.50.par	Steel	0.002	12	(None)	0	0	0	0
Screw_UNI_ISO_7380_M5x16_v9.50.par	Steel	0.003	16	(None)	0	0	0	0
Guide spring-00.par	Stainless steel	0.005	2	(None)	0	0	0	0
ok-del2.par	Aluminum, 5050	0.045	2	(None)	0	0	0	0
Accumulator_screwring-00.par	Aluminum, 6061-T6	0.047	2	(None)	0	0	0	0
ok-del5.par	Steel	0.026	2	(None)	0	0	0	0
Piston_U_flange-00.psm	Stainless Steel, 316	0.032	1	(None)	0	0	0	0
Damping_rod_piston-02.par	Nylon, general purpose	0.006	1	(None)	0	0	0	0
cs13r_M8_ball.par	Steel	0.019	3	(None)	0	0	0	0
MINARB-M6-012-SS.par	Stainless steel	0.003	4	(None)	0	0	0	0
Accumulator_housing-02.par	Aluminum, 6061-T6	0.054	2	(None)	0	0	0	0
Rear_Suspension_arm_damper_plate-03.psm	Aluminum, 5050	0.056	2	(None)	0	0	0	0
Pressure_port-00.par	Stainless Steel, 304	0.007	2	(None)	0	0	0	0
Nut_DIN_EN_24035_M12_v9.00.par	Steel	0.009	4	(None)	0	0	0	0
planet carrier hub.par	Steel	0.061	2	(None)	0	0	0	0
Damper_lock_plate-01.psm	Aluminum, 5050	0.071	2	(None)	0	0	0	0
MINOFF-M5-008-S-4MM-Z.par	Stainless steel	0.001	16	(None)	0	0	0	0
Tverrstag.par	Stainless steel	0.053	1	(None)	0	0	0	0
Steering_rod_Alligt-00.par	Stainless steel	0.054	1	(None)	0	0	0	0
Front hub axle.par	Steel	0.082	1	(None)	0	0	0	0
Planet carrier lid.par	Steel	0.022	4	(None)	0	0	0	0
Rear_Suspension_arm_diagonal_bracket-01.psm	Aluminum, 5050	0.086	2	(None)	0	0	0	0
Minimotor stator holder.par	Aluminum, 6061-T6	0.087	2	(None)	0	0	0	0
StÃ¸tdemperhus.par	Aluminum, 6061-T6	0.175	1	(None)	0	0	0	0
Sun gear.par	Steel	0.05	2	(None)	0	0	0	0

cs13r_M8_joint.par	Steel	0.035	3	(None)	0	0	0	0
Housing_damper_valves-03.par	Aluminum, 6061-T6	0.098	2	(None)	0	0	0	0
A118SAK_Bottom.par	Steel	0.053	2	(None)	0	0	0	0
Rear_Suspension_arm_lower_plate-00.psm	Aluminum, 5050	0.1	2	(None)	0	0	0	0
Planet axle.par	Steel	0.009	6	(None)	0	0	0	0
Bearing_DIN_625_1_1989_608_2RS_v9.00.par	Steel	0.009	6	(None)	0	0	0	0
Minimotor rotor.par	Aluminum, 6061-T6	0.104	2	(None)	0	0	0	0
Longitudional_suspension_rod_Alligt-02.par	Stainless steel	0.077	1	(None)	0	0	0	0
Accumulator_lower_housing-01.par	Aluminum, 6061-T6	0.107	2	(None)	0	0	0	0
160mm disc rotor.par	Stainless steel	0.085	1	(None)	0	0	0	0
Damper metal center.par	Stainless steel	0.09	1	(None)	0	0	0	0
DIN912 M6x16 A4.par	Stainless Steel, 316	0.007	4	(None)	0	0	0	0
Damping_cylinder-02.par	Aluminum, 5050	0.145	2	(None)	0	0	0	0
Minimotor front hub lid.par	Aluminum, 6061-T6	0.153	2	(None)	0	0	0	0
A118SAK_Top.par	Steel	0.083	2	(None)	0	0	0	0
Torque_arm-02.psm	Stainless Steel, 316	0.052	2	(None)	0	0	0	0
Krank arm 140mm.par	Aluminum, 6061-T6	0.174	2	(None)	0	0	0	0
ok-del1.par	Aluminum, 5050	0.023	2	Casting Drilling - Conventional Machines Powder Coating	0	0	0	0
spoke LX.par	Stainless steel	0.005	8	(None)	0	0	0	0
spoke RX.par	Stainless steel	0.005	8	(None)	0	0	0	0
spoke R1.par	Stainless steel	0.005	8	(None)	0	0	0	0
spoke L1.par	Stainless steel	0.005	8	(None)	0	0	0	0
406 rim.par	Aluminum, 6061-T6	0.417	1	(None)	0	0	0	0
Sturmey Archer Drumbrake.par	Aluminum, 6061-T6	0.421	1	(None)	0	0	0	0
Planet carrier rim.par	Steel	0.144	2	(None)	0	0	0	0
ESTM_16_1.par	Nylon, general purpose	0.017	2	(None)	0	0	0	0
Minimotor ring gear.par	Steel	0.155	2	(None)	0	0	0	0
housing_2_2.par	Aluminum, 5050	0.59	1	(None)	0	0	0	0
din912 M4x25-CS.par	Stainless Steel, 316	0.004	16	(None)	0	0	0	0
Minimotor axle.par	Steel	0.183	2	(None)	0	0	0	0
Rear-wheel-inside_left-01.par	Aluminum, 6061-T6	0.377	2	(None)	0	0	0	0
Rear-wheel-inside-right-02.par	Aluminum, 6061-T6	0.377	2	(None)	0	0	0	0
brake_disc_160mm_6hole_v2.par	Stainless Steel, 304	0.14	2	(None)	0	0	0	0
Support_piston-02.par	Nylon, general purpose	0.024	2	(None)	0	0	0	0
Minimotor rotor backing iron.par	Iron	0.269	2	(None)	0	0	0	0
Minimotor front hub.par	Aluminum, 6061-T6	0.609	2	(None)	0	0	0	0
Damping_rod-02.par	Aluminum, 6061-T6	0.081	1	Anodizing Extrusion Turning	0	0	0	0
Tofix_hydropneumatic-00.par	Stainless steel	0.951	1	(None)	0	0	0	0
Rollover protection_20-00.par	Aluminum, 7075-T6	2.748	1	(None)	0	0	0	0
Child_seat-02.par	ABS Plastic, high impact	0.833	1	(None)	0	0	0	0
wheel-cover-01.par	ABS Plastic, high impact	0.916	2	(None)	0	0	0	0

CANOPY20-00.par	Acrylic, high impact grade	3.574	1	(None)	0	0	0	0
VELO20-00C-mirrored.par	Polyethylene, low density	13.066	1	(None)	0	0	0	0
VELO20-00C.par	Polyethylene, low density	13.133	1	(None)	0	0	0	0
Velo_for_LCA-00.asm		50.355			0	0	0	0

3. Individual Part Environmental Impact Results:

Part Name	Environmental Impact	Material Phase	Manufacturing Phase	Transportation Phase	Use Phase	End of Life Phase	Total Result
NK 12_16_PART1.par	GWP (kg CO2 eq)	0	0	0	0	0	0
	TotalEnergy (MJ)	0	0	0	0	0	0
61902_2Z_PART3.par	GWP (kg CO2 eq)	0	0	0	0	0	0
	TotalEnergy (MJ)	0	0	0	0	0	0
I_BIKE_ASSY_QUILT_58_3.par	GWP (kg CO2 eq)	0	0	0	0	0	0
	TotalEnergy (MJ)	0	0	0	0	0	0
Rectifier housing-01.par	GWP (kg CO2 eq)	0	0	0	0	0	0
	TotalEnergy (MJ)	0	0	0	0	0	0
TRM_SRF_23.par	GWP (kg CO2 eq)	0	0	0	0	0	0
	TotalEnergy (MJ)	0	0	0	0	0	0
TRM_SRF_62.par	GWP (kg CO2 eq)	0	0	0	0	0	0
	TotalEnergy (MJ)	0	0	0	0	0	0
TRM_SRF_48.par	GWP (kg CO2 eq)	0	0	0	0	0	0
	TotalEnergy (MJ)	0	0	0	0	0	0
TRM_SRF_5.par	GWP (kg CO2 eq)	0	0	0	0	0	0
	TotalEnergy (MJ)	0	0	0	0	0	0
61902_2Z_PART4.par	GWP (kg CO2 eq)	0	0	0	0	0	0
	TotalEnergy (MJ)	0	0	0	0	0	0
61902_2Z_PART5.par	GWP (kg CO2 eq)	0	0	0	0	0	0
	TotalEnergy (MJ)	0	0	0	0	0	0
I_BIKE_ASSY_QUILT_54_3.par	GWP (kg CO2 eq)	0	0	0	0	0	0
	TotalEnergy (MJ)	0	0	0	0	0	0
TRM_SRF_20.par	GWP (kg CO2 eq)	0	0	0	0	0	0
	TotalEnergy (MJ)	0	0	0	0	0	0
TRM_SRF_42.par	GWP (kg CO2 eq)	0	0	0	0	0	0
	TotalEnergy (MJ)	0	0	0	0	0	0
I_BIKE_ASSY_QUILT_24_2.par	GWP (kg CO2 eq)	0	0	0	0	0	0
	TotalEnergy (MJ)	0	0	0	0	0	0
TRM_SRF_41.par	GWP (kg CO2 eq)	0	0	0	0	0	0
	TotalEnergy (MJ)	0	0	0	0	0	0
ok-del11.par	GWP (kg CO2 eq)	0	0	0	0	0	0
	TotalEnergy (MJ)	0	0	0	0	0	0
I_BIKE_ASSY_QUILT_16_3.par	GWP (kg CO2 eq)	0	0	0	0	0	0
	TotalEnergy (MJ)	0	0	0	0	0	0
NK 12_16_PART2.par	GWP (kg CO2 eq)	0	0	0	0	0	0
	TotalEnergy (MJ)	0	0	0	0	0	0
TRM_SRF_40.par	GWP (kg CO2 eq)	0	0	0	0	0	0
	TotalEnergy (MJ)	0	0	0	0	0	0
TRM_SRF_11.par	GWP (kg CO2 eq)	0	0	0	0	0	0
	TotalEnergy (MJ)	0	0	0	0	0	0
TRM_SRF_37.par	GWP (kg CO2 eq)	0	0	0	0	0	0
	TotalEnergy (MJ)	0	0	0	0	0	0
TRM_SRF_3.par	GWP (kg CO2 eq)	0	0	0	0	0	0
	TotalEnergy (MJ)	0	0	0	0	0	0
TRM_SRF_18.par	GWP (kg CO2 eq)	0	0	0	0	0	0
	TotalEnergy (MJ)	0	0	0	0	0	0
TRM_SRF_38.par	GWP (kg CO2 eq)	0	0	0	0	0	0
	TotalEnergy (MJ)	0	0	0	0	0	0
TRM_SRF_2.par	GWP (kg CO2 eq)	0	0	0	0	0	0
	TotalEnergy (MJ)	0	0	0	0	0	0

One-way-roller-spring-00.par	GWP (kg CO2 eq)	0	0	0	0	0	0
	TotalEnergy (MJ)	0	0	0	0	0	0
I_BIKE_ASSY_QUILT_66_2.par	GWP (kg CO2 eq)	0	0	0	0	0	0
	TotalEnergy (MJ)	0	0	0	0	0	0
TRM_SRF_54.par	GWP (kg CO2 eq)	0	0	0	0	0	0
	TotalEnergy (MJ)	0	0	0	0	0	0
original clean_47.par	GWP (kg CO2 eq)	0	0	0	0	0	0
	TotalEnergy (MJ)	0	0	0	0	0	0
TRM_SRF_14.par	GWP (kg CO2 eq)	0	0	0	0	0	0
	TotalEnergy (MJ)	0	0	0	0	0	0
TRM_SRF_26.par	GWP (kg CO2 eq)	0	0	0	0	0	0
	TotalEnergy (MJ)	0	0	0	0	0	0
V4_2-13--_-_ISO7050_C_2.par	GWP (kg CO2 eq)	0	0	0	0	0	0
	TotalEnergy (MJ)	0	0	0	0	0	0
TRM_SRF_39.par	GWP (kg CO2 eq)	0	0	0	0	0	0
	TotalEnergy (MJ)	0	0	0	0	0	0
TRM_SRF_0.par	GWP (kg CO2 eq)	0	0	0	0	0	0
	TotalEnergy (MJ)	0	0	0	0	0	0
DIN 125 M5 A4-00.par	GWP (kg CO2 eq)	0	0	0	0	0	0
	TotalEnergy (MJ)	0	0	0	0	0	0
16003_2Z_PART5.par	GWP (kg CO2 eq)	0	0	0	0	0	0
	TotalEnergy (MJ)	0	0	0	0	0	0
TRM_SRF_47.par	GWP (kg CO2 eq)	0	0	0	0	0	0
	TotalEnergy (MJ)	0	0	0	0	0	0
TRM_SRF_24.par	GWP (kg CO2 eq)	0	0	0	0	0	0
	TotalEnergy (MJ)	0	0	0	0	0	0
Gyuru_W_DIN_471_8x0.8_A_v9.00.par	GWP (kg CO2 eq)	0	0	0	0	0	0
	TotalEnergy (MJ)	0	0	0	0	0	0
TRM_SRF_31.par	GWP (kg CO2 eq)	0	0	0	0	0	0
	TotalEnergy (MJ)	0	0	0	0	0	0
TRM_SRF_63.par	GWP (kg CO2 eq)	0	0	0	0	0	0
	TotalEnergy (MJ)	0	0	0	0	0	0
TRM_SRF_25.par	GWP (kg CO2 eq)	0	0	0	0	0	0
	TotalEnergy (MJ)	0	0	0	0	0	0
DIN912 M5x20 T2.par	GWP (kg CO2 eq)	0	0	0	0	0	0
	TotalEnergy (MJ)	0	0	0	0	0	0
TRM_SRF_34.par	GWP (kg CO2 eq)	0	0	0	0	0	0
	TotalEnergy (MJ)	0	0	0	0	0	0
Valve_pin.par	GWP (kg CO2 eq)	0	0	0	0	0	0
	TotalEnergy (MJ)	0	0	0	0	0	0
TRM_SRF_33.par	GWP (kg CO2 eq)	0	0	0	0	0	0
	TotalEnergy (MJ)	0	0	0	0	0	0
TRM_SRF_19.par	GWP (kg CO2 eq)	0	0	0	0	0	0
	TotalEnergy (MJ)	0	0	0	0	0	0
TRM_SRF_35.par	GWP (kg CO2 eq)	0	0	0	0	0	0
	TotalEnergy (MJ)	0	0	0	0	0	0
Valve_spring-00.par	GWP (kg CO2 eq)	0	0	0	0	0	0
	TotalEnergy (MJ)	0	0	0	0	0	0
TRM_SRF_27.par	GWP (kg CO2 eq)	0	0	0	0	0	0
	TotalEnergy (MJ)	0	0	0	0	0	0
Valve_seat-00.par	GWP (kg CO2 eq)	0	0	0	0	0	0
	TotalEnergy (MJ)	0	0	0	0	0	0
Valve_end-00.par	GWP (kg CO2 eq)	0	0	0	0	0	0
	TotalEnergy (MJ)	0	0	0	0	0	0
Valve_threads-00.par	GWP (kg CO2 eq)	0	0	0	0	0	0
	TotalEnergy (MJ)	0	0	0	0	0	0
TRM_SRF_1.par	GWP (kg CO2 eq)	0	0	0	0	0	0
	TotalEnergy (MJ)	0	0	0	0	0	0
TRM_SRF_17.par	GWP (kg CO2 eq)	0	0	0	0	0	0
	TotalEnergy (MJ)	0	0	0	0	0	0
crankaxle_fixed.par	GWP (kg CO2 eq)	0	0	0	0	0	0

	TotalEnergy (MJ)	0	0	0	0	0	0
TRM_SRF_50.par	GWP (kg CO2 eq)	0	0	0	0	0	0
	TotalEnergy (MJ)	0	0	0	0	0	0
TRM_SRF_6.par	GWP (kg CO2 eq)	0	0	0	0	0	0
	TotalEnergy (MJ)	0	0	0	0	0	0
TRM_SRF_7.par	GWP (kg CO2 eq)	0	0	0	0	0	0
	TotalEnergy (MJ)	0	0	0	0	0	0
TRM_SRF_12.par	GWP (kg CO2 eq)	0	0	0	0	0	0
	TotalEnergy (MJ)	0	0	0	0	0	0
TRM_SRF_30.par	GWP (kg CO2 eq)	0	0	0	0	0	0
	TotalEnergy (MJ)	0	0	0	0	0	0
TRM_SRF_53.par	GWP (kg CO2 eq)	0	0	0	0	0	0
	TotalEnergy (MJ)	0	0	0	0	0	0
MCM_16_02_1.par	GWP (kg CO2 eq)	0	0	0	0	0	0
	TotalEnergy (MJ)	0	0	0	0	0	0
TRM_SRF_46.par	GWP (kg CO2 eq)	0	0	0	0	0	0
	TotalEnergy (MJ)	0	0	0	0	0	0
TRM_SRF_32.par	GWP (kg CO2 eq)	0	0	0	0	0	0
	TotalEnergy (MJ)	0	0	0	0	0	0
TRM_SRF_21.par	GWP (kg CO2 eq)	0	0	0	0	0	0
	TotalEnergy (MJ)	0	0	0	0	0	0
TRM_SRF_16.par	GWP (kg CO2 eq)	0	0	0	0	0	0
	TotalEnergy (MJ)	0	0	0	0	0	0
TRM_SRF_28.par	GWP (kg CO2 eq)	0	0	0	0	0	0
	TotalEnergy (MJ)	0	0	0	0	0	0
TRM_SRF_44.par	GWP (kg CO2 eq)	0	0	0	0	0	0
	TotalEnergy (MJ)	0	0	0	0	0	0
TRM_SRF_55.par	GWP (kg CO2 eq)	0	0	0	0	0	0
	TotalEnergy (MJ)	0	0	0	0	0	0
TRM_SRF_61.par	GWP (kg CO2 eq)	0	0	0	0	0	0
	TotalEnergy (MJ)	0	0	0	0	0	0
original clean_36.par	GWP (kg CO2 eq)	0	0	0	0	0	0
	TotalEnergy (MJ)	0	0	0	0	0	0
TRM_SRF_57.par	GWP (kg CO2 eq)	0	0	0	0	0	0
	TotalEnergy (MJ)	0	0	0	0	0	0
TRM_SRF_43.par	GWP (kg CO2 eq)	0	0	0	0	0	0
	TotalEnergy (MJ)	0	0	0	0	0	0
TRM_SRF_10.par	GWP (kg CO2 eq)	0	0	0	0	0	0
	TotalEnergy (MJ)	0	0	0	0	0	0
blind rivet Ã¸3.2 L6.par	GWP (kg CO2 eq)	0	0	0	0	0	0
	TotalEnergy (MJ)	0	0	0	0	0	0
I_BIKE_ASSY_QUILT_70_2.par	GWP (kg CO2 eq)	0	0	0	0	0	0
	TotalEnergy (MJ)	0	0	0	0	0	0
din127 M4 A4.par	GWP (kg CO2 eq)	0	0	0	0	0	0
	TotalEnergy (MJ)	0	0	0	0	0	0
TRM_SRF_36.par	GWP (kg CO2 eq)	0	0	0	0	0	0
	TotalEnergy (MJ)	0	0	0	0	0	0
TRM_SRF_29.par	GWP (kg CO2 eq)	0	0	0	0	0	0
	TotalEnergy (MJ)	0	0	0	0	0	0
TRM_SRF_45.par	GWP (kg CO2 eq)	0	0	0	0	0	0
	TotalEnergy (MJ)	0	0	0	0	0	0
Final-drivewheel-00.par	GWP (kg CO2 eq)	0	0	0	0	0	0
	TotalEnergy (MJ)	0	0	0	0	0	0
Washer_DIN_125_1_A_6.4_v9.00.par	GWP (kg CO2 eq)	0.002	0	0	0	0	0.002
	TotalEnergy (MJ)	0.028	0	0	0	0	0.028
Rivet_DIN_7338_A_M_6_v9.00.par	GWP (kg CO2 eq)	0.003	0	0	0	0	0.003
	TotalEnergy (MJ)	0.042	0	0	0	0	0.042
Washer_DIN_125_1_A_8.4_v9.50.par	GWP (kg CO2 eq)	0.003	0	0	0	0	0.003
	TotalEnergy (MJ)	0.056	0	0	0	0	0.056
Screw_ISO_7380_M4x10_v9.00.par	GWP (kg CO2 eq)	0.003	0	0	0	0	0.003
	TotalEnergy (MJ)	0.056	0	0	0	0	0.056

16003_2Z_PART3.par	GWP (kg CO2 eq)	0.003	0	0	0	0	0.003
	TotalEnergy (MJ)	0.056	0	0	0	0	0.056
16003_2Z_PART4.par	GWP (kg CO2 eq)	0.003	0	0	0	0	0.003
	TotalEnergy (MJ)	0.056	0	0	0	0	0.056
Ring_UNI_7435_17_v9.00.par	GWP (kg CO2 eq)	0.003	0	0	0	0	0.003
	TotalEnergy (MJ)	0.056	0	0	0	0	0.056
din7 3x15-316.par	GWP (kg CO2 eq)	0.004	0	0	0	0	0.004
	TotalEnergy (MJ)	0.068	0	0	0	0	0.068
Screw_ISO_7380_M6x16_v9.00.par	GWP (kg CO2 eq)	0.004	0	0	0	0	0.004
	TotalEnergy (MJ)	0.07	0	0	0	0.001	0.071
Brake retainer spacer.par	GWP (kg CO2 eq)	0.006	0	0	0	0	0.006
	TotalEnergy (MJ)	0.072	0	0	0	0	0.072
DIN 471x16.par	GWP (kg CO2 eq)	0.005	0	0	0	0	0.005
	TotalEnergy (MJ)	0.082	0.006	0	0	0.001	0.088
Short spring.par	GWP (kg CO2 eq)	0.006	0	0	0	0	0.006
	TotalEnergy (MJ)	0.092	0	0	0	0.002	0.094
Ring_UNI_7435_15_v9.00.par	GWP (kg CO2 eq)	0.007	0	0	0	0	0.007
	TotalEnergy (MJ)	0.112	0	0	0	0.001	0.112
ok-del10.par	GWP (kg CO2 eq)	0.007	0	0	0	0	0.007
	TotalEnergy (MJ)	0.112	0	0	0	0.001	0.112
ok-del7.par	GWP (kg CO2 eq)	0.005	0	0	0	0	0.005
	TotalEnergy (MJ)	0.125	0	0	0	0	0.126
DIN 71802_cs2_M 6 (10).par	GWP (kg CO2 eq)	0.008	0	0	0	0	0.008
	TotalEnergy (MJ)	0.126	0	0	0	0.001	0.127
Nut_DIN_917_M8_Custom.par	GWP (kg CO2 eq)	0.009	0	0	0	0	0.009
	TotalEnergy (MJ)	0.139	0	0	0	0.002	0.141
Rear_motor_spacer-00.par	GWP (kg CO2 eq)	0.012	0	0	0	0	0.012
	TotalEnergy (MJ)	0.145	0	0	0	0	0.145
kula x6.par	GWP (kg CO2 eq)	0.01	0	0	0	0	0.01
	TotalEnergy (MJ)	0.167	0	0	0	0.001	0.168
Rivet_UNI_748_H_3x14_v9.50.par	GWP (kg CO2 eq)	0.01	0	0	0	0	0.01
	TotalEnergy (MJ)	0.167	0	0	0	0.001	0.168
Washer_ISO_7093_1_2000_8_v9.50.par	GWP (kg CO2 eq)	0.01	0	0	0	0	0.01
	TotalEnergy (MJ)	0.167	0	0	0	0.001	0.168
Nut_ISO_4032_1999_M8_v9.50.par	GWP (kg CO2 eq)	0.01	0	0	0	0	0.01
	TotalEnergy (MJ)	0.167	0	0	0	0.001	0.168
Rivet_DIN_7338_A_M_6_v9.00_1.par	GWP (kg CO2 eq)	0.01	0	0	0	0	0.01
	TotalEnergy (MJ)	0.167	0	0	0	0.001	0.168
ok-del9.par	GWP (kg CO2 eq)	0.01	0	0	0	0	0.01
	TotalEnergy (MJ)	0.167	0	0	0	0.001	0.168
valve nut big.par	GWP (kg CO2 eq)	0.01	0	0	0	0	0.01
	TotalEnergy (MJ)	0.171	0	0	0	0.001	0.171
valve cap.par	GWP (kg CO2 eq)	0.01	0	0	0	0	0.01
	TotalEnergy (MJ)	0.171	0	0	0	0.001	0.171
Screw_DIN_7991_M8x12_v9.00.par	GWP (kg CO2 eq)	0.012	0	0	0	0	0.012
	TotalEnergy (MJ)	0.195	0	0	0	0.001	0.196
Ring_UNI_7434_28_v9.00.par	GWP (kg CO2 eq)	0.014	0	0	0	0	0.014
	TotalEnergy (MJ)	0.223	0	0	0	0.001	0.224
RUbber-boot-washer-00.par	GWP (kg CO2 eq)	0.014	0	0	0	0	0.014
	TotalEnergy (MJ)	0.23	0	0	0	0	0.23
Spring center plug.par	GWP (kg CO2 eq)	0.006	0	0	0	0	0.006
	TotalEnergy (MJ)	0.239	0	0	0	0	0.239
Rod_end_screw-00.par	GWP (kg CO2 eq)	0.014	0	0	0	0	0.014
	TotalEnergy (MJ)	0.23	0	0	0	0.002	0.231
ok-del4.par	GWP (kg CO2 eq)	0.019	0	0	0	0.002	0.02
	TotalEnergy (MJ)	0.231	0	0	0	0.005	0.237
socket button head cap screw_am_B18.3.4M - 5 x 0.8 x 10 SBHCS --N.par	GWP (kg CO2 eq)	0.015	0	0	0	0.001	0.016
	TotalEnergy (MJ)	0.251	0	0	0	0.003	0.254
Longitudional_fixture_right-00.par	GWP (kg CO2 eq)	0.02	0	0	0	0.002	0.022
	TotalEnergy (MJ)	0.246	0	0	0	0.006	0.252
Piston_seal-00.par	GWP (kg CO2 eq)	0.01	0.003	0	0	0	0.012

cs13r_M8_ball.par	TotalEnergy (MJ)	0.206	0.057	0	0	0	0.264
	GWP (kg CO2 eq)	0.016	0	0	0	0.001	0.017
DIN 471x30.par	TotalEnergy (MJ)	0.265	0	0	0	0.003	0.268
	GWP (kg CO2 eq)	0.015	0	0	0	0	0.015
Ring_DIN_472_26mm.par	TotalEnergy (MJ)	0.273	0	0	0	0.001	0.274
	GWP (kg CO2 eq)	0.015	0	0	0	0	0.015
Nut_M12_thin.par	TotalEnergy (MJ)	0.273	0	0	0	0.001	0.274
	GWP (kg CO2 eq)	0.017	0	0	0	0	0.017
16003_2Z_PART1.par	TotalEnergy (MJ)	0.279	0	0	0	0.002	0.281
	GWP (kg CO2 eq)	0.017	0	0	0	0.001	0.018
Wedgenut-00.par	TotalEnergy (MJ)	0.279	0	0	0	0.003	0.282
	GWP (kg CO2 eq)	0.024	0	0	0	0	0.024
ok-del3_mirrored.par	TotalEnergy (MJ)	0.289	0	0	0	0.001	0.29
	GWP (kg CO2 eq)	0.025	0	0	0	0.002	0.027
One-way-roller-00.par	TotalEnergy (MJ)	0.304	0	0	0	0.007	0.311
	GWP (kg CO2 eq)	0.021	0	0	0	0	0.021
ok-del14.par	TotalEnergy (MJ)	0.335	0	0	0	0.002	0.337
	GWP (kg CO2 eq)	0.021	0	0	0	0	0.021
ok-del8.par	TotalEnergy (MJ)	0.335	0	0	0	0.002	0.337
	GWP (kg CO2 eq)	0.021	0	0	0	0	0.021
Hubspacer.par	TotalEnergy (MJ)	0.335	0	0	0	0.002	0.337
	GWP (kg CO2 eq)	0.03	0	0	0	0	0.03
Front wheel Upper suspension mount right-00.par	TotalEnergy (MJ)	0.362	0	0	0	0.001	0.362
	GWP (kg CO2 eq)	0.03	0	0	0	0.003	0.032
Suspension_rod_bearing_reinforcement-00.par	TotalEnergy (MJ)	0.362	0	0	0	0.008	0.37
	GWP (kg CO2 eq)	0.031	0	0	0	0.003	0.033
61902_2Z_PART2.par	TotalEnergy (MJ)	0.376	0	0	0	0.009	0.385
	GWP (kg CO2 eq)	0.024	0	0	0	0.001	0.025
Brake shield 1.par	TotalEnergy (MJ)	0.391	0	0	0	0.005	0.395
	GWP (kg CO2 eq)	0.031	0	0	0	0.003	0.034
16003_2Z_PART2.par	TotalEnergy (MJ)	0.383	0	0	0	0.009	0.392
	GWP (kg CO2 eq)	0.026	0	0	0	0.001	0.027
Rod-hollow-bolt-00.par	TotalEnergy (MJ)	0.418	0	0	0	0.005	0.423
	GWP (kg CO2 eq)	0.035	0	0	0	0	0.035
ok-del12.par	TotalEnergy (MJ)	0.434	0	0	0	0.001	0.435
	GWP (kg CO2 eq)	0.028	0	0	0	0	0.028
Washer_id12od19t1.5.par	TotalEnergy (MJ)	0.446	0	0	0	0.003	0.449
	GWP (kg CO2 eq)	0.028	0	0	0	0	0.028
ok-del6.par	TotalEnergy (MJ)	0.446	0	0	0	0.003	0.449
	GWP (kg CO2 eq)	0.028	0	0	0	0.001	0.029
Bearing_DIN_625_1_1989_6001_2RS_v9.00.par	TotalEnergy (MJ)	0.446	0	0	0	0.005	0.452
	GWP (kg CO2 eq)	0.028	0	0	0	0.001	0.029
DIN 985 M6 A4.par	TotalEnergy (MJ)	0.446	0	0	0	0.005	0.452
	GWP (kg CO2 eq)	0.027	0	0	0	0	0.027
DIN 71802_cs1__M 6_0.par	TotalEnergy (MJ)	0.46	0	0	0	0.001	0.461
	GWP (kg CO2 eq)	0.029	0	0	0	0.001	0.03
cs13r_M8_joint.par	TotalEnergy (MJ)	0.474	0	0	0	0.006	0.48
	GWP (kg CO2 eq)	0.03	0	0	0	0.001	0.031
Screw_DIN_912_M5x10_v9.00.par	TotalEnergy (MJ)	0.488	0	0	0	0.006	0.494
	GWP (kg CO2 eq)	0.031	0	0	0	0.001	0.032
Schrader_tube_18,5x7.7.par	TotalEnergy (MJ)	0.502	0	0	0	0.006	0.508
	GWP (kg CO2 eq)	0.029	0	0	0	0	0.03
Front wheel arm right.par	TotalEnergy (MJ)	0.512	0	0	0	0.002	0.514
	GWP (kg CO2 eq)	0.043	0	0	0	0.004	0.047
61902_2Z_PART1.par	TotalEnergy (MJ)	0.528	0	0	0	0.012	0.54
	GWP (kg CO2 eq)	0.034	0	0	0	0	0.035
ok-del13.par	TotalEnergy (MJ)	0.558	0	0	0	0.003	0.561
	GWP (kg CO2 eq)	0.034	0	0	0	0.001	0.036
Damper bushing.par	TotalEnergy (MJ)	0.558	0	0	0	0.006	0.564
	GWP (kg CO2 eq)	0.018	0	0	0	0	0.018
	TotalEnergy (MJ)	0.676	0	0	0	0.001	0.678

Brake retainer.psm	GWP (kg CO2 eq)	0.04	0	0	0	0.001	0.042
	TotalEnergy (MJ)	0.656	0	0	0	0.008	0.663
Screw_UNI_ISO_7380_M5x10_v9.50.par	GWP (kg CO2 eq)	0.041	0	0	0	0	0.041
	TotalEnergy (MJ)	0.67	0	0	0	0.004	0.673
Screw_UNI_ISO_7380_M5x16_v9.50.par	GWP (kg CO2 eq)	0.041	0	0	0	0.002	0.043
	TotalEnergy (MJ)	0.67	0	0	0	0.008	0.677
Guide spring-00.par	GWP (kg CO2 eq)	0.039	0	0	0	0	0.039
	TotalEnergy (MJ)	0.683	0	0	0	0.002	0.684
ok-del2.par	GWP (kg CO2 eq)	0.053	0	0	0	0.005	0.058
	TotalEnergy (MJ)	0.651	0	0	0	0.015	0.666
Accumulator_screwring-00.par	GWP (kg CO2 eq)	0.055	0	0	0	0.005	0.06
	TotalEnergy (MJ)	0.68	0	0	0	0.016	0.695
ok-del5.par	GWP (kg CO2 eq)	0.045	0	0	0	0.002	0.046
	TotalEnergy (MJ)	0.725	0	0	0	0.008	0.734
Piston_U_flange-00.psm	GWP (kg CO2 eq)	0.043	0	0	0	0.001	0.045
	TotalEnergy (MJ)	0.736	0	0	0	0.005	0.741
Damping_rod_piston-02.par	GWP (kg CO2 eq)	0.056	0	0	0	0	0.056
	TotalEnergy (MJ)	0.733	0	0	0	0.001	0.734
cs13r_M8_ball.par	GWP (kg CO2 eq)	0.049	0	0	0	0.002	0.051
	TotalEnergy (MJ)	0.795	0	0	0	0.009	0.804
MINARB-M6-012-SS.par	GWP (kg CO2 eq)	0.046	0	0	0	0	0.046
	TotalEnergy (MJ)	0.819	0	0	0	0.002	0.821
Accumulator_housing-02.par	GWP (kg CO2 eq)	0.064	0	0	0	0.005	0.069
	TotalEnergy (MJ)	0.781	0	0	0	0.018	0.799
Rear_Suspension_arm_damper_plate-03.psm	GWP (kg CO2 eq)	0.066	0	0	0	0.006	0.072
	TotalEnergy (MJ)	0.81	0	0	0	0.019	0.829
Pressure_port-00.par	GWP (kg CO2 eq)	0.054	0	0	0	0	0.054
	TotalEnergy (MJ)	0.956	0	0	0	0.002	0.958
Nut_DIN_EN_24035_M12_v9.00.par	GWP (kg CO2 eq)	0.062	0	0	0	0	0.062
	TotalEnergy (MJ)	1.004	0	0	0	0.006	1.01
planet carrier hub.par	GWP (kg CO2 eq)	0.063	0	0	0	0.005	0.068
	TotalEnergy (MJ)	1.021	0	0	0	0.02	1.041
Damper_lock_plate-01.psm	GWP (kg CO2 eq)	0.084	0	0	0	0.007	0.091
	TotalEnergy (MJ)	1.027	0	0	0	0.024	1.051
MINOFF-M5-008-S-4MM-Z.par	GWP (kg CO2 eq)	0.062	0	0	0	0	0.062
	TotalEnergy (MJ)	1.092	0	0	0	0.003	1.095
Tverrstag.par	GWP (kg CO2 eq)	0.061	0	0	0	0.002	0.064
	TotalEnergy (MJ)	1.086	0	0	0	0.009	1.094
Steering_rod_Alligt-00.par	GWP (kg CO2 eq)	0.063	0	0	0	0.002	0.065
	TotalEnergy (MJ)	1.106	0	0	0	0.009	1.115
Front hub axle.par	GWP (kg CO2 eq)	0.07	0	0	0	0.003	0.073
	TotalEnergy (MJ)	1.144	0	0	0	0.013	1.157
Planet carrier lid.par	GWP (kg CO2 eq)	0.076	0	0	0	0.003	0.078
	TotalEnergy (MJ)	1.227	0	0	0	0.014	1.242
Rear_Suspension_arm_diagonal_bracket-01.psm	GWP (kg CO2 eq)	0.101	0	0	0	0.009	0.11
	TotalEnergy (MJ)	1.244	0	0	0	0.029	1.273
Minimotor stator holder.par	GWP (kg CO2 eq)	0.103	0	0	0	0.009	0.111
	TotalEnergy (MJ)	1.259	0	0	0	0.029	1.287
StÃ¸tdemperhus.par	GWP (kg CO2 eq)	0.103	0	0	0	0.009	0.112
	TotalEnergy (MJ)	1.266	0	0	0	0.029	1.295
Sun gear.par	GWP (kg CO2 eq)	0.086	0	0	0	0.003	0.089
	TotalEnergy (MJ)	1.395	0	0	0	0.016	1.411
cs13r_M8_joint.par	GWP (kg CO2 eq)	0.09	0	0	0	0.003	0.094
	TotalEnergy (MJ)	1.465	0	0	0	0.017	1.482
Housing_damper_valves-03.par	GWP (kg CO2 eq)	0.116	0	0	0	0.01	0.126
	TotalEnergy (MJ)	1.418	0	0	0	0.033	1.45
A118SAK_Bottom.par	GWP (kg CO2 eq)	0.091	0	0	0	0.003	0.095
	TotalEnergy (MJ)	1.479	0	0	0	0.017	1.496
Rear_Suspension_arm_lower_plate-00.psm	GWP (kg CO2 eq)	0.118	0	0	0	0.01	0.128
	TotalEnergy (MJ)	1.447	0	0	0	0.033	1.48
Planet axle.par	GWP (kg CO2 eq)	0.093	0	0	0	0	0.093

Bearing_DIN_625_1_1989_608_2RS_v9.00.par	TotalEnergy (MJ)	1.506	0	0	0	0.008	1.515
	GWP (kg CO2 eq)	0.093	0	0	0	0	0.093
Minimotor rotor.par	TotalEnergy (MJ)	1.506	0	0	0	0.008	1.515
	GWP (kg CO2 eq)	0.123	0	0	0	0.01	0.133
Longitudional_suspension_rod_Alligt-02.par	TotalEnergy (MJ)	1.504	0	0	0	0.035	1.539
	GWP (kg CO2 eq)	0.089	0	0	0	0.003	0.092
Accumulator_lower_housing-01.par	TotalEnergy (MJ)	1.577	0	0	0	0.013	1.59
	GWP (kg CO2 eq)	0.126	0	0	0	0.011	0.137
160mm disc rotor.par	TotalEnergy (MJ)	1.548	0	0	0	0.036	1.583
	GWP (kg CO2 eq)	0.098	0	0	0	0.003	0.102
Damper metal center.par	TotalEnergy (MJ)	1.741	0	0	0	0.014	1.755
	GWP (kg CO2 eq)	0.104	0	0	0	0.004	0.108
DIN912 M6x16 A4.par	TotalEnergy (MJ)	1.843	0	0	0	0.015	1.858
	GWP (kg CO2 eq)	0.126	0	0	0	0	0.126
Damping_cylinder-02.par	TotalEnergy (MJ)	2.145	0	0	0	0.004	2.15
	GWP (kg CO2 eq)	0.171	0	0	0	0.015	0.186
Minimotor front hub lid.par	TotalEnergy (MJ)	2.098	0	0	0	0.048	2.146
	GWP (kg CO2 eq)	0.181	0	0	0	0.015	0.196
A118SAK_Top.par	TotalEnergy (MJ)	2.213	0	0	0	0.051	2.264
	GWP (kg CO2 eq)	0.143	0	0	0	0.005	0.148
Torque_arm-02.psm	TotalEnergy (MJ)	2.315	0	0	0	0.027	2.342
	GWP (kg CO2 eq)	0.14	0	0	0	0.004	0.145
Krank arm 140mm.par	TotalEnergy (MJ)	2.39	0	0	0	0.017	2.408
	GWP (kg CO2 eq)	0.205	0	0	0	0.018	0.223
ok-del1.par	TotalEnergy (MJ)	2.517	0	0	0	0.058	2.575
	GWP (kg CO2 eq)	0.014	0.194	0	0	0.002	0.21
spoke LX.par	TotalEnergy (MJ)	0.166	2.444	0	0	0.008	2.618
	GWP (kg CO2 eq)	0.154	0	0	0	0	0.155
spoke RX.par	TotalEnergy (MJ)	2.731	0	0	0	0.006	2.737
	GWP (kg CO2 eq)	0.154	0	0	0	0	0.155
spoke R1.par	TotalEnergy (MJ)	2.731	0	0	0	0.006	2.737
	GWP (kg CO2 eq)	0.154	0	0	0	0	0.155
spoke L1.par	TotalEnergy (MJ)	2.731	0	0	0	0.006	2.737
	GWP (kg CO2 eq)	0.154	0	0	0	0	0.155
406 rim.par	TotalEnergy (MJ)	2.731	0	0	0	0.006	2.737
	GWP (kg CO2 eq)	0.246	0	0	0	0.021	0.267
Sturmey Archer Drumbrake.par	TotalEnergy (MJ)	3.016	0	0	0	0.069	3.085
	GWP (kg CO2 eq)	0.248	0	0	0	0.021	0.27
Planet carrier rim.par	TotalEnergy (MJ)	3.045	0	0	0	0.07	3.115
	GWP (kg CO2 eq)	0.248	0	0	0	0.009	0.257
ESTM_16_1.par	TotalEnergy (MJ)	4.017	0	0	0	0.047	4.064
	GWP (kg CO2 eq)	0.315	0	0	0	0	0.315
Minimotor ring gear.par	TotalEnergy (MJ)	4.153	0	0	0	0.005	4.158
	GWP (kg CO2 eq)	0.267	0	0	0	0.01	0.276
housing_2_2.par	TotalEnergy (MJ)	4.324	0	0	0	0.05	4.374
	GWP (kg CO2 eq)	0.348	0	0	0	0.03	0.378
din912 M4x25-CS.par	TotalEnergy (MJ)	4.267	0	0	0	0.098	4.365
	GWP (kg CO2 eq)	0.288	0	0	0	0.001	0.289
Minimotor axle.par	TotalEnergy (MJ)	4.904	0	0	0	0.01	4.914
	GWP (kg CO2 eq)	0.315	0	0	0	0.012	0.326
Rear-wheel-inside_left-01.par	TotalEnergy (MJ)	5.105	0	0	0	0.059	5.165
	GWP (kg CO2 eq)	0.445	0	0	0	0.038	0.483
Rear-wheel-inside-right-02.par	TotalEnergy (MJ)	5.454	0	0	0	0.125	5.579
	GWP (kg CO2 eq)	0.445	0	0	0	0.038	0.483
brake_disc_160mm_6hole_v2.par	TotalEnergy (MJ)	5.454	0	0	0	0.125	5.579
	GWP (kg CO2 eq)	0.324	0	0	0	0.012	0.336
Support_piston-02.par	TotalEnergy (MJ)	5.735	0	0	0	0.046	5.781
	GWP (kg CO2 eq)	0.445	0	0	0	0	0.445
Minimotor rotor backing iron.par	TotalEnergy (MJ)	5.863	0	0	0	0.008	5.87
	GWP (kg CO2 eq)	0.408	0	0	0	0.017	0.425
	TotalEnergy (MJ)	6.213	0	0	0	0.087	6.3

Minimotor front hub.par	GWP (kg CO2 eq)	0.719	0	0	0	0.061	0.78
	TotalEnergy (MJ)	8.81	0	0	0	0.202	9.012
Damping_rod-02.par	GWP (kg CO2 eq)	0.048	1.065	0	0	0.004	1.117
	TotalEnergy (MJ)	0.586	17.532	0	0	0.013	18.131
Tofix_hydropneumatic-00.par	GWP (kg CO2 eq)	1.101	0	0	0	0.039	1.14
	TotalEnergy (MJ)	19.478	0	0	0	0.156	19.634
Rollover protection_20-00.par	GWP (kg CO2 eq)	1.621	0	0	0	0.138	1.76
	TotalEnergy (MJ)	19.876	0	0	0	0.456	20.332
Child_seat-02.par	GWP (kg CO2 eq)	1.83	0	0	0	0.027	1.857
	TotalEnergy (MJ)	41.374	0	0	0	0.135	41.509
wheel-cover-01.par	GWP (kg CO2 eq)	4.026	0	0	0	0.058	4.084
	TotalEnergy (MJ)	90.992	0	0	0	0.297	91.289
CANOPY20-00.par	GWP (kg CO2 eq)	7.635	0	0	0	0.147	7.782
	TotalEnergy (MJ)	137.95	0	0	0	0.587	138.537
VELO20-00C-mirrored.par	GWP (kg CO2 eq)	8.224	0	0	0	0.537	8.76
	TotalEnergy (MJ)	311.771	0	0	0	2.145	313.916
VELO20-00C.par	GWP (kg CO2 eq)	8.266	0	0	0	0.54	8.805
	TotalEnergy (MJ)	313.37	0	0	0	2.156	315.525

4. Skipped Part List:

Part Name	Material	No. of Instances
o-ring 015,47 x 3,53 nbr, 70 shore.par	NBR	2
Rod_glider-00.par	PTFE	2
O-ring 005,23x2,62 NBR 70 shore.par	NBR	1
V6-404 428849(240).par	Polychloroprene	1
Poppet_seal-00.par	Polychloroprene	2
Vale_outer_seal-00.par	Polychloroprene	2
Valve_cap_seal-00.par	Polychloroprene	2
BFA 50 45 40 2365 Rollmembran unten.par	NBR	2
o-ring.par	NBR	2
Cylinder_plug_w_rod_hole-01.par	PTFE	2
o-ring 20x2.6.par	NBR	2
o-ring 004,47 x 1,78 NBR, 70 Shore.par	NBR, 70 sh	2
Hydraulic_fluid-00.par	Hydraulic fluid	2
bromskloss1.par	Friction pad	4
DIN 125 M6 A4-02.par	A4	4
DIN 912 M6x20 A4.par	A4	4
DIN912 M6x45 A480.par	Stainless Steel, 316	4
Minimotor rotor magnet.psm	NdFeB magnet	40
DIN 7991 M4x8 A4.par	A4	6
Planet -1.5m.par	POM	6
Minimotor stator laminate insulator.par	Epoxy, glass fibre reinforced	4
Minimotor stator laminat.par	Steel, structural	2
DIN912 M8x15 A4 80.par	Stainless Steel, 316	2
torsion bar-00.par	Stainless steel	1
Zit_alligt_11.par	ABS Plastic, high impact	1
Lid handle bracket-00_2.par	Aluminum, 5050	1
Rubber bushing ID13 OD23(18).par	Nitrile rubber	1
Damper rod protector.par	Polypropylene, shrinkable	1
406 tire.par	Tyre rubber	1
Rubber washer ID7 OD24 T4.2.par	Nitrile rubber	1
Rubber washer ID 6.5 OD 20 T3.par	Nitrile rubber	1
TRM_SRF_51.par	Epoxy, cast rigid	1
original clean.par	Epoxy, cast rigid	1
HENGLI-SQL-00.par	Epoxy, cast rigid	1

5. Material Usage Analysis:

Material	Mass(kg)	Percentage (%) mass in assembly
NdFeB magnet	0	0
Aluminum, 5050	1.72	3.42

Silicone	0.002	0
Acrylic, high impact grade	3.574	7.1
Polyethylene, low density	26.202	52.03
Epoxy, glass fibre reinforced	0.008	0.02
Polyurethene	0.002	0
Tyre rubber	0.2	0.4
Steel	2.635	5.23
Epoxy, cast rigid	0.027	0.05
Polypropylene, shrinkable	0.007	0.01
Polypropylene, high impact	0.009	0.02
Polychloroprene	0.078	0.15
Nylon, general purpose	0.088	0.17
NBR	0.018	0.04
Steel, structural	0.02	0.04
Aluminum, 6061-T6	5.744	11.41
Hydraulic fluid	0.206	0.41
Aluminum, 7075-T6	2.748	5.46
ABS Plastic, high impact	3.568	7.09
NBR, 70 sh	0	0
A4	0.042	0.08
Nitrile rubber	0.006	0.01
Stainless Steel, 316	0.325	0.65
Brass, yellow brass	0.02	0.04
Stainless Steel, 304	0.295	0.59
Stainless steel	2.055	4.08
PTFE	0.01	0.02
Iron	0.538	1.07
POM	0.048	0.1
Friction pad	0.16	0.32

COMPARISON BETWEEN SERIES-HYBRID VELOMOBILE AND OTHER MODES OF TRANSPORT FOR COMMUTING WITHIN A CITY

PER H. SØRENSEN[1]
Faculty of Science and Technology
University of Stavanger

Summary: *Seven metrics are used to qualitative compare six different transport modes for a 10 km commute twice every working day. Car, bus, ICE-scooter, bicycle, Pedelec (electric assisted bicycle) and series-hybrid velomobile are compared in a Norwegian city scenario, comparing speed, time consumption, cost with and without travel time, CO_2 emissions, exercise benefit, damage potential in collision in a single radar chart.*

Key words: *Transport modes, emissions, sustainability, pedelec, velomobile*

Introduction

The car has been seen as a vital part of modern society. Unfortunately, the massive implementations of private cars have caused a collection of more or less severe problems in all countries. It is well known that car accidents are a major cause of death and hospitalization. But the huge number of cars also causes a lot of secondary problems as well. For example are air pollution from traffic as lethal as the traffic itself, causing at least as many deaths as road accidents (1).

In Norway, cars are seen as the fastest mode of transport. But when putting the cost of vehicle, plus cost of use including travel time based on labor rates together, the use of cars become extremely expensive, requiring the need to work more than an hour extra to cover the costs. In addition, the non-personal negative impact of massive car use should be part of the equation when selecting transport mode for commuting.

ICE-scooters, scooters with internal combustion engines including mopeds and motorcycles, are quite time efficient and not as expensive as a car but give low or zero weather protection. Bus is very time consuming and becomes extremely costly when calculating travel time as cost on labor rates. Local train and trams are costly and have limited practicality due to low frequency except in the few areas with more than 100-150 000 citizens. Highly functional multi modality like bringing bicycles along on the train has not been examined as this is generally not available in rush hour.

Bicycling is the least costly transport mode available when disregarding time to travel, with the exception of bare walking, which is not included due to the distance selected for modality comparison. Unfortunately, bicycles are not very efficient with regard to speed and Norwegian weather, often being wet or windy or both. In addition, the distance of 10 km each way would normally require a shower and clothes change unless using pedelec, adding either time or additional cost. The benefit of a bicycle is clearly the low cost. Also the longest exercise could be regarded as a plus, depending on training requirements.

A new type of vehicle, a series-hybrid velomobile, *SHV*, has aerodynamic shell over a pedal driven recumbent bicycle with electric assist that offer major improvements over the bicycle. Use of SHV would reduce time consumption to less than half compared to a regular bicycle, due to twice the speed and no need for shower and exchange of clothes, sharing these benefits with pedelecs. Velomobiles offers at least some collision protection and variable weather protection depending on construction.

Some extra time is used riding a SHV compared to a car or ICE-scooter. But work hours must be even longer to pay for the extra cost of the car or scooter. In addition, if one include the time used for exercising while riding as saved time that has a monetary value, the SHV cost becomes even less.

[1] E-mail perhassel@gmail.com

Results of the comparison can be found in *Figure 1 - Comparison of key criteria for various modes of city transport.*

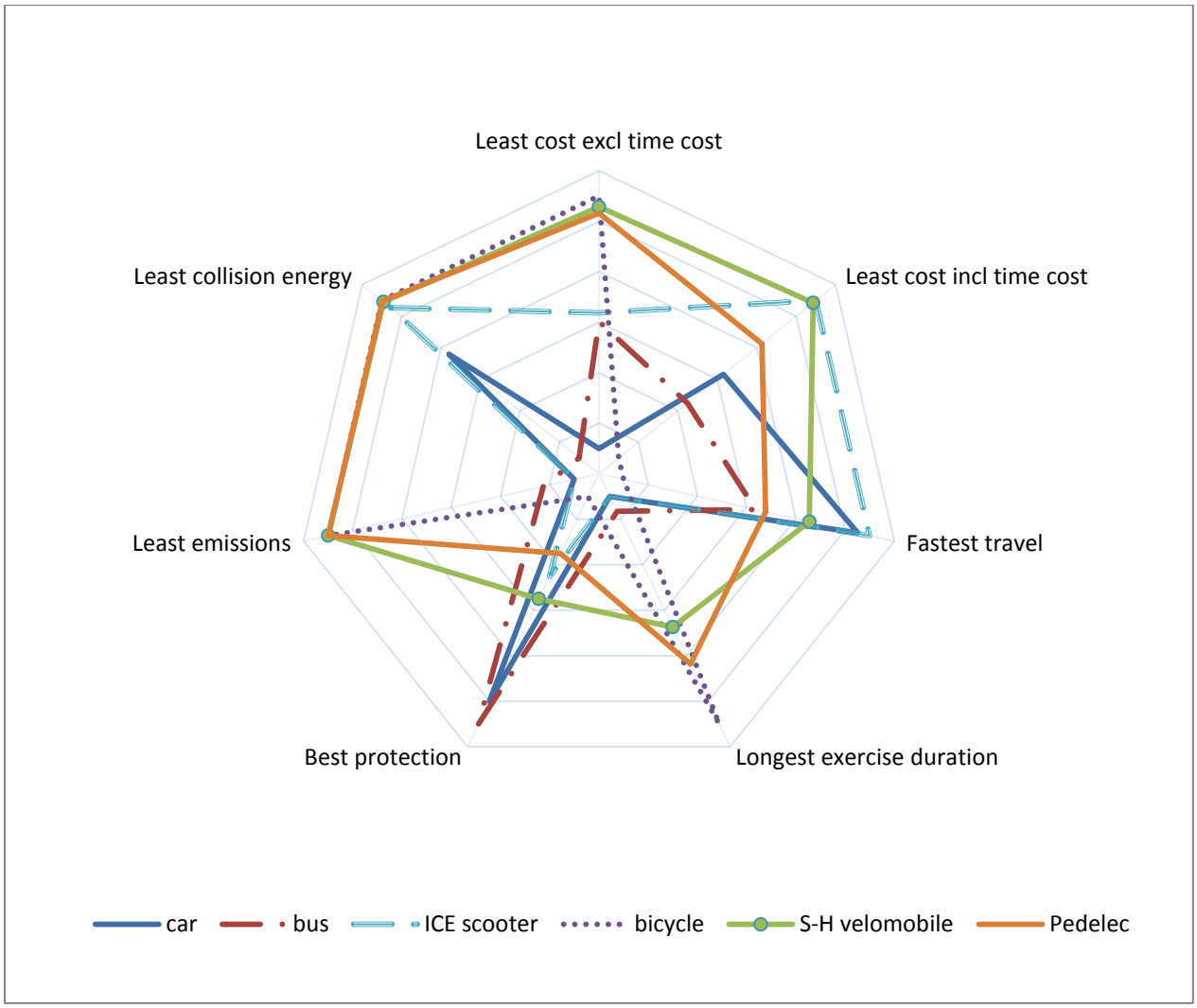

Figure 1 - Comparison of key criteria for various modes of city transport

Costs of using vehicle

Car: Cost of using a private car, for example Volkswagen Passat, Toyota Avensis or Peugeot 508 is NOK 262 per day when driven 15 000 km **Ugyldig kilde er angitt.**, **Ugyldig kilde er angitt.**. That gives a cost of NOK 6.375 /km.

Bus: NOK 15700 is the price for a one year travel card in Oslo (2013). With 235 working days this cost is split on 470 trips, each 10 km, resulting in a travel cost of NOK 3.340 /km.

ICE-scooter: The cost of owning and using a small ICE based moped/scooter is estimated to NOK 625 per month when driven 300 km per month **Ugyldig kilde er angitt.**. This is only 3/4 of the distance traveled in the base case which will decrease cost per km. In addition the cost does not include interest for the vehicle which will increase cost per km. It is estimated that these two deviations compensate for each other resulting in cost of NOK 3.125 /km.

Bicycle: As sources for documenting the cost of using a bicycle has not been found, the following estimates has been used: Liftetime before bike is replaced is 4 years. Estimated purchase cost NOK 4000. Estimated NOK 1000 per year in total running costs that includes locks, spares, service, insurance, parking and storage etc. Estimated distance travelled is 4700 km for 235 working days plus 1300 km additional travel, total 6000 km per year. This result in a cost of NOK 0.33 /km.

Pedelec: As sources for documenting the cost of using a pedelec has not been found, the following estimates has been used: Liftetime before pedelec is replaced (or stolen) is 6 years. Estimated purchase cost NOK 17500. Estimated NOK 1500 per year in total running costs that includes locks, spares, service, insurance, parking and storage etc. Estimated distance travelled is 4700 km for 235 working days plus 1300 km additional travel, total 6000 km per year. This result in a cost of NOK 0.74/km.

SHV: Reliable sources documenting the cost of owning and using a series-hybrid velomobile is not yet available. Based on limited volume production estimated cost is NOK 40 000 with running cost estimated to twice the running cost of bicycle; NOK 2000 per year partly due to addition of more tires, battery, and protective cover. Higher purchase price also result in more costly insurance. Electric energy used for charging is not relevant. On a trip author did in hilly areas using a not very efficient electric assisted velomobile, the average electric consumption measured from the battery was only 5.5 Wh/km **Ugyldig kilde er angitt.**, adding up to less than NOK 1 for a 227 km trip. When using the s-h velomobile as a car replacement it is estimated that the vehicle travel 10 000 km, 2/3 of the km travelled by the example car. It is also estimated that the relatively low cost of the vehicle can be financed without a loan and thus 2.5% interest, i.e. NOK 1000 per year is reasonable. A velomobile is typically sold at ½ price if well treated. If kept for 7 year the ownership costs NOK 20 000 + 7 (1 000 + 2 000) = NOK 41 000 which is NOK 0.59/km.

Equivalent CO_2 emissions

Car: Average equivalent CO_2 emissions of a petrol car is 106.8 g /km/passenger – see table 5 **Ugyldig kilde er angitt.**. This does not include additional emissions caused by cold motor, queue for typical rush hour traffic. In addition this is based on average occupancy of 1.6 persons per car, see page 37 **Ugyldig kilde er angitt.**. Single occupancy transport will increase emissions further.

Bus: Average equivalent CO_2 emissions for a diesel bus in city traffic is 94 g/km/passenger, see table 5 in **Ugyldig kilde er angitt.**. This is based on average occupancy of 19.3 passengers per bus in average, see page 47 **Ugyldig kilde er angitt.**.

ICE-scooter: In average, ICE based two wheelers have unproportionally high greenhouse gas emissions when compared to cars **Ugyldig kilde er angitt.**. Even if CO_2 emissions are somewhat reduced due to less fuel used, other emissions are much higher than for cars, adding GHG constituents that results in approximate same carbon footprint as an average petrol car, i.e. 106,8 g/km. New European directives that will be enforced within a few years may lower emissions from two wheelers.

Speed of travel

Car: Average speed of a car in city is highly dependent on local traffic. Maximum speed in town in Norway is 50 km/h. Some queue and and traffic jams in cross sections will reduce the average speed. Assuming 40 km/h would be a reasonable estimate,. It is possibly overestimated but not to far off.

Bus: Speed of bus in a city is 22.3 km/h based on median value for bus statistics presented in**Ugyldig kilde er angitt.**.

ICE-scooter: Average speed of an ICE-scooter is estimated to 45 km/h, achievable by most two wheeled ICE vehicles and slightly faster than cars due to ease of passing queues. Many Norwegian cities have reduced speed in many streets to 40 km/h. That makes 45 km/h a reasonable maximum speed for ICE two wheelers.

Bicycle: Speed of bicycle in city traffic including time to park and lock is 15 km/h, see page 18 in **Ugyldig kilde er angitt.**.

Pedelec: Speed of pedelec in city traffic including time to park and lock is 20 km/h. Max speed for pedelec in EU is 25 km/h but in city traffic average becomes less than max.

SHV: Assuming a fast series hybrid velomobile, 27.5 km/h average is achievable. Author regularly travel 27-28 km/h in average using a less aerodynamic velomobile in hilly terrain.

Additional time consumption

Car: Assuming 2 minutes to locate parking space and drive off or park at each end of journey, 4 min per day.

Bus: Average distance to nearest bus stop is 300-400 m according to**Ugyldig kilde er angitt.**. Assume 2 x 350 m resulting in 9 min walking per day for average commuter travel by bus.

ICE-scooter: Assuming 2 minutes to locate parking space and drive off or park at each end of journey, 4 min per day.

Bicycle: 20 minutes additional time in wardrobe/shower. Time to park and lock is included in travel time estimate.

Pedelec: Time to park and lock is included in travel time estimate.

SHV: Assuming 2 minutes to locate parking space and drive off or park at each end of journey, 4 min per day.

Cost of time

Average yearly income before tax is NOK 470 900 **Ugyldig kilde er angitt.**. Average tax is 29.8% **Ugyldig kilde er angitt.** resulting in average available income of NOK 330 572. A working year consists of 1762.5 hours. Income per minute is then:

$$\frac{NOK\ 470\ 900\ (1-0.298)}{1762.5\ hour\ \frac{60\ min}{1\ hour}} = NOK\ 3.126\ \text{ per minute.}$$

Training as part of journey

Training time is all time spent on the journey while not sitting in/on a fully motorized vehicle (bus, car, ICE-scooter).

Collision energy

Potential collision energy is based on the following estimates:

Person:	A person has a mass of 75 kg, as used officially for car legislation.
Car:	Mass of car with 1.6 occupants is estimated to 1600 kg.
Bus:	Mass of bus with 19.3 passengers is estimated to 15 000 kg.
ICE-scooter:	Mass of scooter with driver is estimated to 180 kg.
Bicycle:	Mass of bicycle plus rider is estimated to 90 kg.
Pedelec:	Mass of pedelec plus rider is estimated to 100 kg.
SHV:	Mass of series hybrid velomobile including rider is estimated to 110 kg.

Best protection

Protection values are estimated values based on risk for occupants of vehicle to be seriously damaged in a traffic accident.

Car:	Modern car has very good protection when driven in city with low and moderate speed. Slightly higher risk than bus passengers, P = 0.9
Bus:	Best protection, least risk, P = 1
ICE-scooter:	Moderate to high risk, P = 0.35
Bicycle:	Highest risk, P = 0
Pedelec:	No protection but slightly less risk taking in traffic compared to bicycle due to less cost involved when reducing speed, P = 0.25
SHV:	Some protection, moderate risk, P = 0.45

Bibliography:

1. Caiazzo, F., Ashok A., Waitz, I., Yim, S., Barrett, S. *Air pollution and early deaths in the United States. Part I: Quantifying the impact of major sectors in 2005*. 2013. Atmospheric Environment vol. 79 p. 198-208.